

University of Warwick institutional repository: <http://go.warwick.ac.uk/wrap>

A Thesis Submitted for the Degree of PhD at the University of Warwick

<http://go.warwick.ac.uk/wrap/45786>

This thesis is made available online and is protected by original copyright.

Please scroll down to view the document itself.

Please refer to the repository record for this item for information to help you to cite it. Our policy information is available from the repository home page.

**Verdazyl Radicals as Mediators in Living
Radical Polymerisation**

And

**Dopamine End-Functionalised Polymers for
Application as Friction Modifiers**

Georgina Rayner

A thesis submitted in partial fulfilment of the requirements for the
degree of

Doctor of Philosophy in Chemistry

Department of Chemistry
THE UNIVERSITY OF
WARWICK

October 2011

Table of Contents

Table of Contents	i
List of Figures	ix
List of Schemes	xxi
List of Tables.....	xxiv
List of abbreviations.....	xxvii
Acknowledgements	xxxii
Declaration	xxxiii
Abstract	XXXIV
1. Verdazyl Radicals as Mediators in Living Radical Polymerisation.....	1
1.1. Introduction	1
1.1.1. The development of living radical polymerisation	1
1.1.1.1. Conventional radical polymerisation	1
1.1.1.2. Living polymerisation	3
1.1.1.3. Living radical polymerisation	3
1.1.2. Living radical polymerisation techniques	4
1.1.2.1. Atom transfer radical polymerisation.....	4
1.1.2.2. Reversible addition- fragmentation chain transfer.....	5
1.1.2.3. Stable free radical polymerisation.....	7
1.1.2.4. Other stable radicals for SFRP.....	15
1.1.3. Electron paramagnetic resonance.....	17

1.1.3.1. The theory of EPR.....	17
1.1.3.2. Hyperfine interactions.....	20
1.1.3.3. Sample preparation and experimental considerations.....	21
1.1.4. Verdazyl radicals.....	22
1.1.4.1. Synthesis of verdazyl radicals.....	23
1.1.4.2. Properties of verdazyl radicals.....	26
1.1.4.3. Applications of verdazyl radicals.....	31
1.1.5. Verdazyl radicals as mediators in stable free radical polymerisations ...	31
1.1.6. Aim of this work.....	41
1.2. Verdazyl radicals: Synthesis and characterisation.....	42
1.2.1. Radical synthesis.....	42
1.2.2. Verdazyl characterisation.....	48
1.3. Verdazyl initiator synthesis.....	63
1.3.1. Exchange reaction.....	63
1.3.2. Atom transfer radical addition reaction.....	70
1.4. Verdazyl mediated polymerisation.....	79
1.4.1. Polymerisation of styrene.....	79
1.4.2. Polymerisation of <i>n</i> -butyl acrylate.....	87
1.4.2.1. Polymerisation of styrene at a lower temperature.....	98
1.4.3. Polymerisation of MMA.....	100
1.4.4. Copolymerisation of MMA and styrene.....	104
1.5. High Temperature EPR studies.....	112
1.5.1. High temperature cavity calibration.....	114

1.5.2. Polymer end-group analysis.....	115
1.5.3. In-situ EPR analysis of the polymerisation of styrene.....	118
1.5.4. Initiator characterisation.....	125
1.5.4.1. Initiator decomposition.....	126
1.5.5. Radical decomposition.....	128
1.6. Conclusions and future work.....	132
1.7. Experimental.....	134
1.7.1. Materials.....	134
1.7.2. Characterisation techniques.....	134
1.7.3. Synthesis of compounds in Chapter 1.....	136
1.7.3.1. 2,4-dimethylcarbonohydrazide ⁹⁸ (1).....	136
1.7.3.2. 1,5-dimethyl-tetrazinan-6-one ⁹⁷ (2).....	137
1.7.3.3. 1,5-dimethyl-3-phenyl-tetrazinan-6-one ⁹⁷ (3).....	138
1.7.3.4. 1,5-dimethyl-3-(4-methylphenyl)tetrazinan-6-one ⁹⁹ (4).....	139
1.7.3.5. 1,5-dimethyl-3-(4-methoxyphenyl)tetrazinan-6-one ⁹⁷ (5).....	140
1.7.3.6. 1,5-dimethyl-3-(4-nitrophenyl)tetrazinan-6-one ⁹⁷ (6).....	141
1.7.3.7. 1,5-dimethyl oxoverdazyl ⁶³ (7).....	142
1.7.3.8. 1,5-dimethyl-3-phenyl-6-oxoverdazyl ⁶³ (8).....	143
1.7.3.9. 1,5-dimethyl-3-(4-methylphenyl)-6-oxoverdazyl ⁹⁹ (9).....	144
1.7.3.10. 1,5-dimethyl-3-(4-methoxyphenyl)-6-oxoverdazyl ⁶³ (10).....	145
1.7.3.11. 1,5-dimethyl-3-(4-nitrophenyl)-6-oxoverdazyl ⁶³ (11).....	146
1.7.3.12. Sample preparation of TEMPO and verdazyl radicals 7, 8, 9, 10 and 11 for EPR.....	147

1.7.3.13. 2-phenyl-2-(2,2,6,6-tetramethylpiperidin-1-oxy)ethyl benzoate ²⁴ (12).....	148
1.7.3.14. Synthesis of 2-phenyl-2-(1,5-dimethyl-3-Phenyl-6-oxoverdazyl)ethyl benzoate (13) via an exchange reaction ⁵³	149
1.7.3.15. 2-bromo-2-phenyl ethanol ¹¹⁶ (14).....	150
1.7.3.16. 2-bromo-2-phenylethyl benzoate (15).....	151
1.7.3.17. 2-phenyl-2-(1,5-dimethyl-6-oxoverdazyl) ethyl benzoate unimer (16).....	152
1.7.3.18. Synthesis of 2-phenyl-2-(1,5-dimethyl-3-Phenyl-6-oxoverdazyl)ethyl benzoate (13).....	154
1.7.3.19. Synthesis of 2-phenyl-2-(1,5-dimethyl-3-methoxyphenyl-6-oxoverdazyl)ethyl benzoate (17).....	155
1.7.3.20. Synthesis of 2-phenyl-2-(1,5-dimethyl-3-nitrophenyl-6-oxoverdazyl)ethyl benzoate (18).....	156
1.7.4. Polymerisation procedures for Chapter 1.....	158
1.7.4.1. Polymerisation of verdazyl stabilised and non stabilised styrene using 16 (R = H).....	158
1.7.4.2. Polymerisation of styrene with 0, 25 and 50% toluene using 13 (R = Ph)	158
1.7.4.3. Polymerisation of styrene using 13 (R = Ph), 16 (R = H), 17 (R = PhOMe) and 18 (PhNO ₂)	159
1.7.4.4. Polymerisation of styrene using 12	160
1.7.4.5. Polymerisation of <i>n</i> -butyl acrylate using 13 (R = Ph)	161
1.7.4.6. Polymerisation of verdazyl stabilised <i>n</i> -butyl acrylate at different volumes using 13 (R = Ph).....	161

1.7.4.7. Polymerisation of verdazyl stabilised <i>n</i> -butyl acrylate using verdazyl initiators 16 (R = H), 17 (R = PhOMe) and 18 (R = PhNO ₂)	162
1.7.4.8. Polymerisation of verdazyl stabilised <i>n</i> -butyl acrylate using 12 ...	163
1.7.4.9. Polymerisation of <i>n</i> -butyl acrylate at different temperatures using 17 (R = PhOMe).....	164
1.7.4.10. Polymerisation of styrene at a lower temperature.....	165
1.7.4.11. Polymerisation of MMA using 13 (R = Ph), 16 (R = H), 17 (R = PhOMe) and 18 (R = PhNO ₂)	166
1.7.4.12. Polymerisation of verdazyl stabilised MMA using 16 (R = H) ...	167
1.7.4.13. Copolymerisation of styrene and MMA using 13 (R = Ph) with the addition of 0.05 equivalents of 8 ³¹	167
1.7.4.14. Copolymerisation of styrene and MMA using 13 (R = Ph).....	168
1.7.5. High Temperature EPR procedures for Chapter 1	169
1.7.5.1. Polymer end-group analysis by EPR	169
1.7.5.2. High temperature cavity calibration.....	170
1.7.5.3. High temperature EPR study of the polymerisation of styrene using 13.....	171
1.7.5.4. High temperature EPR study of radical decomposition using 8....	171
1.7.5.5. Initiator characterisation.....	172
1.7.5.6. High temperature EPR study of initiator decomposition using 13	173
1.8. Appendix	174
1.8.1. Crystallographic data	174
1.8.1.1. 1,5-dimethyl-tetrazinan-6-one.....	174
1.8.1.2. 1,5-dimethyl-3-phenyl-tetrazinan-6-one	180

1.8.1.3. 2-phenyl-2-(1,5-dimethyl-3-phenyl-6-oxoverdazyl)ethyl benzoate	187
1.9. References	196
2. Dopamine End-Functionalised Polymers for Application as Friction Modifiers	205
2.1. Introduction	205
2.1.1. Dopamine and polymer adhesion.....	205
2.1.1.1. Taking inspiration from nature.....	205
2.1.1.2. The role of DOPA in adhesion.....	208
2.1.1.3. Mussel inspired adhesive polymers	213
2.1.2. Living radical polymerisation	215
2.1.2.1. Atom transfer radical polymerisation.....	215
2.1.2.2. Single electron transfer living radical polymerisation	216
2.1.3. Reduction of friction and wear by lubrication	219
2.1.3.1. Friction and wear.....	219
2.1.3.2. The role of lubricants	219
2.1.3.3. The Stribeck curve	220
2.1.4. Mechanical measurement of friction.....	223
2.1.5. The aim of this work	226
2.2. Initiator synthesis and characterisation	227
2.2.1. Initiator synthesis	227
2.2.2. Initiator characterisation.....	230
2.3. Initial polymerisation studies	232
2.3.1. Cu(I) mediated polymerisation of MMA	232

2.3.1.1. Polymer end-group analysis	234
2.3.2. Cu(0) mediated polymerisation of <i>t</i> -butyl acrylate	236
2.3.2.1. Low molecular weight polymer end-group analysis	242
2.3.2.2. Deprotection of low molecular weight polymer	244
2.4. Polymerisation of lauryl methacrylate	246
2.4.1. Initial investigations	246
2.4.2. Polymerisation of lauryl methacrylate using a Cu(I)Cl system	247
2.4.2.1. Copolymerisation of lauryl methacrylate and MMA	249
2.4.2.2. Initiator scale up	253
2.4.2.3. Scale up polymerisations	253
2.5. Tribological testing	256
2.6. Conclusions and future work	265
2.7. Experimental	267
2.7.1. Materials	267
2.7.2. Characterisation techniques	267
2.7.3. Synthesis of compounds for Chapter 2	269
2.7.3.1. Synthesis of 2-bromo- <i>N</i> -[2-(3,4-dihydroxyphenyl)ethyl] propionamide (unprotected dopamine initiator)	269
2.7.3.2. Synthesis of 2-bromo- <i>N</i> -[2-(3,4-dihydroxyphenyl)ethyl] propionamide acetonide (protected dopamine initiator)	270
2.7.3.3. Deprotection 2-bromo- <i>N</i> -[2-(3,4-dihydroxyphenyl)ethyl] propionamide acetonide (deprotected dopamine initiator)	272
2.7.4. Polymerisation procedures for Chapter 2	273

2.7.4.1. Cu(I) mediated polymerisation of MMA using the unprotected/protected dopamine initiators.....	273
2.7.4.2. Cu(0) mediated polymerisation of <i>t</i> -butyl acrylate using the unprotected/protected dopamine initiators.....	274
2.7.4.3. Deprotection of poly <i>t</i> -butyl acrylate made using the protected dopamine initiator	276
2.7.4.4. Polymerisation of lauryl methacrylate using Cu(I)Cl.....	276
2.7.4.5. Copolymerisation of lauryl methacrylate and MMA using Cu(I)Cl	277
2.7.4.6. Copolymerisation of lauryl methacrylate and MMA using Cu(I)Cl and the protected dopamine initiator.....	278
2.7.4.7. Deprotection of lauryl methacrylate/MMA copolymer ($M_n = 18,900$ g/mol; PDI = 1.29)	279
2.7.4.8. Copolymerisation of lauryl methacrylate and MMA using Cu(I)Cl and ethyl 2-bromopropionate	280
2.7.5. Scale up polymerisations for industrial testing.....	281
2.7.5.1. Copolymerisation of lauryl methacrylate and MMA using Cu(I)Cl and ethyl 2-bromopropionate	281
2.7.5.2. Copolymerisation of lauryl methacrylate and MMA using Cu(I)Cl and the protected dopamine initiator.....	281
2.7.5.3. Deprotection of lauryl methacrylate/MMA copolymer	282
2.8. References	283

List of Figures

Figure 1.1-1. 2,2'-Azobisisobutyronitrile (AIBN, left) or benzoyl peroxide (BPO, right).....	2
Figure 1.1-2. General structure of chain transfer agents used in RAFT	6
Figure 1.1-3. Structures of TIPNO (left) and SG1 (right).....	11
Figure 1.1-4. 2,2-diphenyl-3-phenylimino-2,3-dihydroindol-1-yloxyl (DPAIO, left) and DPAIO based alkoxyamine initiator (right)	14
Figure 1.1-5. <i>N</i> -phenylalkoxyamine initiator.....	15
Figure 1.1-6. Alternative stable radicals for use in SFRP.....	15
Figure 1.1-7. Energy diagram for a free electron in an applied magnetic field illustrating the Zeeman effect.....	18
Figure 1.1-8. Effect of field modulation to produce the first derivative of an absorption curve ⁵⁶	19
Figure 1.1-9. EPR spectrum of TEMPO	20
Figure 1.1-10. EPR spectra of polycrystalline DPPH and a 0.6 mM solution of DPPH in toluene ⁵⁸	21
Figure 1.1-11. Type I (left) and Type II (right) verdazyl radicals with atom numbering scheme, X = O or S.....	23
Figure 1.1-12. Simulated EPR spectra of 1,3,5-diphenylverdazyl (bottom) and 1,5-dimethyl-3-phenyl-6-oxoverdazyl (top) using hyperfine couplings from the literature ^{63, 75}	30
Figure 1.1-13. Coupling products of triphenylverdazyl with 2'-azobis-2,4-dimethylvaleronitrile (left) and methyl 2,2'-azobisbutylate (right).....	32

Figure 1.1-14. Change in triphenylverdazyl concentration during the polymerisation of styrene by (i) determined by EPR ⁵¹	35
Figure 1.1-15. Unimolecular verdazyl initiators employed by Georges <i>et al.</i>	37
Figure 1.2-1. Molecular structure of 1,5-dimethyl-3-tetrazinan-6-one (2) determined by X-ray crystallography.....	45
Figure 1.2-2. Molecular structure of 1,5-dimethyl-3-phenyl-tetrazinan-6-one (3) determined by X-ray crystallography	46
Figure 1.2-3. 1,5-dimethyl-6-oxoverdazyl (7) straight after purification (left) and after standing at ambient temperature for 1 day (right)	47
Figure 1.2-4. General numbering scheme used for verdazyl radicals.....	49
Figure 1.2-5. Verdazyl radicals (from left to right); 1,5-dimethyl-6-oxoverdazyl (7), 1,5-dimethyl-3-phenyl-6-oxoverdazyl (8), 1,5-dimethyl-3-methylphenyl-6-oxoverdazyl (9), 1,5-dimethyl-3-methoxyphenyl-6-oxoverdazyl (10) and 1,5-dimethyl-3-nitrophenyl-6-oxoverdazyl (11)	49
Figure 1.2-6. UV-vis spectra of verdazyl radicals 7-11 in 1,4-dioxane.....	50
Figure 1.2-7. Experimental (top) and simulated (bottom) EPR spectrum of 7.....	51
Figure 1.2-8. Experimental EPR spectrum of a 1 mM solution of 8 in toluene	52
Figure 1.2-9. Experimental (top) and simulated (bottom) EPR spectrum of a 0.2 mM solution of 8 in toluene.....	53
Figure 1.2-10. Experimental (top) and simulated (bottom) EPR spectrum of a 0.05 mM solution of 9 in toluene	54
Figure 1.2-11. Experimental (top) and simulated (bottom) EPR spectrum of a 0.05 mM solution of 10 in toluene	55
Figure 1.2-12. Experimental (top) and simulated (bottom) EPR spectrum of a 0.05 mM solution of 11 in toluene	56

Figure 1.2-13. Calculated molecular orbital (top left), spin density plot (top right) for verdazyl radical 8 (R = Ph)	58
Figure 1.2-14. Atom numbering scheme for used for Table 1.2-2	59
Figure 1.2-15. Structure of 1,5-diphenyl-6-oxoverdazyl (left) and 1,5-dimethyl-3-nitro-6-oxoverdazyl (right).....	61
Figure 1.3-1. EPR of spectra of samples taken at 0 and 2 hours for the synthesis of 2-phenyl-2-(1,5-dimethyl-3-phenyl-6-oxoverdazyl)ethyl benzoate (13) via an exchange reaction.....	65
Figure 1.3-2. Simulation of 8 (left) and TEMPO (right) at t = 2 h from the exchange reaction.....	66
Figure 1.3-3. Comparison of EPR spectra from the exchange reaction at t = 0 (—) and 0.5 (—) hours zoomed in to the signal for 8 (R = Ph).....	68
Figure 1.3-4. ¹ H NMR spectrum of TEMPO initiator (—), the first attempt at the exchange reaction (—), attempt at the exchange reaction using ascorbic acid (—) ...	69
Figure 1.3-5. EPR traces from the ATRA reaction for the synthesis of 2-phenyl-2-(1,5-dimethyl-6-oxoverdazyl)ethyl benzoate (16)	72
Figure 1.3-6. Verdazyl initiators 2-phenyl-2-(1,5-dimethyl-6-oxoverdazyl)ethyl benzoate (16), 2-phenyl-2-(1,5-dimethyl-3-phenyl-6-oxoverdazyl)ethyl benzoate (13), 2-phenyl-2-(1,5-dimethyl-3-methoxyphenyl-6-oxoverdazyl)ethyl benzoate (17) and 2-phenyl-2-(1,5-dimethyl-3-nitrophenyl-6-oxoverdazyl)ethyl benzoate (18) ...	73
Figure 1.3-7. Assigned ¹ H NMR spectrum of 16.....	74
Figure 1.3-8. Assigned ¹ H NMR spectrum of 13.....	74
Figure 1.3-9. Assigned ¹ H NMR spectrum of 17.....	75
Figure 1.3-10. Assigned ¹ H NMR spectrum of 18.....	75
Figure 1.3-11. ¹ H NMR spectra of 2-phenyl-2-(1,5-dimethyl-3-phenyl-6-oxoverdazyl)ethyl benzoate (13) at room temperature (—) and at -20 °C (—)	76

Figure 1.3-12. Molecular structure of 2-phenyl-2-(1,5-dimethyl-3-phenyl-6-oxoverdazyl)ethyl benzoate (13) determined by X-ray crystallography with selected atom distances and atom labels.....	77
Figure 1.4-1. First order kinetic plot for the verdazyl mediated polymerisation of styrene by 16 (R = H) using verdazyl stabilised styrene (●), styrene (●) and results from the literature (◆) ⁵³	80
Figure 1.4-2. Evolution of molecular weight (M_n) and PDI versus conversion for the verdazyl mediated polymerisation of styrene by 16 (R = H) using verdazyl stabilised styrene (●), styrene (●) and results from the literature (◆) ⁵³ , DP = 380, target M_n = 39,500 g/mol (- - -).....	80
Figure 1.4-3. Overlaid differential molecular weight distribution curves for the verdazyl mediated polymerisation of styrene (●) by 16 (R = H).....	81
Figure 1.4-4. First order kinetic plot for the verdazyl mediated polymerisation of styrene with 0% (▲), 25% (▲), 50% (▲) and literature values for 0% (◆) ⁵³ toluene with respect to monomer by 13 (R = Ph).....	82
Figure 1.4-5. Evolution of molecular weight (M_n) and PDI versus conversion for the verdazyl mediated polymerisation of styrene with 0% (▲), 25% (▲), 50% (▲) and literature values for 0% (◆) ⁵³ toluene with respect to monomer by 13 (R = Ph), DP = 485, target M_n = 50,500 g/mol (- - -).....	83
Figure 1.4-6. First order kinetic plot for the verdazyl mediated polymerisation of styrene by 12 (■), 16 (●), 13 (▲), 17 (★), 18 (▶) and literature values for 16 (◆) ⁵³	84
Figure 1.4-7. Evolution of molecular weight (M_n) and PDI versus conversion for the verdazyl mediated polymerisation of styrene by 12 (■), 16 (●), 13 (▲), 17 (★), 18 (▶) and literature values for 16 (◆) ⁵³ , DP = 485, target M_n = 50,500 g/mol (- - -).....	85
Figure 1.4-8. Overlaid differential molecular weight distribution curves for the verdazyl mediated polymerisation of styrene by 16 (R = H, ●, top) and 18 (R = PhNO ₂ , ▶, bottom).....	86

Figure 1.4-9. First order kinetic plot for the verdazyl mediated polymerisation of <i>n</i> -butyl acrylate by 13 (R = Ph)	88
Figure 1.4-10. Evolution of molecular weight (M_n) and PDI versus conversion for the verdazyl mediated polymerisation of <i>n</i> -butyl acrylate by 13 (R = Ph), DP = 280, target M_n = 35,900 g/mol (- - -)	88
Figure 1.4-11. First order kinetic plot for the verdazyl mediated polymerisation of verdazyl stabilised <i>n</i> -butyl acrylate by 13 (R = Ph) at different volumes (3 (▲), 9 (▲) and 15 (▲) mL) and results from the literature ⁵³ (▲)	90
Figure 1.4-12. Evolution of molecular weight (M_n) and PDI versus conversion for the verdazyl mediated polymerisation of verdazyl stabilised <i>n</i> -butyl acrylate by 13 (R = Ph) at different volumes (3 (▲), 9 (▲) and 15 (▲) mL) and results from the literature ⁵³ (▲), DP = 478, target M_n = 61,300 g/mol (- - -)	91
Figure 1.4-13. First order kinetic plot for the verdazyl mediated polymerisation of verdazyl stabilised <i>n</i> -butyl acrylate by 12 (■), 16 (●), 13 (▲), 17 (★), 18 (▶) and literature values for 13 (◆) ⁵³	92
Figure 1.4-14. Evolution of molecular weight (M_n) and PDI versus conversion for the verdazyl mediated polymerisation of verdazyl stabilised <i>n</i> -butyl acrylate by 12 (■), 16 (●), 13 (▲), 17 (★), 18 (▶) and literature values for 13 (◆) ⁵³ , DP = 478, target M_n = 61,300 g/mol (- - -)	93
Figure 1.4-15. Overlaid differential molecular weight distribution curves for the verdazyl mediated polymerisation of verdazyl stabilised <i>n</i> -butyl acrylate by 17 (R = PhOMe, ★)	94
Figure 1.4-16. Overlaid differential molecular weight distribution curves for the verdazyl mediated polymerisation of verdazyl stabilised <i>n</i> -butyl acrylate by 13 (R = Ph, ▲)	95
Figure 1.4-17. First order kinetic plot for the verdazyl mediated polymerisation of <i>n</i> -butyl acrylate by 17 (R = PhOMe) at 90 °C (★), 100 °C (★) and 110 °C (★)	96
Figure 1.4-18. Evolution of molecular weight (M_n) and PDI versus conversion for the verdazyl mediated polymerisation of verdazyl stabilised <i>n</i> -butyl acrylate by 17	

(R = PhOMe) at 90 °C (★), 100 °C (☆) and 110 °C (▲), DP = 524, target $M_n = 67,100$ g/mol (- - -).....	97
Figure 1.4-19. First order kinetic plot for the verdazyl mediated polymerisation of styrene by 13 (R = Ph, ▲) and 17 (R = PhOMe, ★) at 100 °C	99
Figure 1.4-20. Evolution of molecular weight (M_n) and PDI versus conversion for the verdazyl mediated polymerisation of styrene by 13 (R = Ph, ▲) and 17 (R = PhOMe, ★) at 100 °C, DP = 485, target $M_n = 50,500$ g/mol (- - -).....	99
Figure 1.4-21. First order kinetic plot for the verdazyl mediated polymerisation of MMA by 16 (●), 13 (▲), 17 (★) and 18 (▶)	101
Figure 1.4-22. Evolution of molecular weight (M_n) and PDI versus conversion for the verdazyl mediated polymerisation of MMA by 16 (●), 13 (▲), 17 (★) and 18 (▶), DP = 485, target $M_n = 50,500$ g/mol (- - -)	102
Figure 1.4-23. Overlaid differential molecular weight distribution curves for the verdazyl mediated polymerisation of MMA by 17 (PhOMe, ★)	103
Figure 1.4-24. First order kinetic plot for the verdazyl mediated copolymerisation of MMA and styrene by 13 (R = Ph) at ratios of 1:1 (▲), 3:1 (■) and 9:1 (◆) using 0.05 equivalents of free verdazyl radical (8) for every equivalent of initiator	105
Figure 1.4-25. Evolution of molecular weight (M_n) and PDI versus conversion for the verdazyl mediated copolymerisation of MMA and styrene by 13 (R = Ph) at ratios of 1:1 (▲), 3:1 (■) and 9:1 (◆) using 0.05 equivalents of free verdazyl radical (8) for every equivalent of initiator. DP = 200, target $M_n = 20,000$ g/mol (- - -).....	105
Figure 1.4-26. First order kinetic plot for the verdazyl mediated copolymerisation of MMA and styrene by 13 (R = Ph) at ratios of 1:1 (▲), 3:1 (■) and 9:1 (◆).....	106
Figure 1.4-27. Evolution of molecular weight (M_n) and PDI versus conversion for the verdazyl mediated copolymerisation of MMA and styrene by 13 (R = Ph) at ratios of 1:1 (▲), 3:1 (■) and 9:1 (◆), DP = 200, target $M_n = 20,000$ g/mol (- - -)	107

Figure 1.4-28. Overlaid differential molecular weight distribution curves for the verdazyl mediated copolymerisation of MMA and styrene with 0.5 equivalents of free verdazyl (left) and without (right) at ratios of 1:1 (top), 3:1 (middle) and 9:1 (bottom).....	110
Figure 1.4-29. ¹ H NMR of polystyrene homopolymer (PS, —), poly methyl methacrylate homopolymer (PMMA, —) and poly methyl methacrylate/polystyrene copolymer (—).....	111
Figure 1.5-1. Ambient temperature EPR spectrum of 8 (0.2 mM)	113
Figure 1.5-2. Plot of normalised double integral vs. concentration for 0.1, 0.5, 1.2, 2.4 and 7.9 mM solutions of 8 at ambient temperature (■), during heating (■) and after heating (■).....	114
Figure 1.5-3. EPR spectrum of poly <i>n</i> -butyl acrylate synthesised using 13 recorded at 142 °C.....	117
Figure 1.5-4. Plot of normalised double integral vs. time for the first attempt at the polymerisation of styrene in the EPR spectrometer.....	120
Figure 1.5-5. ¹ H NMR traces for the polymerisation by styrene at <i>t</i> = 0 (—), the EPR polymerisation after 20 h (—) and the remaining polymerisation mixture heated in an oil bath for 22 h (—)	121
Figure 1.5-6. EPR traces from the second attempt at the polymerisation of styrene in the EPR machine at 0, 23, 42 and 67 h	122
Figure 1.5-7. Plot of normalised double integral vs. time for the second attempt at the polymerisation of styrene in the EPR spectrometer.....	123
Figure 1.5-8. Plot of normalised double integral vs. time for all four verdazyl initiators demonstrating the reversible nature of the cleavage of the C-N bond using EPR	126
Figure 1.5-9. Plot of normalise double integral vs. time for the EPR decomposition study of 13 at polymerisation temperature.....	127

Figure 1.5-10. Plot of normalised double integral vs. time for the EPR study of the decomposition of 8 at polymerisation temperature	129
Figure 1.5-11. EPR traces from the polymerisation of styrene by 13.....	130
Figure 1.5-12. First order kinetic plot for the verdazyl mediated polymerisation of styrene using 13	131
Figure 2.1-1. Mussels in their natural environment ¹	205
Figure 2.1-2. Mussel with the byssus used to adhere to a rock ⁴	206
Figure 2.1-3. Time lapse photography showing the mussel foot (left) and the rubber plunger model (right) for the five steps of thread formation ³	207
Figure 2.1-4. Schematic of the mussel adhesive plaque and the approximate location of the mussel foot proteins and their DOPA content	208
Figure 2.1-5. A) Schematic of the DOPA functionalised AFM tip and the force-distance curves for the single molecule interaction of DOPA with a titanium surface; B) Schematic of the oxidised DOPA functionalised AFM tip and force-distance curves for the single molecule interaction of dopaquinone with an organic surface ¹³	210
Figure 2.1-6. Modification of surfaces by DOPA by ‘grafting from’ or ‘grafting to’ approaches.....	214
Figure 2.1-7. UV-vis spectra of Cu(II)Br ₂ (red) and Cu(I)Br (green) in (a) DMSO and (b) DMSO and Me ₆ Tren ³⁹	218
Figure 2.1-8. The Stribeck curve.....	221
Figure 2.1-9. Schematic of hydrodynamic, mixed and boundary lubrication regimes	221
Figure 2.1-10. Schematic of the use of chemical modification to reduce friction by the adsorption of molecules onto a surface	223
Figure 2.1-11. High frequency reciprocating rig	224

Figure 2.1-12. Mini traction machine	224
Figure 2.1-13. Schematic of the HFRR system	225
Figure 2.1-14. Schematic of the MTM system	226
Figure 2.2-1. ^1H NMR spectra of unprotected dopamine initiator (top), protected dopamine initiator (middle) and deprotected dopamine initiator (bottom) in deuterated methanol	231
Figure 2.3-1. First order kinetic plot for the Cu(I) mediated polymerisation of MMA using the unprotected dopamine initiator (■) and protected dopamine initiator (■)	233
Figure 2.3-2. Evolution of molecular weight (M_n) and PDI versus conversion for the Cu(I) mediated polymerisation of MMA using the unprotected dopamine initiator (■) and protected dopamine initiator (■), DP = 100, target M_n = 10,000 g/mol (- - -)	233
Figure 2.3-3. ^1H NMR of precipitated polymers from the Cu(I) mediated polymerisation of MMA by the unprotected dopamine initiator (top) and protected dopamine initiator (bottom) in deuterated chloroform.....	235
Figure 2.3-4. UV-vis GPC traces for the protected dopamine initiator at a retention time of 18.36 mins (—) and for PMMA synthesised using the protected dopamine initiator at 12.89 mins (—).....	236
Figure 2.3-5. First order kinetic plot for the Cu(0) mediated polymerisation of <i>t</i> -butyl acrylate using the unprotected dopamine initiator (■, DP = 200) and protected dopamine initiator (■, DP = 160).....	238
Figure 2.3-6. Evolution of molecular weight (M_n) and PDI versus conversion for the Cu(0) mediated polymerisation of <i>t</i> -butyl acrylate using the unprotected dopamine initiator (■) and protected dopamine initiator (■), DP = 200, target M_n = 25,600 g/mol (- - -), DP = 160, target M_n = 20,500 g/mol (- - -)	238
Figure 2.3-7. Cu(0) mediated polymerisation of <i>t</i> -butyl acrylate by the unprotected dopamine initiator (left) and protected dopamine initiator (right).....	239

Figure 2.3-8. First order kinetic plot for the Cu(0) mediated polymerisation of <i>t</i> -butyl acrylate using the unprotected dopamine initiator (■) and protected dopamine initiator (■).....	241
Figure 2.3-9. Evolution of molecular weight (M_n) and PDI versus conversion for the Cu(0) mediated polymerisation of <i>t</i> -butyl acrylate using the unprotected dopamine initiator (■) and protected dopamine initiator (■), DP = 39, target M_n = 5,000 g/mol (- - -).....	242
Figure 2.3-10. ^1H NMR of precipitated polymers from the Cu(0) mediated polymerisation of <i>t</i> -butyl acrylate using the unprotected dopamine initiator (top) and protected dopamine initiator (bottom) in deuterated methanol.....	243
Figure 2.3-11. UV-vis GPC traces for the protected dopamine initiator at a retention time of 18.36 mins (—) and for PBuA synthesised using the protected dopamine initiator at 14.77 mins (—).....	244
Figure 2.3-12. ^1H NMR of the precipitated polymer from the Cu(0) mediated polymerisation of <i>t</i> -butyl acrylate using the protected dopamine initiator (top) and after deprotection (bottom) in deuterated methanol.....	245
Figure 2.4-1. First order kinetic plot for the polymerisation of lauryl methacrylate by EBiB using Cu(I)Cl.....	248
Figure 2.4-2. Evolution of molecular weight (M_n) and PDI versus conversion for the polymerisation of lauryl methacrylate by EBiB using Cu(I)Cl, DP = 200, target M_n = 55,300 g/mol (- - -).....	248
Figure 2.4-3. First order kinetic plot for the copolymerisation of lauryl methacrylate and MMA by EBiB using Cu(I)Cl.....	249
Figure 2.4-4. Evolution of molecular weight (M_n) and PDI versus conversion for the copolymerisation of lauryl methacrylate and MMA by EBiB using Cu(I)Cl, target M_n = 20,000 g/mol (- - -).....	250
Figure 2.4-5. First order kinetic plot for the copolymerisation lauryl methacrylate and MMA using the protected dopamine initiator using Cu(I)Cl aiming for 20,000	

g/mol (■), 10,000 g/mol (●), 15,000 g/mol (▲) and 10,000 g/mol at 50% solids (★)	252
Figure 2.4-6. Evolution of molecular weight (M_n) and PDI versus conversion for the copolymerisation of lauryl methacrylate and MMA using the protected dopamine initiator with Cu(I)Cl aiming for 20,000 g/mol (■), 10,000 g/mol (●), 15,000 g/mol (▲) and 10,000 g/mol at 50% solids (★), target $M_n = 20,000$ g/mol (---), target $M_n = 10,000$ g/mol (---), target $M_n = 15,000$ g/mol (---)	252
Figure 2.4-7. First order kinetic plot for the copolymerisation lauryl methacrylate and MMA using EBiB aiming for 20,000 g/mol (■) and the protected dopamine initiator aiming for 10,000 g/mol (●, ▲) with Cu(I)Cl	254
Figure 2.4-8. Evolution of molecular weight (M_n) and PDI versus conversion for the copolymerisation of lauryl methacrylate and MMA using EBiB aiming for 20,000 g/mol (■), and the protected dopamine initiator aiming for 10,000 g/mol (●, ▲) with Cu(I)Cl	254
Figure 2.5-1. Plot of test run on HFRR for the baseline polymer.....	258
Figure 2.5-2. Plot of test run on HFRR for the protected dopamine polymer	258
Figure 2.5-3. Plot of test run on HFRR for the deprotected dopamine polymer	259
Figure 2.5-4. Wear scars for the base line (left), protected dopamine (middle) and deprotected dopamine (right) polymers from HFRR.....	259
Figure 2.5-5. Test pieces from the HFRR tests for the baseline (left), protected dopamine (middle) and deprotected dopamine (right) polymers.....	261
Figure 2.5-6. Test pieces from the MTM tests for the baseline (left), protected dopamine (middle) and deprotected dopamine (right) polymers.....	262
Figure 2.5-7. Overlaid Stribeck curves from the MTM tests for the baseline polymer	262
Figure 2.5-8. Overlaid Stribeck curves from the MTM tests for the protected dopamine polymer.....	263

Figure 2.5-9. Overlaid Stribeck curves from the MTM tests for the deprotected dopamine polymer..... 263

List of Schemes

Scheme 1.1-1. General mechanism for conventional radical polymerisation.....	2
Scheme 1.1-2. A proposed mechanism for ATRP	5
Scheme 1.1-3. Proposed mechanism for RAFT ¹⁵	6
Scheme 1.1-4. Proposed reaction pathway for NMP using a a) bimolecular or b) unimolecular initiating system	7
Scheme 1.1-5. The use of TEMPO as a radical trap for determining the mechanism of initiation in radical polymerisation	8
Scheme 1.1-6. TEMPO alkoxyamine synthesis for unimolecular initiation in NMP.	9
Scheme 1.1-7. Mayo thermal auto-initiation of styrene.....	10
Scheme 1.1-8. Ascorbic acid reduction of TEMPO.....	10
Scheme 1.1-9. Proposed mechanism for hydrogen abstraction from methacrylates during NMP.....	12
Scheme 1.1-10. Kuhn method for the synthesis of verdazyl radicals from formazan	24
Scheme 1.1-11. Neugebauer method for the synthesis of 1,5-dimethyl-6-oxoverdazyl radicals	24
Scheme 1.1-12. Milcent method for the synthesis of 1,5-diaryl substituted verdazyls ⁵⁴	25
Scheme 1.1-13. Pare method for the synthesis of 1,5-diisopropyl substituted oxoverdazyls ⁵⁴	26
Scheme 1.1-14. Disproportionation reaction of 1,5-dimethyl-6-oxoverdazyls ⁵⁴	27
Scheme 1.1-15. Synthesis of unimolecular initiator from the coupling product of AIBN and triphenylverdazyl.....	32

Scheme 1.1-16. Mechanism of leuco-verdazyl formation from the polymerisation of MMA by (i)	33
Scheme 1.1-17. Exchange reaction for the synthesis of verdazyl unimolecular initiators	36
Scheme 1.1-18. ATRA reaction for the synthesis of verdazyl unimolecular initiators	36
Scheme 1.2-1. General synthesis of 1,5-dimethyl-6-oxoverdazyl radicals.....	42
Scheme 1.2-2. Barr method for the synthesis of 2,4-dimethylcarbonohydrazide (1)	43
Scheme 1.2-3. Plater method for the synthesis of 2,4-dimethylcarbonohydrazide (1)	43
Scheme 1.2-4. Synthesis of 1,5-dimethyl-3-R-tetrazinan-6-one.....	44
Scheme 1.2-5. Synthesis of 1,5-dimethyl-3-R-6-oxoverdazyl.....	46
Scheme 1.3-1. Synthesis of 2-phenyl-2-(2,2,6,6-tetramethylpiperidin-1-oxy)ethyl benzoate.....	63
Scheme 1.3-2. Exchange reaction for the synthesis of 2-phenyl-2-(1,5-dimethyl-3-phenyl-6-oxoverdazyl)ethyl benzoate (13)	64
Scheme 1.3-3. Atom transfer radical addition reaction for the synthesis of 2-phenyl-2-(1,5-dimethyl-6-oxoverdazyl)ethyl benzoate (16).....	71
Scheme 1.3-4. Synthesis of 2-bromo-2-phenylethyl benzoate (15).....	71
Scheme 1.5-1. Expected bond cleavage on heating polymers synthesised using 13 (R = Ph).....	116
Scheme 1.5-2. Controlled radical mechanism for the polymerisation of styrene by 13	119
Scheme 1.5-3. Expected initiator cleavage mechanism at polymerisation temperature	127
Scheme 2.1-1. Oxidation of DOPA to dopaquinone.....	209

Scheme 2.1-2. Oxidation and reduction of DOPA in mfp-3 by thiols present in mfp-6 ¹⁴	211
Scheme 2.1-3. Proposed mechanism of mussel adhesion and crosslinking based on by the formation of an Fe(DOPA) ₃ complex ¹⁷	212
Scheme 2.1-4. A proposed mechanism for ATRP	215
Scheme 2.1-5. Proposed mechanism for SET-LRP	216
Scheme 2.1-6. Proposed route to the propagating radical by the outer sphere electron transfer.....	217
Scheme 2.2-1. Synthesis of 2-bromo- <i>N</i> -[2-(3,4-dihydroxyphenyl)ethyl] propionamide.....	227
Scheme 2.2-2. Soloshonok and Ueki method for the acetonide protection of 2-bromo- <i>N</i> -[2-(3,4-dihydroxyphenyl)ethyl] propionamide	228
Scheme 2.2-3. Messersmith method for the acetonide protection of 2-bromo- <i>N</i> -[2-(3,4-dihydroxyphenyl)ethyl] propionamide.....	229
Scheme 2.2-4. Deprotection of 2-bromo- <i>N</i> -[2-(3,4-dihydroxyphenyl)ethyl] propionamide acetonide	230

List of Tables

Table 1.1-1. Nitrogen hyperfine couplings and calculated spin densities for both type I and type II verdazyls ⁵⁴	29
Table 1.1-2. Final results from the polymerisation of MMA with initiators (i) – (iii) ⁵⁰	33
Table 1.1-3. Results for the polymerisation of styrene by verdazyl unimolecular initiators	38
Table 1.1-4. Results for the polymerisation of <i>n</i> -butyl acrylate using verdazyl unimolecular initiators	39
Table 1.2-1. Hyperfine coupling constants and g-factor values for verdazyl radicals 7-11 at room temperature in toluene	57
Table 1.2-2. Mulliken spin populations for verdazyl radicals 7-11	60
Table 1.2-3. Mulliken spin populations for 1,5-diphenyl-6-oxoverdazyl and 1,5-dimethyl-3-nitro-6-oxoverdazyl	62
Table 1.3-1. Approximate concentrations of 1,5-dimethyl-3-phenyl-6-oxoverdazyl (8) and TEMPO at selected time intervals during the exchange reaction.....	67
Table 1.3-2. Concentrations of 1,5-dimethyl-6-oxoverdazyl (7) at selected time intervals during the ATRA reaction.....	73
Table 1.4-1. Molecular weights and polydispersities for the verdazyl mediated polymerisation of MMA before and after precipitation.....	103
Table 1.4-2. Molecular weights and polydispersities for the verdazyl mediated copolymerisation of MMA and styrene before and after precipitation.....	108
Table 1.7-1. Quantities of sample for the EPR of verdazyl radicals.....	147
Table 1.7-2. Final polymerisation data for the polymerisation of styrene with 0, 25 and 50% toluene using 13 (R = Ph)	159

Table 1.7-3. Final polymerisation data for the verdazyl mediated polymerisation of styrene	160
Table 1.7-4. Final polymerisation data for the verdazyl mediated polymerisation of <i>n</i> -butyl acrylate by 13 (R = Ph) at different volumes.....	162
Table 1.7-5. Final polymerisation data for the verdazyl mediated polymerisation of <i>n</i> -butyl acrylate.....	163
Table 1.7-6. Final polymerisation data for the verdazyl mediated polymerisation of <i>n</i> -butyl acrylate by 17 (R = PhOMe) at different temperatures	164
Table 1.7-7. Final polymerisation data for the verdazyl mediated polymerisation of styrene by 13 (R = Ph) and 17 (R = PhOMe) at 100 °C.....	165
Table 1.7-8. Final polymerisation data for the verdazyl mediated polymerisation of MMA.....	166
Table 1.7-9. Final polymerisation data for the verdazyl mediated copolymerisation of verdazyl stabilised styrene and MMA	168
Table 1.7-10. Final polymerisation data for the verdazyl mediated copolymerisation of styrene and MMA by 13 (R = Ph)	169
Table 1.7-11. Quantities of 8 (R = H) for calibration of high temperature cavity..	170
Table 1.7-12. Sample preparation of verdazyl initiators for high temperature EPR analysis.....	172
Table 1.8-1. Crystal data for 1,5-dimethyl-tetrazinan-6-one	174
Table 1.8-2. Crystal data for 1,5-dimethyl-3-phenyl-tetrazinan-6-one.....	180
Table 1.8-3. Crystal data for 2-phenyl-2-(1,5-dimethyl-3-phenyl-6-oxoverdazyl)ethyl benzoate	187
Table 2.3-1. Effect of initiator on the species formed in solution with Cu(0), Cu(I)Br and Cu(II)Br ₂	240

Table 2.4-1. Final polymerisation data for the scale up polymerisations for mechanical testing.....	255
Table 2.5-1. Polymer blend formulation.....	257
Table 2.5-2. Average friction coefficients for the baseline, protected dopamine and deprotected dopamine polymers recorded using HFRR.....	260
Table 2.7-1. Final polymerisation data for the Cu(I) mediated polymerisation of MMA using the unprotected/protected dopamine initiators.....	274
Table 2.7-2. Reagent quantities for the Cu(0) mediated polymerisation of <i>t</i> -butyl acrylate using the unprotected/protected dopamine initiators.....	275
Table 2.7-3. Final polymerisation data for the Cu(0) mediated polymerisation of <i>t</i> -butyl acrylate using the unprotected/protected dopamine initiators.....	275
Table 2.7-4. Reagent quantities for the Cu(I)Cl mediated copolymerisation of lauryl methacrylate and MMA using the unprotected dopamine initiator.....	278
Table 2.7-5. Final polymerisation data for the Cu(I)Cl mediated copolymerisation of lauryl methacrylate and MMA using the unprotected dopamine initiator.....	279

List of abbreviations

AFM	Atomic force microscopy
AIBN	2,2'-azobisisobutyronitrile
ATRA	Atom transfer radical addition
ATRP	Atom transfer radical polymerisation
AVN	2,2'-azobis-2,4-di-methylvaleronitrile
Boc	<i>t</i> -Butoxycarbonyl
BPO	Benzoyl peroxide
CRP	Controlled radical polymerisation
CTA	Chain transfer agent
DCC	<i>N,N'</i> dicyclohexylcarbodiimide
DCM	Dichloromethane
DMAP	4-(dimethylamino)pyridine
DMF	Dimethylformamide
DMSO	Dimethylsulfoxide
DOPA	3,4-dihydroxyphenyl-L-alanine
DP	Number average degree of polymerisation
DPAIO	2,2-diphenyl-3phenylimino-2,3-dihydroindol-1-yloxy
DPPH	2,2-diphenyl-1-picrylhydrazyl
DRI	Differential refractive index
EBiB	Ethyl 2-bromoisobutyrate
ENDOR	Electron nuclear double resonance
EPR	Electron paramagnetic resonance

ESR	Electron spin resonance
EtOH	Ethanol
<i>g</i>	<i>g</i> -factor (EPR)/ grams
G	Gauss
GPC	Gel permeation chromatography
h	Hour(s)
HCl	Hydrochloric acid
HFRR	High frequency reciprocating rig
IPA	Isopropyl alcohol, propan-2-ol
IR	Infra red
K	Activation-deactivation equilibrium rate constant
k_d	Rate constant of dissociation/dissociation constant
k_p	Rate constant of propagation
k_{tc}	Rate constant of combination
k_{td}	Rate constant of disproportionation
KV	Kinematic viscosity
LMA	Lauryl methacrylate
LRP	Living radical polymerisation
[M]	Concentration of monomer at $t = t$
[M] ₀	Concentration of monomer at $t = 0$
MAIB	Methyl 2,2'-azobisbutylrate
Me ₆ Tren	<i>N,N,N',N',N'',N''</i> -hexamethyl-tris[2-(dimethylamino)ethyl]amine
MeOH	Methanol
mfp	Mussel foot protein

min(s)	Minute(s)
MMA	Methyl methacrylate
M_n	Number average molecular weight
MTM	Mini traction machine
M_w	Weight average molecular weight
N	Normal/Newton
nBA	n-Butyl acrylate
NMP	Nitroxide mediated polymerisation
NMR	Nuclear magnetic resonance
NOE	Nuclear Overhauser effect
PDi	Polydispersity
PMDETA	<i>N,N,N',N'',N'''</i> -pentamethyldiethylenetriamine
PRE	Persistent radical effect
RAFT	Reversible addition fragmentation chain transfer
SET-LRP	Single electron transfer living radical polymerisation
SFRP	Stable free radical polymerisation
SG1	<i>N</i> -(2-methylpropyl)- <i>N</i> -(1-diethylphosphono-2-dimethylpropyl)- <i>N</i> -oxyl
<i>t</i>	Tertiary
t	Time
TEMPO	2,2,6,6-tetramethylpiperdinyloxy
TFA	Trifluoroacetic acid
THF	Tetrahydrofuran
TIPNO	2,2,5-tri-methyl-4-phenyl-3-azahexane-3-nitroxide

TLC	Thin layer chromatography
UV-vis	Ultra violet - visible

Acknowledgements

First and foremost I would like to thank Professor Dave Haddleton. I would like to thank him for giving me the opportunity to work in his group and for his continuous encouragement. Thanks to Dave I have gained another qualification from Warwick, met some amazing people, travelled the world a little bit and have become a much more well rounded, confident and happy person. I never intended to do a PhD, but now consider it to be one of the best decisions I ever made.

I would also like to thank the University of Warwick and Lubrizol Ltd. for providing the funding that allowed me to conduct my research. I would also like to thank my contacts at Lubrizol; Tim Smith, David Price and Will Barton. I would also like to thank David Moreton for organising all the contacts meetings which undoubtedly kept me organised.

There are also many people here at Warwick and at Lubrizol that have helped me obtain data presented in this thesis. Thanks to Dr. Adam Clarke, Dr. Ivan Prokes, Dr. Guy Clarkson, Prof. Rob Deeth, Dr. Mark Newton, Chris Hartland, Dr. Radek Kowalczyk, Dr. Tim Smith, John Durham and Zahra Hussain.

A very big thank you goes to everyone in the Haddleton group past and present, it has been a pleasure working with you. I would especially like to thank Dr. Beppe

Mantovani and Dr. Chris Fidge for all their help when I first joined the group, my conference buddy Kay and everyone in office C210 with whom I have enjoyed many entertaining conversations.

I would like to thank all my family, and in particular my mum and dad who have always been there for me and supported me in everything I have decided to do. I would also like to thank Ant's family for all their help and for making me feel like part of their family, especially as I am so far away from mine.

Finally I would like to thank Ant. Without him writing up would have taken much longer. Thanks for staying up late with me, making me laugh and for all the cooking and washing up you did even though you protested occasionally, I really appreciated it all.

Declaration

Experimental work contained within this thesis is original research carried out by the author, unless otherwise stated, in the Department of Chemistry at the University of Warwick, between October 2008 and October 2011. No material contained herein has been submitted for any other degree, or at any other institution.

Results from other authors are referenced in the usual manner throughout the text.

Signed: _____

Georgina Rayner

Date:

Abstract

Verdazyl Radicals as Mediators in Living Radical Polymerisation

The aim of this work was to investigate verdazyl radicals as an alternative to nitroxides as mediators in stable free radical polymerisation. Verdazyl radicals and their unimolecular initiators were synthesised and utilised in the polymerisation of styrene and *n*-butyl acrylate. Varying degrees of success was observed in the polymerisations depending on the structure of the verdazyl radical. The polymerisation of methyl methacrylate and the copolymerisation of styrene and methyl methacrylate were also investigated. Correlations between observed molecular weight and theoretical molecular weight were poor but may be improved by optimisation of the reaction conditions. Electron paramagnetic resonance was used to elucidate the radical structure as well as to confirm the living nature of the polymerisation technique. Electron paramagnetic resonance was also utilised to provide an insight into radical stability and reactivity in the various reactions undertaken.

Dopamine End-Functionalised Polymers for Application as Friction Modifiers

The aim of this work was to synthesise oil soluble dopamine end-functionalised polymers for mechanical testing to determine if the polymers can reduce friction by film formation at a surface. A dopamine based initiator was synthesised and used in

Cu(I) and Cu(0) mediated polymerisations with little success and the dopamine catecholic end-group could not be identified as the polymer end-group. To enable a successful living polymerisation, the catechol groups on dopamine required protection. Complete deprotection of the catechol group can be achieved post polymerisation. The polymerisation of lauryl methacrylate was achieved using a polymerisation method designed for the long chain, non-polar molecule which utilised Cu(I)Cl. The polymerisations were scaled up to obtain a baseline, protected dopamine and deprotected dopamine polymers for mechanical testing. A reduction in friction and wear observed for the deprotected dopamine polymer, however, corrosion was also observed and may have affected the results.

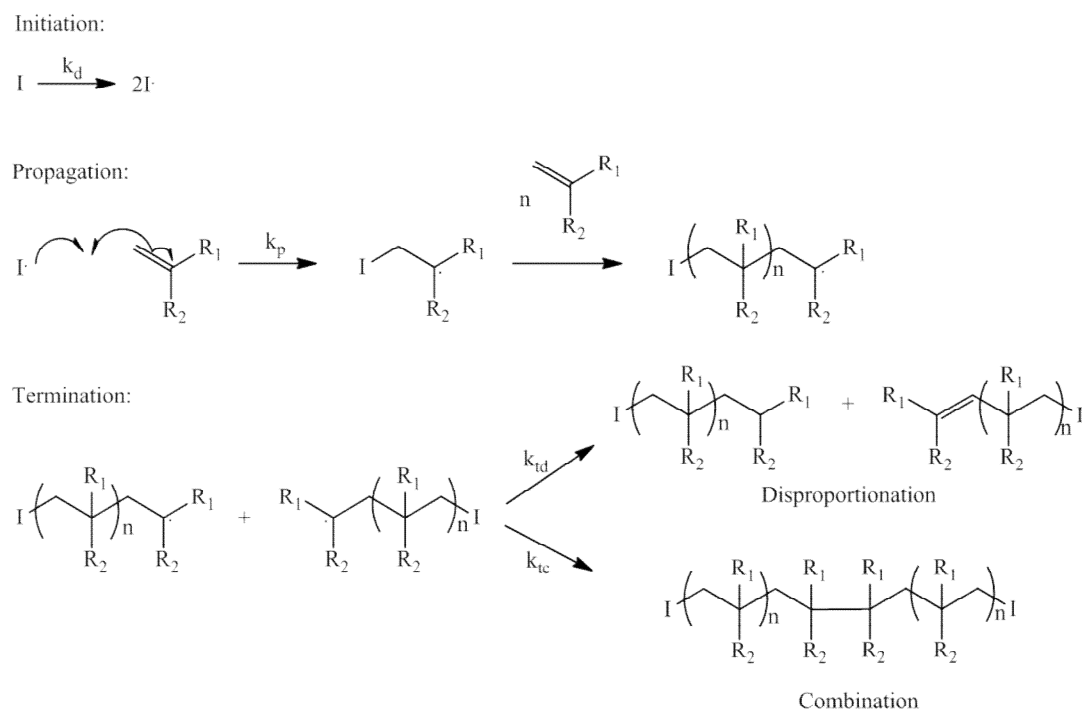
1. Verdazyl Radicals as Mediators in Living Radical Polymerisation

1.1. Introduction

1.1.1. The development of living radical polymerisation

1.1.1.1. Conventional radical polymerisation

The three main steps in a conventional radical polymerisation are initiation, propagation and termination (Scheme 1.1-1). Initiation begins with the generation of radicals either thermally, photolytically or via a redox reaction from a free radical initiator such as 2,2'-azobisisobutyronitrile (AIBN) or benzoyl peroxide (BPO), Figure 1.1-1. Propagation continues until all the monomer has been consumed or termination occurs. Chain termination can be divided into two different mechanisms: coupling and disproportionation. In termination by coupling, two chains meet and combine to give a chain with an increased molecular weight. Termination by disproportionation occurs by the transfer of a hydrogen atom from one chain to another resulting in one saturated and one unsaturated chain end. Chain transfer to solvent, monomer, initiator or polymer can also occur through the abstraction of a hydrogen atom. Although a new radical is formed, often it cannot undergo further propagation.



Scheme 1.1-1. General mechanism for conventional radical polymerisation

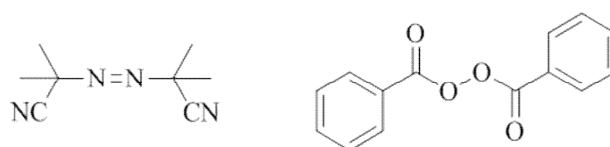


Figure 1.1-1. 2,2'-Azobisisobutyronitrile (AIBN, left) or benzoyl peroxide (BPO, right)

Conventional radical polymerisations are tolerant to various reaction conditions, temperatures, impurities and solvents, including water, enabling suspension and emulsion polymerisations to be undertaken.¹ However, polymers of well defined molecular weight or structure are unobtainable due to a high level of termination reactions and as a result led to the development of living radical polymerisation.

1.1.1.2. Living polymerisation

The use of strongly nucleophilic anions to mediate vinyl addition polymerisation reported by Szwarc²⁻⁴ was the start of the development of living polymerisation. The use of anions instead of an unpaired electron removed termination reactions due to repulsion of like charges. As the field of anionic polymerisation developed, Quirk and Lee⁵ established a set of criteria to define a living polymerisation. A polymerisation is defined as living if: i) the polymerisation proceeds until all the monomer is consumed and will continue to grow if more monomer is added; ii) a linear increase in molecular weight with conversion is observed; iii) the concentration of active species remains constant so that a plot of $\ln([M]_0/[M])$ versus time is linear; iv) a narrow polydispersity (PDI) or molecular weight distribution; v) sequential monomer addition results in the formation of block copolymers and vi) the polymer end-groups retain their functionality. A polymerisation is only deemed to be living if all the aforementioned criteria are met.

1.1.1.3. Living radical polymerisation

Living radical polymerisation (LRP) reintroduces a free radical into the polymerisation system, and as a result, requires a method to ideally prevent completely termination reactions occurring. The addition of a mediating agent in living radical polymerisations serves to reversibly activate and deactivate the propagating radical, thus controlling the concentration of radicals in solution. Keeping the concentration of propagating radicals low forces propagation and helps to reduce termination reactions to a minimum. It is often preferred to use the term

controlled when describing these systems, however, the term living can still be applied as termination reactions have been reduced to a minimum and as such the system meets most of the requirements described in Section 1.1.1.2. The term living has been preferentially used throughout this body of work.

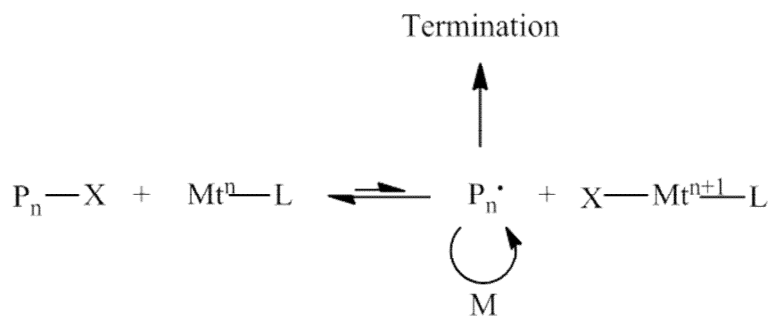
Over the last few decades three main systems for LRP have been developed: stable free radical polymerisation (SFPR), atom transfer radical polymerisation (ATRP) and reversible addition-fragmentation chain transfer (RAFT) polymerisation. ATRP and RAFT will be introduced briefly in the following section. A more detailed discussion of SFPR is included at the end of the following section as it forms the basis of the technique used in this work.

1.1.2. Living radical polymerisation techniques

1.1.2.1. Atom transfer radical polymerisation

ATRP was developed independently by Sawamoto⁶ and Matyjaszewski⁷ in 1995. Developed from the Karasch⁸ and the atom transfer radical addition (ATRA) reaction⁹, ATRP utilises the radical addition of a halogen atom across a double bond. The technique uses a transition metal-ligand complex as the mediating species. The transfer of a halogen atom to and from the propagating radical to the transition metal complex results in the oxidation and reduction of the metal as it

activates and deactivates the propagating chain. Scheme 1.1-2 outlines a proposed mechanism for ATRP.



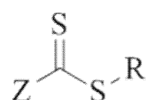
Scheme 1.1-2. A proposed mechanism for ATRP

Since its discovery a variety of metals have been investigated including copper, ruthenium, nickel and iron, although copper is the most widely used.¹⁰ Initiators are typically alkyl halides and nitrogen based ligands are used.¹¹ A variety of monomers can be polymerised using ATRP including styrenes, acrylates, methacrylates and acrylamides.¹¹

1.1.2.2. Reversible addition- fragmentation chain transfer

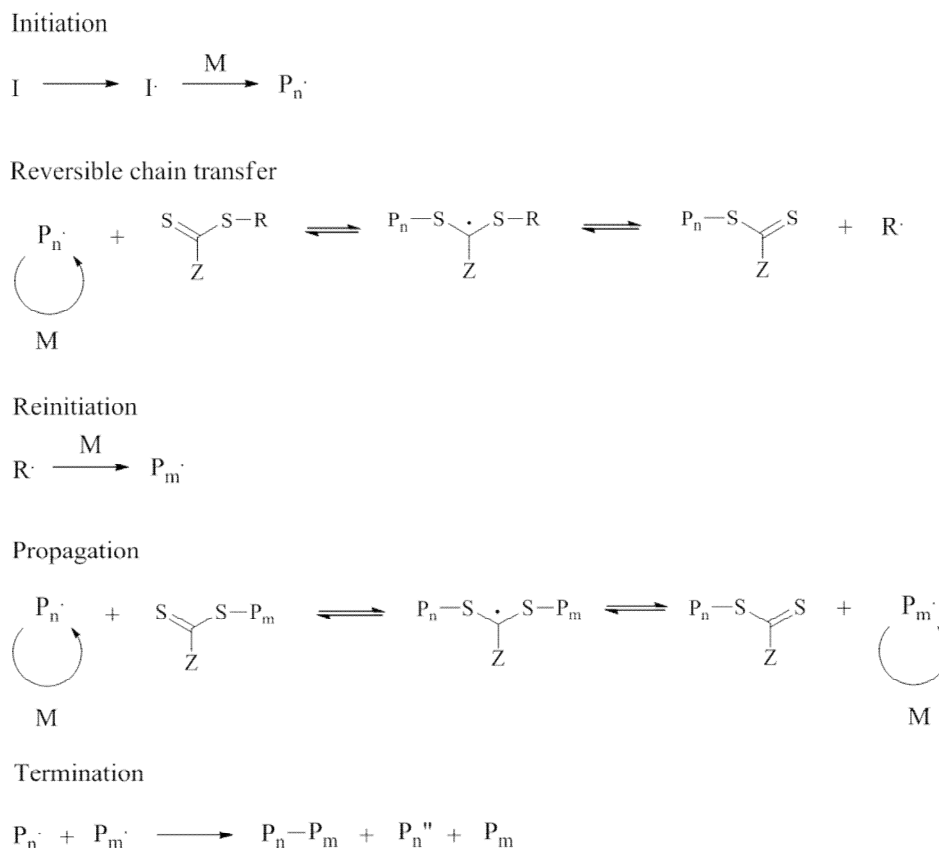
RAFT was first reported in the 1980s, although at the time, only macromonomers were used and high polydispersities were observed.^{12, 13} The technique has since continued to develop and uses reversible chain transfer agents (CTAs) (Figure 1.1-2), which when applied to a polymerisation system act as mediators.¹⁴ The proposed mechanism for a RAFT polymerisation is shown in Scheme 1.1-3. A conventional

initiator is used to form active radicals which react with the monomer to form propagating chains. A radical can then be transferred from the propagating chain to the CTA expelling another radical group which initiates a second propagating chain. This process repeats throughout the reaction. Monomers that can be polymerised by RAFT include styrenes, acrylates, methacrylates and vinyl acetate.¹⁵



R = leaving group
Z = activating group

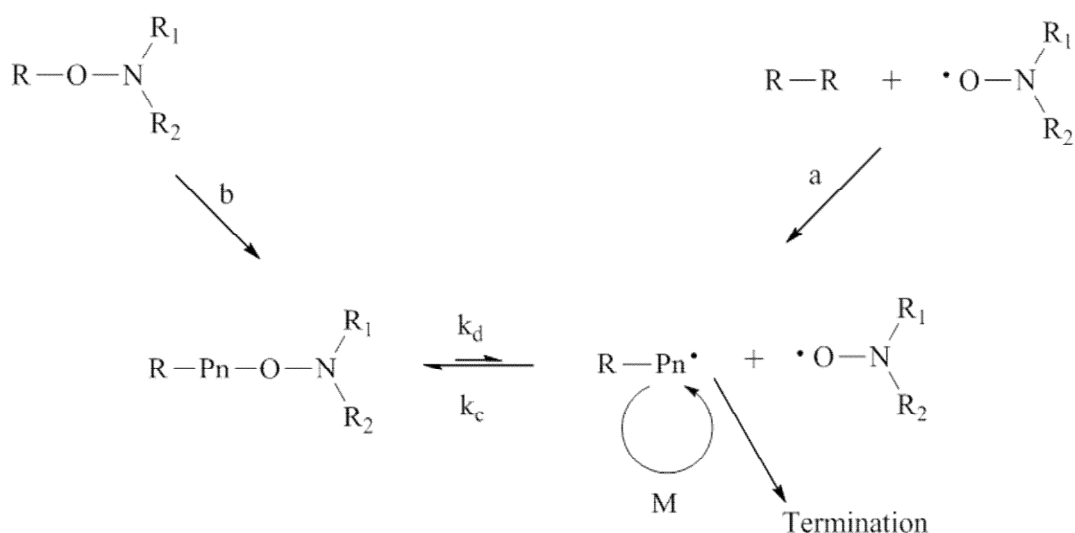
Figure 1.1-2. General structure of chain transfer agents used in RAFT



Scheme 1.1-3. Proposed mechanism for RAFT¹⁵

1.1.2.3. Stable free radical polymerisation

SFRP was the earliest living radical technique to be discovered and uses stable free radicals as mediators in the polymerisation. The most widely studied family of stable radicals for SFRP are the nitroxides and the technique is often referred to as nitroxide mediated polymerisation (NMP). NMP offers an advantage over other LRP techniques as there is no contamination of the polymer by metals, halides or sulfur as it is governed by thermal activation thereby the addition of a catalyst is not required and only a simple precipitation is required to remove unreacted monomer.

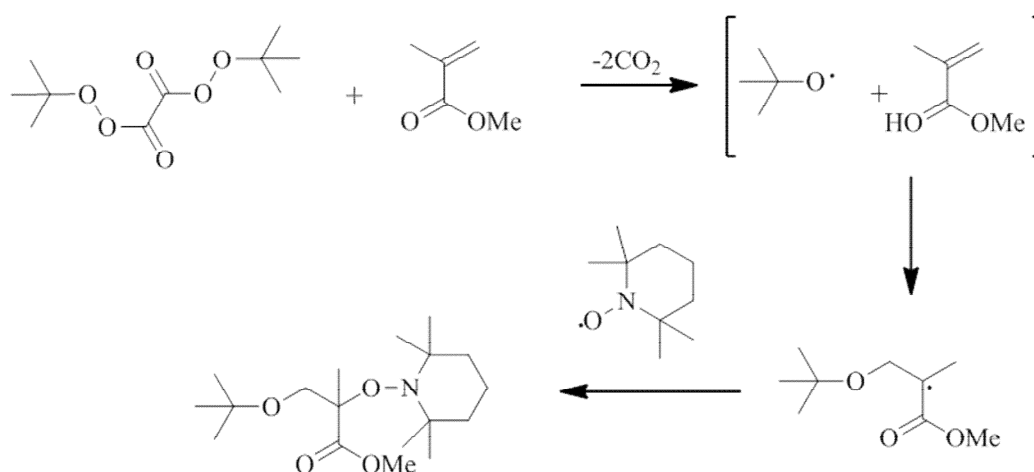


Scheme 1.1-4. Proposed reaction pathway for NMP using a) bimolecular or b) unimolecular initiating system

In a general NMP system an initiator undergoes homolytic bond cleavage to form an active radical and a mediating radical (Scheme 1.1-4). The active/nucleophilic radicals initiate polymerisation. The coupling of the mediating radical with the

active radical, which has now become a propagating chain, produces a dormant species. The propagating chain and dormant chain are in equilibrium. The mediating radical is often referred to as the persistent radical and the prevention of bimolecular termination by the radical is known as the persistent radical effect (PRE).¹⁶⁻²⁰

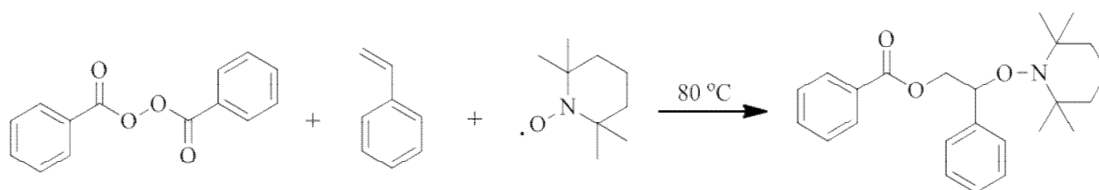
The development of nitroxides for SFRP stems from radical trapping experiments conducted by Rizzardo, Solomon and Moad.^{21, 22} In these experiments 2,2,6,6-tetramethylpiperdinyloxy (TEMPO) was found to react with a carbon centred free radical formed during the initiation stages of a polymerisation (Scheme 1.1-5). The resulting alkoxyamine derivatives were stable at the reaction temperatures (40-60 °C) and did not participate in further reactions.



Scheme 1.1-5. The use of TEMPO as a radical trap for determining the mechanism of initiation in radical polymerisation

Georges *et al.*²³ prepared high molecular weight polystyrene of narrow polydispersity in bulk using a molar ratio of benzoyl peroxide to TEMPO of 1.3:1 at an increased temperature of 130 °C. At higher temperatures the C-ON bond becomes unstable releasing the nitroxide radical to act as a mediator for the polymerisation.

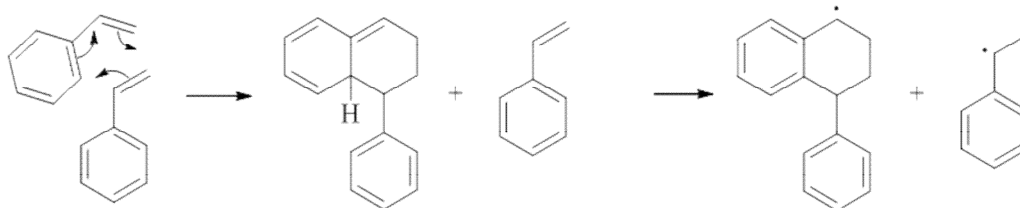
This work demonstrates the use of a bimolecular initiating system where an alkoxyamine is formed *in situ*. However, the yield of alkoxyamine is not quantitative with respect to the amount of benzoyl peroxide added due to side reactions in the alkoxyamine synthesis.¹⁰ The efficiency factor of a radical initiator such as AIBN <1, whereas with an alkoxyamine the value is ~1. This poorly defined initiating system led to the development of unimolecular initiating systems^{24, 25} where an alkoxyamine is synthesised separately and then used to initiate a polymerisation (Scheme 1.1-6).



Scheme 1.1-6. TEMPO alkoxyamine synthesis for unimolecular initiation in NMP

NMP with TEMPO is generally limited to styrenes and requires high temperatures (125-145 °C) and long reaction times (24-72 hours).²⁶ The polymerisation of acrylates proceeds only to low conversions before stopping without the use of

additives.²⁷ Random copolymers of styrene with either n-butyl acrylate (nBA) or methyl methacrylate (MMA) have been demonstrated, however over 50% styrene was required.²⁸ The inability of TEMPO to mediate acrylate polymerisations has been shown to be due to irreversible termination reactions, causing the increase in the concentration of TEMPO in solution which shifts the polymerisation equilibrium to the dormant side.²⁷ Styrene possesses an auto-initiation mechanism (Scheme 1.1-7) which generates new radicals that can consume the excess TEMPO²⁹, making the polymerisation of styrene by TEMPO possible.



Scheme 1.1-7. Mayo thermal auto-initiation of styrene

The use of additives, such as ascorbic acid, reduces the concentration of TEMPO in solution by the formation of hydroxylamine (Scheme 1.1-8)³⁰ pushing the equilibrium back towards the propagating species and allows the polymerisation of butyl acrylate with TEMPO to proceed.²⁷



Scheme 1.1-8. Ascorbic acid reduction of TEMPO

The desire to have polymerisation systems that do not require additives has led to the development of a large family of structurally modified nitroxides. The development of nitroxides that bear little resemblance to TEMPO, such as the acyclic nitroxides 2,2,5-tri-methyl-4-phenyl-3-azahexane-3-nitroxide (TIPNO)³¹ and *N*-(2-methylpropyl)-*N*-(1-diethylphosphono-2-dimethylpropyl)-*N*-oxyl (SG1)³² illustrated in Figure 1.1-3, showed a greater improvement as mediating radicals. The nitroxides that possess a hydrogen atom on an α -carbon that is not present in TEMPO display faster living polymerisations with good control over molecular weight and polydispersity at lower temperatures without additives.²⁶ Work published by Nielsen and Braslau³³ detailed a decomposition mechanism that exists for the acyclic nitroxide TIPNO at 120 °C which prevents accumulation of the nitroxide. These new nitroxides increased the range of monomers to acrylates, dienes, acrylic acid and substituted acrylamides.²⁶

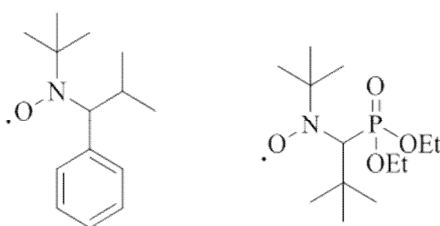
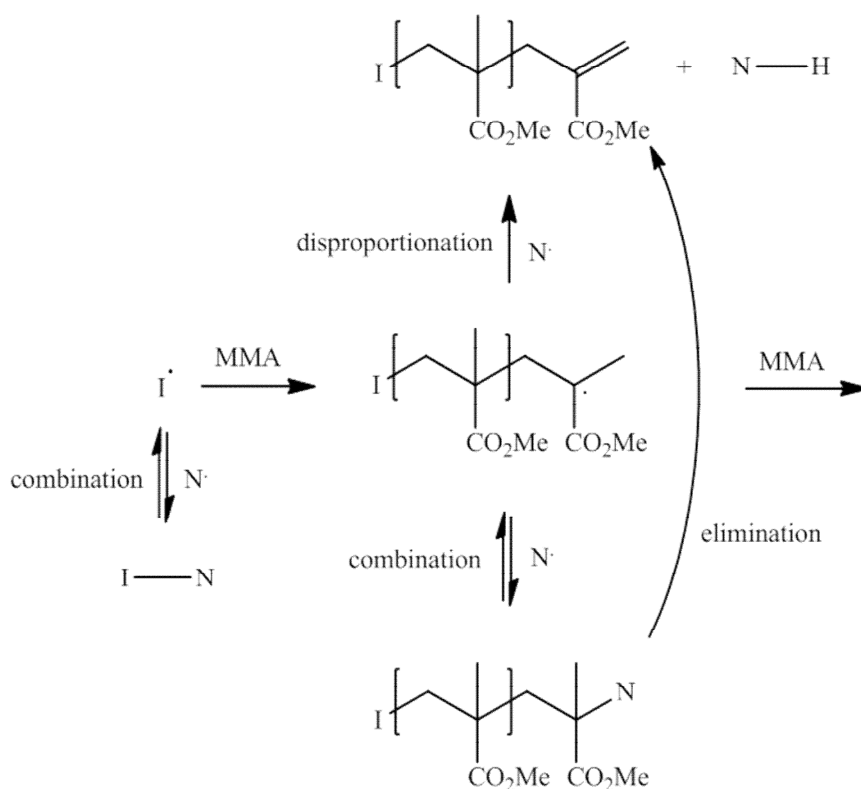


Figure 1.1-3. Structures of TIPNO (left) and SG1 (right)

Despite these successes, the polymerisation of methacrylates by nitroxides is still considered to be difficult. The attempted TEMPO mediated polymerisation of MMA

by Moad *et al.*³⁴ displayed no living character, stopping between 30-40% conversion. The authors attributed these results to the occurrence of a hydrogen abstraction reaction between the propagating chain end and the nitroxide radical to form a saturated chain end and a hydroxylamine. The suggested mechanism of hydrogen abstraction is shown in Scheme 1.1-9.



Scheme 1.1-9. Proposed mechanism for hydrogen abstraction from methacrylates during NMP

With SG1 and TIPNO a large equilibrium constant (K) is seen in the NMP of MMA (Equation 1.1-1).³⁵ The high value of K leads to an increased concentration of propagating chains which leads to an increase in termination reactions. The case of SG1 is further complicated as success depends on $[SG1_0]$. When the concentration is

low, there is no control due to a high value for K . When the concentration is high hydrogen abstraction, as seen with TEMPO, becomes predominant.



Equation 1.1-1.

The addition of a comonomer can be used to lower the value of K if the second monomer has a lower K value, such as styrene. Charleux et al.³⁶ demonstrated a living polymerisation of MMA using BlocBuilder[®], an SG1 based alkoxyamine³⁷, could be obtained by the addition of 4.4-8.8 mol% styrene to the polymerisation. Charleux et al.³⁷ have also demonstrated the nitroxide mediated copolymerisation of MMA under living conditions with the addition of 2.2–8.8 mol% acrylonitrile.

The successful nitroxide mediated homopolymerisation of MMA was reported in 2007 by Guillaneuf et al.³⁸ The authors used an indole based nitroxide, 2,2-diphenyl-3-phenylimino-2,3-dihydroindol-1-yloxyl (DPAIO), Figure 1.1-4. The radical was chosen as it was theorised that delocalisation of the radical onto the phenyl ring would decrease the spin density on the oxygen atom, reducing its ability to undergo hydrogen abstraction reactions.³⁸

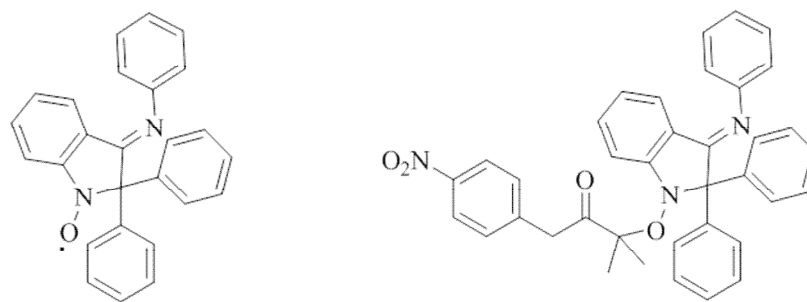


Figure 1.1-4. 2,2-diphenyl-3-phenylimino-2,3-dihydroindol-1-yloxy (DPAIO, left) and DPAIO based alkoxyamine initiator (right)

The decomposition of DPAIO has been investigated to confirm the absence of the hydrogen abstraction reaction.³⁹ However, it was noted that DPAIO may undergo C-ON bond homolysis to give an alkoxy and aminyl radical which may affect the living nature of the polymerisation.³⁹ The polymerisation of MMA was performed at 100 °C using a DPAIO based alkoxyamine (Figure 1.1-4), and proceeded up to 80% conversion with polydispersity values between 1.3 and 1.4. Molecular weights were generally lower than the theoretical and this was attributed to a slower initiation rate and slow decomposition of DPAIO.³⁸

More recently, the NMP of MMA has also been reported using a *N*-phenylalkoxyamine initiator (Figure 1.1-5), achieving a living polymerisation with conversions up to 50% with polydispersity values between 1.12 and 1.30.⁴⁰ The NMP of MMA has also been performed in the presence of sulfuric acid, which acts as an accelerating agent⁴¹, as well as in supercritical CO₂⁴².

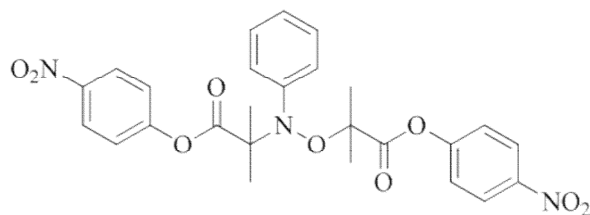


Figure 1.1-5. *N*-phenylalkoxyamine initiator

1.1.2.4. Other stable radicals for SFRP

SFRP has mainly focused on the use of nitroxides, however, the technique is not limited to nitroxides. Other stable radicals include triazoliny⁴³⁻⁴⁶, borinate⁴⁷, (aryloxy)oxyl^{48, 49} and verdazyl radicals⁵⁰⁻⁵³ (Figure 1.1-6). The latter of which is the focus of the first chapter of this thesis and will be discussed further in Sections 1.1.4 and 1.1.5.

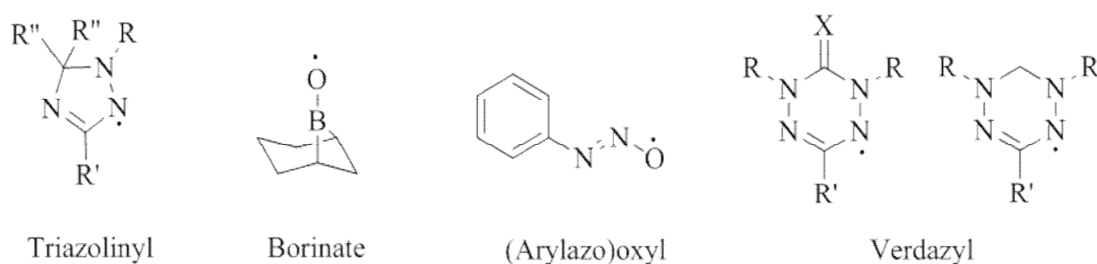


Figure 1.1-6. Alternative stable radicals for use in SFRP

Triazoliny radicals have been used as mediators in the synthesis of homo and block copolymers of styrene and methacrylates. At elevated temperatures triazoliny

radicals decompose which prevents the build up of excess triazolanyl radical. During decomposition a phenyl radical is produced which is capable of initiating further polymerisation reactions leading to a broader PDI than seen when using nitroxides.

Borinate radicals are formed *in situ* from the decomposition of a peroxyborinate. As decomposition yields an alkoxy and borinate radical, peroxyborinates act in the same way as the nitroxide based alkoxyamines. Borinate radicals have been used as mediators in the polymerisation of methacrylates where an increase in M_n with conversion was observed although alongside broad PDI's.

(Arylazo)oxyl radicals are also formed *in situ* by the one electron oxidation of an arenedihyponitrite or cyanate anion with an arenediazonium or by an electron transfer reaction between an activated carbon-halogen compound with an (arenediazo)oxyl anion.⁵⁴ The formation of the (arylazo)oxyl radical also creates an initiating radical. Both the polymerisation of MMA and n-butyl acrylate has been attempted, however similar trends seen in polymerisations using borinate radicals were observed.

1.1.3. Electron paramagnetic resonance

Electron paramagnetic resonance (EPR), or electron spin resonance (ESR) spectroscopy as it is sometimes known, studies the interactions of unpaired electrons with nearby nuclei and has such been an important tool in the characterisation of stable radicals. EPR is a similar technique to the more widely known nuclear magnetic resonance (NMR), although it looks at the interaction of unpaired electrons in a magnetic field rather than nuclei. As this technique has been used throughout this body of work an outline of the method and some experimental considerations are given in the following sections.

1.1.3.1. The theory of EPR

The interaction of an unpaired electron in a magnetic field creates differences in energy, known as the Zeeman effect.⁵⁵ A single unpaired electron has two energy states which lose their degeneracy when a magnetic field is applied. When introduced to a magnetic field, an electron behaves like a bar magnet due to its magnetic moment. When aligned with the magnetic field, a lower energy state is observed. A higher energy state is observed when aligned against the magnetic field (Figure 1.1-7). The lower energy state is denoted $m_s = -1/2$ and the higher energy state $m_s = +1/2$.

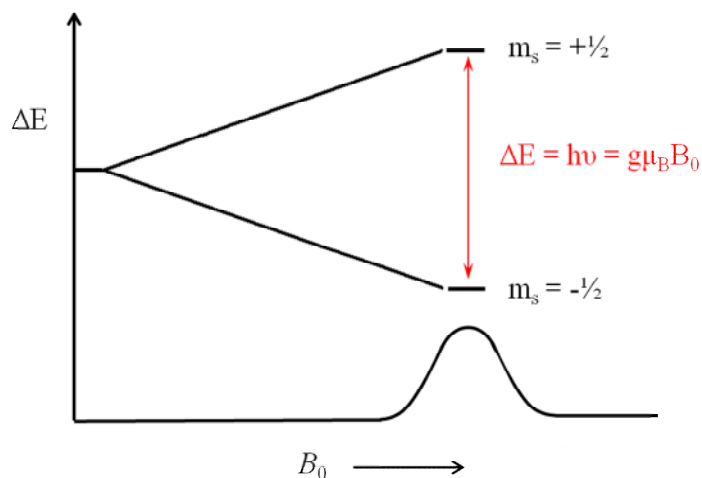


Figure 1.1-7. Energy diagram for a free electron in an applied magnetic field illustrating the Zeeman effect

The energy difference (ΔE) required for a transition between the two states is shown by Equation 1.1-2⁵⁵;

$$\Delta E = g \mu_B B_0 = h\nu$$

Equation 1.1-2

Where g is the electrons g -factor, μ_B is the Bohr magneton (9.2740×10^{-24} J/T), B_0 is the applied magnetic field, h is Plank's constant (6.626×10^{-34} J/s) and ν is the frequency of the electromagnetic radiation.

Two possible approaches exist for obtaining EPR spectra. The most common method involves scanning the magnetic field whilst the frequency of

electromagnetic radiation is held constant, illustrated in Figure 1.1-7. This is called the continuous wave EPR method.⁵⁵ The reverse is also possible. An absorption occurs when the electron moves between the two energy levels and this occurs when ΔE matches the energy of the applied radiation, known as the 'field for resonance'.⁵⁵

Although absorption curves are recorded, continuous wave EPR spectra are reported as the first derivative of the absorption curve. This is the result of applying field modulation with phase sensitive detection, used to improve the signal to noise ratio and enhance the observed signal intensity.⁵⁶ If the applied field modulation is smaller than the line width, the detected signal is proportional to the slope of the absorption curve, shown in Figure 1.1-8 taken from the literature.⁵⁶

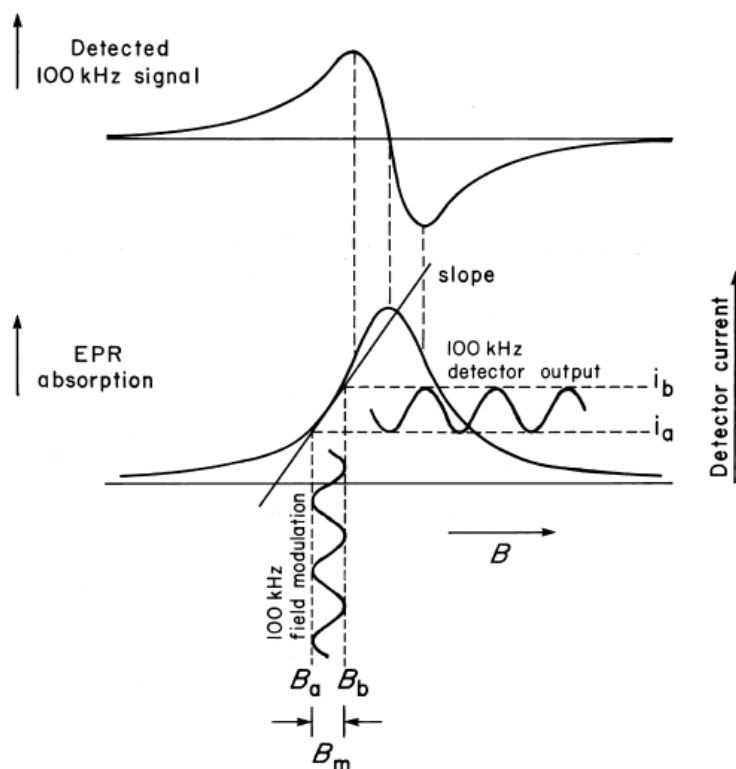


Figure 1.1-8. Effect of field modulation to produce the first derivative of an absorption curve⁵⁶

1.1.3.2. Hyperfine interactions

When an unpaired electron interacts with nearby nuclei with spin (I) > 0 splitting of the EPR signal is observed.⁵⁶ This is called a hyperfine interaction or hyperfine coupling and is analogous in effect to observed J couplings in NMR. As a result, an abundance of structural information is obtained, in particular the identity and number of atoms that interact with the electron.⁵⁵ The number of hyperfine lines in a spectrum is equal to:

$$2nI + 1$$

Equation 1.1-3

Where n is the number of symmetry equivalent nuclei with spin I .⁵⁵ For example, ^{14}N has $I = 1$, so the interaction of the electron with one nitrogen would give three lines, as seen for TEMPO (Figure 1.1-9).

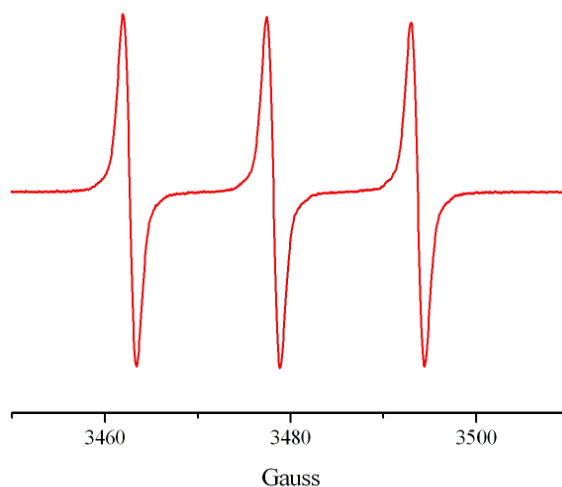


Figure 1.1-9. EPR spectrum of TEMPO

As the number of nuclei which interact with the electron increases, so do the number of signals, resulting in a complex multi-line spectrum. On occasion, broadening of the signal can be seen due to overlap occurring from multiple signals.⁵⁵

1.1.3.3. Sample preparation and experimental considerations

For stable free radicals, solution samples show more hyperfine structure compared to solid samples as shown for 2,2-diphenyl-1-picrylhydrazyl (DPPH) in Figure 1.1-10.^{57, 58} When preparing a sample, concentrations should generally be $< 10^{-3}$ M otherwise line broadening may occur resulting in the loss of some of the smaller hyperfine interactions.^{58, 59}

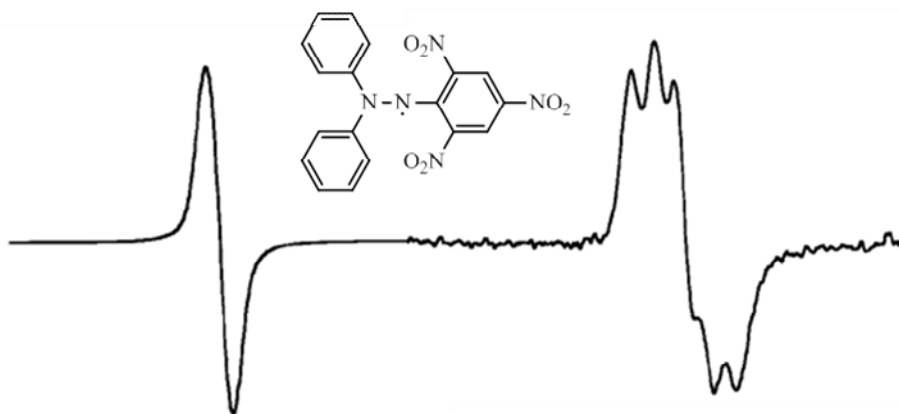


Figure 1.1-10. EPR spectra of polycrystalline DPPH and a 0.6 mM solution of DPPH in toluene⁵⁸

Non-polar solvents are advisable as polar solvents can cause difficulties in tuning the cavity, which is required to obtain a signal, due to interaction with the microwaves.⁵⁷ Samples should also be carefully prepared to ensure the absence of oxygen. Oxygen is paramagnetic and its interaction with the electron will result in line broadening and the loss of hyperfine structure.⁵⁹ Experimental parameters (microwave power, modulation amplitude, frequency, time constant) also need to be carefully chosen to ensure EPR signals do not get distorted.⁵⁵ As EPR spectra are reported as first derivative of the absorption signal, the spectra must be integrated twice to first obtain the absorption spectra and then secondly to calculate the area under the absorption curve. The integrated intensity is proportional to the concentration of radical and as such can be used for quantitative analysis.⁵⁵

1.1.4. Verdazyl radicals

Verdazyl radicals were first discovered by Kuhn and Trischmann in the 1960s.⁶⁰ They are considered stable radicals rather than persistent owing to the fact that they can be isolated.⁶¹ The general structure consists of a six membered ring substituted with four nitrogen atoms as shown in Figure 1.1-11. Verdazyl radicals are classed as either Type I or Type II depending on the nature of the carbon atom at the 6 position. The second class of verdazyl was discovered in the 1980s by Neugebauer and Fischer.⁶²

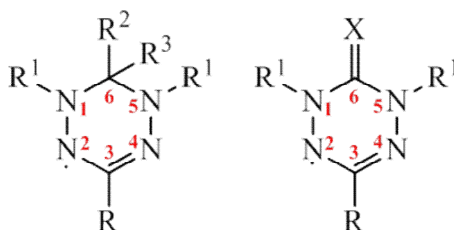


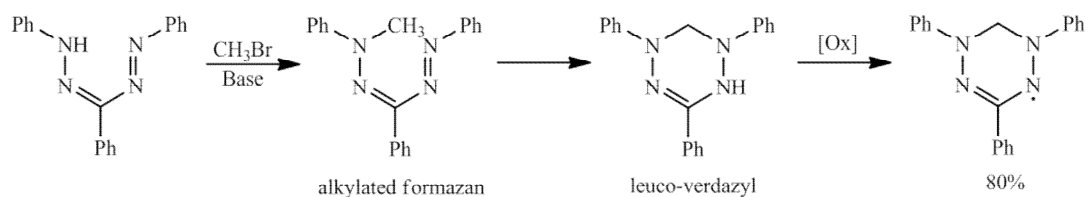
Figure 1.1-11. Type I (left) and Type II (right) verdazyl radicals with atom numbering scheme,

X = O or S

Type I verdazyls have a saturated carbon atom at the 6 position and R¹ is generally aromatic. Type II verdazyls have a carbonyl or thiocarbonyl group at the 6 position and R¹ can be alkyl or aryl.

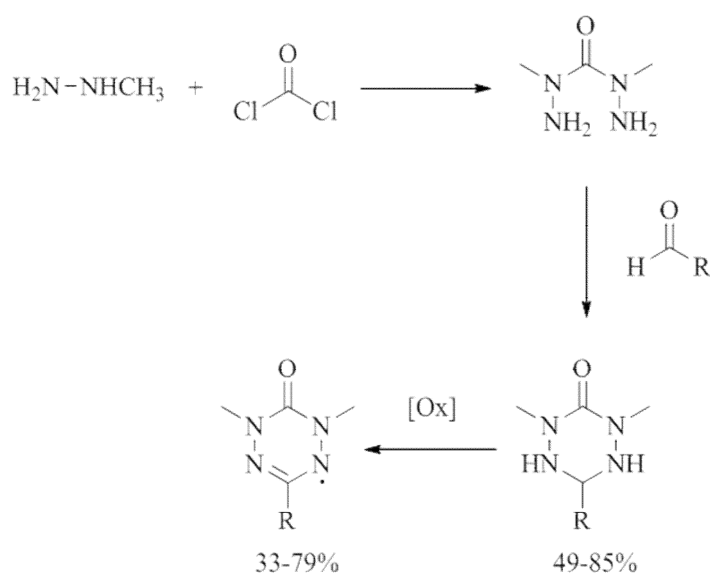
1.1.4.1. Synthesis of verdazyl radicals

Verdazyl radicals were accidentally discovered in 1963 by Kuhn and Trischmann when attempting the alkylation of formazans.⁶⁰ Triphenylformazan was reacted with methyl bromide in the presence of air which yielded triphenylverdazyl instead of the expected alkylated formazan (Scheme 1.1-10). In the mechanism, the alkylated formazan cyclises to give a leuco-verdazyl, which is in turn oxidised in air to give the resulting verdazyl radical.



Scheme 1.1-10. Kuhn method for the synthesis of verdazyl radicals from formazan

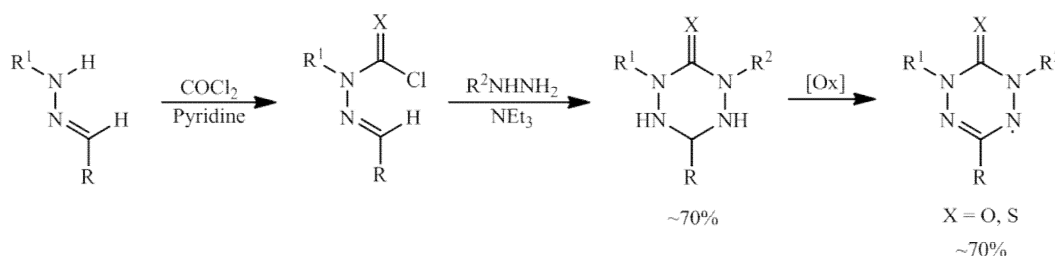
In 1980, Neugebauer and Fischer reported the synthesis of 1,5-dimethyl-6-oxoverdazyl and 1,5-dimethyl-3-phenyl-6-oxoverdazyl.⁶² This work was followed in 1988 with a publication by Neugebauer *et al.* detailing the synthesis of a series of 6-oxo and 6-thioverdazyls.⁶³ The general scheme for the synthesis of 6-oxoverdazyls is shown in Scheme 1.1-11.



Scheme 1.1-11. Neugebauer method for the synthesis of 1,5-dimethyl-6-oxoverdazyl radicals

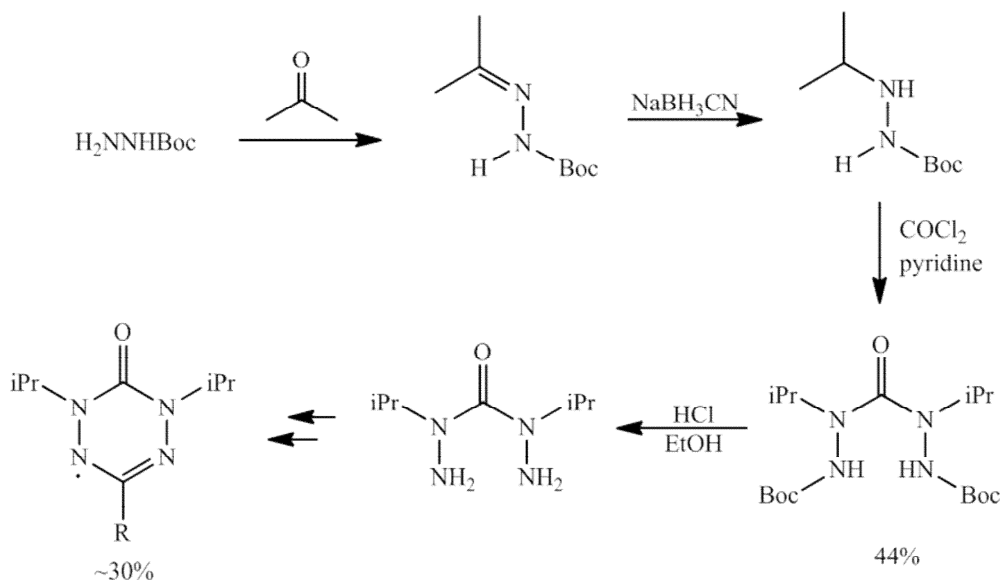
In the first step methyl hydrazine is reacted with phosgene to give 2,4-dimethylcarbonohydrazide. For the synthesis of 6-thioverdazyls, phosgene is replaced by thiophosgene. The condensation of 2,4-dimethylcarbonohydrazide with a substituted aldehyde yields 1,2,4,5-tetrazinane-6-one, referred to as the tetrazinanone intermediate, which is then oxidised to give the 6-oxoverdazyl radical. A number of oxidants have been used including potassium ferricyanide⁶³, lead oxide⁶⁴, sodium periodate⁶⁵ and benzoquinone⁶⁶.

The incorporation of aromatic substituents on the nitrogen atoms at the 1 and 5 positions can be afforded by constructing the tetrazinanone intermediate in a stepwise process developed by Milcent *et al.* (Scheme 1.1-12).⁶⁷ A hydrazone, synthesised from the appropriate aldehyde and hydrazine, is reacted in phosgene or thiophosgene to give a chloroformylhydrazone. The hydrazone is ring-closed with an aryl hydrazine to give the tetrazinanone intermediate which is then oxidised to give the corresponding verdazyl radical.



Scheme 1.1-12. Milcent method for the synthesis of 1,5-diaryl substituted verdazyls⁵⁴

More recently, Paré *et al.* developed the synthesis of 1,5-diisopropyl substituted verdazyls (Scheme 1.1-13).⁶⁶



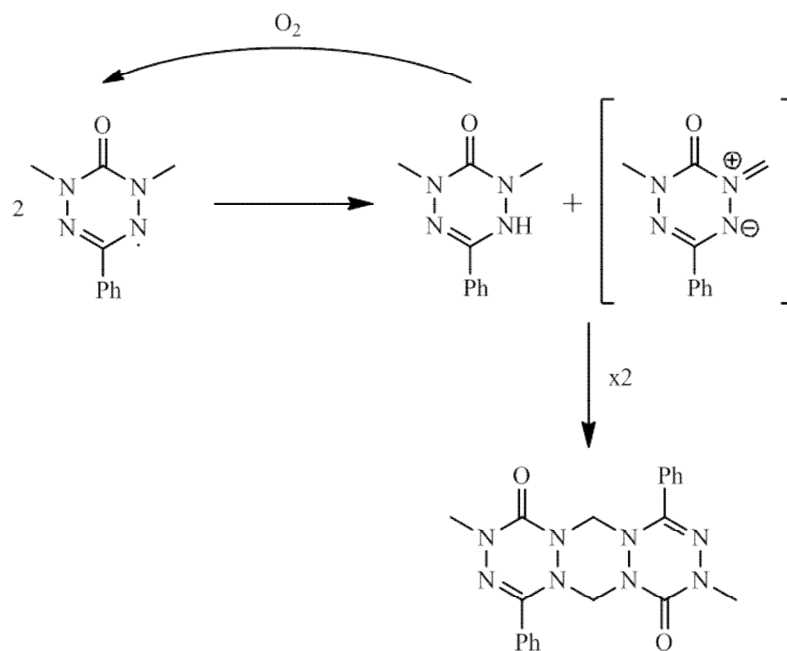
Scheme 1.1-13. Pare method for the synthesis of 1,5-diisopropyl substituted oxoverdazyls⁵⁴

In this method, the *t*-butyloxycarbonyl (Boc) protected isopropyl hydrazine is reacted with phosgene in the presence of triethylamine. Removal of the Boc protecting group yields the desired 2,4-diisopropylcarbonohydrazide. The condensation reaction with an aldehyde and oxidation steps are similar to that already described.

1.1.4.2. Properties of verdazyl radicals

Verdazyl radicals can be isolated, handled and stored without decomposition, are air and water stable, and do not dimerise when in solution or in the solid state.^{54, 68}

Verdazyls substituted with small groups at the 3 position, such as H or Me, are known to gradually decompose; however, this is over a period of weeks.⁶⁹ Larger substituents at the 3 positions can sterically shield the verdazyl ring, thus increasing its stability.⁶⁹ The 1,5-dimethyloxoverdazyls disproportionate very slowly over time and as such can still be referred to as stable rather than persistent (Scheme 1.1-14).^{54, 63, 70} In the disproportionation reaction, a hydrogen atom is abstracted from one of the methyl groups creating an azomethine imine intermediate and a leuco-verdazyl.⁷⁰ The leuco-verdazyl is air oxidised back to the verdazyl radical whilst the azomethine imine undergoes a [3+3] cycloaddition reaction.⁵⁴



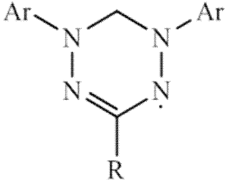
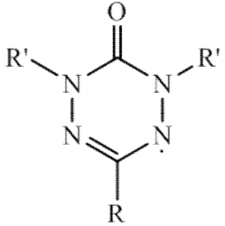
Scheme 1.1-14. Disproportionation reaction of 1,5-dimethyl-6-oxoverdazyls⁵⁴

Verdazyl radicals are brightly coloured and the colours vary depending on the type of verdazyl and its substituents. Type I verdazyls are typically green with an

absorption wavelength at approximately 700 nm.^{69, 71} Type II verdazyls range from dark yellow to brown, with absorptions between 400 and 600 nm.^{63, 66} Both types of verdazyl generally show two overlapping bands in UV-vis spectra. The latter band varies upon changing the substituent at the 3 position.^{69, 72} In particular, when the substituent at the 3 position is small, such as R = H or Me, a shift to a lower wavelength by about 50 nm is observed in comparison to the corresponding verdazyl with R = Ph.⁵⁴

Nitrogen hyperfine coupling constant ranges and calculated spin density distributions recorded in the literature are summarised in Table 1.1-1⁵⁴ for both types of verdazyl. Both type I and type II verdazyls display a general nine line pattern in EPR spectra corresponding to the hyperfine coupling of the unpaired electron to the four nitrogen atoms on the verdazyl ring. In type I verdazyls the hyperfine couplings for both sets of nitrogen atoms (N2,4 and N1,5) are generally equivalent (Table 1.1-1). In type II verdazyls the measured hyperfine coupling constant for N1 and N5 is smaller than for N2 and N4 and this has the effect of splitting the observed nine lines.

Table 1.1-1. Nitrogen hyperfine couplings and calculated spin densities for both type I and type II verdazyls⁵⁴

Verdazyl general structure	N1/N5 hyperfine coupling (G) <i>N1/N5 calculated spin density</i>	N2/N4 hyperfine coupling (G) <i>N2/N4 calculated spin density</i>
	5.7-6.2 <i>0.24</i>	5.4.-6.1 <i>0.16</i>
	5.1-5.4 <i>0.18-0.21</i>	6.4-6.6 <i>0.34-0.40</i>

The spectra of the type II verdazyls are further complicated by the addition of hyperfine coupling of the unpaired electron with the substituents on the N1 and N5 positions on the verdazyl. This hyperfine interaction varies depending on the substituent with values ranging from 5.2-5.8 for R = methyl, 2.9-3.0 for R = CH₂Ph and 1.2-1.5 for R = isopropyl.⁵⁴ Hyperfine interactions with the substituent at the 3 position is generally small (< 1 G) and often requires a more sensitive technique such as electron nuclear double resonance (ENDOR) spectroscopy⁷³ for its calculation.^{63, 74} Figure 1.1-12 compares the simulated EPR spectra of 1,3,5-triphenyl verdazyl and 1,5-dimethyl-3-phenyl-6-oxoverdazyl and illustrates how additional hyperfine interactions serve to complicate the spectrum.

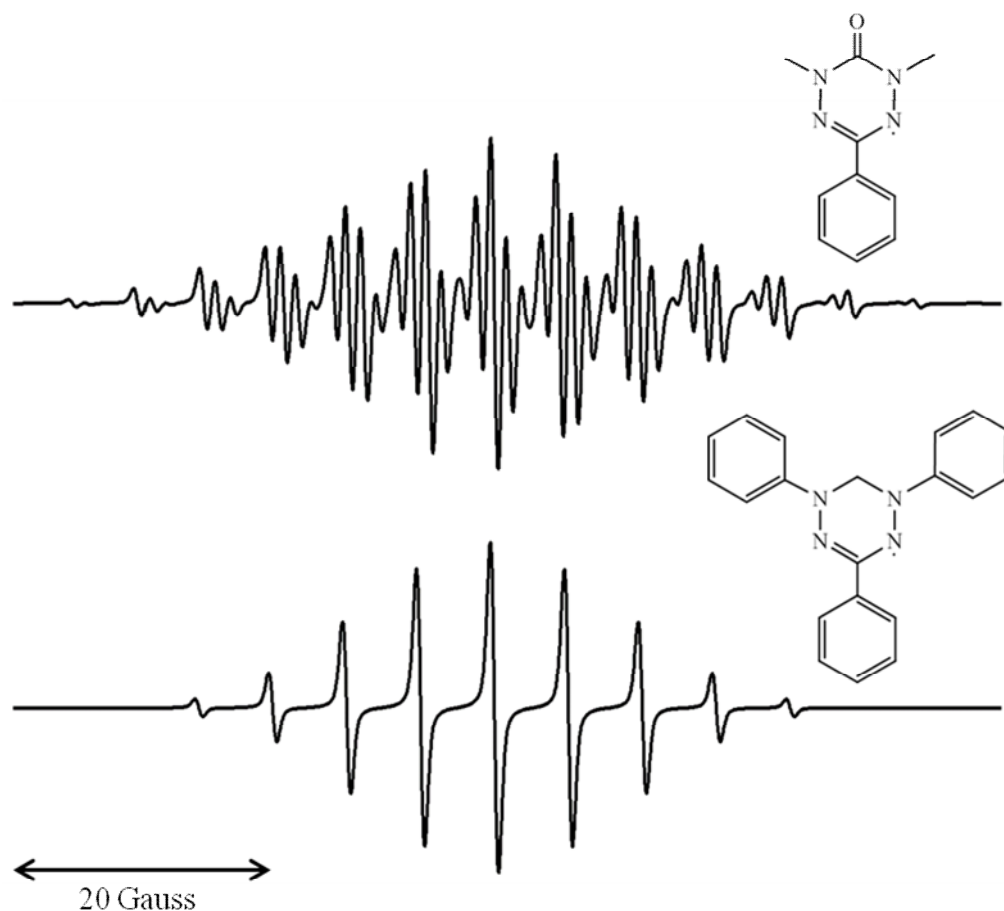


Figure 1.1-12. Simulated EPR spectra of 1,3,5-diphenylverdazyl (bottom) and 1,5-dimethyl-3-phenyl-6-oxoverdazyl (top) using hyperfine couplings from the literature^{63, 75}

Spin density distributions on verdazyl radicals are commonly determined computationally to support hyperfine coupling values determined from EPR.⁷⁶⁻⁸¹ For both types of verdazyl the unpaired electron is in a π system delocalised over N1,2,4,5 and C3.^{54, 82} The calculated singly occupied molecular orbital (SOMO) is a π^* orbital that resides mostly over the four nitrogen atoms.^{54, 83} A nodal plane passes through the carbon atom at the 3 and 6 positions, however, spin polarisation effects produce some spin density on the substituent at the 3 position.^{54, 83} For both types of

verdazyl the four nitrogen atoms carry the majority of the spin density. Calculated spin densities (Table 1.1-1) are close in magnitude for both sets of nitrogen atoms in the type I verdazyls, although slightly higher values are seen for N1 and N5. In type II verdazyls N2 and N4 carry almost double the spin density seen on N1 and N5.

1.1.4.3. Applications of verdazyl radicals

Since their discovery, verdazyl radicals have found themselves in a number of applications including spin labels⁸⁴, ligands for transition metals^{65, 85, 86} which in turn can be used as building block for magnetic materials⁸⁷⁻⁹¹, substrates for organic synthesis^{70, 92}, polymerisation inhibitors⁹³ and polymerisation mediators^{50-53, 94}. The latter is the focus of the first chapter of this thesis and is discussed in more detail in Section 1.1.5.

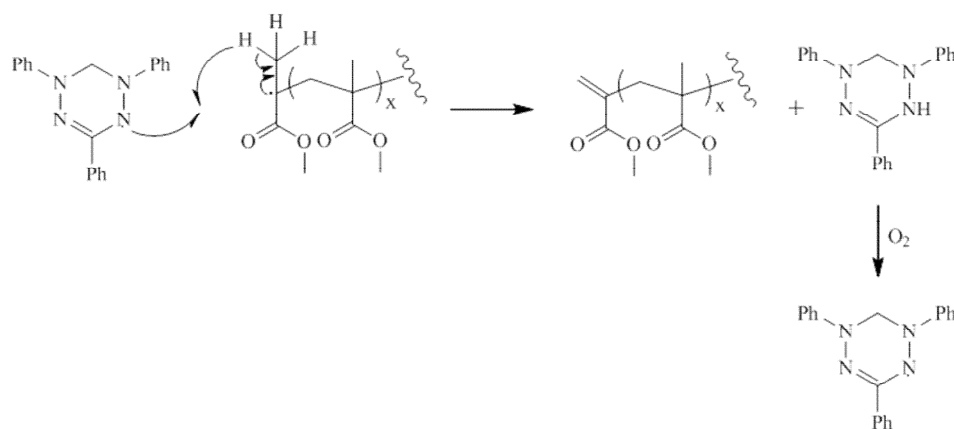
1.1.5. Verdazyl radicals as mediators in stable free radical polymerisations

Yamada *et al.* reported the first use of verdazyls in SFRP with their attempts to mediate the polymerisation of MMA and styrene with triphenylverdazyl.⁵⁰ The authors used a unimolecular initiator formed from the coupling product of triphenylverdazyl with a 2-cyano-2-propyl radical formed from the decomposition of AIBN (Scheme 1.1-15).

The polymerisation of MMA was performed at 80 °C. After 24 hours low conversions, low molecular weights and high polydispersities were observed for all three initiating systems (Table 1.1-2). The polymerisation mixture went from colourless to green, indicating the presence of free verdazyl and was attributed by the authors to the slow recombination of the propagating chain with the verdazyl.⁵⁰ The colour was observed to become more intense on exposure to air indicating the presence of leuco-verdazyl.⁵⁰ The formation of leuco-verdazyl was accounted for by the abstraction of a hydrogen atom from the propagating chain (Scheme 1.1-16). From these results it was concluded that triphenylverdazyl was unsuitable for mediating the SFRP of MMA.⁵⁰

Table 1.1-2. Final results from the polymerisation of MMA with initiators (i) – (iii)⁵⁰

Unimolecular initiator	Time (h)	Conversion (%)	M _n (g/mol)
(i)	40	9.9	4,700
(ii)	29	3.6	1,600
(iii)	29	4.4	1,700



Scheme 1.1-16. Mechanism of leuco-verdazyl formation from the polymerisation of MMA by (i)

The polymerisation of styrene was performed at 60 °C. After 24 hours no polymer formation was observed and the polymerisation mixture remained colourless, even on exposure to air. It was concluded that a strong carbon-nitrogen (C-N) bond, formed between the propagating radical and the verdazyl radical, did not dissociate at the polymerisation temperature preventing the formation of polymer.⁵⁰

In 1998 the polymerisation of styrene was revisited by Yamada *et al.*⁵¹ The coupling product of the 2,-cyano-2-propyl radical and triphenylverdazyl (**i**) was again used as the unimolecular initiator, however, this time higher polymerisation temperatures were investigated (90-120 °C). Nearly linear first order kinetics with respect to monomer was observed alongside an increase in molecular weight with conversion at 110 °C, however, polydispersity values remained > 1.5. The use of ¹H NMR confirmed that 40% of polymer chains contained the triphenylverdazyl end-group indicating a large amount of bimolecular termination was occurring. Through the use of EPR spectroscopy it was determined that at 110 °C the triphenylverdazyl radical decomposed, resulting in a reduced concentration of radical that was insufficient to cap all the growing polymer chains (Figure 1.1-14⁵¹). Reducing (90 °C) or increasing (120 °C) the temperature did not improve on the observed results. It was concluded by the authors that the use of a structurally modified verdazyl radical that was more stable at the polymerisation temperature would be able to mediate a SFRP.⁵¹

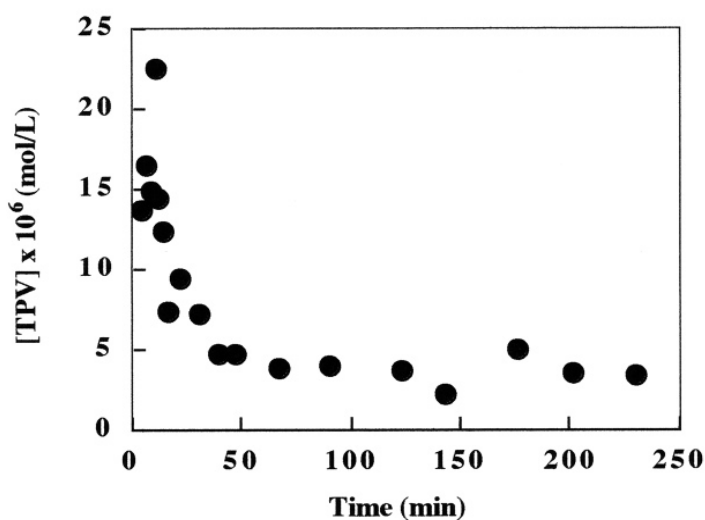
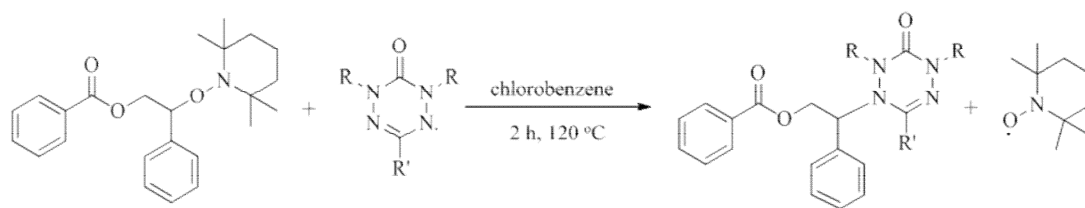
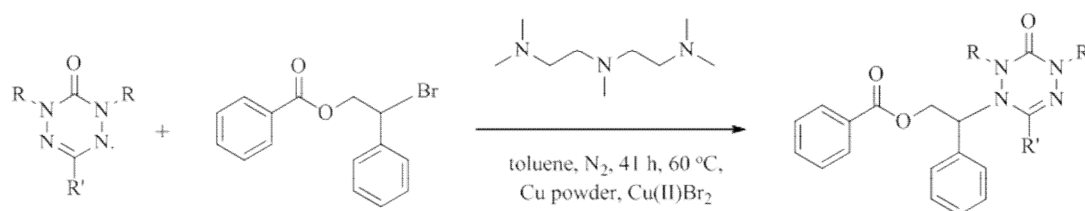


Figure 1.1-14. Change in triphenylverdazyl concentration during the polymerisation of styrene by (i) determined by EPR⁵¹

The area of verdazyl mediated SFRP remained dormant until 2007 when Georges *et al.* investigated the polymerisation of styrene and butyl acrylate mediated by 6-oxoverdazyls.⁵³ After some initial, largely unsuccessful work using a bimolecular initiating system, work was then focused on the use of a verdazyl based unimolecular initiator similar in structure to a unimolecular initiator utilised in NMP.^{52, 53} It was speculated by the authors that the use of a unimolecular initiator would introduce the correct ratio of propagating species to verdazyl radical that was not seen in the bimolecular systems.⁵³ The unimolecular initiators were prepared by either a radical exchange reaction or an atom transfer radical addition (ATRA) reaction (Schemes 1.1-17 and 1.1-18).



Scheme 1.1-17. Exchange reaction for the synthesis of verdazyl unimolecular initiators



Scheme 1.1-18. ATRA reaction for the synthesis of verdazyl unimolecular initiators

A selection of unimolecular initiators were investigated (Figure 1.1-15). Initiator (**iv**) was used to polymerise styrene at 130 °C resulting in high molecular weight growth and a high polydispersity. The poor result was attributed to the slow dissociation and recombination of the verdazyl radical to and from the propagating polymer chain.⁵³ In contrast, initiator (**v**) was demonstrated to control the polymerisation of styrene well with low polydispersities and molecular weights close to theoretical values. This illustrated how altering the verdazyl structure, in this case by making it less sterically bulky by changing the phenyl groups at N1 and N5 to methyl, increased the radicals ability to mediate a polymerisation.

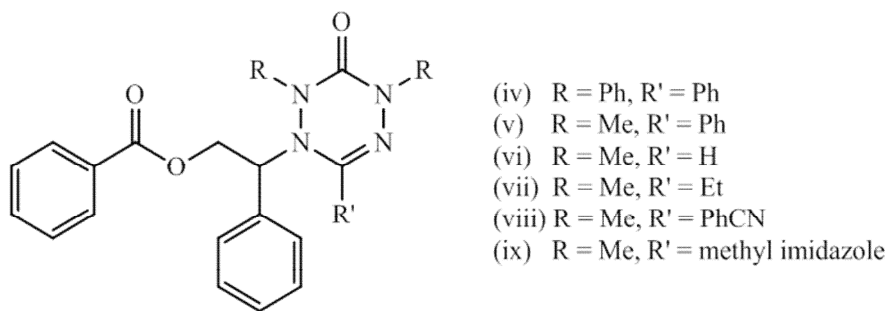


Figure 1.1-15. Unimolecular verdazyl initiators employed by Georges *et al.*

The polymerisation of styrene was also discussed for initiator **(vi)**. High conversions and molecular weights close to theoretical values were observed alongside low polydispersity values in the same timescales used for **(v)**. It had been expected by the authors that less steric crowding around the radical site would increase the dissociation constant (k_d) for the C-N bond, thus increasing the amount of energy required resulting in a slower polymerisation.⁹⁵ The calculated k_d values for **(v)** and **(vi)** were in fact similar ($2.6 \times 10^{-3} \text{ s}^{-1}$ and $2.7 \times 10^{-3} \text{ s}^{-1}$ respectively) and it was concluded that a radical's ability to mediate a controlled polymerisation was not completely due to steric effects around the C-N bond.⁹⁵

Table 1.1-3. Results for the polymerisation of styrene by verdazyl unimolecular initiators

Initiator	Time (h)	Conversion (%)	M_n (g/mol)	M_n^{theo} (g/mol)	PDi	Temperature (°C)
(iv)	6	39	32,700	20,000	1.60	130
(v)	5	40	12,100	15,500	1.22	125
(vi)	7	59	19,900	23,000	1.09	123
(viii)	10	45	6,600	17,700	1.14	125

The polymerisation of *n*-butyl acrylate with initiator (v) proceeded under controlled conditions. The ability of the radical to mediate the polymerisation without any additives, often required with nitroxides^{27, 30}, was attributed to the radical possessing some form of instability under the polymerisation conditions, resulting in slow decomposition.^{53, 95} This controlled the amount of free radical in the polymerisation mixture and prevented the equilibrium being pushed toward the dormant side. Initiator (vi) displayed less control with high polydispersity values being observed (Table 1.1-3). The authors speculated that this was due to the verdazyl radical being more susceptible to participate in the abstraction of a hydrogen atom to form a leuco-verdazyl due to the lack of steric hindrance around the radical centre than radicals with larger substituents.⁹⁵ The presence of leuco-verdazyl was confirmed by the polymerisation mixture changing from colourless to yellow, the colour of the free verdazyl, on exposure to air.

Table 1.1-4. Results for the polymerisation of *n*-butyl acrylate using verdazyl unimolecular initiators

Initiator	Time (h)	Conversion (%)	M_n (g/mol)	M_n^{theo} (g/mol)	PDi	Temperature (°C)
(v)	28	40	14,300	23,000	1.20	130
(vi)	8	68	23,200	24,300	1.54	125
(vii) with ascorbic acid	27	53	13,100	18,700	1.21	132
(viii)	24	40	11,500	22,000	1.17	130
(ix)	5	57	56,000	25,500	2.06	130

The polymerisation of styrene and *n*-butyl acrylate by **(vii)** was briefly addressed by the authors. They observed a decrease in the rate of polymerisation from styrene and a similar rate for the polymerisation of butyl acrylate compared to **(v)** (Table 1.1-4). It was concluded from this that the ability of a verdazyl radical to mediate a polymerisation could be varied between different monomers based on the choice of substituent at the 3 position on the radical.⁵³

Initiators **(viii)** and **(ix)** were separately reported.⁹⁵ Improved results on those previously published were not observed (Table 1.1-4). Noticeably, the polymerisation of *n*-butyl acrylate by **(ix)** was fast and lacked control (Table 1.1-4). This was suggested to be either the result of faster decomposition of the radical at the polymerisation temperature or the substituent at the 3 position sterically hindering the recombination of the radical with the propagating chain.⁹⁵

Three main differences between the polymerisation of styrene and *n*-butyl acrylate were commented upon by the authors.^{53, 95} Longer reaction times were required for the butyl acrylate polymerisations, no low molecular weight tailing was seen for butyl acrylate, in contrast to styrene, and the rate of polymerisation was seen to slow over time for the butyl acrylate polymerisations whereas the rate of styrene remained constant. The longer reaction times for butyl acrylate were accounted for by a larger k_d value for the C-N bond in the acrylate polymerisation compared to the analogous styrene bond.⁹⁵ The last two observations were accounted for by the build up of free verdazyl due to bimolecular termination which reduces the rate of the polymerisation.^{53, 95} This had a greater effect in butyl acrylate polymerisations as it lacks the auto-initiation reaction seen with styrene polymerisations that prevents the build up of free verdazyl.^{27, 96} The addition of ascorbic acid to butyl acrylate polymerisations resulted in increased conversion confirming the author's theories.^{53,}

95

The authors concluded that verdazyl radicals could successfully mediate polymerisation reactions; however, different substituents on the radical resulted in them having different mediating abilities, consistent with the behaviour seen by nitroxides.^{53, 95}

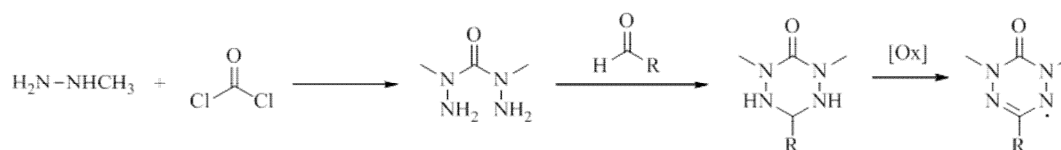
1.1.6. Aim of this work

Previous studies have shown that the structure of a nitroxide radical can have a great effect on its ability to mediate polymerisation reactions. With a variety of structural modifications possible, verdazyl radicals could potentially be designed to specifically mediate polymerisation reactions. This work aims to further evaluate the use of verdazyl radicals as an alternative to nitroxides in the SFRP of styrene, butyl acrylate and MMA.

1.2. Verdazyl radicals: Synthesis and characterisation

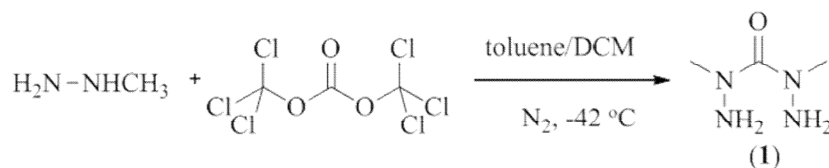
1.2.1. Radical synthesis

The focus of this work was the investigation of 1,5-dimethyl-6-oxoverdazyls used previously to mediated living polymerisations in the work described by Georges *et al.*⁵³ The general synthesis for a range of substituents at the 3 position was developed by Neugebauer (Scheme 1.2-1).^{63, 97}



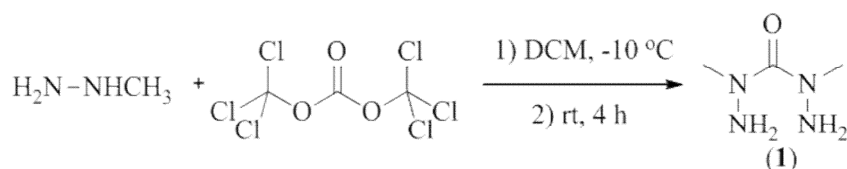
Scheme 1.2-1. General synthesis of 1,5-dimethyl-6-oxoverdazyl radicals

The first step is the synthesis of 2,4-dimethylcarbonohydrazide (**1**). Initially a procedure described by Barr *et al.*⁶⁵ was used (Scheme 1.1-2) which utilised solid triphosgene over more traditionally used phosgene gas.



Scheme 1.2-2. Barr method for the synthesis of 2,4-dimethylcarbonohydrazide (1)

Triphosgene dissolved in toluene was added dropwise to methyl hydrazine in dichloromethane cooled to $-42\text{ }^\circ\text{C}$ using a dry ice/acetonitrile bath. After stirring overnight, the solution was filtered and the solvent/volatiles were removed *in vacuo*. ^1H NMR analysis showed a mixture of products which were difficult to purify using column chromatography and **1** could not be isolated. A second method described by Plater et al.⁹⁸ (Scheme 1.2-3) was then investigated.

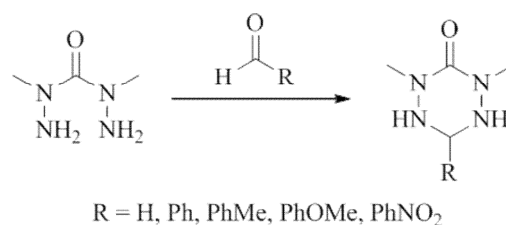


Scheme 1.2-3. Plater method for the synthesis of 2,4-dimethylcarbonohydrazide (1)

In this method triphosgene dissolved in dichloromethane was added dropwise to a solution of methyl hydrazine in dichloromethane cooled to below $0\text{ }^\circ\text{C}$. As with the previous method the reaction mixture was stirred overnight before removing solids and solvent. No further purification was required and high yields ($> 80\%$) were

observed. Compound **1** is hygroscopic and requires drying on a high vacuum line before being stored under nitrogen in the fridge.

The second step in the synthesis is the condensation of the appropriately substituted aldehyde with **1** to give the tetrazinanone intermediate, 1,5-dimethyl-3-R-tetrazinan-6-one (Scheme 1.2-4).



Scheme 1.2-4. Synthesis of 1,5-dimethyl-3-R-tetrazinan-6-one

- (a) **2**, R = H, formaldehyde, MeOH/H₂O, 52%; (b) **3**, R = Ph, benzaldehyde, MeOH, 29%; (c) **4**, R = PhMe, *p*-tolualdehyde, MeOH, 63%; (d) **5**, R = PhOMe, 4-methoxybenzaldehyde, MeOH, 60%; (e) **6**, R = PhNO₂, nitrobenzaldehyde, MeOH, 17%.

Following the described literature procedures^{97, 99}, the dissolved aldehyde is added dropwise to a solution of **1** and stirred at ambient temperature for 1-2 hours. Note that it is important not to add the aldehyde too quickly as this results in the formation of the acyclic bis-hydrazone over the desired cyclic tetrazinanone.^{95, 97}

The volatiles are removed to give 1,5-dimethyl-tetrazinan-6-one (**2**), 1,5-dimethyl-3-phenyl-tetrazinan-6-one (**3**), 1,5-dimethyl-3-methylphenyl-tetrazinan-6-one (**4**) and 1,5-dimethyl-3-methoxyphenyl-tetrazinan-6-one (**5**) and, in the case of 1,5-

dimethyl-3-nitrophenyl-tetrazinan-6-one (**6**), filtered. All tetrazinanone intermediates were purified by recrystallisation from appropriate solvents.

Molecular structures determined by X-ray crystallography have been obtained for intermediates **2** and **3** (Figures 1.2-1 and 1.2-2). In **2** (R = H), the tetrazinanone ring is in a distorted boat conformation with all the nitrogen atoms nearly coplanar. In **3** (R = Ph), the phenyl group sits orthogonal to the tetrazinanone ring, which is itself more planar than **2** (R = H), with only the carbon in the three position out of plane. Crystals suitable for X-ray crystallography for the other tetrazinanone intermediates were unfortunately not obtained.

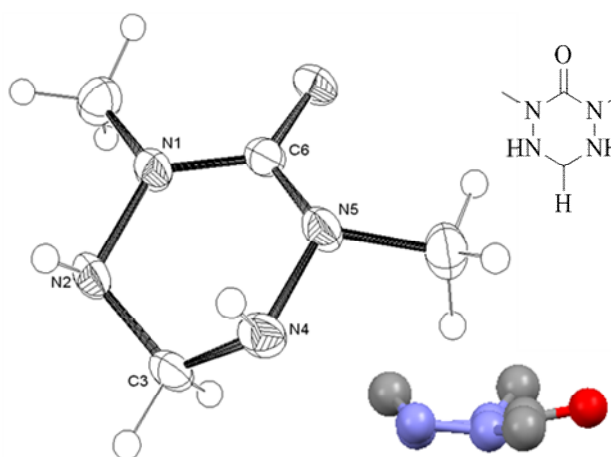


Figure 1.2-1. Molecular structure of 1,5-dimethyl-3-tetrazinan-6-one (2**) determined by X-ray crystallography**

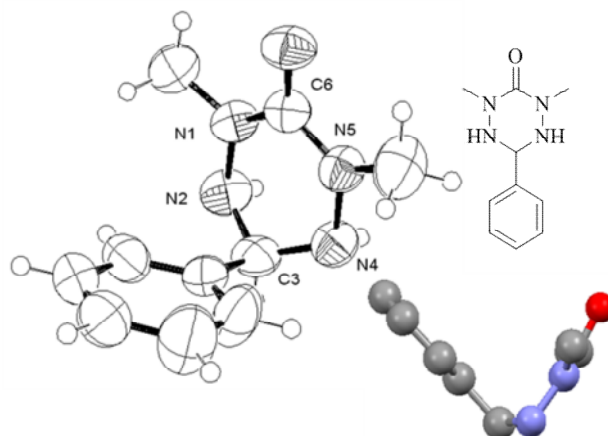
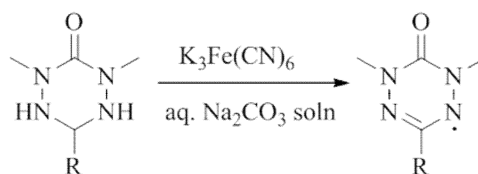


Figure 1.2-2. Molecular structure of 1,5-dimethyl-3-phenyl-tetrazinan-6-one (3) determined by X-ray crystallography

The final step is the oxidation of tetrazinanone intermediates **2-6** to give the corresponding verdazyl radical, 1,5-dimethyl-3-R-6-oxoverdazyl (Scheme 1.1-5).



Scheme 1.2-5. Synthesis of 1,5-dimethyl-3-R-6-oxoverdazyl

(a) **7**, R = H, 82%; (b) **8**, R = Ph, 89%; (c) **9**, R = PhMe, 46%; (d) **10**, R = PhOMe, 81%; (e) **11**, R = PhNO₂, 66%.

Following a literature procedure⁶³, potassium ferricyanide dissolved in water and a 2N aqueous solution of sodium carbonate were used to synthesise 1,5-dimethyl-6-

oxoverdazyl (**7**). The reaction was completed at ambient temperature, with the product then extracted into diethyl ether. The radical was purified using an activated alumina (basic) column eluted using 1:1 dichloromethane/petroleum ether yielding a dark red crystalline solid. This crystalline material decomposes to a viscous liquid that is largely insoluble if left at ambient temperature (Figure 1.2-3).

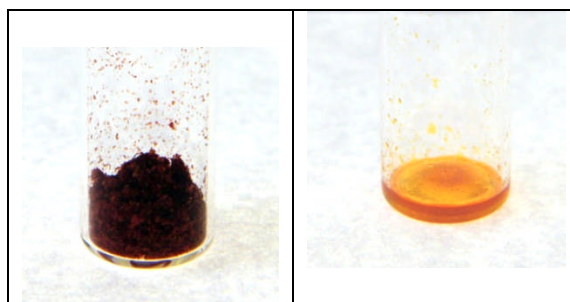


Figure 1.2-3. 1,5-dimethyl-6-oxoverdazyl (7**) straight after purification (left) and after standing at ambient temperature for 1 day (right)**

The crystalline material can be stored in the freezer; however, this is not a permanent solution as it only slows the degradation of the crystals. It is better to store the eluent from the column in the freezer, removing portions of solvent *in vacuo* to obtain ‘fresh’ crystalline material as required. Crystals of **7** (R = H) which may be suitable for x-ray crystallography can be grown in petroleum ether on storing in the freezer, however, these crystals disappear into solution quickly on warming so obtaining a crystal structure has thus far not been possible.

The synthesis of radicals 1,5-dimethyl-3-phenyl-6-oxoverdazyl (**8**), 1,5-dimethyl-3-methylphenyl-6-oxoverdazyl (**9**), 1,5-dimethyl-3-methoxyphenyl-6-oxoverdazyl (**10**) and 1,5-dimethyl-3-nitrophenyl-6-oxoverdazyl (**11**) follow a similar synthetic route to **7** (R = H), all described in the literature.^{63, 99} Tetrazinanone intermediate **3** (R = Ph) was found to be difficult to dissolve if not used soon after synthesis. When adding the potassium ferricyanide to tetrazinanone intermediates **3** (R = Ph) and **6** (R = PhNO₂), a large amount of white precipitate is formed alongside the radical. This can be mostly removed once the solids have been collected by extensive washing with water. Radicals **9-11** were purified by recrystallisation from appropriate solvents. Purifying **8** (R = Ph) proved problematic and was therefore used without further purification.

1.2.2. Verdazyl characterisation

Five radicals were synthesised during this body of work, focused on varying the substituent at the 3 position of the verdazyl (Figure 1.2-4). The aim was to investigate whether changing the substituent would affect the outcome of a verdazyl mediated polymerisation through both steric and electronic effects. Steric effects have been introduced by the use of a phenyl substituent and electronic effects by the use of electron donating (CH₃, OCH₃) and electron withdrawing (NO₂) groups.

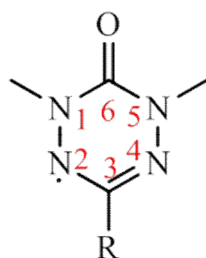


Figure 1.2-4. General numbering scheme used for verdazyl radicals

Figure 1.2-5 shows a sample of each radical and illustrates how each radical is a different colour as a result of the substituent at the 3 position on the radical.

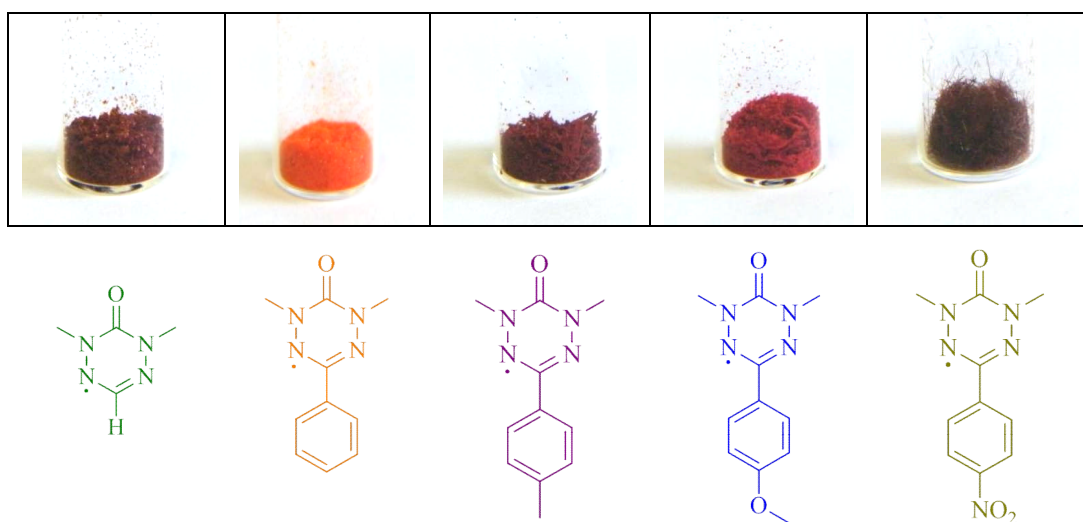


Figure 1.2-5. Verdazyl radicals (from left to right); 1,5-dimethyl-6-oxoverdazyl (7), 1,5-dimethyl-3-phenyl-6-oxoverdazyl (8), 1,5-dimethyl-3-methylphenyl-6-oxoverdazyl (9), 1,5-dimethyl-3-methoxyphenyl-6-oxoverdazyl (10) and 1,5-dimethyl-3-nitrophenyl-6-oxoverdazyl

(11)

It is documented in the literature that the substituent at the 3 position effects the absorption wavelength, λ_{\max} , of the radicals.⁵⁴ Figure 1.2-6 compares the electronic spectra for the five radicals (1, 4-dioxane) and each radical displays two overlapping bands with λ_{\max} values between 350 and 600 nm. The verdazyl with R = H, ie. when the verdazyl is the least substituted, has the lowest λ_{\max} value of all the radicals synthesised. A shift in λ_{\max} towards the red wavelength was seen when the verdazyl was substituted with electron rich aromatic groups (R = PhMe or PhOMe), concurrent with existing data.⁷²

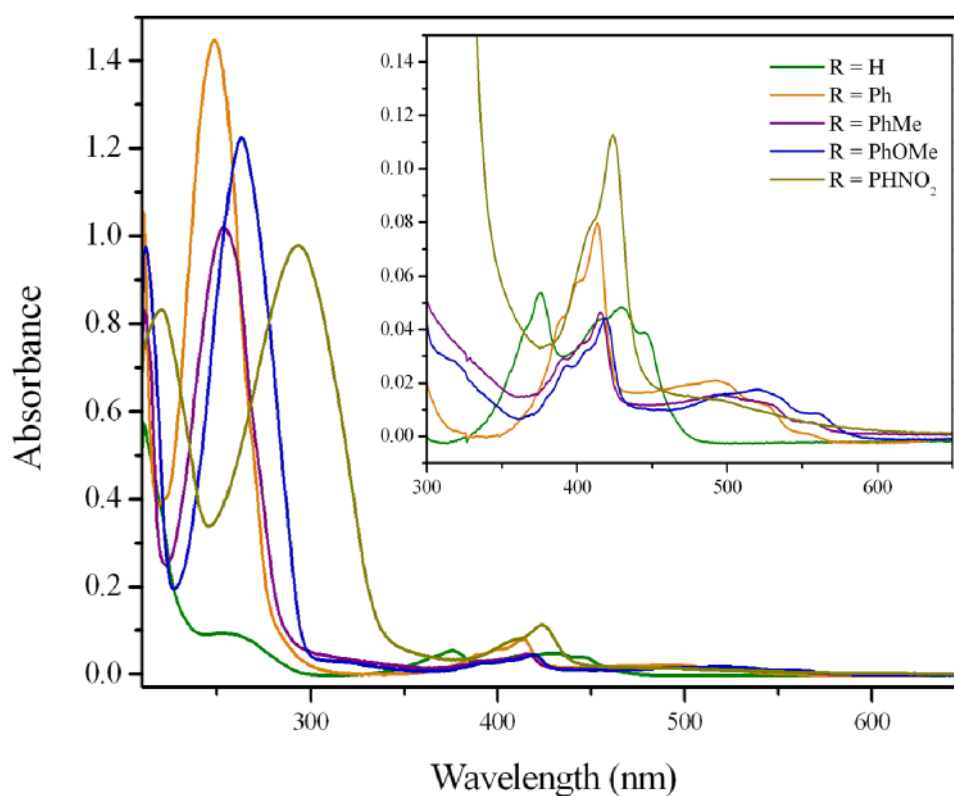


Figure 1.2-6. UV-vis spectra of verdazyl radicals 7-11 in 1, 4-dioxane

Along with traditional characterisation techniques, EPR has been used to gain further insight into the electronic structure of the verdazyl radicals. The solution EPR spectrum of **7** (R = H, 1 mM, toluene) is shown in Figure 1.2-7 (—). The hyperfine structure of **7** arises from the coupling of the free electron to the four nitrogen atoms, the six methyl hydrogen atoms and the hydrogen at the 3 position and the hyperfine coupling constants (Table 1.2-1) were calculated by simulating the experimental spectrum (Figure 1.2-7, —).

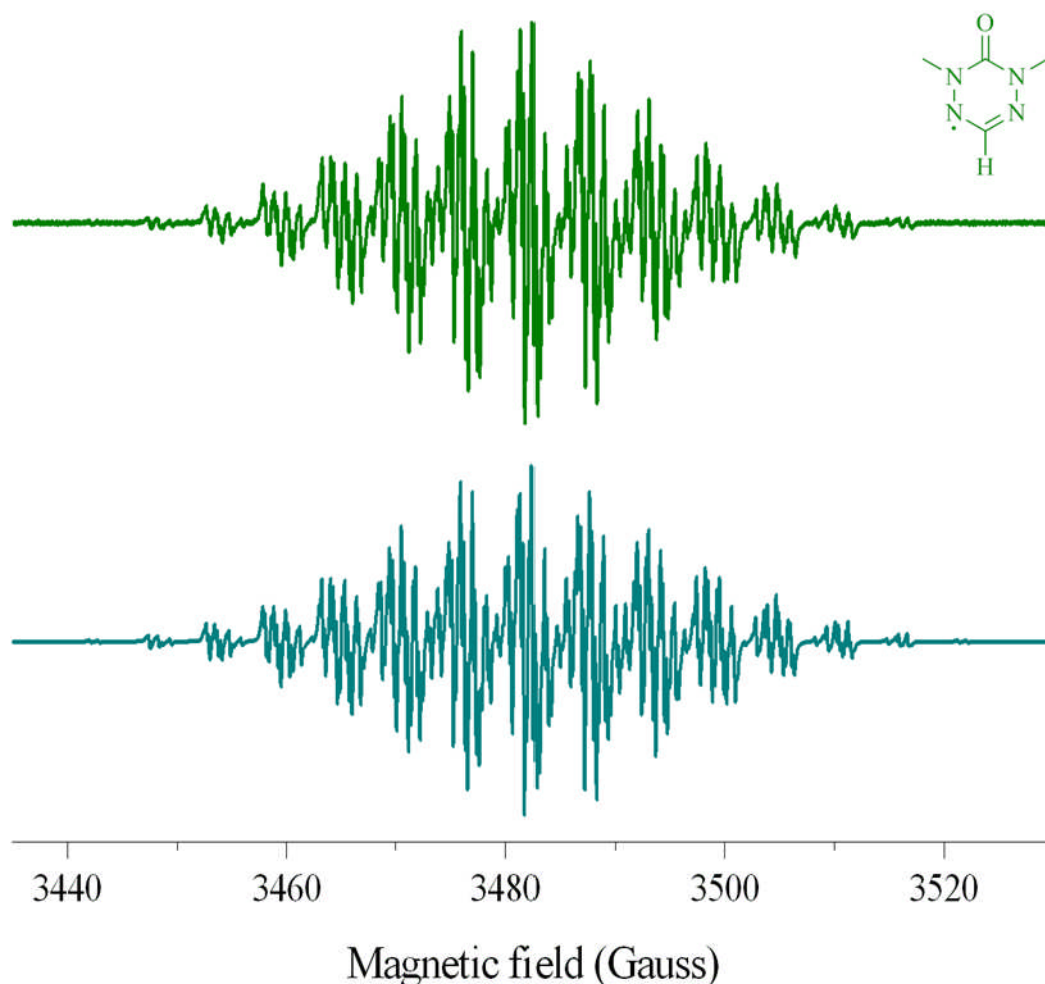


Figure 1.2-7. Experimental (top) and simulated (bottom) EPR spectrum of **7**

The solution EPR spectrum of **8** (R = Ph) was initially recorded at the same 1 mM concentration as **7** (R = H) and is displayed in Figure 1.2-8.

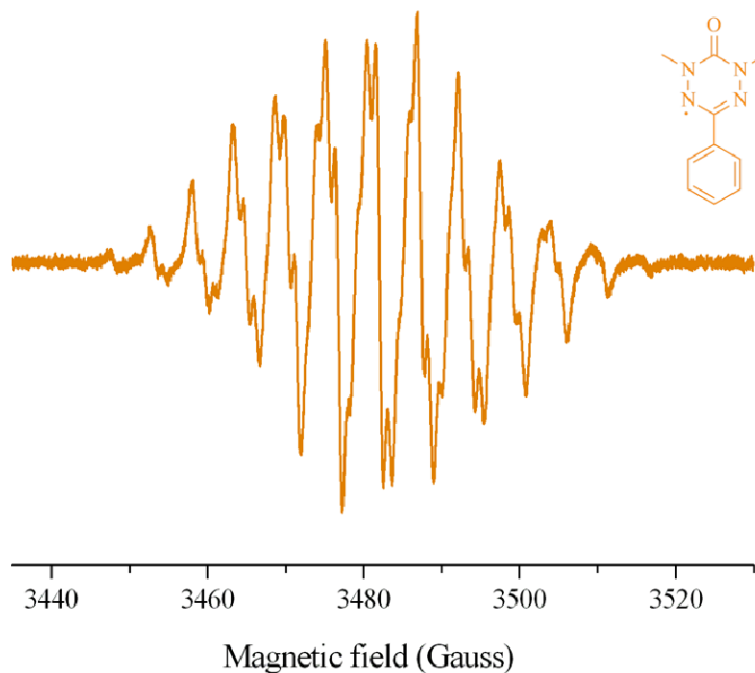


Figure 1.2-8. Experimental EPR spectrum of a 1 mM solution of **8 in toluene**

The EPR spectrum of **8** displays less hyperfine coupling than **7**, illustrated by a reduction in the number of lines in the spectrum. To investigate whether this spectrum accurately showed the full extent of the coupling or whether broadening of the signal was occurring, a second sample was run at a concentration of 0.2 mM (Figure 1.2-9). The spectrum of the 0.2 mM solution showed less broadening of the signal. This determined that there was some saturation of the signal in the 1 mM sample. Again, a simulation was done to obtain the hyperfine coupling constants (Table 1.2-1). The simulation revealed that there was no hyperfine coupling observed with the phenyl group at the 3 position on the verdazyl.

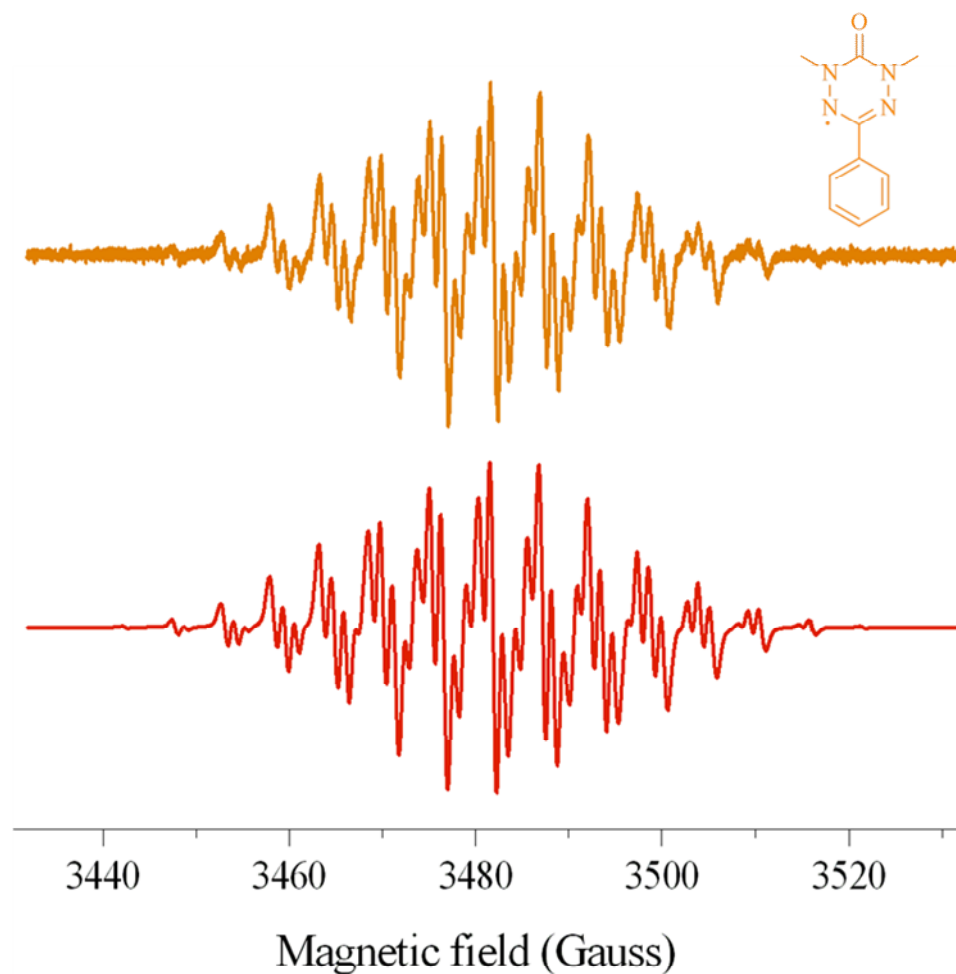


Figure 1.2-9. Experimental (top) and simulated (bottom) EPR spectrum of a 0.2 mM solution of **8 in toluene**

It was expected that the EPR spectra of verdazyl radicals **9-11** should be that similar to that of 1,5-dimethyl-3-phenyl-6-oxoverdazyl. However, the group at the 4 position on the phenyl ring may exhibit some electronic effect on the coupling of the radical. Figures 1.1-10-1.1-12 displays the recorded EPR spectra of radicals **9** (R = PhMe), **10** (R = PhOMe) and **11** (R = PhNO₂). A 0.05 mM concentration of radical was used instead of a 0.1 mM concentration, the concentration used for **8**, as the

higher concentration resulted in significant line broadening. The lower concentration reduced the amount of line broadening significantly for **10**. Less of an effect was seen in the spectra of **9** and **11**, and the line broadening was taken into account during the simulations of the two radicals.

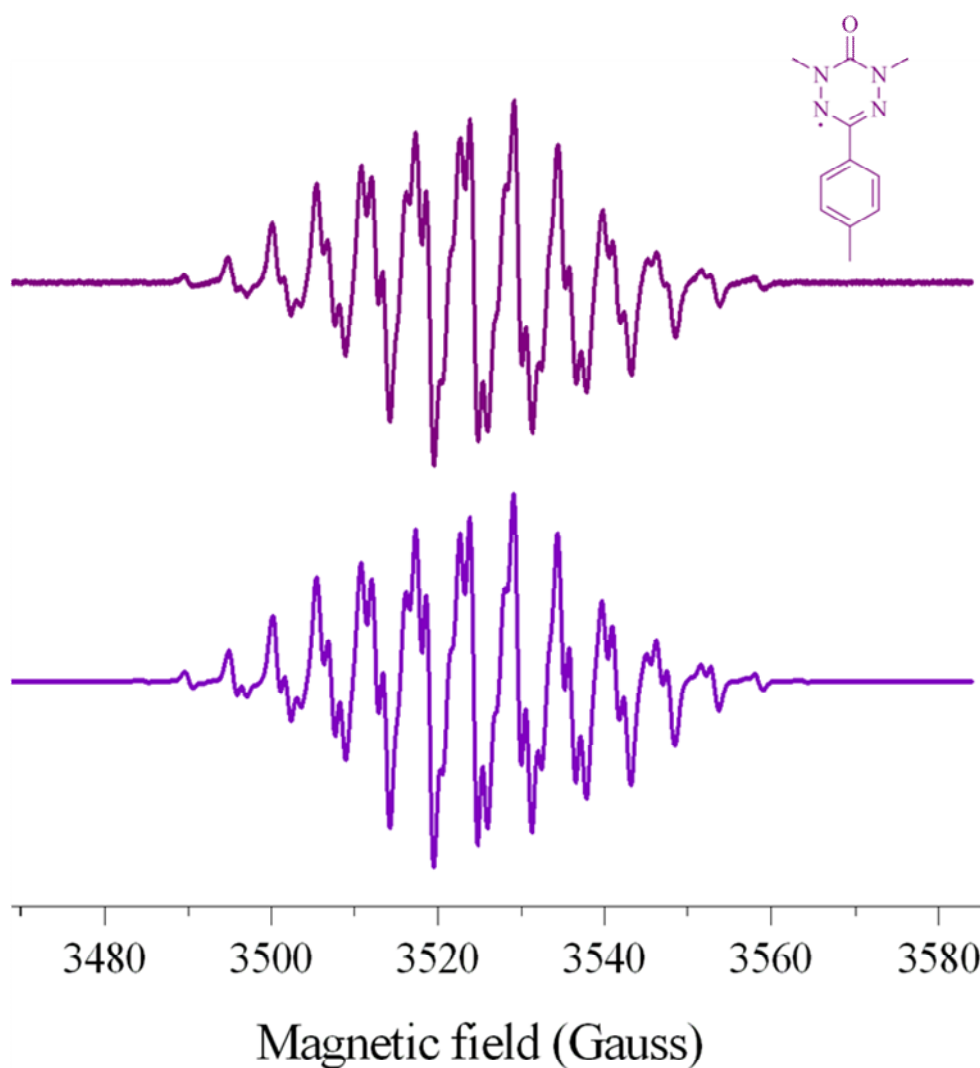


Figure 1.2-10. Experimental (top) and simulated (bottom) EPR spectrum of a 0.05 mM solution of **9 in toluene**

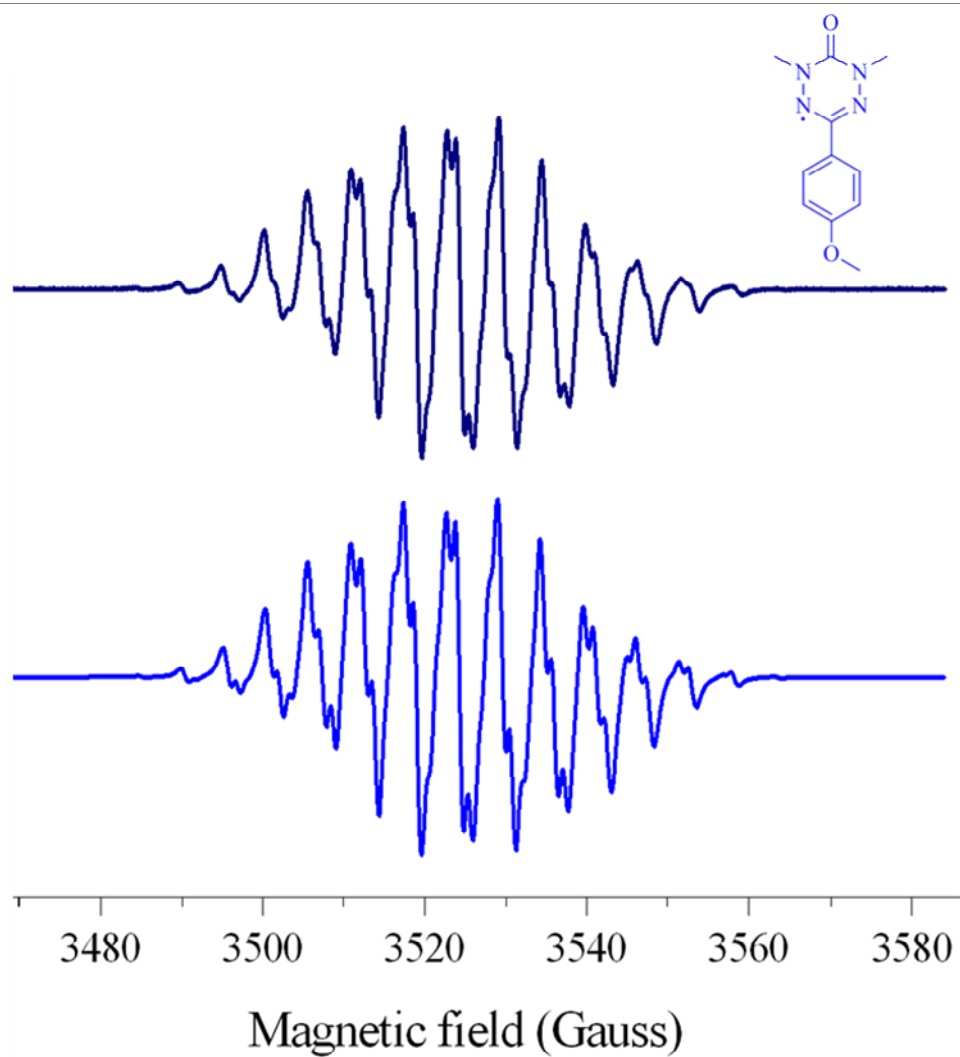


Figure 1.2-11. Experimental (top) and simulated (bottom) EPR spectrum of a 0.05 mM solution of 10 in toluene

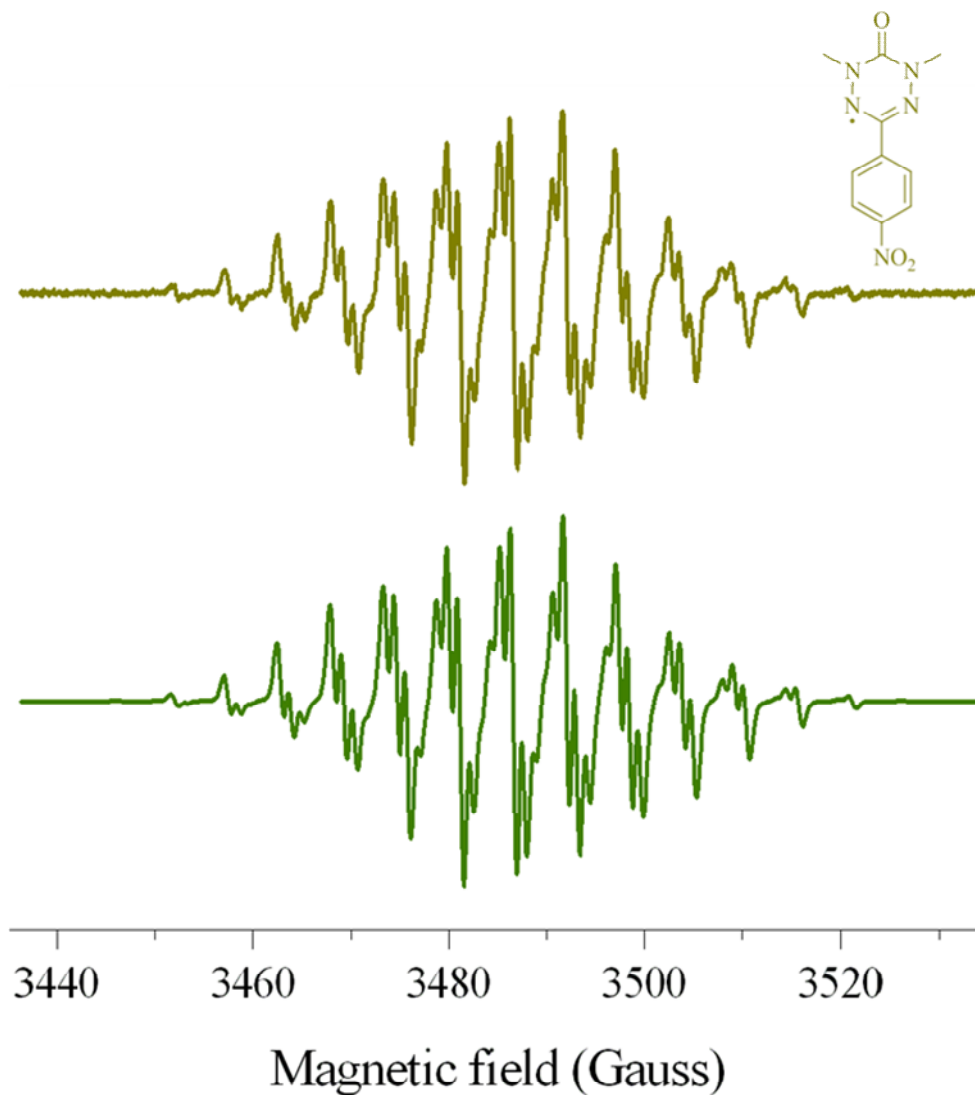


Figure 1.2-12. Experimental (top) and simulated (bottom) EPR spectrum of a 0.05 mM solution of 11 in toluene

As expected, similar spectra to **8** (R = Ph) were observed with coupling seen with the four nitrogen atoms and the six methyl hydrogen atoms. Table 1.2-1 displays the calculated values for the hyperfine coupling constants and g-factors for all the radicals and shows that small changes were observed in the values on changing the

substituent at the 3 position. The values were in the expected range for oxoverdazyls⁵⁴ and were similar to literature values⁶³ with the exception of **9** (R = PhMe) as no EPR data was recorded by the authors who developed the synthesis⁹⁹.

Table 1.2-1. Hyperfine coupling constants and g-factor values for verdazyl radicals 7-11 at room temperature in toluene

R	a(N _{2,4})	a(N _{1,5})	a(H _{CH₃}) (6H)	a(H _{CH})	g-factor
H	6.50	5.19	5.45	0.78	2.0045
Ph	6.50	5.10	5.45	-	2.0045
PhMe	6.52	5.15	5.42	-	2.0099
PhOMe	6.53	5.37	5.15	-	2.0100
PhNO ₂	6.45	5.35	5.48	-	2.0101

No obvious trends are visible from the data in Table 1.2-1 relating to the changes in substituent at the 3 position. In the future it may be beneficial to use the advanced EPR method ENDOR to obtain more accurate values for the hyperfine coupling values.⁷³ This technique has previously shown a small hyperfine coupling (< 1 G) to the phenyl group in the 3 position of **8** (R = Ph) exists.⁶³

A short computational study was completed by Professor Rob Deeth, University of Warwick, to compliment the observed EPR results. The structures of the spin-doublet radicals were optimised using spin-unrestricted density functional theory (DFT). The B3LYP functional with 3-21G* basis sets as implemented in Gaussian 03¹⁰⁰ was used throughout. The results of molecular orbital and spin density calculations for **8** (R = Ph) are shown in Figure 1.2-13, and Mulliken spin

populations are recorded in Table 1.2-2. Figure 1.2-14 shows the atom numbering scheme used in Table 1.2-2.

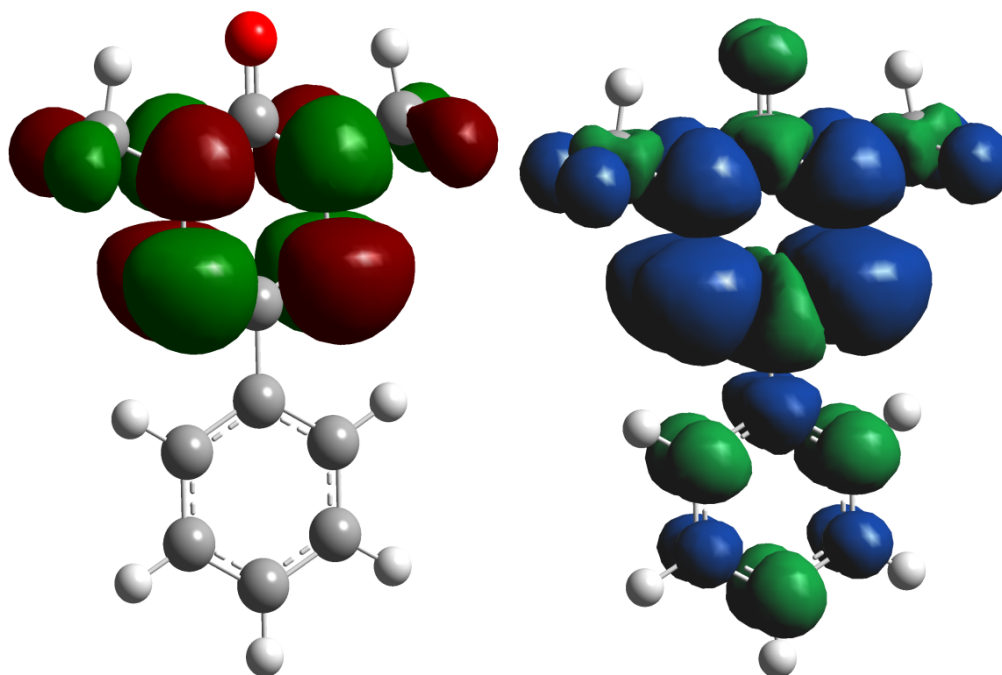


Figure 1.2-13. Calculated molecular orbital (top left), spin density plot (top right) for verdazyl radical **8** (R = Ph)

The calculated molecular orbital explains why the substituent at the 3 position does not have a greater effect on the hyperfine coupling seen in EPR. A nodal plane passes through the 3 and 6 positions on the radical making the molecular orbital relatively insensitive to the substituent at the 3 position. However, a small amount of spin density can be seen on the C3 atom and the phenyl ring as a result of spin polarisation⁵⁴; however, this effect is very small. This fits with the observed hyperfine coupling seen in the literature for **8** when ENDOR is used.⁶³ The molecular orbital spans the four nitrogen atoms and as such they carry the majority

of the spin density. The nitrogen atoms at the 2 and 4 positions carry double the spin density of those at the 1 and 5 positions, which correlates with the larger hyperfine coupling seen in EPR for N2 and N4.

When calculated, the verdazyl radicals appeared planar. This has been seen in crystals structures of 1,5-dimethyloxoverdazyls published in the literature.^{74, 101} To determine if this was a correct representation for these radicals, the molecular orbital for **3** (R = H) was calculated. The same boat conformation as illustrated in Figure 1.2-1 was observed.

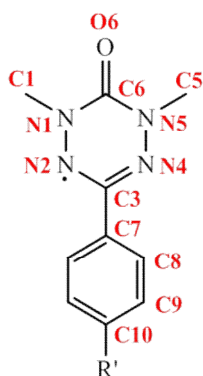


Figure 1.2-14. Atom numbering scheme for used for Table 1.2-2

In general the verdazyl ring carries the same distributions of spin densities in all radicals. An increased amount of spin density was observed for the nitrophenyl substituent on **11**, less so on the methoxy and methyl substituents on **10** and **9** respectively, and with the least on **8**.

Table 1.2-2. Mulliken spin populations for verdazyl radicals 7-11

Atom	Verdazyl radical				
	7	8	9	10	11
	(R = H)	(R = Ph)	(R = PhMe)	(R = PhOMe)	(R = PhNO ₂)
C6	-0.03	-0.03	-0.03	-0.03	-0.03
O6	-0.02	-0.02	-0.02	-0.02	-0.01
N1,5	0.20	0.20	0.20	0.20	0.20
N2,4	0.42	0.41	0.42	0.42	0.42
C3	-0.19	-0.19	-0.19	-0.19	-0.19
C1	-0.02	-0.02	-0.02	-0.02	-0.02
C5	-0.02	-0.02	-0.02	-0.02	-0.02
H3	0.01	-	-	-	-
C7	-	0.02	0.04	0.04	0.09
C8	-	-0.01	-0.03	-0.03	-0.06
C9	-	0	0.02	0.02	0.07, 0.06
C10	-	0	-0.03	-0.02	-0.07
R' CH ₃	-	-	0	-	-
R' OCH ₃	-	-	-	-0.01	-
R' NO ₂	-	-	-	-	0.18, 0.44, -0.69

A brief second study was completed by Professor Rob Deeth. The differences observed between the dimethyl substituted verdazyl and the diphenyl substituted verdazyl were investigated. Removing the phenyl from the substituent at the 3 position i.e. having a nitro group instead of a nitrophenyl group was also investigated. The structures of the radicals are displayed in Figure 1.2-5 and the calculated Mulliken spin populations are displayed in Table 1.2-3.

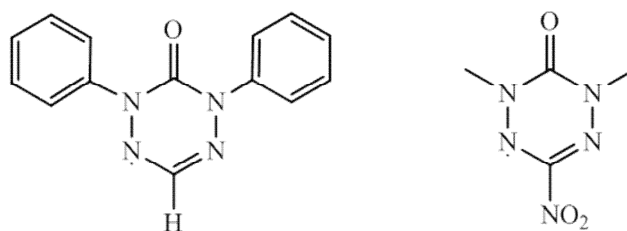


Figure 1.2-15. Structure of 1,5-diphenyl-6-oxoverdazyl (left) and 1,5-dimethyl-3-nitro-6-oxoverdazyl (right)

The 1,5-diphenyl substituted verdazyl displayed less spin density on the 1 and 5 nitrogen atoms, and more on those at the 2 and 4 positions compared with radicals **8-11**. The opposite was observed for the nitro substituted verdazyl.

It has been observed from these calculations and from EPR data that only very small differences in electronic structure occur on changing substituents on the verdazyl radicals **7-11**. Whether these small differences within the verdazyl structure will translate to some kind of effect when used in polymerisation reactions is explored in Section 1.4. It should be noted that any differences observed may not only be due to electronic effects as steric effects may also play a role.

Table 1.2-3. Mulliken spin populations for 1,5-diphenyl-6-oxoverdazyl and 1,5-dimethyl-3-nitro-6-oxoverdazyl

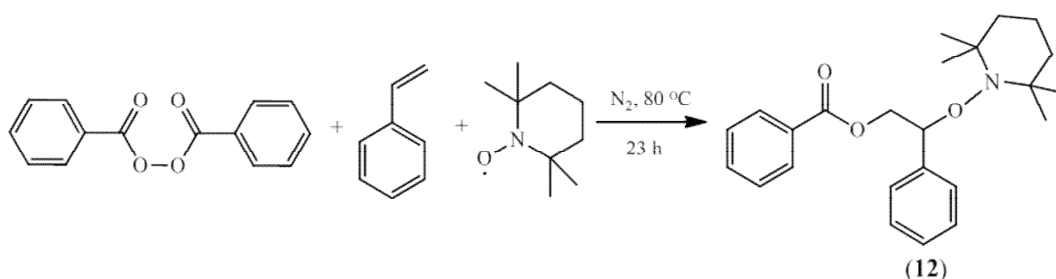
Atom	Verdazyl radical	
	N-Ph	c-NO ₂
C6	-0.03	-0.03
O6	-0.02	-0.02
N1,5	0.18	0.21
N2,4	0.44	0.40
C3	-0.21	-0.19
C1	-	-0.02
C5	-	-0.02
H3	0.01	-
Ph1	-0.01, 0.01(2), 0.00 (2)	-
Ph5	-0.01, 0.01(2), 0.00 (2)	-
NO ₂	-	0.01, -0.01(2)

1.3. Verdazyl initiator synthesis

To synthesise the verdazyl initiators analogous to the nitroxide based unimolecular initiator synthesised by Hawker²⁴, two synthetic routes are possible, firstly via an exchange reaction or secondly via an atom transfer radical addition (ATRA) reaction.^{53, 95}

1.3.1. Exchange reaction

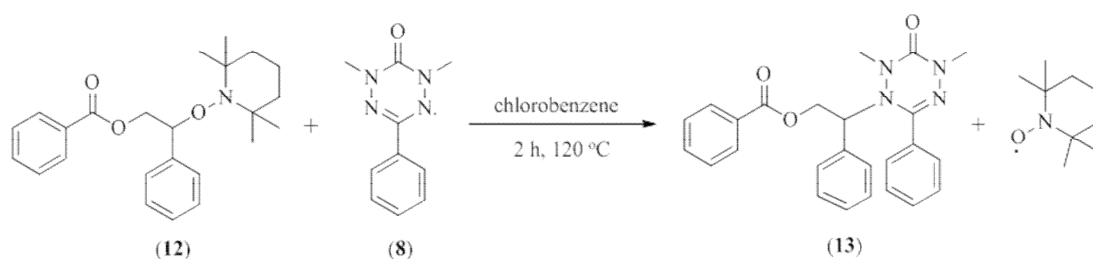
The first method investigated was the radical exchange reaction. Prior to the reaction, 2-phenyl-2-(2,2,6,6-tetramethylpiperidin-1-oxy)ethyl benzoate (**12**) was synthesised from 2,2,6,6-tetramethyl-1-piperidinyloxy (TEMPO), benzoyl peroxide (BPO) and styrene (Scheme 1.3-1).²⁴



Scheme 1.3-1. Synthesis of 2-phenyl-2-(2,2,6,6-tetramethylpiperidin-1-oxy)ethyl benzoate

The reagents were deoxygenated by bubbling with nitrogen for one hour before being heated at 80 °C for 23 hours. Any remaining styrene was removed on a high vacuum line. Repeated column chromatography on a silica gel column with 1:1 dichloromethane/petroleum ether 40-60 changing to 9:1 dichloromethane/petroleum ether 40-60 and 30:1 petroleum ether 40-60/diethyl ether changing to 20:1 petroleum ether 40-60/diethyl ether as eluent was required to obtain **12** as a pure compound as verified by ^1H NMR at a 20% yield.

The radical exchange reaction was attempted for the synthesis of 2-phenyl-2-(1,5-dimethyl-3-phenyl-6-oxoverdazyl)ethyl benzoate (**13**, Scheme 1.3-2)



Scheme 1.3-2. Exchange reaction for the synthesis of 2-phenyl-2-(1,5-dimethyl-3-phenyl-6-oxoverdazyl)ethyl benzoate (**13**)

Following the method described by Georges *et al.*⁵³, a deoxygenated solution of the TEMPO based initiator (**12**) and verdazyl radical **8** (R = Ph) in chlorobenzene was heated at 120 °C under nitrogen for 2 hours. The exchange reaction was initially completed on a small scale (1.2 mg of **8**). EPR was used to analyse samples taken from the reaction mixture every half an hour for the duration of the experiment. It

was expected, that if the reaction proceeded as described, that initially only the signal for **8** (R = Ph) would be visible and that over time it would decrease in intensity and a signal for TEMPO would appear, indicating that the TEMPO radical and verdazyl radical had exchanged.

Figure 1.3-1 shows the EPR traces for $t = 0$ and 2 hours. At time zero only the signal for **8** (R = Ph) is visible as expected and at $t = 2$ hours a TEMPO signal was visible alongside the verdazyl signal.

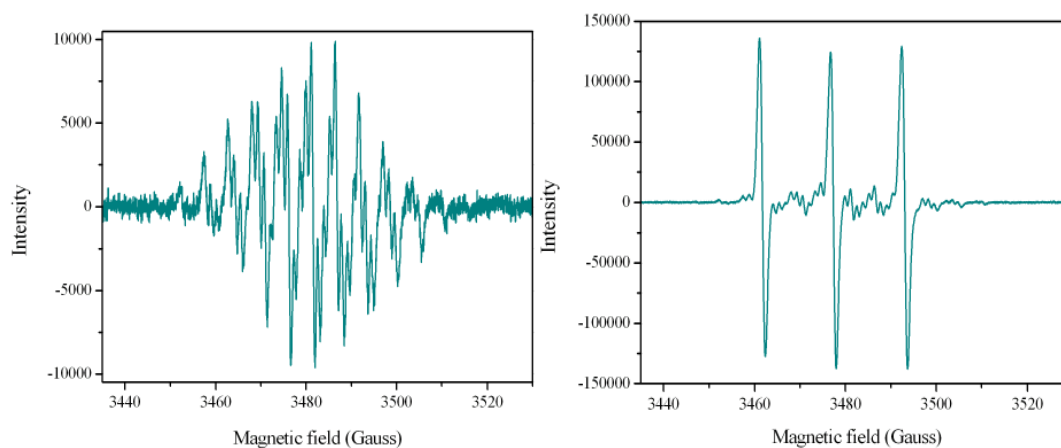


Figure 1.3-1. EPR of spectra of samples taken at 0 and 2 hours for the synthesis of 2-phenyl-2-(1,5-dimethyl-3-phenyl-6-oxoverdazyl)ethyl benzoate (13**) via an exchange reaction**

Initially the results appear to show that in comparison, the verdazyl signal is much weaker than the TEMPO signal at 2 hours, however, the values for the intensity of the signal need to be fully investigated. The intensity signal for **8** (R = Ph) at $t = 0$ was approximately (+/-) 10,000 whereas in $t = 2$ hours, the TEMPO intensity is

approximately (+/-) 150,000 thus the intensity of **8** (R = Ph) would look small in comparison. To analyse the EPR spectra with two radical signals, simulations were performed to separate the signals (Figure 1.3-2).

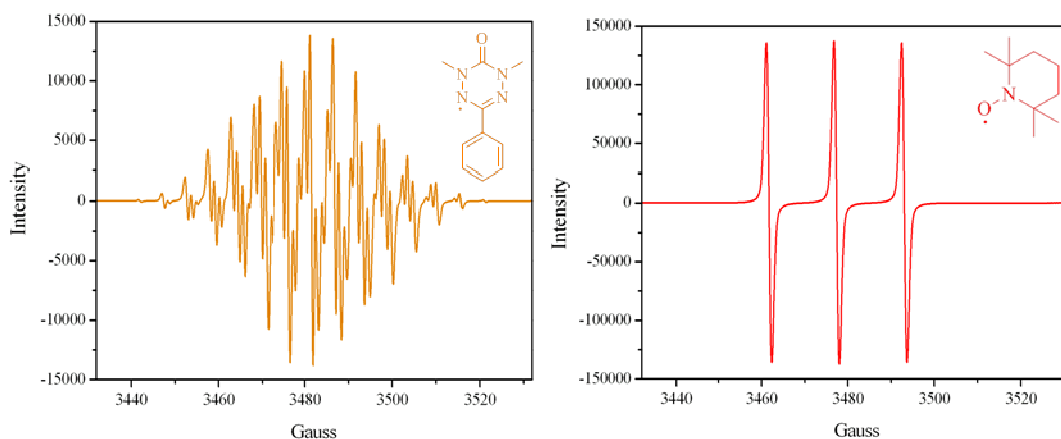


Figure 1.3-2. Simulation of **8 (left) and TEMPO (right) at t = 2 h from the exchange reaction**

It is possible to estimate the concentration of each radical and this was carried out for this reaction. Solutions of radical (both **8** and TEMPO) at known concentrations were run in the EPR spectrometer and the resulting spectra doubly integrated and normalised. The double integration was calculated using the Bruker WinEPR program using the simulations for both radicals. The DI/N values have not been normalised for the correct experimental receiver gain as the WinEPR Simfonia program does not permit the experimental parameter to be changed. The result is a calibration plot which relates intensity to concentration. Table 1.3-1 shows the approximate concentrations of both radicals for the samples taken during the exchange reaction calculated from the calibration.

Table 1.3-1. Approximate concentrations of 1,5-dimethyl-3-phenyl-6-oxoverdazyl (8**) and TEMPO at selected time intervals during the exchange reaction.**

Time (h)	[8] (M)	[TEMPO] (M)
0	0.032	0
0.5	0.061	0.014
1	0.061	0.014
1.5	0.069	0.014
2	0.069	0.015

As expected no signal was seen for TEMPO at $t = 0$ hours. The signal for TEMPO was visible after 0.5 hours and remained constant over the remainder of the reaction. There is some error observed as the concentration of the first sample for the verdazyl radical ($t = 0$) is lower than that observed for other samples. It can be seen from overlaying the EPR traces that the intensity of **8** at $t = 0$ is lower than the signal at 0.5 hours (Figure 1.3-3). The same error can account for the values for the concentration of **8** increasing over the duration of the reaction.

The major problem with these results lies with the simulations. The overlap of the two signals in the EPR spectra has the effect of altering the signal sufficiently to make it difficult to match the intensity of the signal for **8** ($R = Ph$) correctly and the concentrations can therefore not be calculated accurately. It is easier to simulate the TEMPO signal due to it being the more prominent and simpler signal. The TEMPO signal was visible after the first half hour, as expected, and the concentration values do not change greatly throughout the reaction. For more accurate concentration values, the samples from the exchange reaction would need to be reanalysed using a

technique such as ENDOR in order to separate the two signals.¹⁰² This was not followed up for this reaction as ^1H NMR analysis showed this to be an inefficient reaction for initiator synthesis.

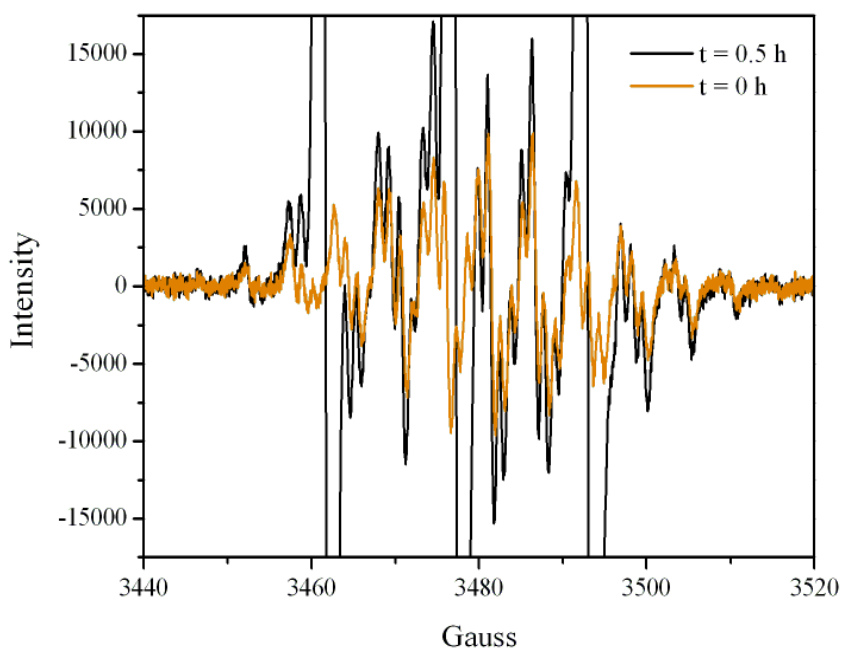


Figure 1.3-3. Comparison of EPR spectra from the exchange reaction at $t = 0$ (—) and 0.5 (—) hours zoomed in to the signal for **8 ($\text{R} = \text{Ph}$)**

The exchange reaction was attempted for a second time using ascorbic acid, which reacts with nitroxides to give the hydroxylamine³⁰, in an attempt to increase the yield by removing the free TEMPO.⁵³ Some of the desired product was visible in ^1H NMR, however, the compound was difficult to purify and the yield was low. Figure 1.3-4 shows the ^1H NMR spectra from the attempts at the exchange reaction along with the spectra for the nitroxide initiator (**12**). Characteristic features of **12** (bottom trace, red) are the broad peaks between 0.6 and 1.8 ppm which relate to the four methyl groups of the TEMPO moiety. If the exchange reaction was successful we

would expect these peaks to disappear and peaks relating to the verdazyl radical (**8**, R = Ph) to appear at approximately 2.65 and 3.34 ppm.⁵³ It is also expected that the peaks relating to the rest of **12** should still be visible, in particular between 4 and 5 ppm, but may change slightly in chemical shift.

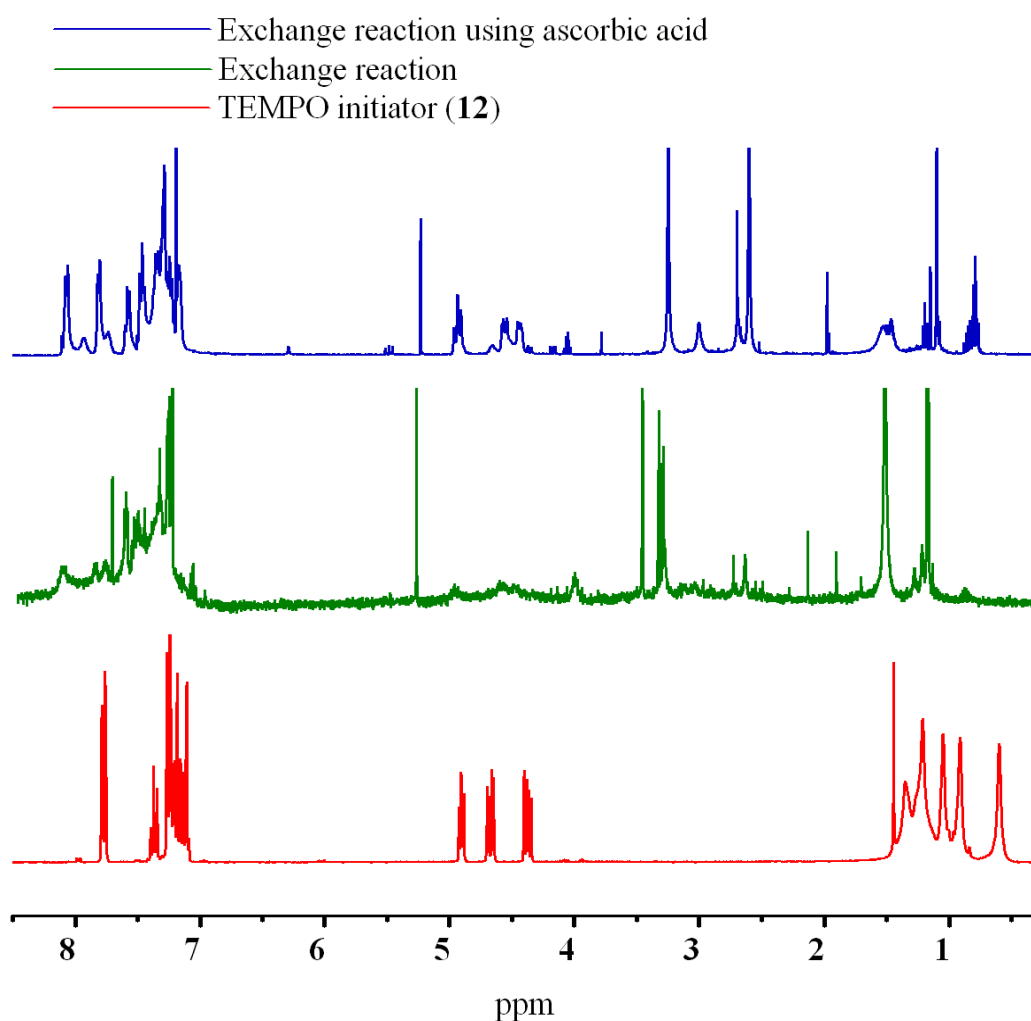
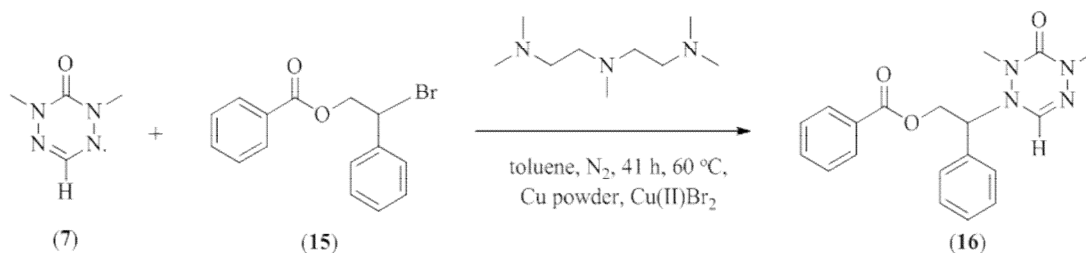


Figure 1.3-4. ¹H NMR spectrum of TEMPO initiator (—), the first attempt at the exchange reaction (—), attempt at the exchange reaction using ascorbic acid (—)

The green trace is the first attempt at the exchange reaction after attempts at purification. The top trace (blue) is the reaction incorporating ascorbic acid after purification. Silica gel column chromatography was attempted to purify the two reactions and removed the peaks associated with the TEMPO moiety. In the green trace the two peaks associated with the verdazyl are small and the other peaks that would be expected for the initiator moiety are also very weak. The two verdazyl peaks are quite strongly visible in the blue trace, however, despite purification there is still a large amount of impurities present. This suggests that this reaction does produce the desired product, however, it is difficult to purify and the yield low.

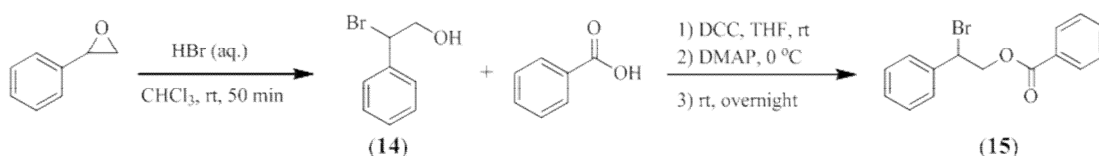
1.3.2. Atom transfer radical addition reaction

The alternative route is to use an ATRA reaction described in the work by Georges⁵³ which is a modified procedure from that described by Matyjaszewski *et al.*¹⁰³ It proceeds by the transfer of a halogen atom to the copper atom leaving a free radical species for the verdazyl to react with and form the initiator. This reaction was attempted initially using **7** (R = H), following the procedure described in the literature⁵³, which described how the exchange reaction did not work for this particular radical (Scheme 1.3-3).



Scheme 1.3-3. Atom transfer radical addition reaction for the synthesis of 2-phenyl-2-(1,5-dimethyl-6-oxoverdazyl)ethyl benzoate (16)

Prior to the reaction 2-bromo-2-phenylethyl benzoate (**15**) was synthesised (Scheme 1.3-4). Hydrobromic acid was added dropwise to a solution of styrene oxide in chloroform. Stirring at ambient temperature for about an hour, washing with saturated sodium hydrocarbonate solution and water and removing the solvent gives 2-bromo-2-phenylethanol (**14**). To synthesise **15**, benzoic acid is added to **14** dissolved in THF, followed by *N,N'*-dicyclohexylcarbodiimide (DCC) and 4-(dimethylamino)pyridine (DMAP). The solution is stirred overnight and purified by silica gel column chromatography with 5:4:1 dichloromethane/petroleum ether 40-60/diethyl ether as the eluent.



Scheme 1.3-4. Synthesis of 2-bromo-2-phenylethyl benzoate (15)

For the ATRA reaction, verdazyl radical **7** (R = H) and **15** was dissolved in toluene and degassed by freeze-pump-thaw cycles in a Schlenk tube also containing PMDETA. The solution was then cannulated into a degassed and nitrogen filled two-neck round bottom flask containing both copper powder and Cu(II)Br₂ and heated at 60 °C under nitrogen for approximately 40 hours. Samples were taken from the reaction at t = 0, 1.5 and 40.5 hours for EPR analysis. It was expected that the strong radical signal observed at the start of the reaction would reduce until almost completely gone as the reaction proceeds. Figure 1.3-5 shows the EPR spectra for the samples.

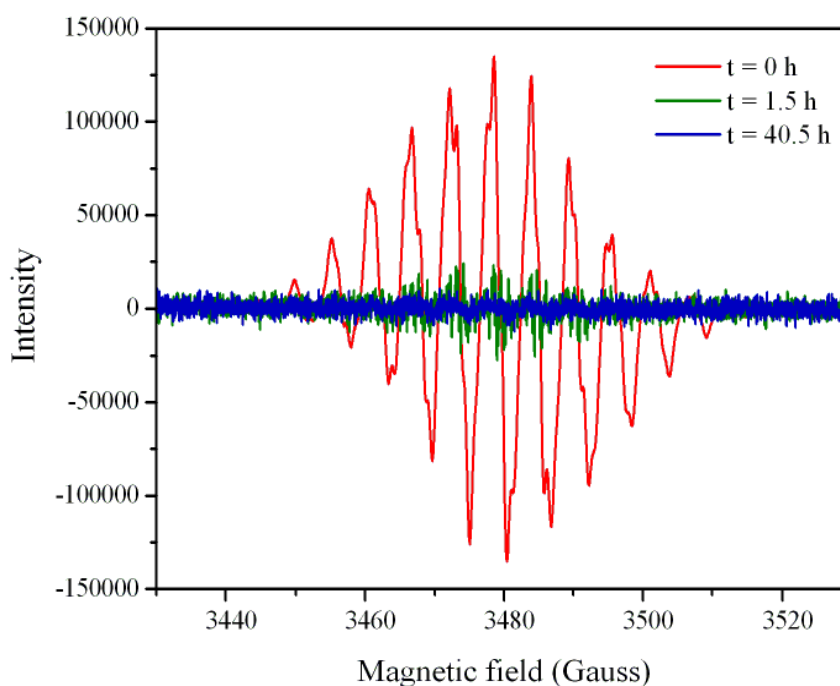


Figure 1.3-5. EPR traces from the ATRA reaction for the synthesis of 2-phenyl-2-(1,5-dimethyl-6-oxoverdazyl)ethyl benzoate (16**)**

As expected the strong signal seen for **7** (R = H) has been dramatically reduced after 1.5 hours. Using a calibration prepared for **7** and TEMPO, the intensity of the signal has been related to concentration (Table 1.3-2).

Table 1.3-2. Concentrations of 1,5-dimethyl-6-oxoverdazyl (7**) at selected time intervals during the ATRA reaction.**

Time (h)	[7] (mM)
0	4.79
1.5	0.03
40.5	0.03

Over the course of this work, four initiators were synthesised using the ATRA method using radicals **7** (R = H), **8** (R = Ph), **10** (R = PhOMe) and **11** (R = PhNO₂) to give **16** (32%), **13** (63%), **17** (36%) and **18** (49%) respectively (Figure 1.3-6). The assigned ¹H NMR spectrum of each initiator is displayed in Figures 1.3-7 to 13.10.

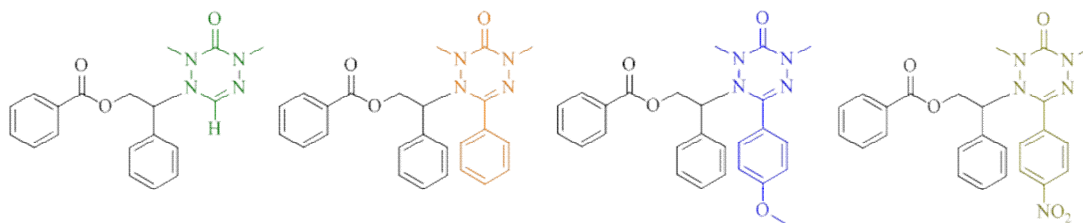


Figure 1.3-6. Verdazyl initiators 2-phenyl-2-(1,5-dimethyl-6-oxoverdazyl)ethyl benzoate (16**), 2-phenyl-2-(1,5-dimethyl-3-phenyl-6-oxoverdazyl)ethyl benzoate (**13**), 2-phenyl-2-(1,5-dimethyl-3-methoxyphenyl-6-oxoverdazyl)ethyl benzoate (**17**) and 2-phenyl-2-(1,5-dimethyl-3-nitrophenyl-6-oxoverdazyl)ethyl benzoate (**18**)**

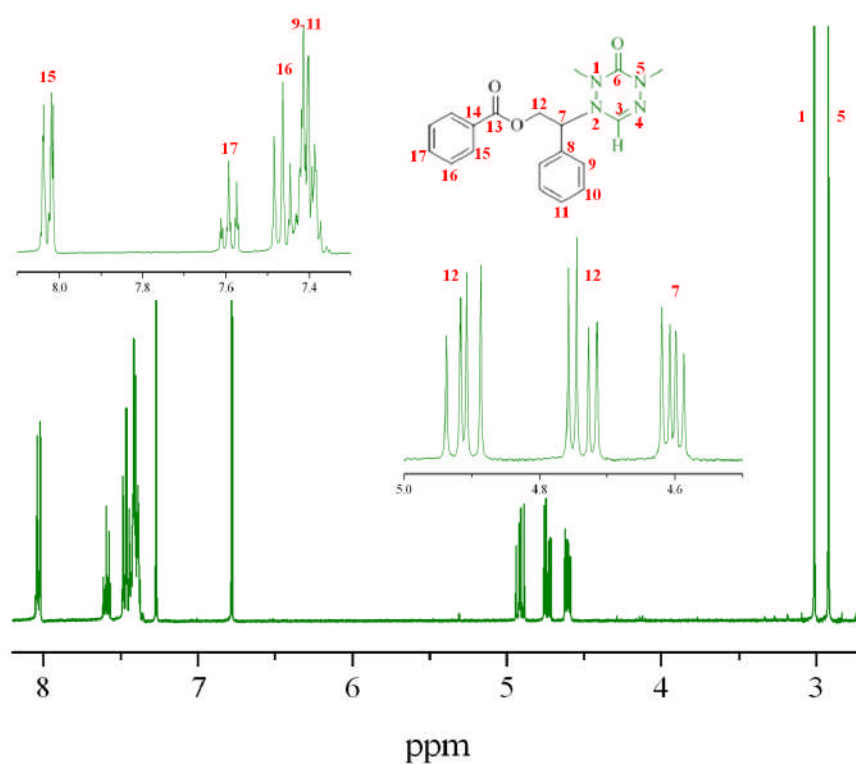


Figure 1.3-7. Assigned ¹H NMR spectrum of 16

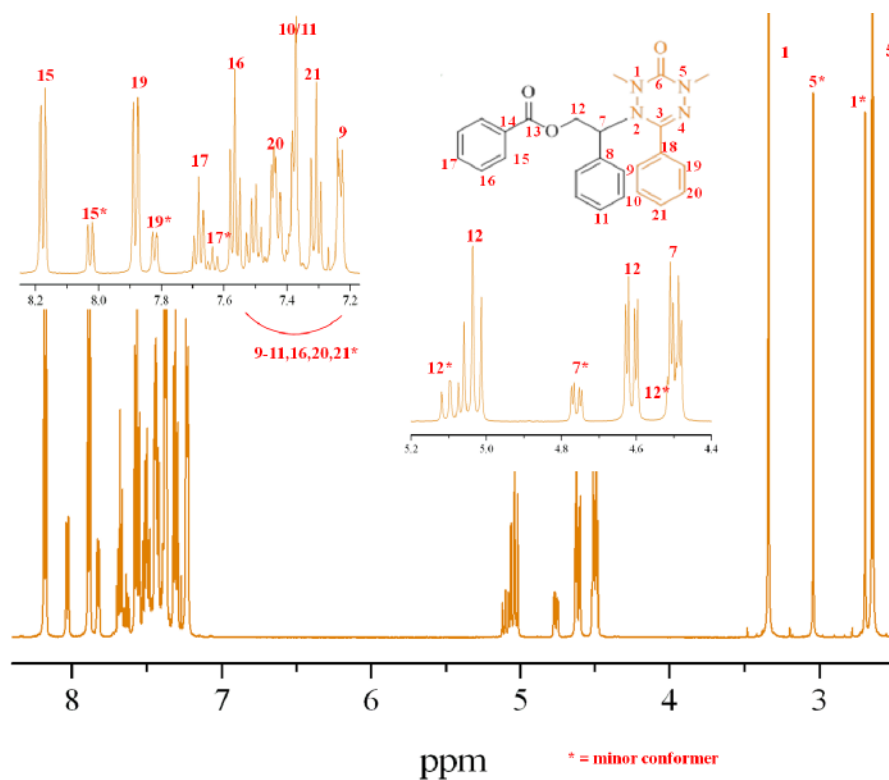


Figure 1.3-8. Assigned ¹H NMR spectrum of 13

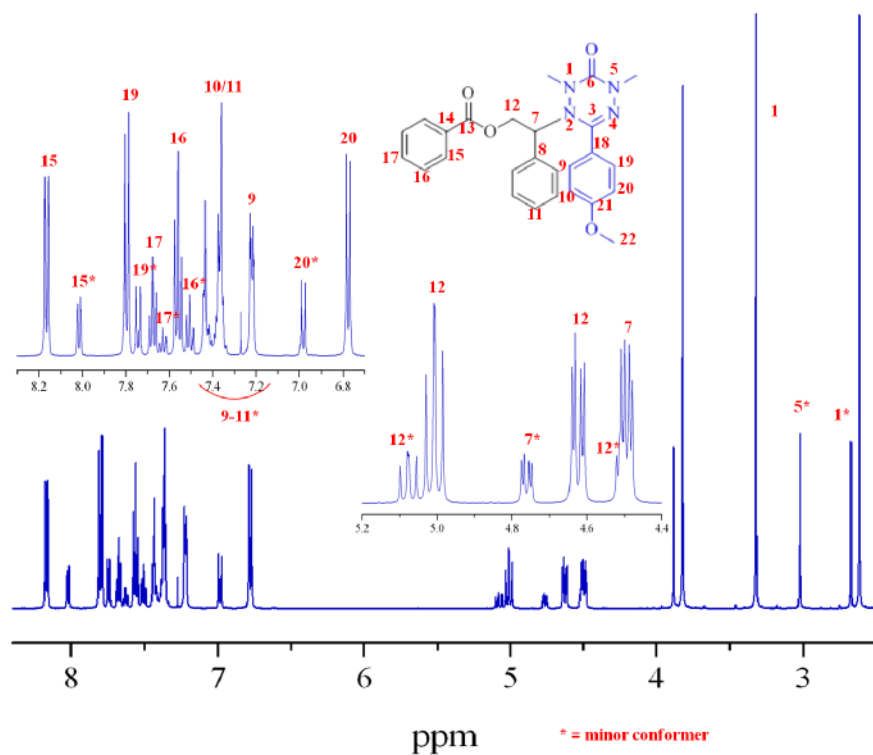


Figure 1.3-9. Assigned ^1H NMR spectrum of 17

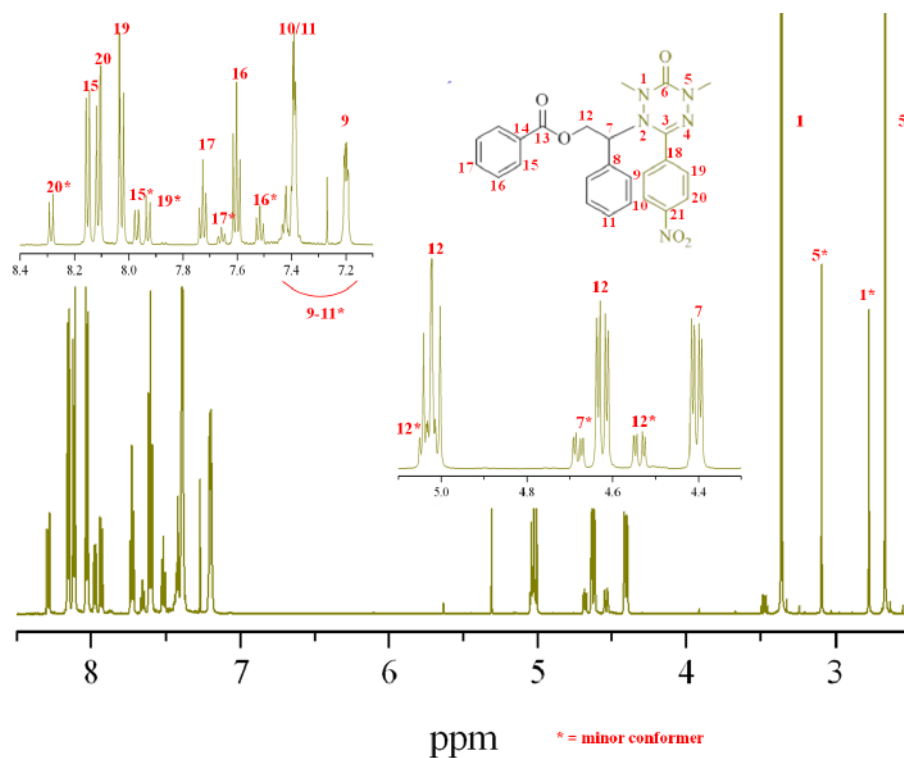


Figure 1.3-10. Assigned ^1H NMR spectrum of 18

At ambient temperature, the ^1H NMR spectra of **13** (R = Ph), **17** (R = PhOMe) and **18** (PhNO₂) are broadened with additional peaks. This is due to the molecules existing as conformers in solution due to rotation around the C-N bond.⁵³ Recording the spectra at -20 °C allows for greater definition and separation of the peaks and is illustrated in Figure 1.3-11 for **13** (R = Ph). The percentage of the two conformers was determined from the integrals of the verdazyl methyl peaks.

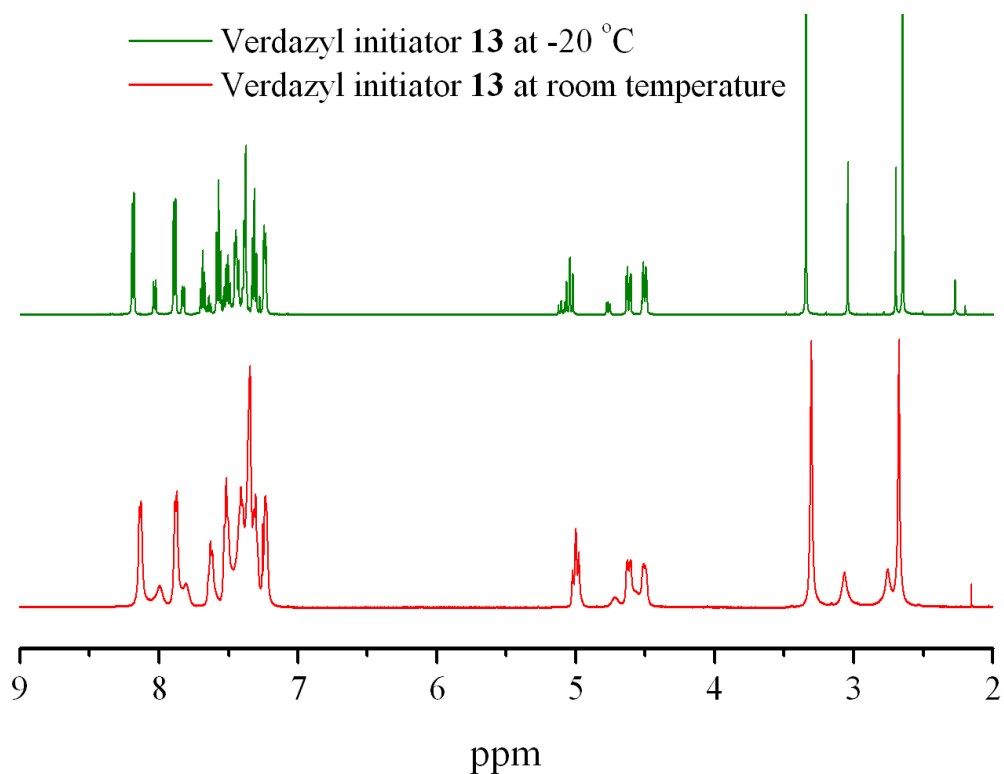


Figure 1.3-11. ^1H NMR spectra of 2-phenyl-2-(1,5-dimethyl-3-phenyl-6-oxoverdazyl)ethyl benzoate (**13**) at room temperature (—) and at -20 °C (—)

Further studies were carried out to investigate the structures of the two conformers for **13** (R = Ph). Initially, Nuclear Overhauser effect (NOE) NMR experiments were

completed by Dr. Ivan Prokes, University of Warwick. Unfortunately it was observed that when irradiating a ‘major’ peak, the corresponding ‘minor’ peak was also affected. This occurred with all the peaks in the spectrum. Further analysis by Dr. Prokes confirmed that there is only one compound in solution and that at different temperatures two different orientations exist, as opposed to two similar compounds. However, as they are so similar, the structures of both of these orientations have yet to be identified using NMR methods.

A molecular structure (Figure 1.3-12) of **13** (R = Ph) has been obtained. Immediately it is noticeable that the orientation of the molecule is completely different to the general structure used throughout this thesis.

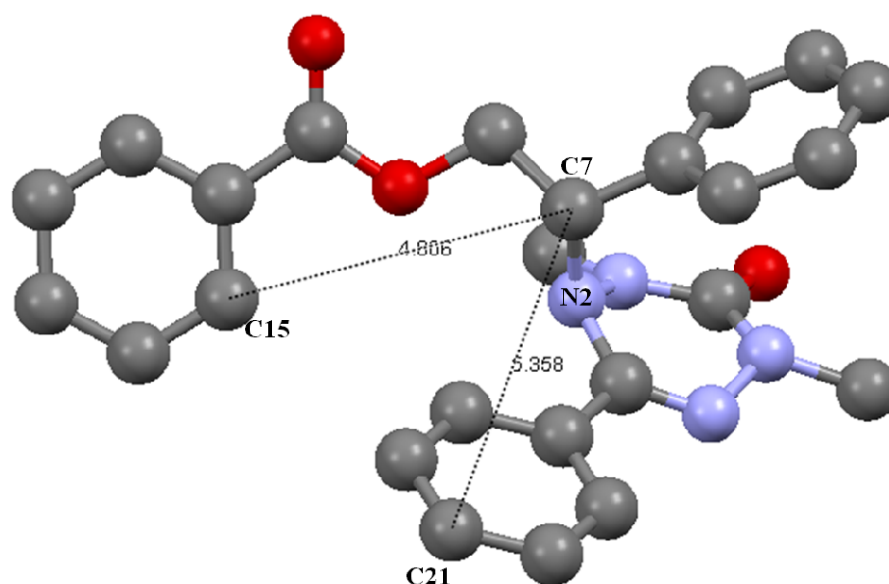


Figure 1.3-12. Molecular structure of 2-phenyl-2-(1,5-dimethyl-3-phenyl-6-oxoverdazyl)ethyl benzoate (13) determined by X-ray crystallography with selected atom distances and atom labels

As seen with the computational studies the phenyl group in the 3 position is planar to the rest of the verdazyl rather than orthogonal to it, as seen for tetrazinanone intermediate **4** (R = Ph) displayed in Figure 1.2-2. The two atomic distances included on the crystal structure may offer some insight to the two possible conformers observed for this molecule. The distance between C7 and C15 is 4.81 Å and the distance between C7 and C21 is 5.36 Å. Rotation about the bond between C7 and N2 may become restricted by the ethyl benzoate moiety incorporating C15. As a result, the two conformers may be the phenyl substituent on the verdazyl being in front of and behind the ethyl benzoate group. This would provide an explanation as to why two conformers are not seen for **16**, which lacks a bulky substituent at the 3 position. Crystals adequate to obtain a structure have not been obtained for the other initiators.

1.4. Verdazyl mediated polymerisation

1.4.1. Polymerisation of styrene

The polymerisation of styrene was attempted using a similar procedure to that described by Georges.⁵³ The monomer was stabilised with free verdazyl at a concentration of 1 mg of verdazyl per 40 mL of styrene. The verdazyl radical used to stabilise the monomer was the same as that in the initiator used in the polymerisation, in this case verdazyl initiator **16** (R = H) and verdazyl radical **7** (R = H). The polymerisation was performed in bulk at 125 °C using mesitylene as an internal standard to determine conversion by ¹H NMR. After 50 hours, 71% conversion had been reached.

The pseudo first order kinetic plot shown in Figure 1.4-1 (●) is linear indicating that the concentration of propagating radicals remains relatively constant throughout the reaction. However, it should be noted that the rate began to slow down over time, seen as the kinetic plot starting to curve (after approximately 40 hours). The polymerisation mixture was yellow at the end of the reaction indicating a build up of free radical, due to termination reactions, which can inhibit the polymerisation reaction. The molecular weight versus conversion plot (Figure 1.4-2, ●) shows that the experimental values for the molecular weight deviated from the calculated theoretical molecular weights, in particular at conversions above 30% where the molecular weight plateaus at a lower molecular weight than targeted.

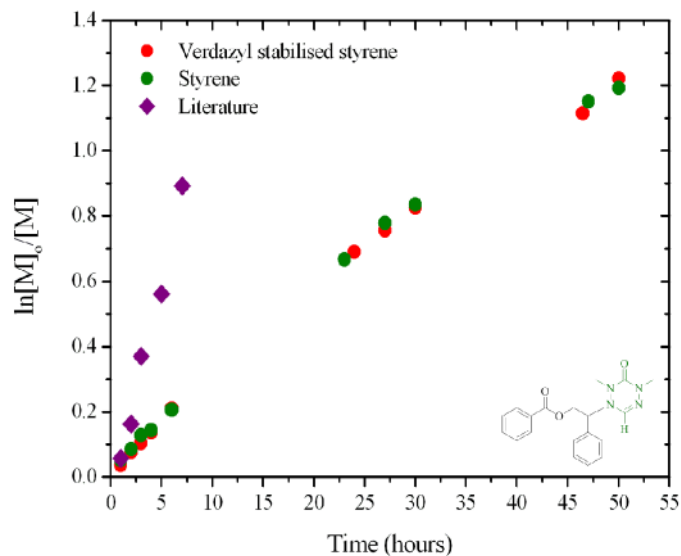


Figure 1.4-1. First order kinetic plot for the verdazyl mediated polymerisation of styrene by 16 (R = H) using verdazyl stabilised styrene (●), styrene (●) and results from the literature (◆)⁵³

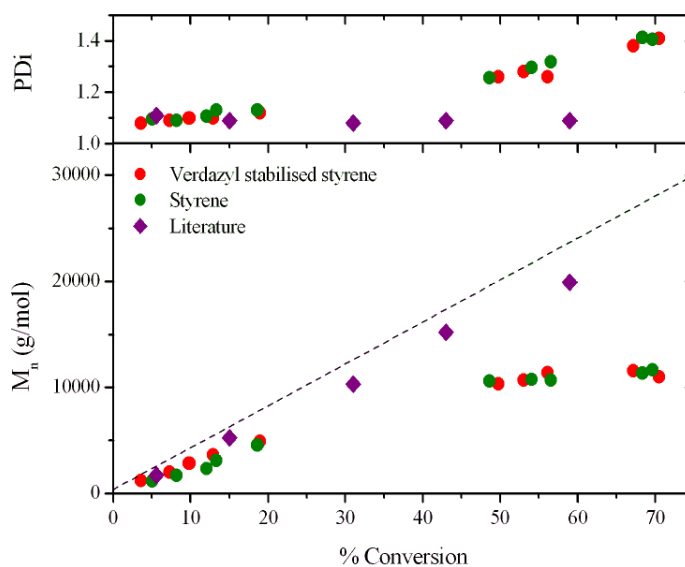


Figure 1.4-2. Evolution of molecular weight (M_n) and PDI versus conversion for the verdazyl mediated polymerisation of styrene by 16 (R = H) using verdazyl stabilised styrene (●), styrene (●) and results from the literature (◆)⁵³, DP = 380, target $M_n = 39,500$ g/mol (- - -)

The kinetic plot shows the concentration of radical to be constant for the majority of the reaction indicating that the monomer is being consumed at a steady rate, however, the levelling out of the molecular weight indicates that chain termination occurs. The number average molecular weight (M_n) is plotted against conversion in Figure 1.4-2 and even though some monomer chains are getting longer, the number of terminated lower molecular weight chains is also increasing which overall averages out for no change in the value. This is confirmed by an increase in polydispersity as the molecular weight plateaus and can be visualised in the differential molecular weight distributions¹⁰⁴ as a low molecular weight tail (Figure 1.4-3).

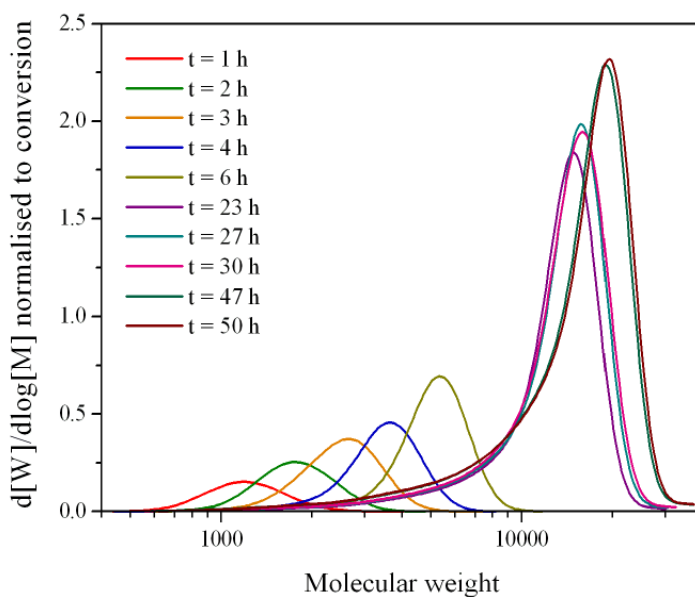


Figure 1.4-3. Overlaid differential molecular weight distribution curves for the verdazyl mediated polymerisation of styrene (●) by 16 (R = H)

The reaction was then repeated, this time without stabilising the monomer with free verdazyl prior to performing the reaction. The polymerisation produced identical results (Figures 1.4-1 and 1.4-2, ●), also reaching 70% conversion in 50 hours. As no differences were observed, styrene was not stabilised in further reactions.

Verdazyl initiator **13** (R = Ph) was investigated and the same trends were seen as with **16** (R = H). A linear kinetic plot was observed (Figure 1.4-4, ▲) and the molecular weight plateaued along with an increase in polydispersity (Figure 1.4-5, ▲) towards the end of the reaction.

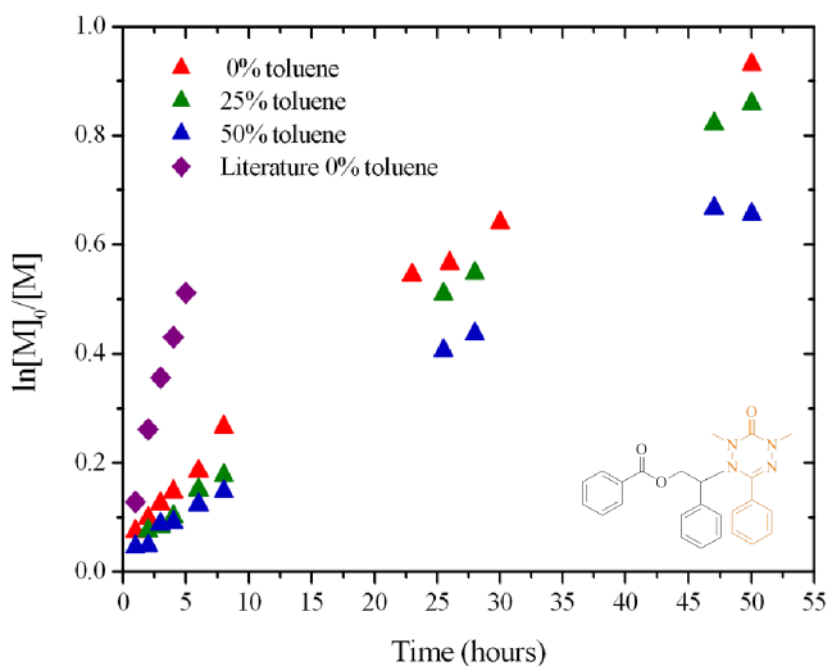


Figure 1.4-4. First order kinetic plot for the verdazyl mediated polymerisation of styrene with 0% (▲), 25% (▲), 50% (▲) and literature values for 0% (◆)⁵³ toluene with respect to monomer by **13 (R = Ph)**

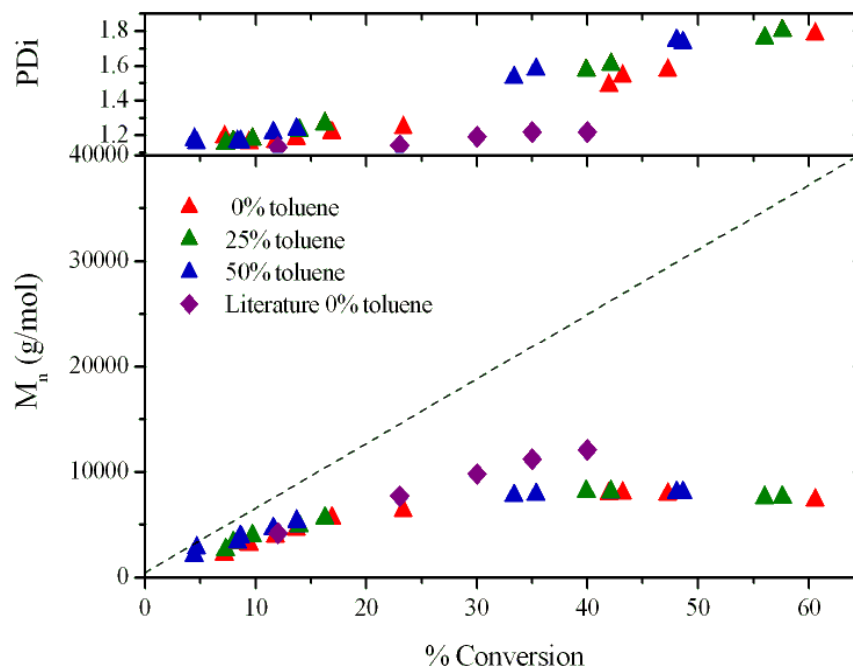


Figure 1.4-5. Evolution of molecular weight (M_n) and PDI versus conversion for the verdazyl mediated polymerisation of styrene with 0% (\blacktriangle), 25% (\blacktriangle), 50% (\blacktriangle) and literature values for 0% (\blacklozenge)⁵³ toluene with respect to monomer by **13 ($R = Ph$), $DP = 485$, target $M_n = 50,500$ g/mol (---)**

As the polymerisations were carried out in bulk it was speculated that increasing viscosity in the polymerisation mixture may affect growth of the polymer. Therefore, two further reactions were performed (Figure 1.4-4) using **13** ($R = Ph$) with either 25% (\blacktriangle) or 50% (\blacktriangle) toluene with respect to styrene. As expected, the rate of polymerisation slowed with increasing amount of solvent, but the molecular weight and polydispersity showed the same trends and almost identical values (Figure 1.4-5).

The polymerisation of styrene in bulk at 125 °C was then repeated for each of the four verdazyl initiators and the TEMPO initiator in order to observe if any differences between radicals. Figure 1.4-6 shows the kinetic data for the five polymerisations.

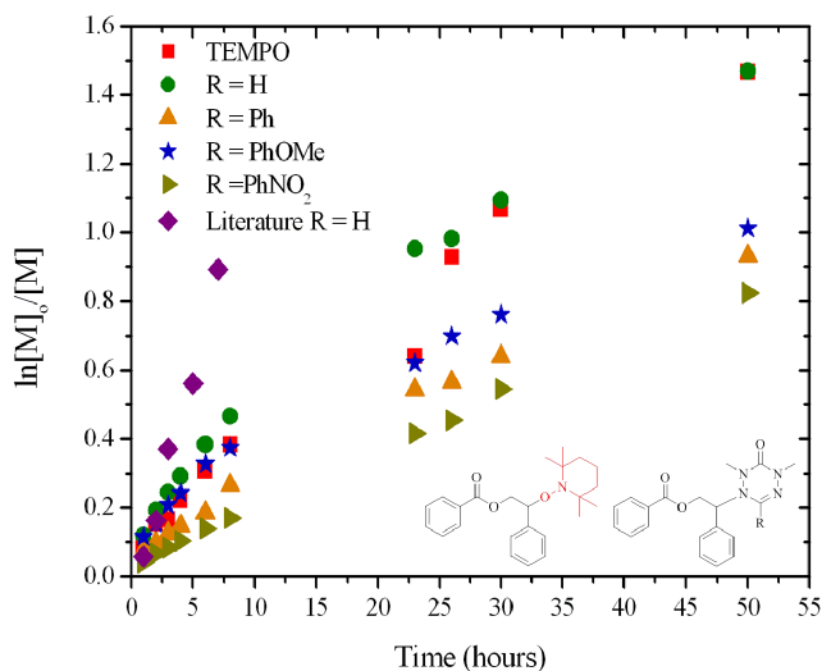


Figure 1.4-6. First order kinetic plot for the verdazyl mediated polymerisation of styrene by **12**

(**12**, **16** (●), **13** (▲), **17** (★), **18** (▶) and literature values for **16** (◆)⁵³

Slight differences were observed between initiators. Verdazyl initiator **16** (R = H, ●) displayed the same rate as the TEMPO initiator (**12**, ■). Adding the phenyl substituents to the verdazyl results in a reduction of the rate in the order of PhNO₂ (▶) < Ph (▲) < PhOMe (★). The rate was seen to slow down over time in a more pronounced fashion for **17** (R = PhOMe, ★) then for any of the other initiators. The

molecular weight plot (Figure 1.4-7) shows that the same trends as already seen with **13** (R = Ph) and **16** (R = H).

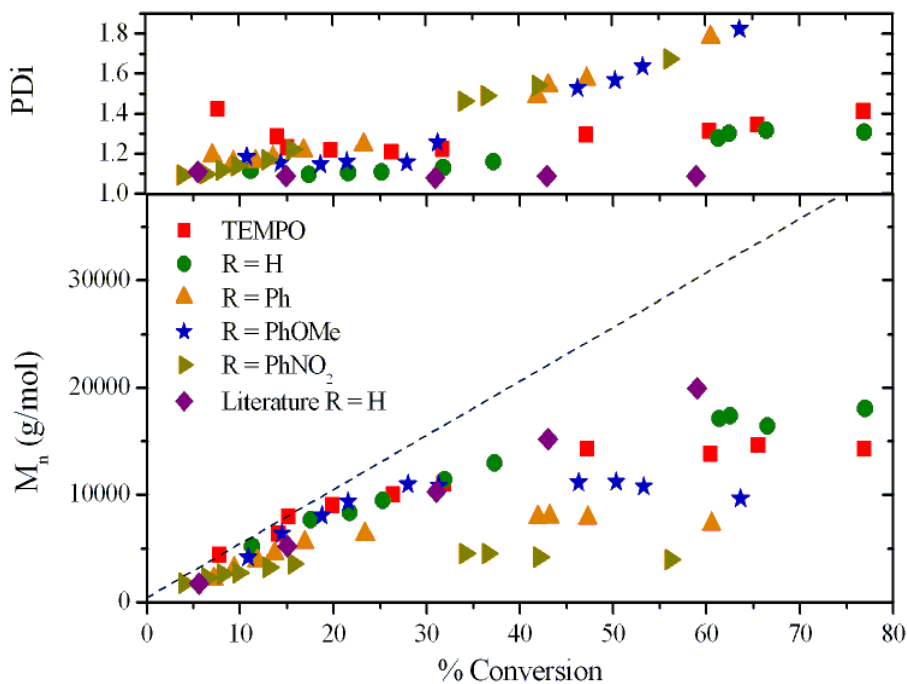


Figure 1.4-7. Evolution of molecular weight (M_n) and PDI versus conversion for the verdazyl mediated polymerisation of styrene by **12 (■), **16** (●), **13** (▲), **17** (★), **18** (▶) and literature values for **16** (◆)⁵³, DP = 485, target M_n = 50,500 g/mol (- -)**

The slower rate resulted in low conversion for **18** (PhNO₂, ▶) and the lowest molecular weight of all five initiators was observed. The trend in rate for the phenyl substituted verdazyls ran through with the molecular weight so that molecular weights were observed in the order PhNO₂ (▶) < Ph (▲) < PhOMe (★). Initiators **16** (R = H, ●) and **12** (TEMPO, ■) reached the same conversion and molecular weights were similar, although were slightly higher for the verdazyl initiator. The polydispersities were substantially higher for the phenyl substituted verdazyls than

for **12** (TEMPO) and **16** (R = H). Figure 1.4-8 compares the differential molecular weight distributions for the polymerisation of styrene by **16** (R = H) and **18** (R = PhNO₂). Low molecular weight tails were visible in both polymerisations after 8 hours; however, the distribution was much broader in the latter.

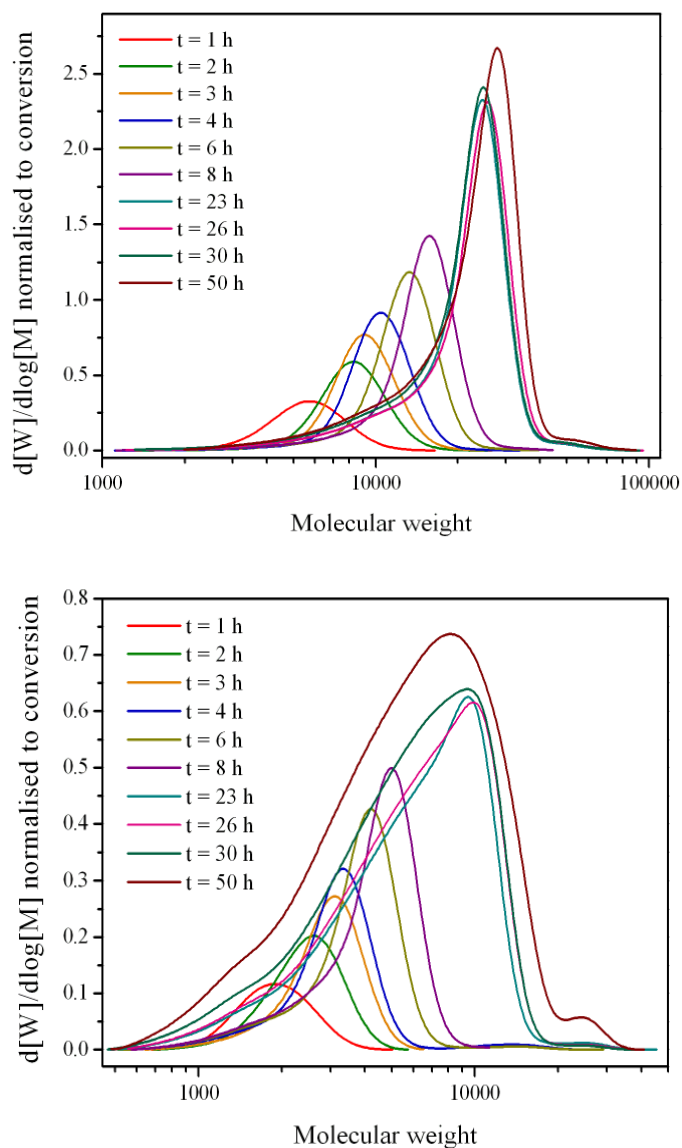


Figure 1.4-8. Overlaid differential molecular weight distribution curves for the verdazyl mediated polymerisation of styrene by **16 (R = H, ●, top) and **18** (R = PhNO₂, ►, bottom)**

In the literature⁵³, results are reported up to between 5-7 hours for the polymerisation of styrene at which conversions were around 40%. This suggests that above this conversion the same low molecular weight tail was observed and were therefore not included. This was confirmed during email correspondence with Georges.¹⁰⁵ These results indicate that it is possible to polymerise styrene using verdazyls; however, an improvement over TEMPO mediated polymerisation has not been established.

1.4.2. Polymerisation of *n*-butyl acrylate

Attention then turned to the polymerisation of *n*-butyl acrylate using the same set of verdazyl radicals. Unstabilised monomer was initially used with **13** (R = Ph) in bulk at 130 °C. The reaction proceeded faster than that observed with styrene (90% conversion in 26 hours) but non-linear first order kinetics with respect to monomer were observed with the reaction starting slowly before accelerating (Figure 1.4-9). The rate constant of propagation (k_p) for butyl acrylate at elevated temperatures is much higher than that observed for styrene, with $k_p = 11,000$ L/mol/s for butyl acrylate and $k_p = 1,800$ L/mol/s for styrene, and as such results in a faster polymerisation at the same temperature.³¹ Polydispersities > 2 were observed along with lower molecular weights than expected (Figure 1.4-10).

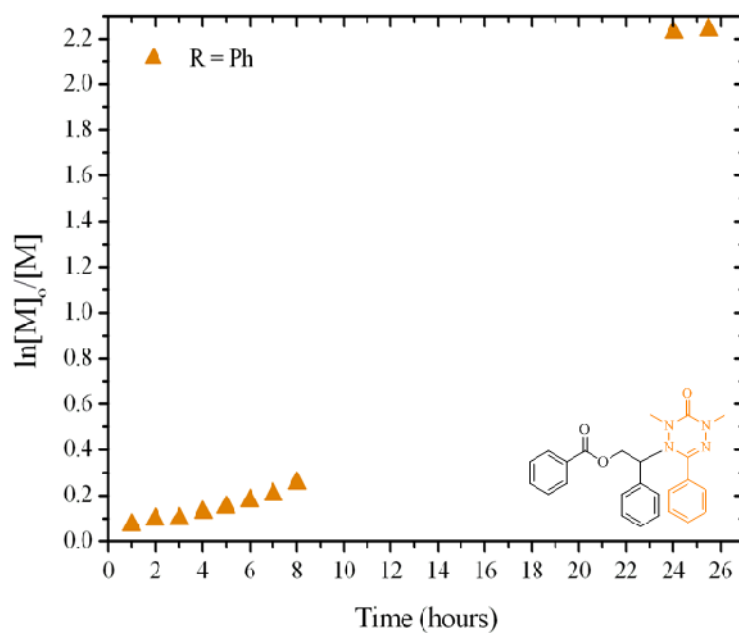


Figure 1.4-9. First order kinetic plot for the verdazyl mediated polymerisation of *n*-butyl acrylate by 13 (R = Ph)

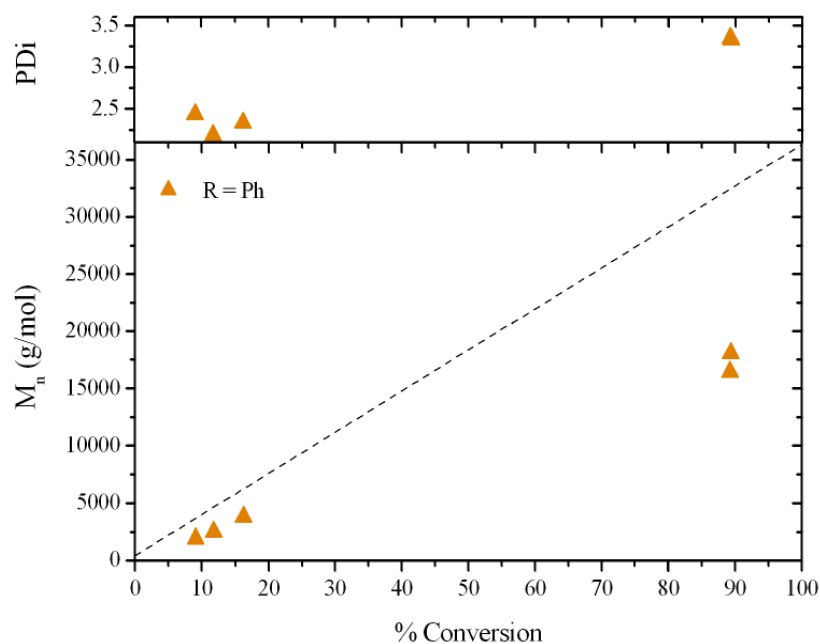


Figure 1.4-10. Evolution of molecular weight (M_n) and PDI versus conversion for the verdazyl mediated polymerisation of *n*-butyl acrylate by 13 (R = Ph), DP = 280, target $M_n = 35,900$ g/mol

(- - -)

These results indicate that the polymerisation did not proceed in a controlled manner as would be expected for a controlled/living system. Repeating the reaction with stabilised *n*-butyl acrylate (1 mg of verdazyl per 40 mL) slowed the polymerisation down and lowered the polydispersity (Figures 1.4-11 and 1.4-12, ▲). It did not provide the linear first order kinetics with respect to monomer expected for a controlled radical polymerisation and the molecular weight was again low.

Due to the limited availability of verdazyl initiators, all polymerisations up until this point in the work had been performed on a small scale (between 1 and 3 mL of monomer). It was therefore deemed prudent to repeat the reaction as described in the literature at the same 15 mL scale (Figures 1.4-11 and 1.4-12, ▲)⁵³. A 9 mL reaction was also performed and is also displayed in Figures 1.4-11 and 1.4-12 (▲) alongside the results published in the literature (▲).

Increasing the volume of the reaction to 15 mL slowed down the reaction further and linear first order kinetics with respect to monomer were obtained although, as seen with styrene and in the literature (▲), the reaction did slow down over time. The 9 mL reaction was slower than the 15 mL (25% conversion in 28 hours) and after 28 hours had only reached 13% conversion. Both reactions were slower than the literature values, however, the observed molecular weights for both reactions was much closer to the theoretical values, and much more so than the literature (Figure

1.4-12). The polydispersities of all four reactions started relatively high, but narrowed as the reaction proceeded.

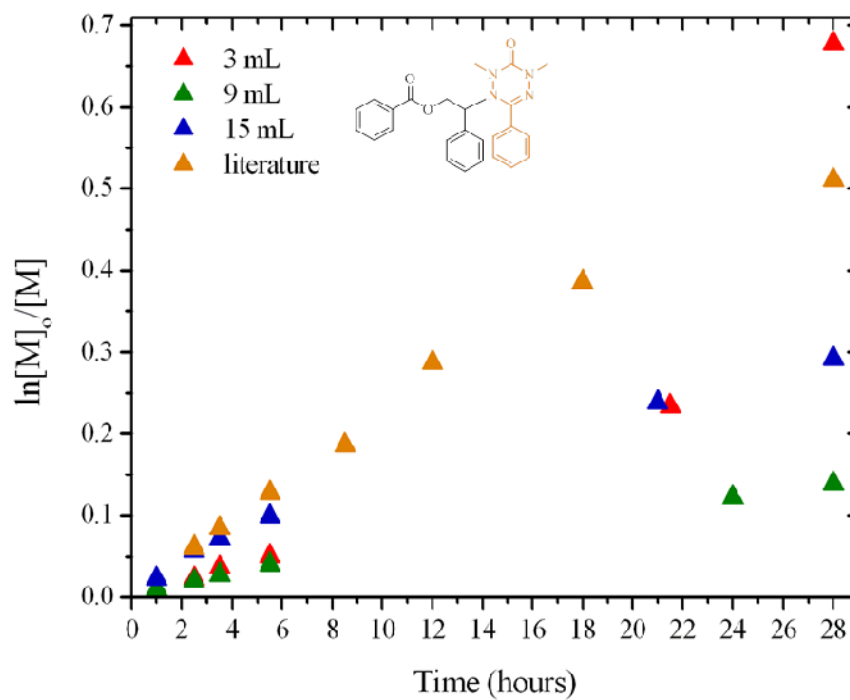


Figure 1.4-11. First order kinetic plot for the verdazyl mediated polymerisation of verdazyl stabilised *n*-butyl acrylate by 13 (R = Ph) at different volumes (3 (▲), 9 (▲) and 15 (▲) mL) and results from the literature⁵³ (▲)

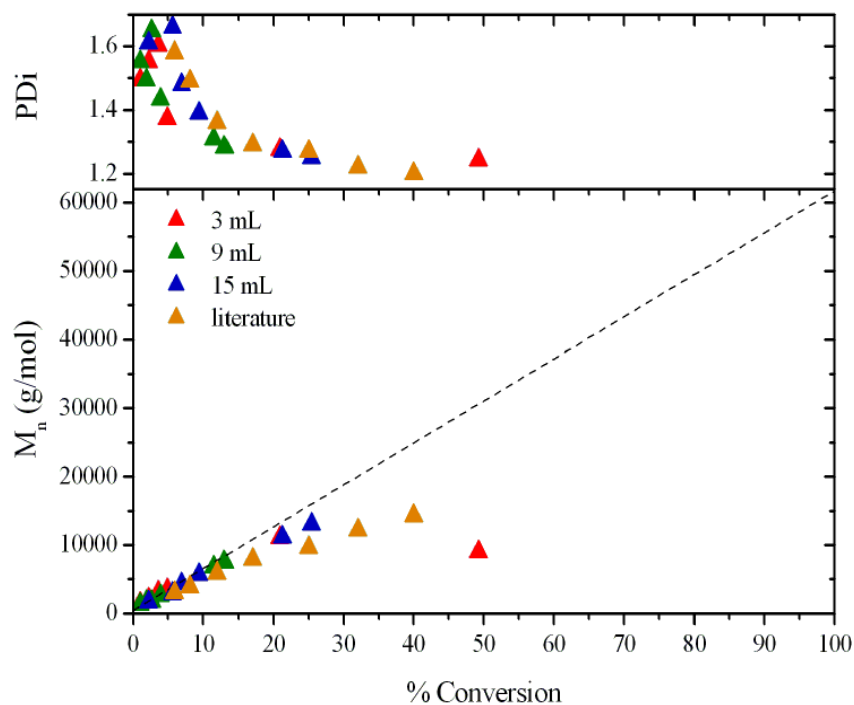


Figure 1.4-12. Evolution of molecular weight (M_n) and PDI versus conversion for the verdazyl mediated polymerisation of verdazyl stabilised *n*-butyl acrylate by **13 ($R = Ph$) at different volumes (3 (\blacktriangle), 9 (\blacktriangle) and 15 (\blacktriangle) mL) and results from the literature⁵³ (\blacktriangle), $DP = 478$, target $M_n = 61,300$ g/mol (---)**

The polymerisation of *n*-butyl acrylate at 130 °C was then performed on the 15 mL scale for the remaining verdazyl initiators **16** - **18** ($R = H$, PhOMe and PhNO₂) and for the TEMPO initiator (**12**) and the results are displayed in Figures 1.4-13 and 1.4-14 along with the results for **13** ($R = Ph$). The polymerisation of *n*-butyl acrylate by **12** (TEMPO, \blacksquare) proceeded to 5% conversion in the first five hours and only increased to 7% after 70 hours; similar to published results.²⁷

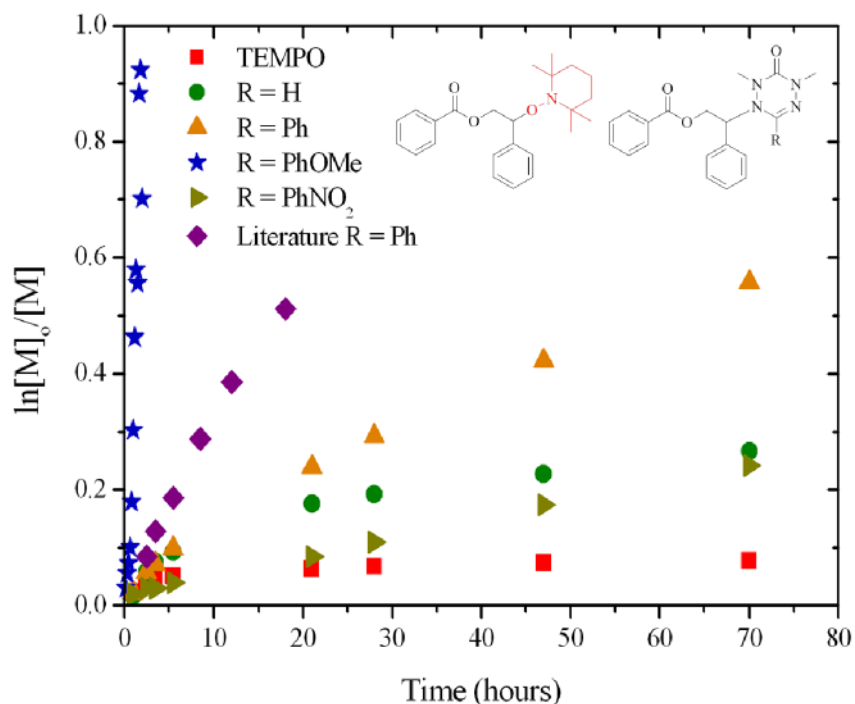


Figure 1.4-13. First order kinetic plot for the verdazyl mediated polymerisation of verdazyl stabilised *n*-butyl acrylate by **12** (■), **16** (●), **13** (▲), **17** (★), **18** (▶) and literature values for **13** (◆)⁵³

In comparison to TEMPO (■), all the verdazyl initiators showed an improvement. The polymerisations using **16** (R = H, ●) and **18** (R = PhNO₂, ▶) were the slowest, reaching approximately 20% conversion over the 70 hour reaction time. In contrast, **17** (R = PhOMe, ★) proceeded much faster, needing to be stopped after 2 hours due to the increased viscosity of the reaction mixture. Despite the speed of the reaction, linear first order kinetics with respect to monomer were observed. The molecular weight also increased linearly with conversion, although typically lower than the theoretical value (1.4-14, ★). Despite these encouraging results, the polydispersity

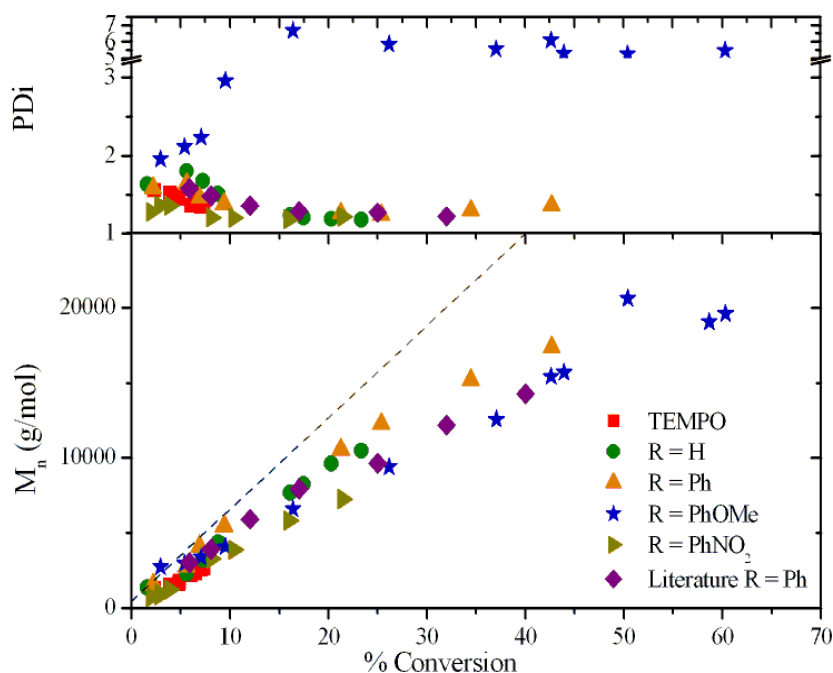


Figure 1.4-14. Evolution of molecular weight (M_n) and PDI versus conversion for the verdazyl mediated polymerisation of verdazyl stabilised *n*-butyl acrylate by **12** (■), **16** (●), **13** (▲), **17** (★), **18** (▶) and literature values for **13** (◆)⁵³, DP = 478, target M_n = 61,300 g/mol (- - -)

was very high (> 5) and the differential molecular weight distribution plot for **17** shows a bimodal system (Figure 1.4-15). This suggests that verdazyl radical **10** (R = PhOMe) is unstable at this polymerisation temperature. The decomposition of the radical would push the equilibrium towards the propagating species leading to an increase in termination reactions resulting in low molecular weights and high polydispersities.

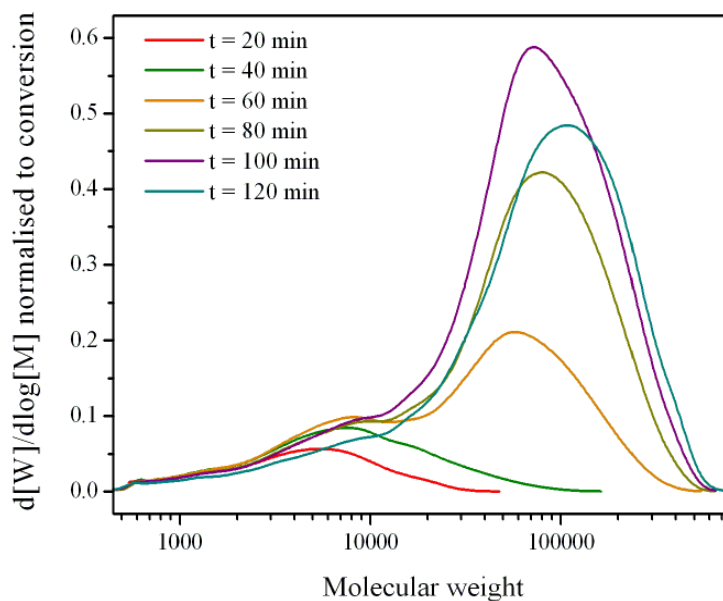


Figure 1.4-15. Overlaid differential molecular weight distribution curves for the verdazyl mediated polymerisation of verdazyl stabilised *n*-butyl acrylate by **17 (R = PhOMe, ★)**

Using **13** (R = Ph, ▲), which is slower than **17** (R = PhOMe), linear first order kinetics with respect to monomer (Figure 1.4-13) and a similar molecular weight to the polymer made using **17** was observed, but in this case an acceptable polydispersity was obtained (Figure 1.4-14). The difference can be seen in the differential molecular weight distribution plot for **13** (Figure 1.4-16) and traces are mono-modal and narrower.

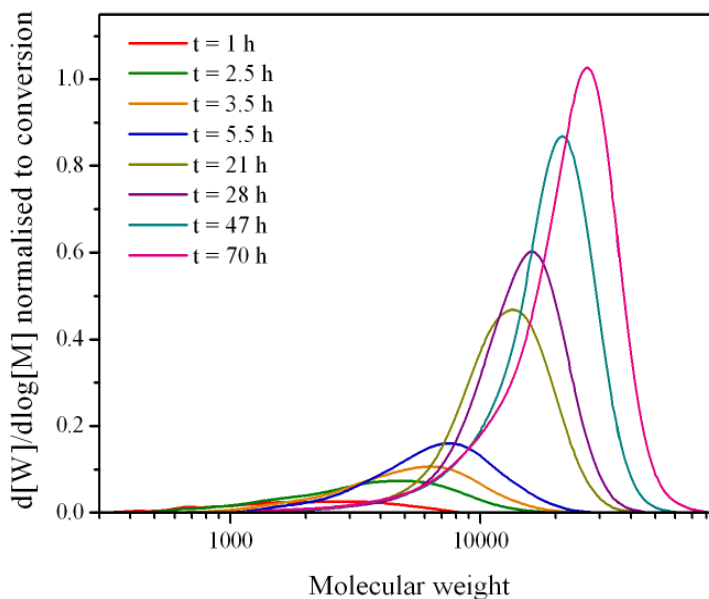


Figure 1.4-16. Overlaid differential molecular weight distribution curves for the verdazyl mediated polymerisation of verdazyl stabilised *n*-butyl acrylate by **13 (R = Ph, ▲)**

The ability of the verdazyls with large substituents at the 3 position on the radical to mediate the polymerisation of *n*-butyl acrylate is likely due to the slow destruction of the radical at the polymerisation temperature due to it being moderately unstable.⁵³ This prevents the build up of verdazyl in solution as seen with the TEMPO mediated polymerisation of acrylates. It is therefore assumed that at 130 °C verdazyl radical **7** (R = H) is more stable than the phenyl substituted verdazyls but less stable than TEMPO.

A small study was completed to investigate whether reducing the temperature would allow for a slower polymerisation of butyl acrylate by **17** (PhOMe) to take place to obtain a living polymerisation. Due to the lack of initiator available, one 15 mL

reaction was prepared and aliquots of 1.5 mL were used. Polymerisations were carried out at 10 degree intervals between 50 and 110 °C. Between 50 and 80 °C no polymerisation was observed over 22 hours. A slow polymerisation (Figure 1.4-17, ★) occurred at 90 °C where 14% conversion was obtained after 22 hours. The molecular weight was approximately as it should be according to the theoretical molecular weight (Figure 1.4-18, ★), however, the polydispersity was relatively high.

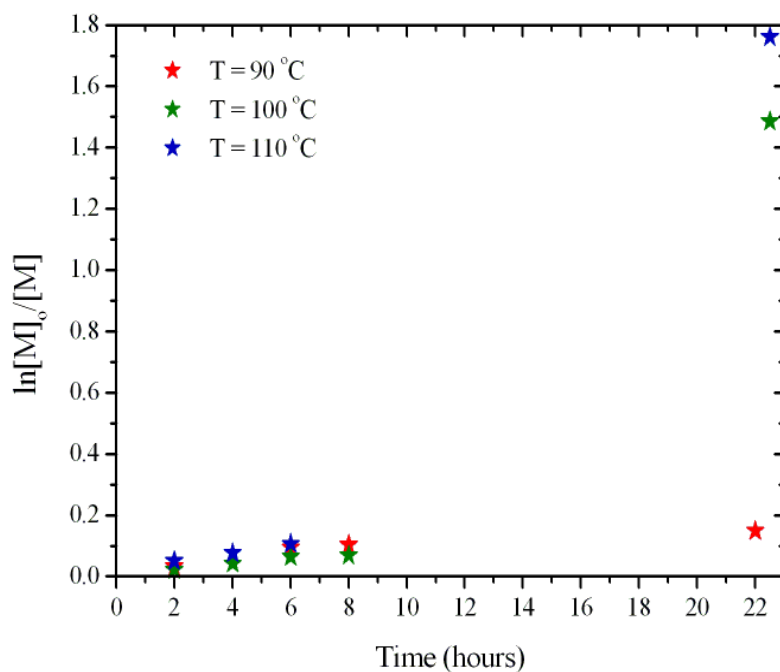


Figure 1.4-17. First order kinetic plot for the verdazyl mediated polymerisation of *n*-butyl acrylate by 17 (R = PhOMe) at 90 °C (★), 100 °C (★) and 110 °C (★)

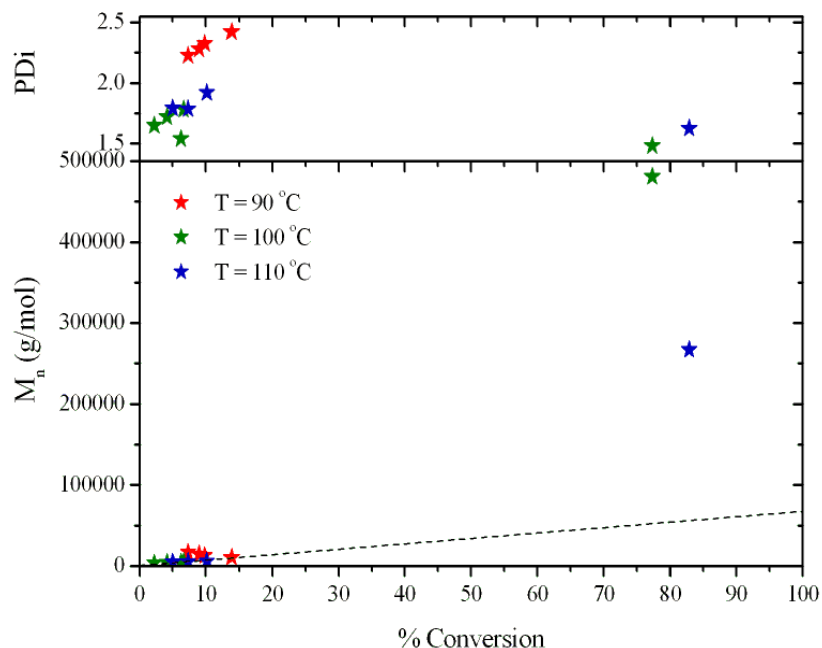


Figure 1.4-18. Evolution of molecular weight (M_n) and PDI versus conversion for the verdazyl mediated polymerisation of verdazyl stabilised *n*-butyl acrylate by 17 ($R = \text{PhOMe}$) at 90 °C (★), 100 °C (★) and 110 °C (★), $DP = 524$, target $M_n = 67,100$ g/mol (---)

The polymerisations at 100 and 110 °C (Figure 1.4-17 and 1.4-18, ★ and ★ respectively) were faster than the polymerisation at 90 °C, however, extremely high molecular weights were observed as the polymerisations got to high conversions. As these butyl acrylate polymerisations were performed on a small scale, already seen to cause some problems with obtaining a controlled reaction, it was decided that these results might not give a true representation of what should happen at those temperatures.

1.4.2.1. Polymerisation of styrene at a lower temperature

As not enough material remained to do a 15 mL scale at lower temperatures using **17** (R = PhOMe) it was decided to use the initiator in a small scale styrene polymerisation, shown to proceed under living conditions on as little as 1 mL monomer scale, at 100 °C. The same polymerisation was also run using **13** (R = Ph) for comparison.

The polymerisation using **13** (R = Ph, ▲) proceeded slower than that using **17** (R = PhOMe, ★) as shown in Figure 1.4-19. The molecular weight and polydispersity for the polymerisation using **13** (Figure 1.4-20, ▲) remained constant for the duration of the experiment indicating that a living polymerisation was not occurring. In contrast, an increase in molecular weight with conversion was seen for **17** (Figure 1.4-20, ★) after an initial jump to approximately 5,000 g/mol at the start of the reaction. The polydispersity, although high at the start of the reaction narrowed as the reaction proceeded. A levelling off in molecular weight was seen towards the end of the polymerisation as well as an increase in the polydispersity. These results indicate that for **17** (R = PhOMe) it is possible to lower the polymerisation temperature, however, a lower temperature may mean that the C-N bond dissociation is slower and as such some optimisation work is required to gain control at the start of the reaction. This can most likely be achieved by adding some free verdazyl at the start, therefore stabilising the monomer, and allowing the equilibrium between propagating and dormant chains to be reached much sooner.

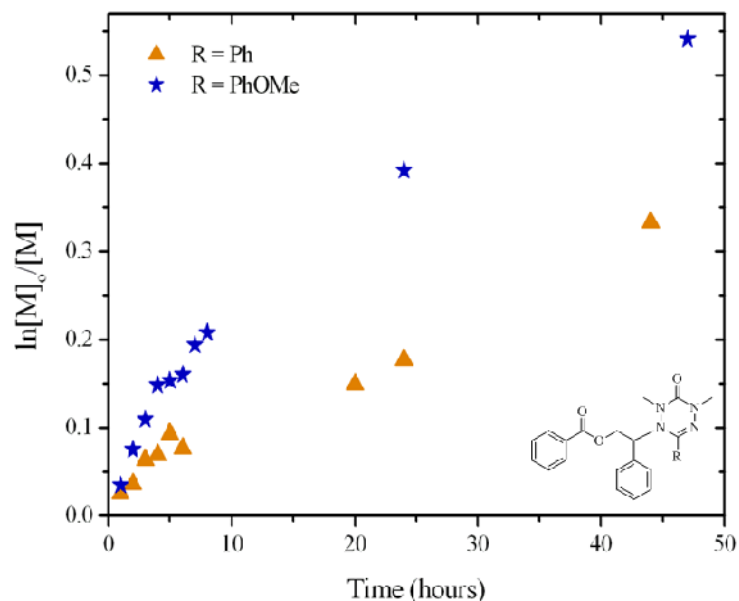


Figure 1.4-19. First order kinetic plot for the verdazyl mediated polymerisation of styrene by 13

($R = \text{Ph}$, \blacktriangle) and 17 ($R = \text{PhOMe}$, \star) at 100 °C

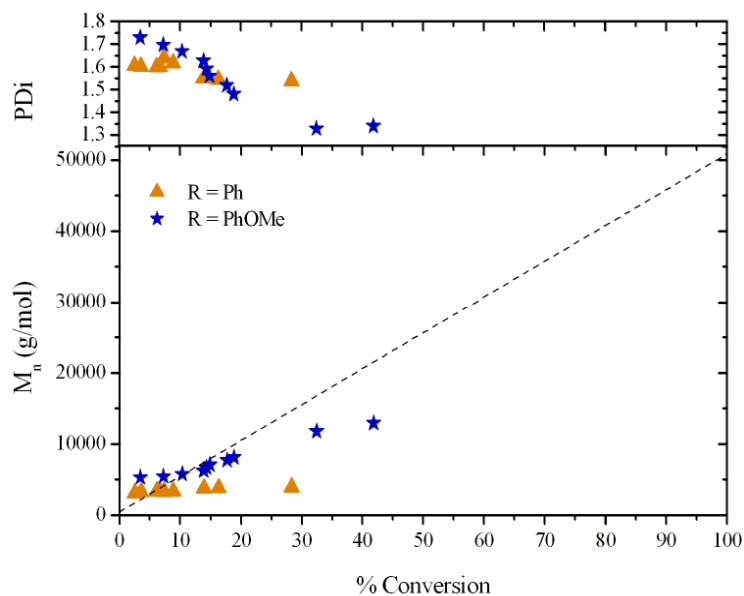


Figure 1.4-20. Evolution of molecular weight (M_n) and PDI versus conversion for the verdazyl mediated polymerisation of styrene by 13 ($R = \text{Ph}$, \blacktriangle) and 17 ($R = \text{PhOMe}$, \star) at 100 °C, DP =

485, target $M_n = 50,500$ g/mol (- - -)

1.4.3. Polymerisation of MMA

Work then progressed to investigate the polymerisation of MMA. The polymerisation was performed under the same conditions used for the polymerisation of styrene (non-stabilised monomer, 125 °C, bulk) using all four verdazyl initiators.

Reasonably similar kinetics were observed for each initiator (Figure 1.4-21) at the start of the polymerisation but differences became more prominent over time. The slowing of the polymerisation rate towards the end of the polymerisations was again attributed to the build up of free radical in solution demonstrated by the bright colour of the polymerisation mixture. The polymerisation using **13** (R = Ph) was stopped after 7 hours as conversion was calculated to be 71%, however errors were introduced by loss of some monomer through evaporation.

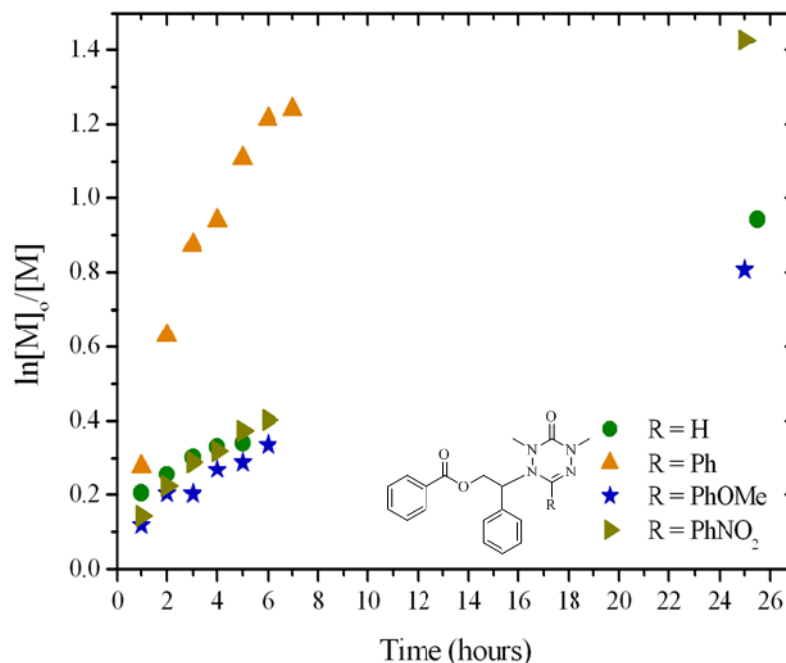


Figure 1.4-21. First order kinetic plot for the verdazyl mediated polymerisation of MMA by 16

(●), 13 (▲), 17 (★) and 18 (▶)

Figure 1.4-22 shows the evolution of molecular weight for the polymerisation of MMA. Unusually, a decrease in molecular weight was observed with conversion. This decrease was accompanied by an increase in polydispersity and multi-modal differential molecular weight distribution curves. These results suggest a high proportion of chain end termination reactions were occurring throughout the polymerisation resulting in a large quantity of low molecular weight chains, reducing the overall value for the molecular weight. When precipitated, some of the low molecular weight chains were removed which served to increase the molecular weight and reduce the polydispersity (Table 1.4-1). The differential molecular

weight distribution curves became more mono-modal after precipitation (Figure 1.4-23).

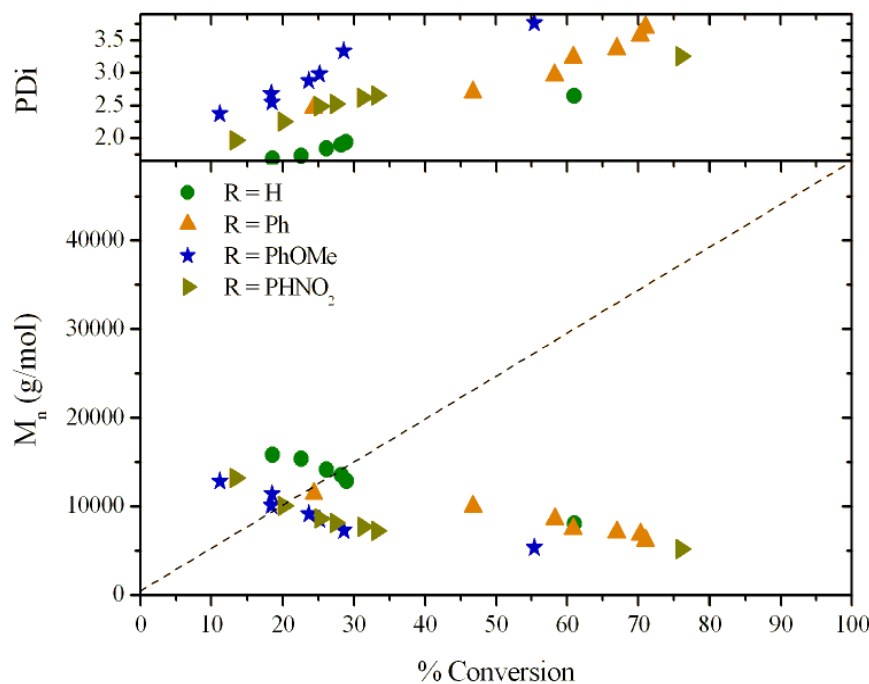


Figure 1.4-22. Evolution of molecular weight (M_n) and PDI versus conversion for the verdazyl mediated polymerisation of MMA by **16 (●), **13** (▲), **17** (★) and **18** (▶), DP = 485, target M_n = 50,500 g/mol (---)**

The homopolymerisation of MMA was repeated using **16** (R = H), however this time the monomer was stabilised with free verdazyl prior to performing the polymerisation. Similar results as with the non-stabilised monomer were observed. The final polymer had a molecular weight of 13,000 g/mol and a polydispersity of 1.70 after precipitation. Based on this result, the polymerisation was not repeated for the other initiators

These results may suggest that it is possible to polymerise MMA using verdazyl radicals. Further work is required to ensure that the polymerisation meets the criteria for a controlled/living system, in particular reducing the amount of termination reactions occurring to address the large proportion of low molecular weight chains that reduce the overall M_n value for the polymerisation.

Table 1.4-1. Molecular weights and polydispersities for the verdazyl mediated polymerisation of MMA before and after precipitation

Initiator	R	Conversion (%)	M_n^a (g/mol)	PDI^a	M_n^b (g/mol)	PDI^b
16	H	61	8,000	2.64	21,900	1.37
13	Ph	71	6,100	3.70	23,600	1.56
17	PhOMe	55	5,300	3.76	18,600	1.86
18	PhNO ₂	76	5,200	3.25	14,800	1.66

^abefore precipitation, ^bafter precipitation

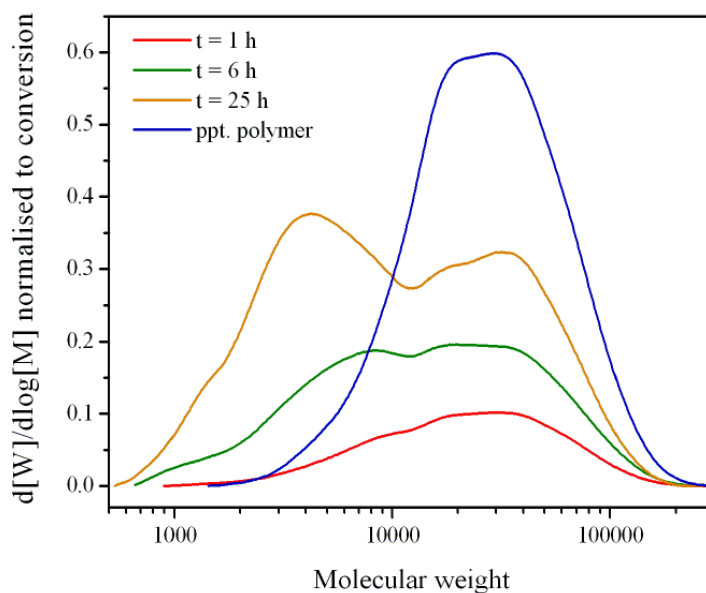


Figure 1.4-23. Overlaid differential molecular weight distribution curves for the verdazyl mediated polymerisation of MMA by 17 (PhOMe, ★)

1.4.4. Copolymerisation of MMA and styrene

Work finally moved on to see if it was possible to improve the polymerisation of MMA by attempting copolymerisation reactions. Styrene was chosen as the comonomer. The method used for the copolymerisation was taken from the literature³¹, in which MMA was copolymerised with butyl acrylate and used 0.05 equivalents of free radical for every equivalent of initiator. Polymerisations were run at 125 °C.

Three sets of experiments were run initially using **13** (R = Ph) varying the amount of MMA and styrene from 1:1 to 3:1 and 9:1. Linear kinetic plots were observed and the rates of polymerisation were similar at the start of the three reactions but started to vary a bit over time (Figure 1.4-24). The polymerisation using 3:1 MMA to styrene proceeded the fastest (▲) followed by 1:1 (▲) and then 9:1 (▲). An increase in molecular weight with conversion was observed but the increase was small over time and much lower than the theoretical molecular weight (Figure 1.4-25). The observed polydispersity was higher than would be expected for an ideal living polymerisation, approximately 1.4 after 25 hours, but was lower than those observed for the homopolymerisation of MMA at 25 hours where the polydispersity was > 2.5 (prior to precipitation).

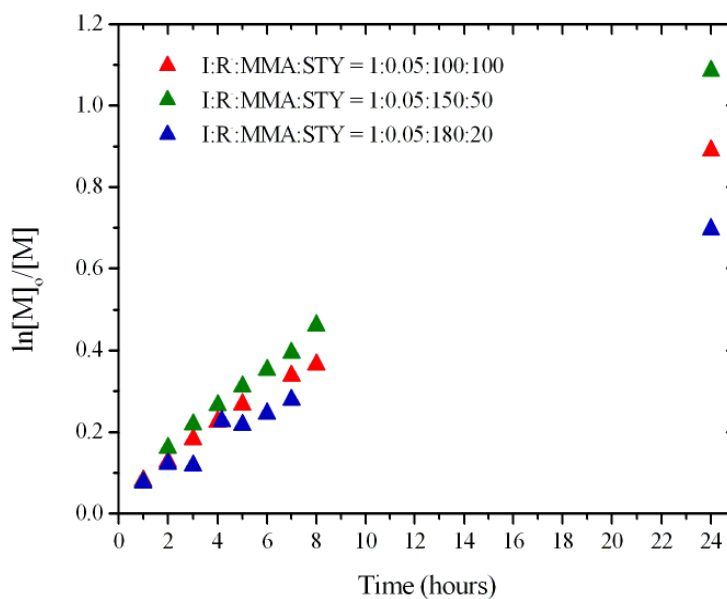


Figure 1.4-24. First order kinetic plot for the verdazyl mediated copolymerisation of MMA and styrene by 13 (R = Ph) at ratios of 1:1 (▲), 3:1 (▲) and 9:1 (▲) using 0.05 equivalents of free verdazyl radical (8) for every equivalent of initiator

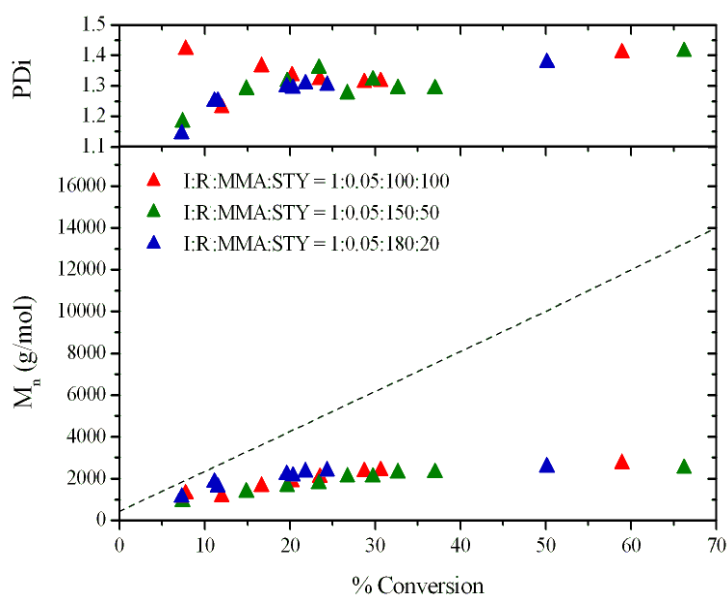


Figure 1.4-25. Evolution of molecular weight (M_n) and PDI versus conversion for the verdazyl mediated copolymerisation of MMA and styrene by 13 (R = Ph) at ratios of 1:1 (▲), 3:1 (▲) and 9:1 (▲) using 0.05 equivalents of free verdazyl radical (8) for every equivalent of initiator.

DP = 200, target M_n = 20,000 g/mol (- - -)

The same three copolymerisations were repeated, however, this time no excess free radical was added to the polymerisation to observe any changes as a result. Similar results were observed with reasonably linear first order kinetics with respect to monomer, with the 3:1 polymerisation the fastest and the 9:1 the slowest (Figure 1.4-26, ▲ and ▲ respectively).

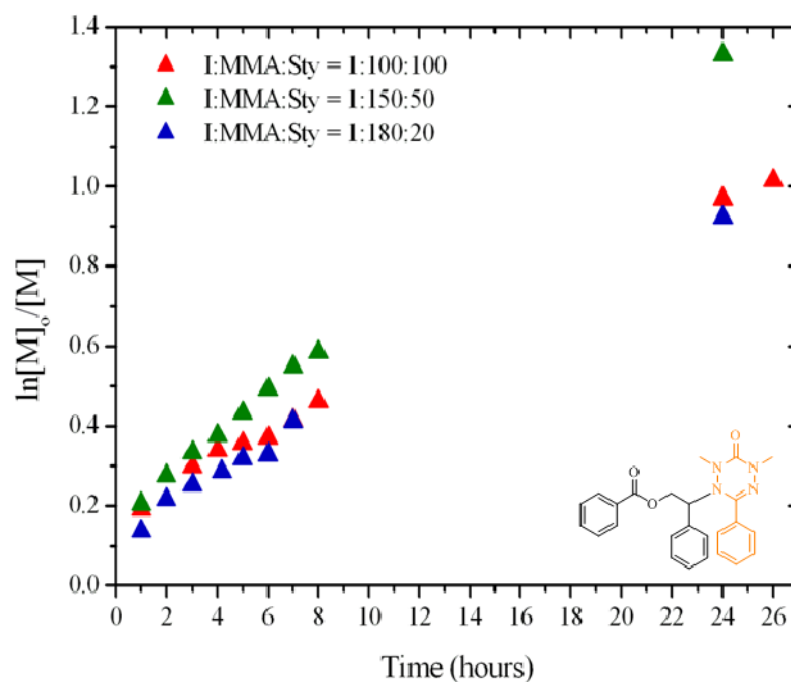


Figure 1.4-26. First order kinetic plot for the verdazyl mediated copolymerisation of MMA and styrene by 13 (R = Ph) at ratios of 1:1 (▲), 3:1 (▲) and 9:1 (▲)

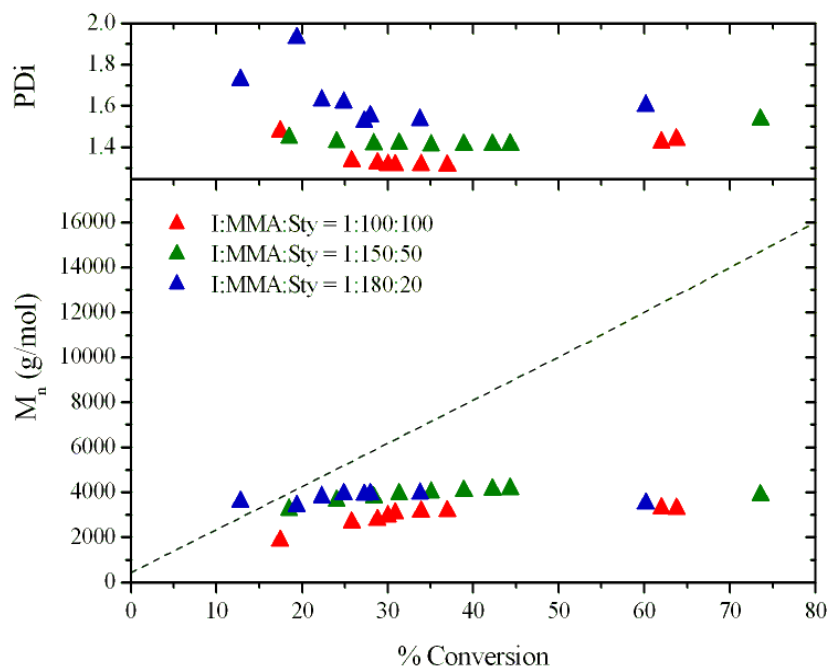


Figure 1.4-27. Evolution of molecular weight (M_n) and PDI versus conversion for the verdazyl mediated copolymerisation of MMA and styrene by 13 ($R = Ph$) at ratios of 1:1 (\blacktriangle), 3:1 (\blacktriangle) and 9:1 (\blacktriangle), $DP = 200$, target $M_n = 20,000$ g/mol (- - -)

After an initial jump in molecular weight, only a small increase in molecular weight was observed (Figure 1.4-27). Polydispersity values were again higher than expected for a living polymerisation. The conversion, molecular weight and polydispersity data for all six aforementioned copolymerisation reactions are presented in Table 1.4-2. The overall conversion was calculated based on the conversions of the individual monomers adjusted for their ratio in the polymerisation.

Table 1.4-2. Molecular weights and polydispersities for the verdazyl mediated copolymerisation of MMA and styrene before and after precipitation

I	V	MMA:Sty	Overall conversion (%)	Conversion (%)		M_n (g/mol) ^a	PDI ^a	M_n (g/mol) ^b	PDI ^b
				MMA	Sty				
1	0.5	100:100	58.3	80.8	35.9	2700	1.41	3600	1.28
1	-	100:100	63.8	87.0	40.5	3300	1.43	3800	1.36
1	0.5	150:50	66.2	68.6	29.5	2500	1.41	3100	1.42
1	-	150:50	73.6	72.3	38.7	3900	1.53	4144	1.55
1	0.5	180:20	50.2	52.0	22.4	2500	1.38	3100	1.33
1	-	180:20	60.2	63.2	33.2	3500	1.60	6300	1.51

^abefore precipitation, ^bafter precipitation

Conversions were higher when free radical was not added at the start of the polymerisation. In each polymerisation, the conversion of MMA was higher than for styrene at the end of the polymerisation. As seen with the homopolymerisation of MMA, after precipitation the copolymers had an increased molecular weight, although to a much lesser extent. Molecular weights rarely exceeded 4,000 g/mol for the copolymerisations, again lower than molecular weights observed for the homopolymerisation of MMA. The changes in polydispersity were small after precipitation. Based on the results displayed in Table 1.4-2, higher molecular weights and polydispersity values were observed in the polymerisations that did not include the addition of free verdazyl at the start of the polymerisation.

The overlaid differential molecular weight distribution curves for all the verdazyl mediated copolymerisations of MMA and styrene are displayed in Figure 1.4-28.

The evolution of molecular weight typically expected for a controlled radical polymerisation was observed when free verdazyl was added at the start of the polymerisation (Figure 1.4-28, left hand side). As conversion increased the low molecular weight tail increased and a shoulder in the trace became more prominent (Figure 1.4-28, top left), similar to the homopolymerisation of MMA (Figure 1.4-23), but to a lesser extent. As the amount of MMA was increased this effect increased. As already seen in Figure 1.4-27, without the addition of free radical at the start of the polymerisation, the evolution of molecular weight was much smaller and decreased further on increasing amounts of MMA (Figure 1.4-28, right hand side). The traces also displayed a low molecular weight tail but were more mono-modal. After precipitation all the molecular weight distributions were mono-modal but they retained the low molecular weight tail.

.

The ^1H NMR of the precipitated polymer was different to both those for polystyrene and poly methyl methacrylate suggesting that a random copolymer has been formed over individual homopolymers or a block copolymer (Figure 1.4-29). Further work is required to optimise the copolymerisation reaction to find the correct conditions to achieve a completely controlled system. All polymerisations were brightly orange coloured after 25 hours indicating the build up of verdazyl radical **8** ($\text{R} = \text{Ph}$) from dissociation. The amount of free radical was not quantified for these polymerisations; however, doing so in the future may improve understanding of the polymerisation system and help to further optimise the reaction conditions.

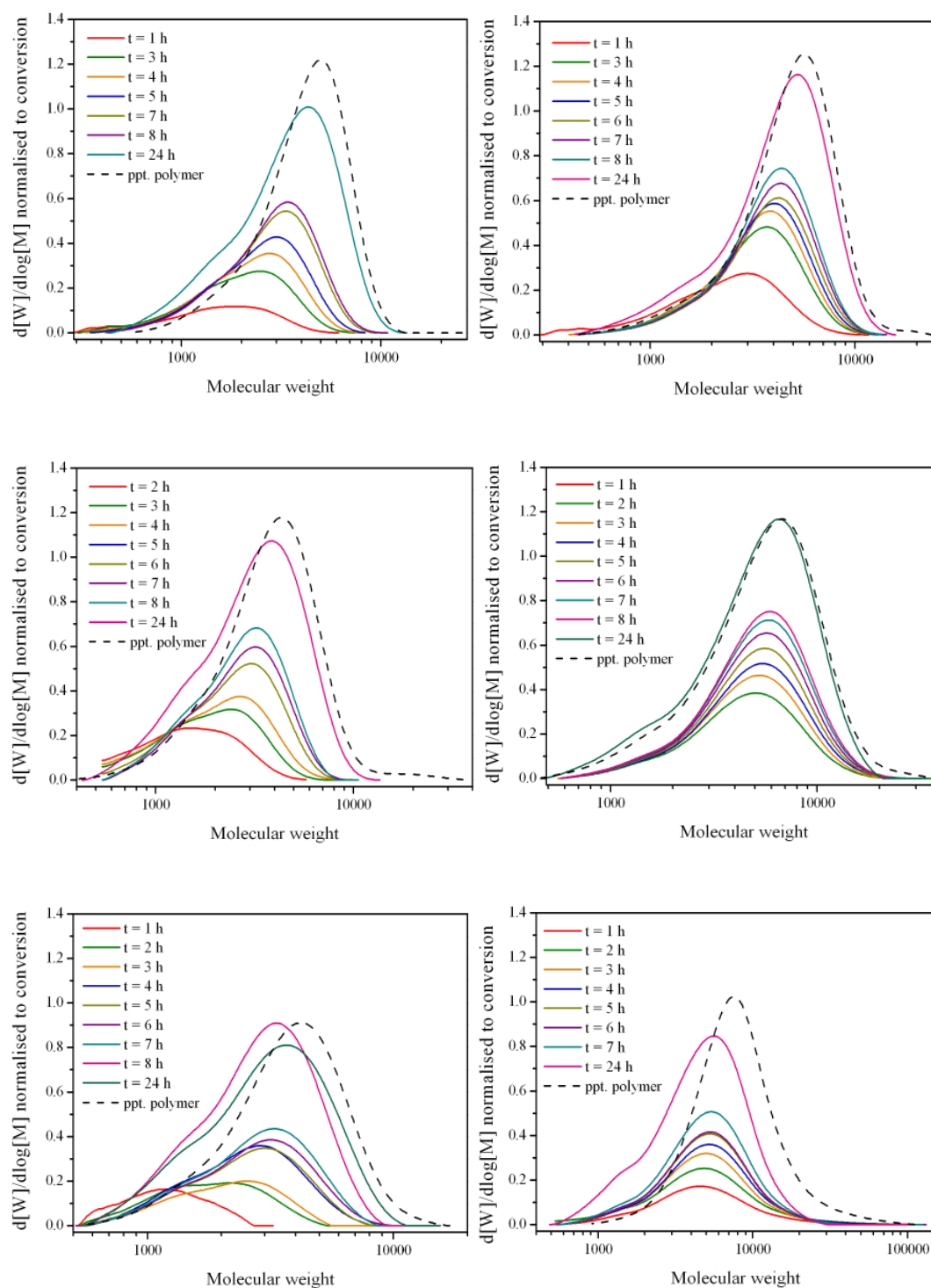


Figure 1.4-28. Overlaid differential molecular weight distribution curves for the verdazyl mediated copolymerisation of MMA and styrene with 0.5 equivalents of free verdazyl (left) and without (right) at ratios of 1:1 (top), 3:1 (middle) and 9:1 (bottom)

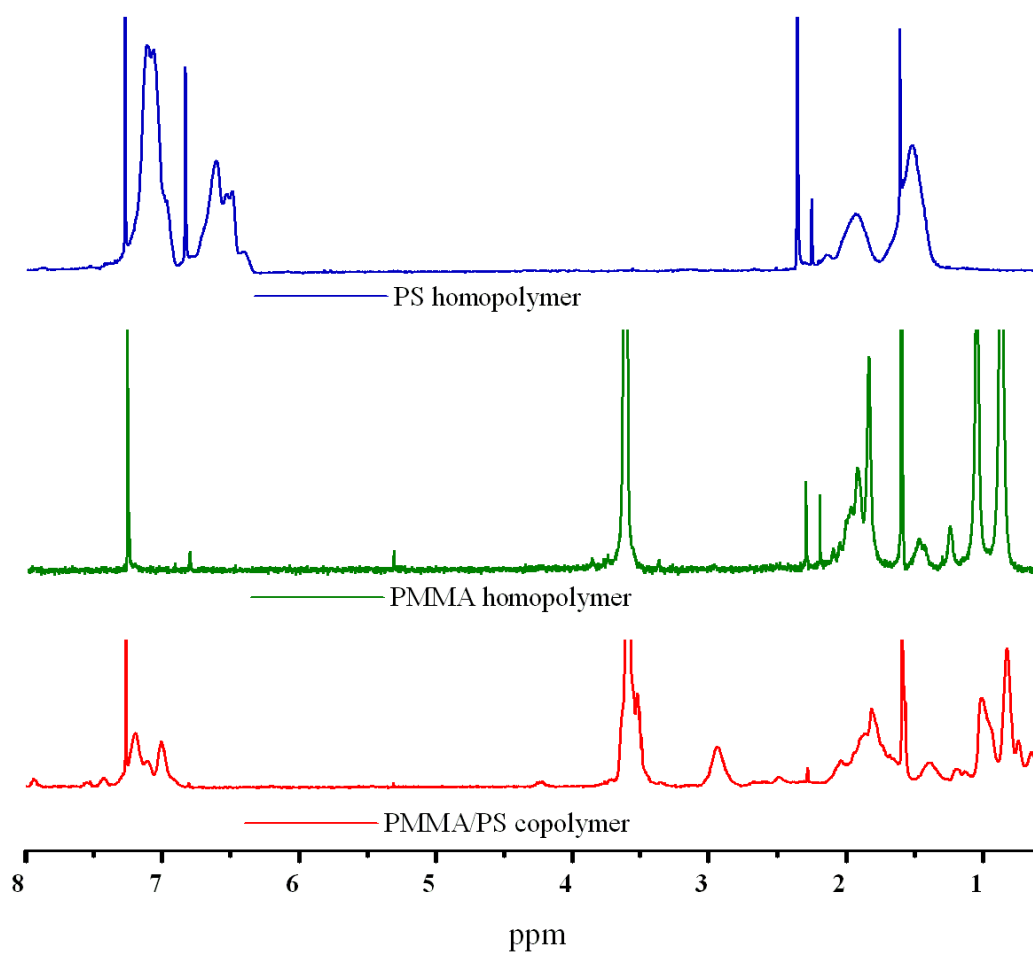


Figure 1.4-29. ^1H NMR of polystyrene homopolymer (PS, —), poly methyl methacrylate homopolymer (PMMA, —) and poly methyl methacrylate/polystyrene copolymer (—)

1.5. High Temperature EPR studies

The facilities at Warwick have made it possible for a small set of high temperature EPR experiments to be carried out. This provided an opportunity to study what happens to the verdazyl radical over time at the polymerisation temperature in various situations which will be discussed in this section of thesis.

Due to limitations with materials and time, studies have mostly been carried out using only verdazyl initiator **13** and radical **8** (both R = Ph). Figure 1.5-1 displays the ambient temperature EPR spectrum of **8**. As previously seen in Section 1.2.2, 11 distinct peaks are visible. The two peaks at the far reaches of the radical spectrum are weak and can be difficult to see if the concentration is low, so in general for these experiments, 9 lines are expected. These 9 lines can broaden depending on concentration, temperature, microwave power, experimental parameters *etc.*⁵⁵ but should always be visible if the verdazyl is present.

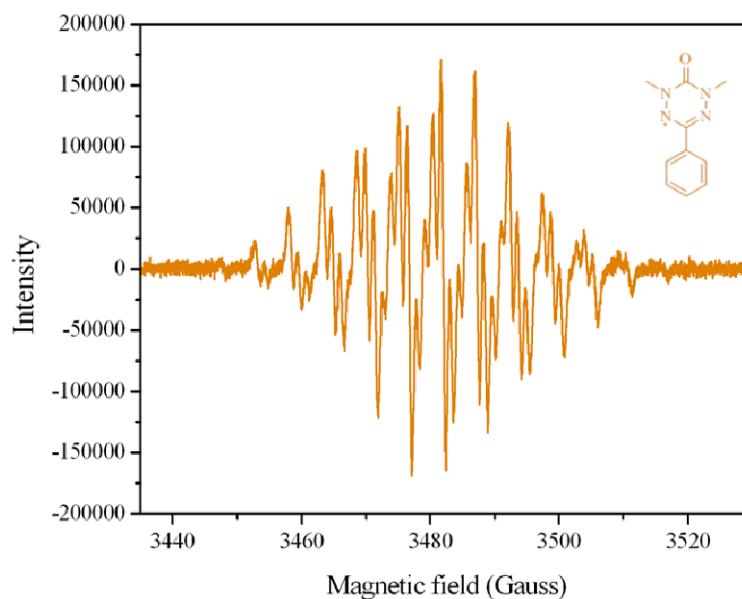


Figure 1.5-1. Ambient temperature EPR spectrum of 8 (0.2 mM)

It should be noted that altering the frequency, which changes depending on which cavity is being used, will result in a shift in the centre field for the radical according to the equation⁵⁵:

$$h\nu = g \mu_B B$$

Equation 1.5-1

The g-factor, which determines the centre field, is the only component in the equation that is not a physical constant or fixed by experimental parameters (frequency, microwaves *etc.*) and thus changes depending on the parameters used.

1.5.1. High temperature cavity calibration

It was hoped that some quantitative analysis could be attempted to determine the concentration of radical at the elevated temperature used during a polymerisation. A calibration of **8** (R = Ph) was completed to enable this quantitative analysis to take place. Similar to the process described in Section 1.3.1, five solutions of known radical concentration were scanned using the same experimental parameters used for all the high temperature experiments (with the exception of the receiver gain which needed to be varied depending on the concentration of the sample). Samples were scanned at ambient temperature before being scanned at 122 °C. The samples were also scanned again once cooled back down to ambient temperature. The graph of normalised double integral vs. concentration for each set of scans is shown in Figure 1.5-2.

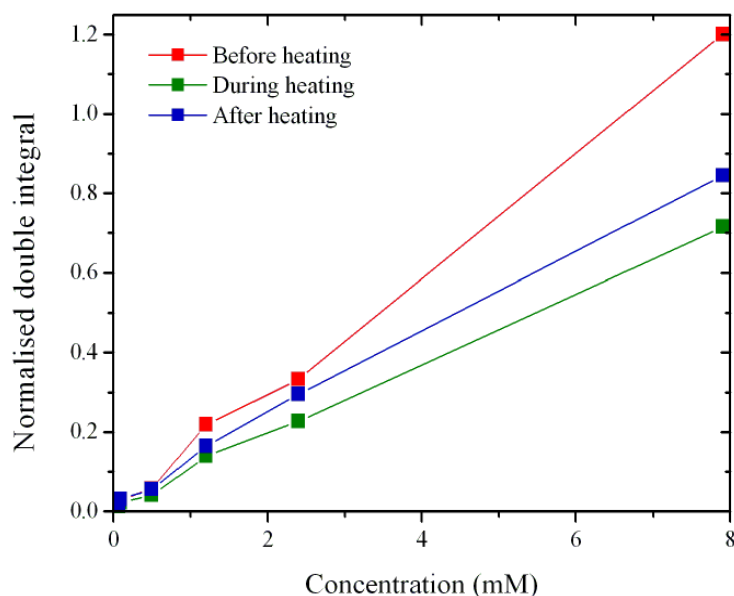
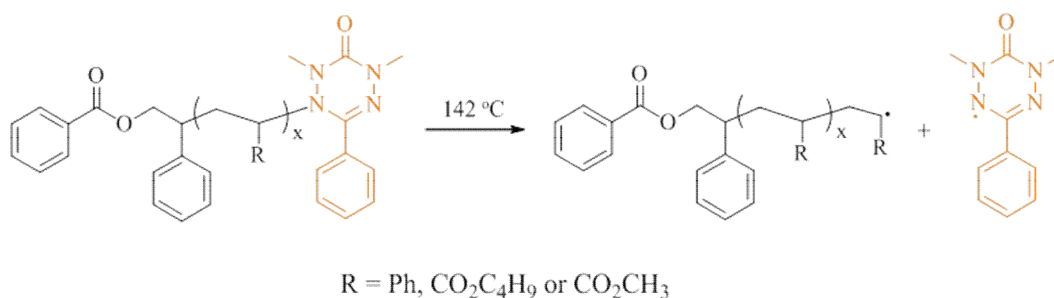


Figure 1.5-2. Plot of normalised double integral vs. concentration for 0.1, 0.5, 1.2, 2.4 and 7.9 mM solutions of **8** at ambient temperature (■), during heating (■) and after heating (■)

The original ambient temperature results (■) represent the concentration of **8** for a given intensity. However, when the same sample is heated the signal was seen to decrease (■). This effect became more prominent on increasing concentration. This may indicate that at elevated temperatures the radical decomposes or that some interaction, such as coupling, occurs between the radicals to reduce the signal. The scan at ambient temperature after heating (■) showed in all cases that the concentration of radical increased, but not to the original value. From this it can be assumed that there is some radical decomposition at elevated temperatures, and as a result the concentration of the heated sample does not match the concentration of the same sample before it was heated. This means that the concentration cannot be determined based on a calibration at high temperature, instead the ambient temperature calibration needs to be used but it may not truly represent the concentration at temperature.

1.5.2. Polymer end-group analysis

A brief investigation into chain end functionality, used to determine whether the polymerisation was living, was first completed for a selection of polymers synthesised using the verdazyl initiators. ¹H NMR can be used to determine the presence of a verdazyl end-group; however, high molecular weights can make it more difficult to use this technique. EPR provides the advantage that if there are polymer-verdazyl bonds present, heating the polymer should cause those bonds to cleave and the signal for the verdazyl should be observed (Scheme 1.5-1).



Scheme 1.5-1. Expected bond cleavage on heating polymers synthesised using **13** ($R = \text{Ph}$)

A deoxygenated solution of polymer in mesitylene was heated at 142 °C for between 15 minutes and 2 hours. The required length of time of heating was found to be dependent on the molecular weight of the polymer, with higher molecular weights requiring an increased amount of time. A higher concentration of polymer in solution was also required as molecular weight increased in order for a signal for the verdazyl radical to be observed. The polymer solution was scanned at ambient temperature initially to confirm that there was no free verdazyl present prior to heating the sample. Figure 1.5-3 displays the high temperature EPR spectrum of poly *n*-butyl acrylate synthesised using **13**.

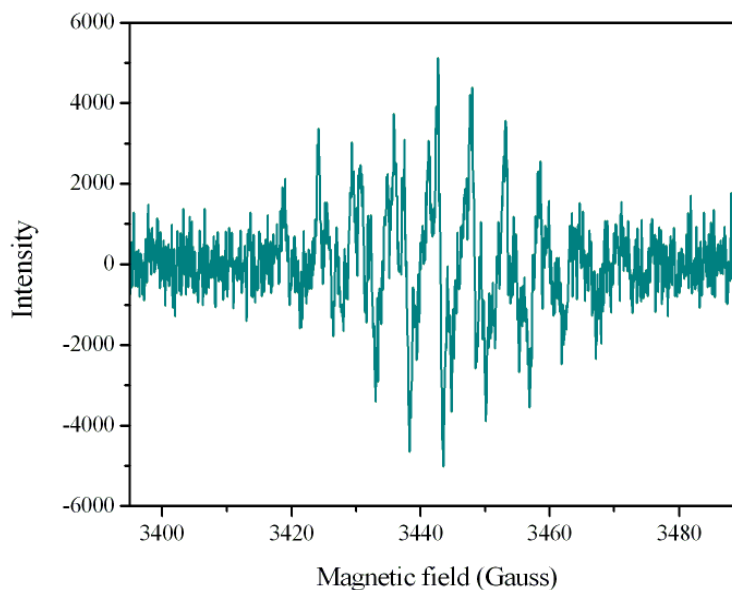


Figure 1.5-3. EPR spectrum of poly *n*-butyl acrylate synthesised using **13** recorded at 142 °C

The expected 9 line spectrum was observed, although weak, and fitted the simulation already recorded for **8**. Interestingly, the polymer fragment was not observed. It was possible that the centre field for the polymer fragment may lay outside of the sweep width used, however when other samples were investigated using a sweep width of 300 G no other signals were observed. The absence of the polymer fragment is most likely due to the molecular weight of the polymer being relatively high (21,200 g/mol) and it is difficult to detect long chain radicals.¹⁰⁶

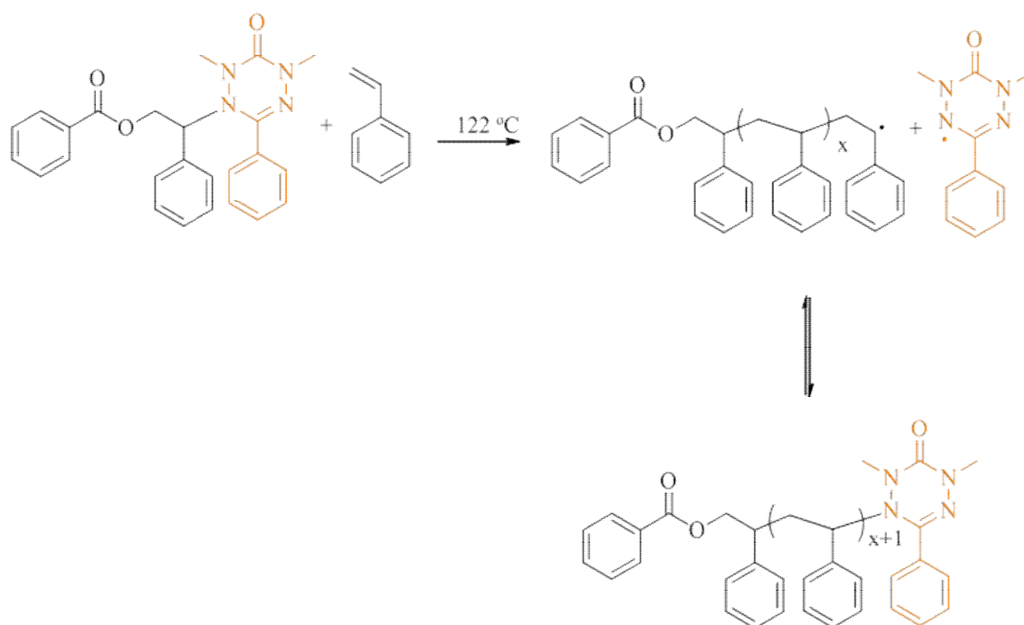
Polystyrene and the MMA/styrene copolymers in the 1:1 and 3:1 ratios were also investigated and displayed a radical signal on heating. The copolymer in the 9:1 ratio and poly methyl methacrylate displayed minimal solubility in mesitylene.

These polymers were dissolved in chlorobenzene, however, the high temperature cavity is very sensitive to changes in dielectric constant and the solvent was found to be too polar for the cavity to be coupled meaning that the EPR spectra could not be obtained.

If this was reinvestigated at a later date, obtaining quantitative analysis for the determination of the percentage of living polymer chains would provide a much better insight to the controlled nature of the polymerisation technique.

1.5.3. In-situ EPR analysis of the polymerisation of styrene

The polymerisation of styrene mediated by **13** was then followed using the EPR spectrometer. The polymerisation mixture was prepared and a sample taken to be recorded. As expected no radical signal was visible at ambient temperature as the monomer was not stabilised with free verdazyl prior to commencing the reaction. On heating the sample it would be expected that the C-N bond would cleave initiating the polymerisation and producing a signal for verdazyl radical **8**. An equilibrium between capped and uncapped polymer chains is expected over the duration of the polymerisation and as such a constant concentration of radical should be observed (Scheme 1.5-2).



Scheme 1.5-2. Controlled radical mechanism for the polymerisation of styrene by 13

The sample was heated to 122 °C and a set of scans recorded every hour up until the radical signal completely disappeared which took just short of 18 hours. Figure 1.5-4 displays the normalised double integral calculated from the recorded spectra and shows that the radical concentration had reached a maximum after approximately two hours and then decreased over the remaining reaction time. The concentration was seen to decrease quite slowly after 6 hours. A ^1H NMR was run of the sample and no polymer was observed indicating that no polymerisation had taken place (Figure 1.5-5, –).

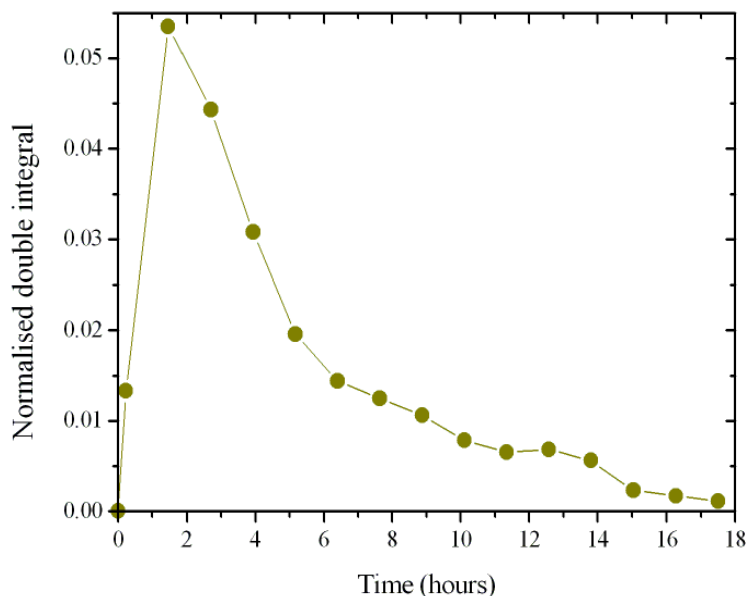


Figure 1.5-4. Plot of normalised double integral vs. time for the first attempt at the polymerisation of styrene in the EPR spectrometer

The remaining polymerisation mixture was heated at the same temperature, without stirring and without the flow of nitrogen to best recreate the conditions experienced by the sample in the cavity. After 22 hours the polymerisation had reached 41% conversion. In the ^1H NMR spectra of a sample taken from the polymerisation reaction (Figure 1.5-5, —), the polymer was clearly visible. This indicated that something had occurred during the transfer of the sample from the Schlenk tube to the EPR tube that stops the polymerisation reaction taking place, most likely the presence of air.

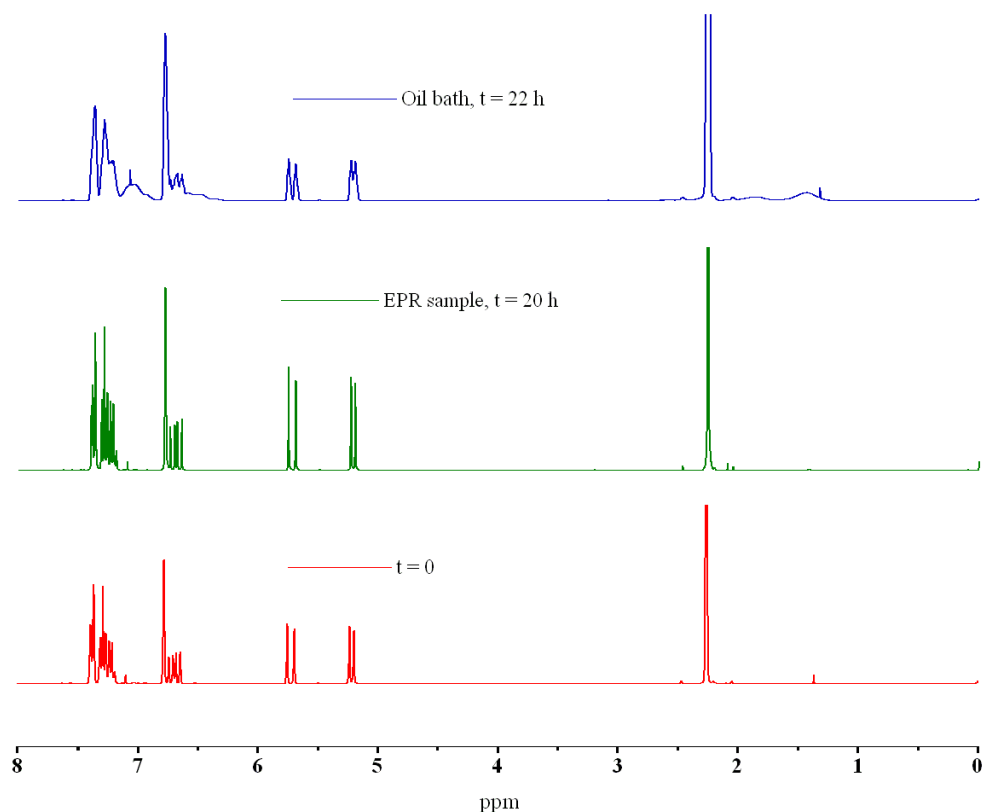


Figure 1.5-5. ^1H NMR traces for the polymerisation by styrene at $t = 0$ (—), the EPR polymerisation after 20 h (—) and the remaining polymerisation mixture heated in an oil bath for 22 h (—)

The EPR tube was normally degassed by placing it into a large (750 mL) Schlenk tube kept under a nitrogen atmosphere. This however, does not mean that the entire length of the narrow EPR tube would be degassed. To address this, the degassed syringe was first used to fill the EPR tube with nitrogen. This was repeated three times prior to syringing in the sample. The sample was run under the same conditions in the EPR spectrometer as the original polymerisation. This time a radical signal was observed at a much lower intensity over the course of the reaction. Figure 1.5-6 displays selected EPR traces which show how the radical signal

intensity changed over the duration of the reaction. The normalised double integral from all the spectra recorded over the course of the reaction are displayed in Figure 1.5-7.

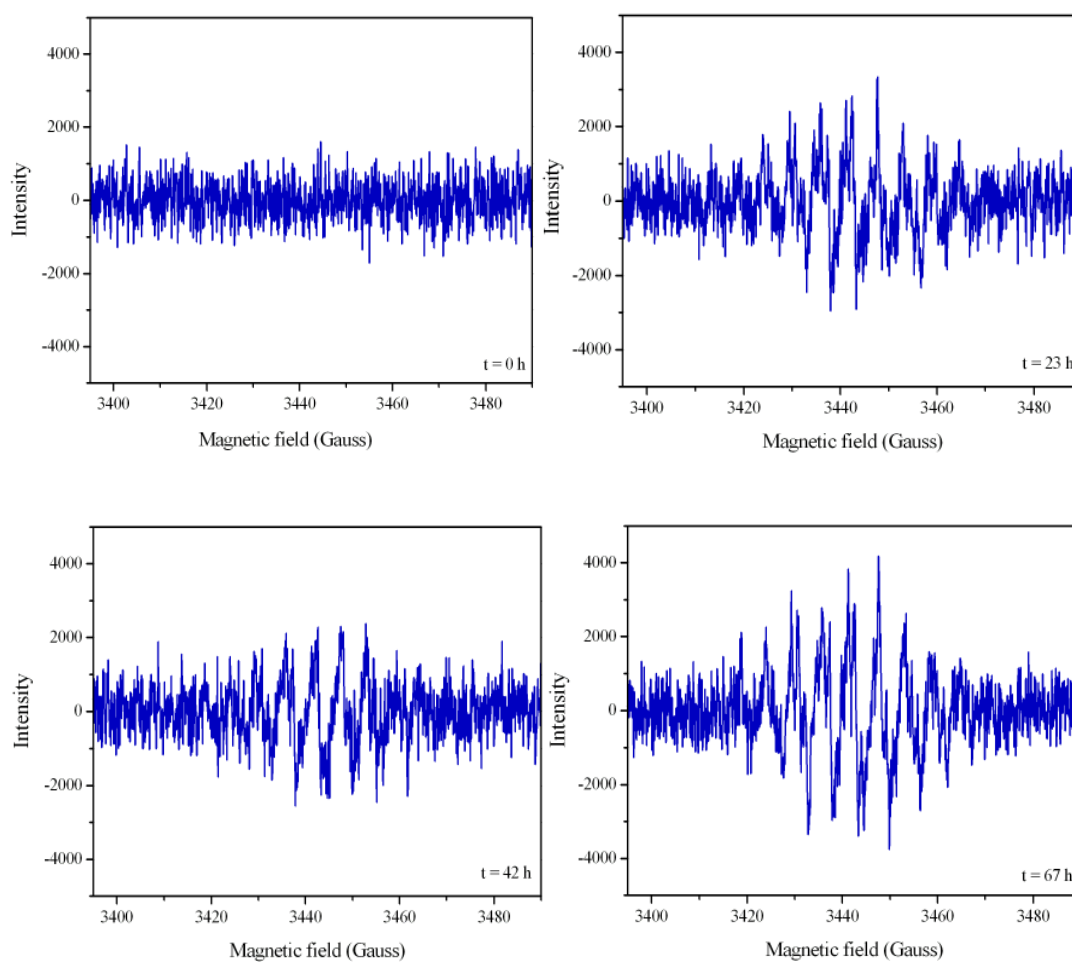


Figure 1.5-6. EPR traces from the second attempt at the polymerisation of styrene in the EPR machine at 0, 23, 42 and 67 h

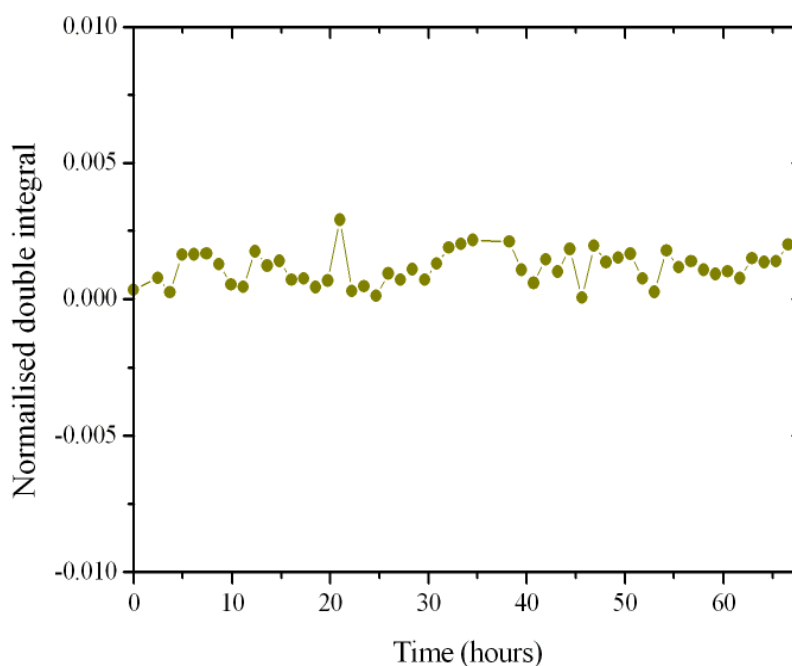


Figure 1.5-7. Plot of normalised double integral vs. time for the second attempt at the polymerisation of styrene in the EPR spectrometer

When the polymerisation was stopped at 67 hours a signal for the verdazyl was still visible. The observed results indicate that the concentration of the radical in solution remained low over the duration of the reaction, important if the reaction is to proceed in a controlled fashion. No particular build up of radical over the course of the polymerisation was observed which would normally be associated with termination reactions. The unprecipitated polymer was analysed using ^1H NMR and GPC and had reached 64% conversion with a molecular weight of 33,400 g/mol and a polydispersity of 1.48 (before precipitation).

The polymer fragment was not seen in the recorded EPR spectra as seen when determining the polymer end-groups. The concentration of stable radical in a controlled living polymerisation can be at least four times greater than that of the propagating radical.¹⁰⁷ Combined with small organic molecules being more easily detectable over long chain radicals in EPR, it is perhaps not surprising that a signal was not seen for the propagating radical. Propagating radicals have been observed before using EPR and has been described in various papers, books and reviews.^{106, 108-113} However, in many cases the EPR experiment was designed using the optimum parameters to capture the propagating radical species. The use of solid state EPR is frequently used as it offers the advantage of longer lived propagating radicals in a much higher concentration¹¹⁴, however this was not included in the scope of this study.

It was hoped that the polymerisation of MMA could be attempted; however, a few problems were encountered. The boiling point of MMA (100 °C) is lower than the desired polymerisation temperature. This would mean that if attempted the polymerisation mixture would be boiling when in the EPR spectrometer and could cause a pressure build which may cause the EPR tube to fail and risk damaging the microwave cavity. This problem was solved by switching to *n*-butyl methacrylate which has a boiling point of 162-165 °C. When it came to running the polymerisation it was discovered that the polarity of the monomer was higher than that of styrene and, as a result, the microwave cavity could not be coupled and the reaction not completed.

1.5.4. Initiator characterisation

It has been shown that the concentration of free radical in a polymerisation, especially for butyl acrylate, can have an effect on the rate of polymerisation. The purity of all four of the verdazyl initiators had already been confirmed by NMR, mass spectrometry and elemental analysis but it was decided to also use EPR as a complimentary technique; this would confirm the absence of any residual free radical in these initiators.

The EPR spectrum of each initiator in mesitylene was recorded at ambient temperature. Initiators **13** (R = Ph), **16** (R = H) and **17** (R = PhOMe) did not show a radical signal. Interestingly, a signal was seen for **18** (R = PhNO₂) at ambient temperature. This result may be a factor as to why polymerisations using **18** were generally observed to be slower than all the other verdazyl initiators. The same samples were individually heated to 122 °C. Spectra were then recorded before cooling back down to ambient temperature. After three hours back at ambient temperature radical signals were still visible in all the initiator samples. The samples were left for between 65-72 hours before being scanned again. This time the radical signal had disappeared, or returned to the same value for **18**, except for **13** where a signal was still visible. The samples were heated back up to temperature where the radical signals reappeared, proving that the initiator-verdazyl bond could be reversibly cleaved. Figure 1.5-8 illustrates the changes in radical concentration on heating and cooling of the samples as described in the text. If more time was available, it would make for a more comprehensive study to extend this experiment

to determine if the initiator could be reversibly cleaved indefinitely or how long it would take before it started to decompose.

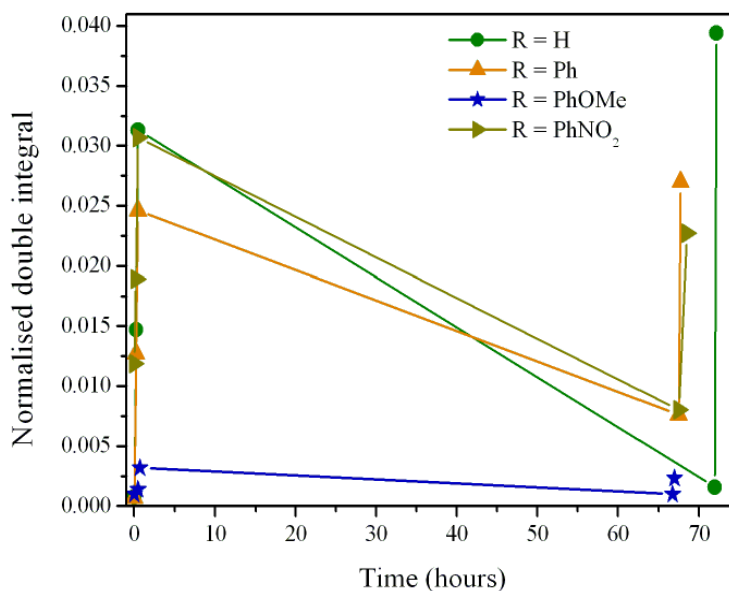
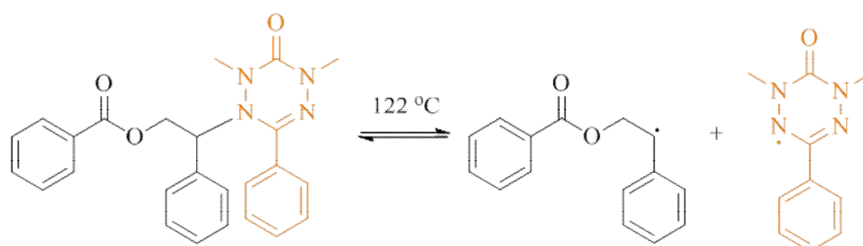


Figure 1.5-8. Plot of normalised double integral vs. time for all four verdazyl initiators demonstrating the reversible nature of the cleavage of the C-N bond using EPR

1.5.4.1. Initiator decomposition

Following on from the previous study it was decided to see how long it took for the initiator to decompose at the elevated reaction temperature. A solution of **13** in mesitylene was heated to cleave the initiator-verdazyl C-N bond (Scheme 1.5-3) and the EPR spectra recorded until the radical signal disappeared. On the first attempt the same result was observed as in the initial attempt of the polymerisation of styrene. There was an initial increase of the radical signal to a maximum before the signal decreased until it completely disappeared, taking approximately 8 hours. The

same reaction was repeated but using the more efficient sample preparation technique that was used to get the polymerisation of styrene to proceed. The normalised double integral values from the EPR spectra recorded during the second attempt are shown in Figure 1.5-9.



Scheme 1.5-3. Expected initiator cleavage mechanism at polymerisation temperature

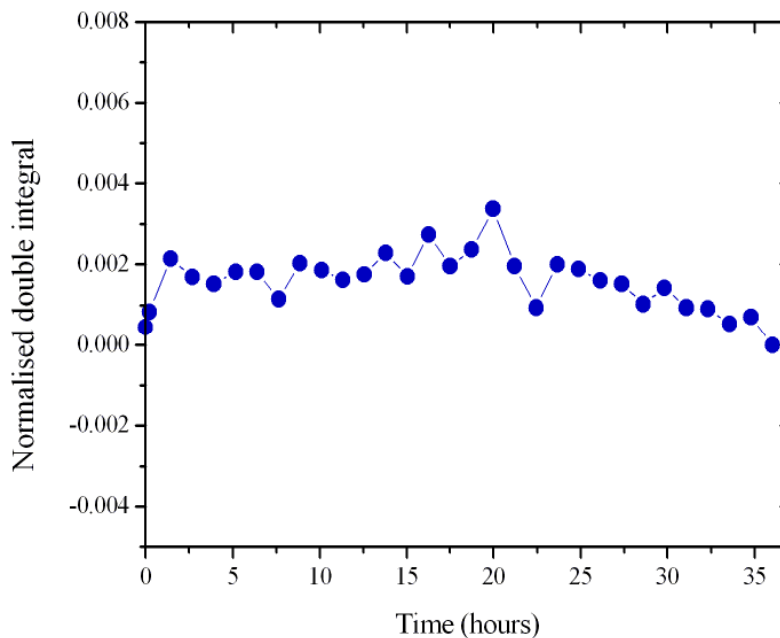


Figure 1.5-9. Plot of normalise double integral vs. time for the EPR decomposition study of 13 at polymerisation temperature

In this instance, and similarly to the polymerisation of styrene, the radical signal was seen to fluctuate. This fluctuation occurred during the first 20 hours before slowly starting to decrease so that by 37 hours no signal was observed.

1.5.5. Radical decomposition

Lastly, the decomposition of radical **8** at the polymerisation temperature was investigated. The amount of **8** used was based on the conditions for the polymerisation of styrene; using the amount of moles of radical that would exist if all the initiator molecules in the polymerisation cleaved all at once. As expected a strong radical signal was observed prior to heating the sample. Upon heating, the concentration of radical decreased dramatically over the first couple of hours before slowing down and eventually disappearing after about 60 hours (Figure 1.5-10).

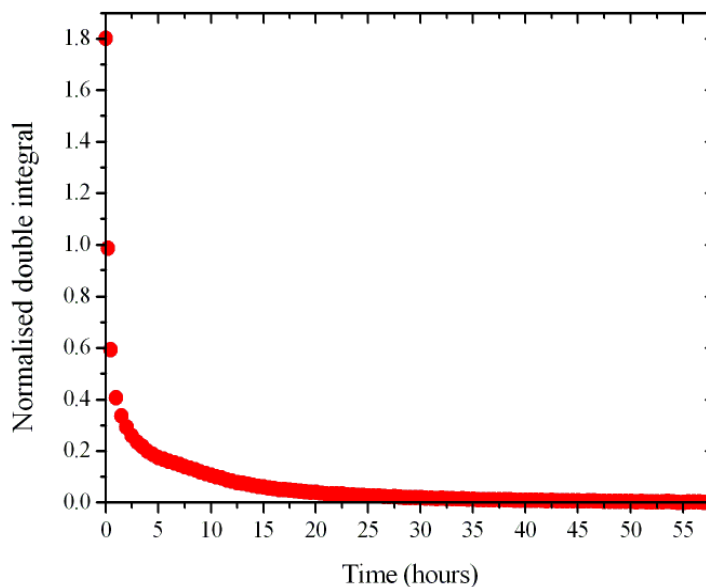


Figure 1.5-10. Plot of normalised double integral vs. time for the EPR study of the decomposition of **8 at polymerisation temperature**

Figure 1.5-11 displays a set of EPR traces recorded at various time intervals during the experiment. The first trace ($t = 0$) illustrates how high concentrations of radical broadens the observed signal. The first set of scans taken immediately after the cavity reached the reaction temperature ($t = 14$ mins) shows a greater extent of signal broadening. This is due to the high concentration combined with the fast tumbling of the radicals in solution at elevated temperatures.¹¹⁵ It was expected that as time progressed and the radical decayed, the concentration of radical would decrease resulting in a reduction in the broadening of the signal and a return to the typical hyperfine splitting pattern for **8**. This was seen in the experiment and is illustrated in the remaining spectra in Figure 1.5-11 ($t = 5.5, 16.5, 42.5$ and 51 hours).

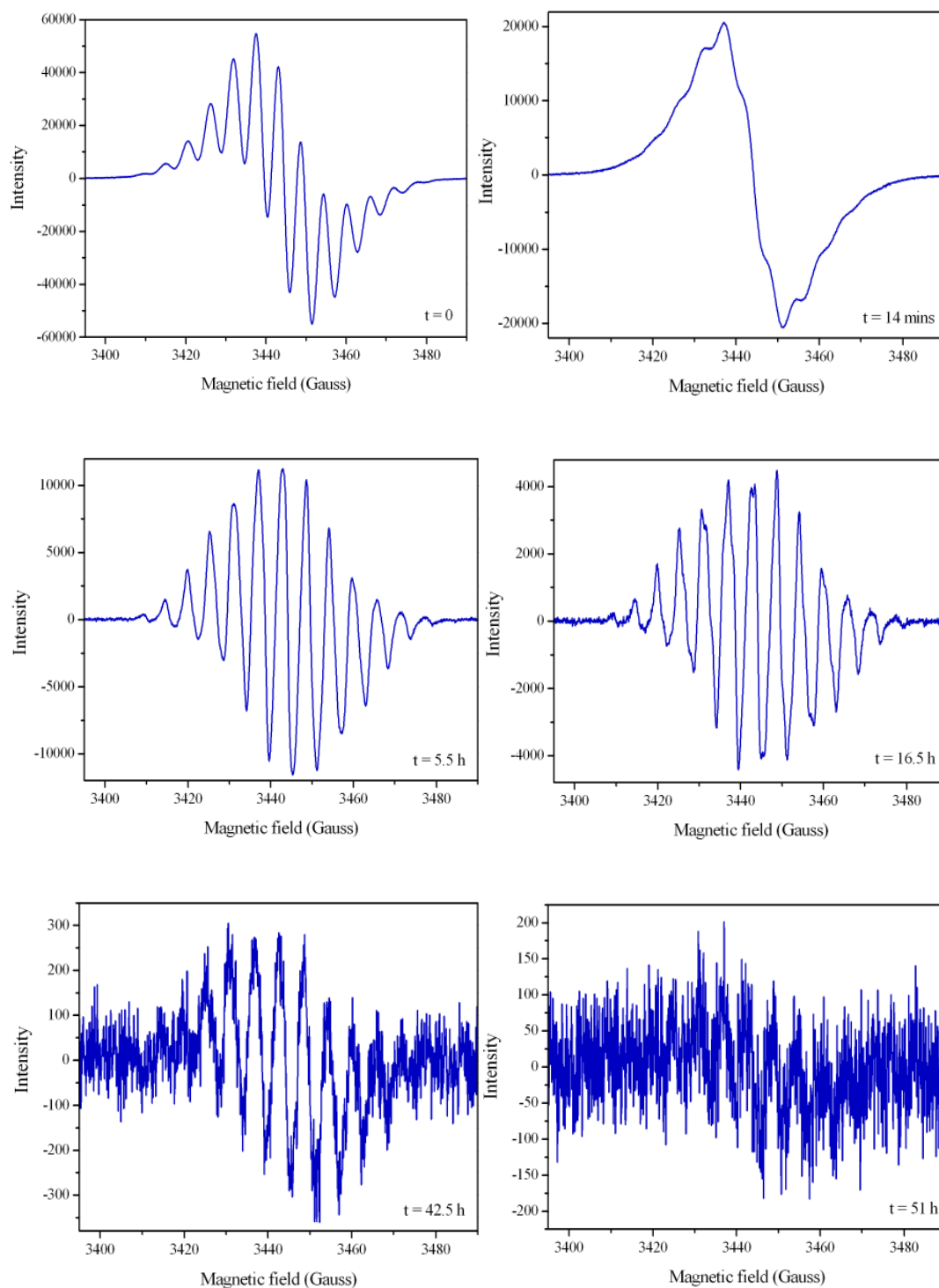


Figure 1.5-11. EPR traces from the polymerisation of styrene by **13**

The kinetics of the reaction were plotted (Figure 1.5-12) and after an initial decrease, linear first order kinetics with respect to monomer were observed. This suggests that there is no interaction of the radical with any external sources, such as the presence of oxygen, that may prevent decomposition. Around 50 hours, where the radical signal was low compared to the signal-to-noise ratio of the spectrum, the integration became more difficult resulting in values deviating from the observed trend.

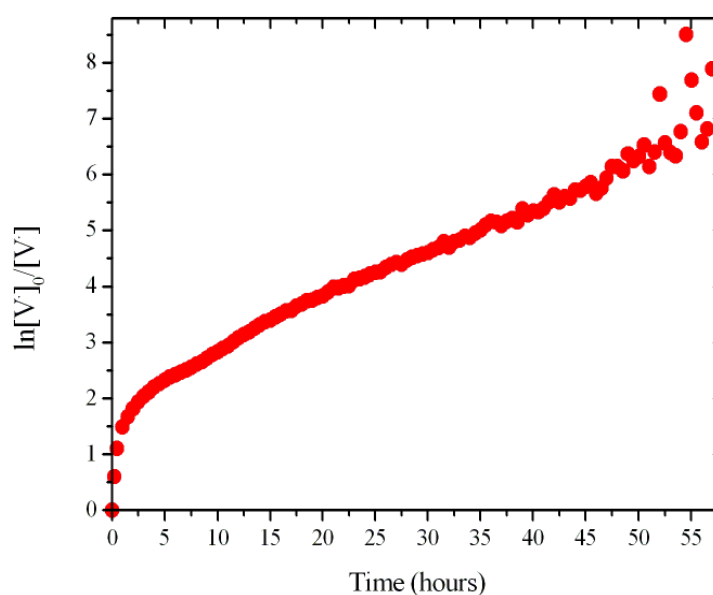


Figure 1.5-12. First order kinetic plot for the verdazyl mediated polymerisation of styrene using

13

The work presented in this section illustrates the various ways in which EPR can be used other than solely for determining a radical's structure. The observations can be used to gain a further understanding of radical action and stability at elevated temperatures for reactions performed in the lab. These studies should ideally be extended by investigating all of the different radicals and initiators described in this thesis allowing further comparisons to be made.

1.6. Conclusions and future work

In summary, five verdazyl radicals with varying substituents at the 3 position were synthesised and four modified to form unimolecular initiators to be investigated as mediators of controlled living radical polymerisations. Polymerisations were undertaken using styrene and n-butyl acrylate to make direct comparison with literature. The polymerisation of MMA and copolymerisation of MMA with styrene was also attempted. Difficulties were encountered in gaining control early on the butyl acrylate polymerisations and MMA polymerisations proved even more difficult to control leading to broad polydispersities and molecular weights that differed from the theoretical values. Varying degrees of success were observed in the polymerisations depending on the substituent at the three position on the verdazyl radical in the aforementioned polymerisations. High temperature EPR has been utilised to study the polymerisation of styrene and to provide an insight into radical stability/activity in various situations based on the observed radical concentration. This work has shown that verdazyl radicals with different structures react differently and as such discrepancies become apparent in their ability to mediate polymerisations, as seen with nitroxides.

Following on from the results discussed in this thesis, more work can be carried out in order to optimise the conditions of the homopolymerisation of all three monomers. One particular area to focus on is increasing the amount of free verdazyl which has already been shown in this work to improve control over the

polymerisation. Better control of the polymerisation temperature to prevent exotherms and aiming for lower molecular weights are also viable options for improving on the observed results. The determination of the C-N bond dissociation constant and kinetic parameters would allow for further correlations between the verdazyl radical structure and its polymerisation mediating ability.

This work could be further extended to investigate a much wider library of verdazyl radicals including those substituted at the 1 and 5 positions. This would undoubtedly lead to the synthesis of novel verdazyls. It may also be worthwhile to investigate other verdazyl families including 6-thio and 6-phosphaverdazyl radicals. With the wide range of possible verdazyl structures potentially available, it may be possible to establish a family of verdazyl radicals designed to mediate the polymerisation of any number of monomers.

1.7. Experimental

1.7.1. Materials

All chemicals were purchased from Sigma Aldrich and used as received unless otherwise stated. Inhibitors were removed from all monomers by passing through a short basic alumina column. *n*-Butyl acrylate was stabilised by adding 1 mg of the appropriate radical for initiator to 40 mL of monomer where stated. Mesitylene, where added, was used as an internal standard for determining conversion. Otherwise conversion was determined by measuring the disappearance of the monomer vinyl peaks with the appearance of polymer.

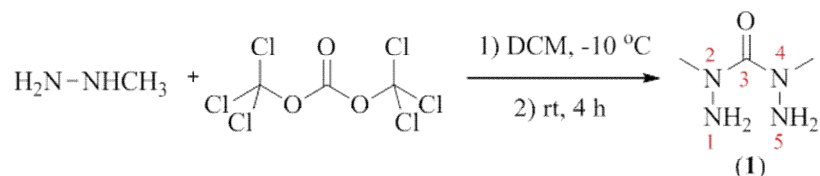
1.7.2. Characterisation techniques

Melting points were recorded using a Stuart Scientific SMP3 melting point apparatus at a rate of 3 °C/minute. Infra-red spectra were recorded using a Bruker Vector 22 FTIR spectrometer fitted with a Golden Gate attenuated total reflection cell. IR transmissions are reported as wavenumbers (cm^{-1}). The following abbreviations have been used; br = broad, w = weak, m = medium, s = strong, Ar = aromatic, adj = adjacent, def = deformation, sym = symmetrical and asym = asymmetrical. NMR spectra were recorded using Bruker DPX-300, DPX-400, DRX-500 and AV III-600 instruments as solutions in deuterated NMR solvents. Chemical shifts are reported in parts per million (ppm) relative to tetramethylsilane (TMS). The following abbreviations are used to abbreviate multiplicities; s = singlet, d =

doublet, t = triplet, q = quartet and m = multiplet. Mesitylene, where added, was used as an internal standard for determining conversion by NMR. Otherwise conversion was determined by measuring the disappearance of the monomer vinyl peaks with the appearance of polymer in NMR spectra. Microanalyses were performed in duplicate where possible by Warwick Analytical Service. High resolution mass spectrometry were performed by the Mass Spectroscopy Facility at Warwick. UV-visible spectra were recorded on a Perkin Elmer Lambdas 25 spectrophotometer using a quartz crystal cuvette. EPR spectra were recorded on Bruker EMX-E, EMX and ECS 080 spectrometers, using either an ER 041X or 041XG X-band microwave bridge and an EIP model 545A microwave frequency counter. The cavity for the ambient temperature measurements were recorded using a Bruker 4103TM/9106 cavity. High temperature measurements were recorded using the EX-102 high temperature cavity and Eurotherm B-V2 2000 control unit. Gel permeation chromatography samples were run on an Agilent 390-LC system equipped with a PL-AS RT autosampler, a 100 μ L injection loop, a 5 μ m PLgel guard column (50 mm x 7.5 mm), 2 5 μ m PLgel Mixed D columns (50mm x 300 mm) and a differential refractive index (DRI) detector. The system was eluted with chloroform at a rate of 1 mL/minute and the detector was calibrated with PL narrow polystyrene (162–371,100 g/mol) and poly methyl methacrylate (200–467,400 g/mol) standard easy vials. Crystallographic data was obtained by Dr Guy Clarkson and theoretical calculations were carried out by Professor Rob Deeth both at the University of Warwick.

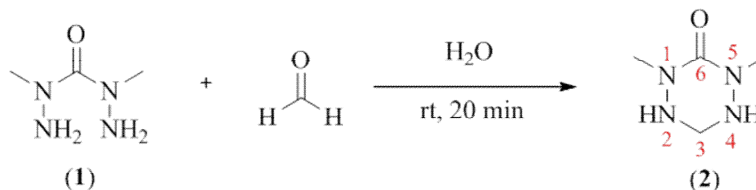
1.7.3. Synthesis of compounds in Chapter 1

1.7.3.1. 2,4-dimethylcarbonohydrazide⁹⁸ (**1**)



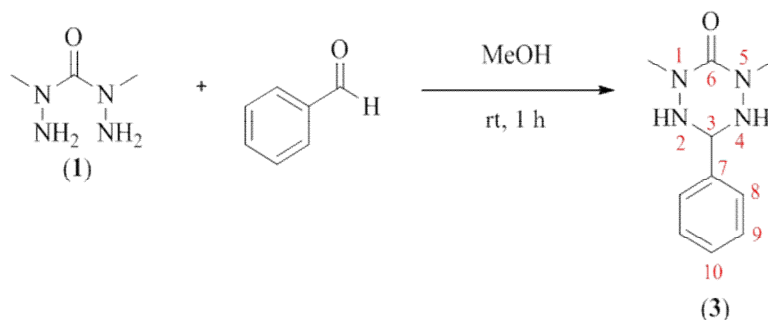
To a stirring solution of methyl hydrazine (54 mL, 1.04 mmol) in dichloromethane (400 mL), cooled to $-10\text{ }^\circ\text{C}$, was added a solution of triphosgene (25.16 g, 84.25 mmol) in dichloromethane (300 mL) dropwise over 1.5 hours. Following the addition, the reaction was allowed to rise to ambient temperature and stirred for a further 4 hours. The reaction mixture was filtered and the solvent removed *in vacuo*. The resulting yellow oil was dried on a high vacuum line to give **1** as a pale yellow solid (26.89 g, 89.5%). The compound is hygroscopic and requires storage under nitrogen in the fridge. Melting point: $49\text{--}51\text{ }^\circ\text{C}$. IR (neat): $\tilde{\nu} = 3308, 3199$ (br s, $>\text{N}-\text{H}$), $3020, 2920, 2839$ (br m, CH stretch), 1583 (br m, $\text{C}=\text{O}$), 1385 (br m, CH_3 sym def) cm^{-1} . ^1H NMR (300.13 MHz, CDCl_3 , 298 K) $\delta = 3.01$ (s, 6H, H2,4); 4.11 (br s, 4H, H1,5). ^{13}C NMR (75.48 MHz, CDCl_3 , 298 K) $\delta = 42.10$ (C2, 4); 164.58 (C3). Mass Spectrometry (+ESI-MS) m/z : 119.09 $[\text{M} + \text{H}]^+$, 141.07 $[\text{M} + \text{Na}]^+$.

1.7.3.2. 1,5-dimethyl-tetrazinan-6-one⁹⁷ (2)

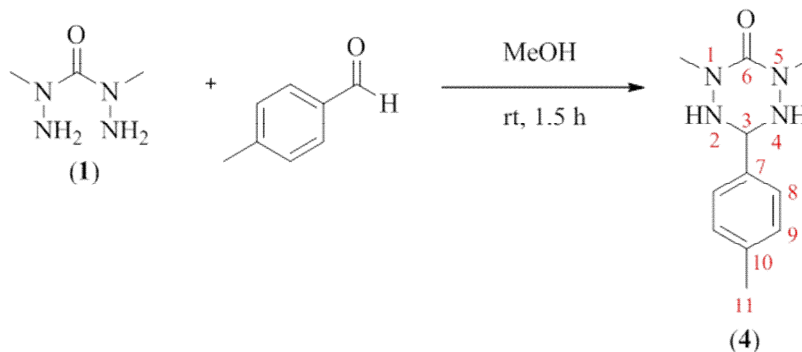


To a solution of **1** (6.00 g, 50.81 mmol) in water (15 mL) stirring at ambient temperature was added dropwise a solution of 37% aqueous formaldehyde (3.80 mL, 43.19 mol) in water (15 mL). The resulting yellow solution was left stirring for 20 minutes. The water was removed on a high vacuum line to give off-white solid. The solid was dissolved in ethanol and the solvent removed *in vacuo*. This was repeated twice more with ethanol resulting in an off white solid which was recrystallised from ethyl acetate to give **2** (2.90 g, 51.5%) as an off white crystalline powder. Melting point: 107–109 °C. IR (neat): $\tilde{\nu}$ = 3244 (br m, >N-H), 2932, 2873 (br w, CH stretch), 1601 (br m, C=O), 1532 (br w, >N-H), 1433 (br m, CH def), 1387 (m, CH₃ sym def) cm⁻¹. ¹H NMR (300.13 MHz, DMSO, 298 K) δ = 2.89 (s, 6H, H1, 5); 3.69 (t, *J* = 7.5 Hz, 2H, H3); 5.29 (t, *J* = 7.5 Hz, 2H, H2, 4). ¹³C NMR (75.48 MHz, DMSO, 298 K) δ = 37.36 (C1, 5); 58.57 (C3); 163.26 (C6). Anal. Calcd. for C₄H₁₀N₄O: C, 36.91; H, 7.74; N, 43.05. Found: C, 36.43; H, 7.73; N, 42.64. Mass Spectrometry (+ESI-MS) *m/z*: 131.09 [M+H]⁺.

1.7.3.3. 1,5-dimethyl-3-phenyl-tetrazinan-6-one⁹⁷ (3)

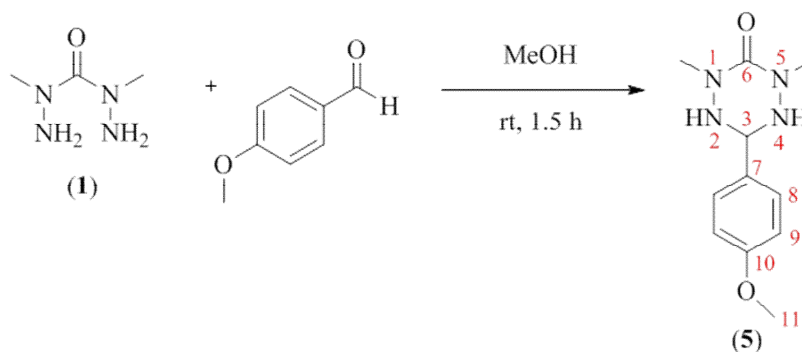


To a solution of **1** (5.00 g, 42.34 mmol) in methanol (53 mL) stirring at ambient temperature was added dropwise a solution of benzaldehyde (4.3 mL, 42.34 mmol) in methanol (42 mL). The resulting solution was left stirring for 1 hour. The solvent was removed *in vacuo* giving a pale orange solid which was recrystallised from methanol to give **3** (2.57 g, 29.4%) as white crystalline needles. Melting point: 124–125 °C. IR (neat): $\tilde{\nu}$ = 3252, 3220 (w, >N-H), 3017 (w, Ar), 2964, 2912, 2868 (w, CH stretch), 1656 (m, C=O), 1596, 1569, 1478 (m, Ar), 1448 (m, CH def), 1400 (m, CH₃ sym def), 1234 (m, C-N stretch), 745, 628 (s, 5 adj H) cm⁻¹. ¹H NMR (300.13 MHz, DMSO, 298 K) δ = 2.95 (s, 6H, H1, 5); 4.90 (t, *J* = 8.0 Hz, 1H, H3); 5.70 (d, *J* = 8.0 Hz, 2H, H2,4); 7.31–7.41 (m, 3H, H9,10), 7.55 (br d, *J* = 7.3 Hz, 2H, H8). ¹³C NMR (100.60 MHz, DMSO, 298 K) δ = 37.64 (C1, 5); 68.56 (C3); 127.01 (C9); 127.88 (C10); 128.19 (C8); 136.71 (C7); 154.47 (C6). Anal. Calcd. for C₁₀H₁₄N₄O: C, 58.24; H, 6.84; N, 27.17. Found: C, 58.02; H, 6.86; N, 27.10. Mass Spectrometry (+ESI-MS) *m/z*: 207.12 [M+H]⁺.

1.7.3.4. 1,5-dimethyl-3-(4-methylphenyl)tetrazinan-6-one⁹⁹ (4)

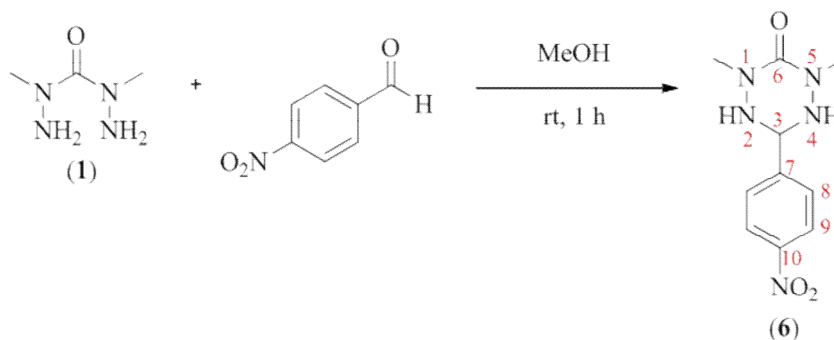
To a solution of **1** (1.20 g, 10.20 mmol) in methanol (10 mL) stirring at ambient temperature was added dropwise a solution of *p*-tolualdehyde (1.28 mL, 10.80 mmol) in methanol (10 mL). The resulting solution was stirred 1.5 hours. The solvent was removed to give a white solid with yellow staining which was recrystallised from ethanol to give **4** (1.42 g, 63.3%) as white crystalline needles. Melting point: 173–175 °C. IR (neat): $\tilde{\nu}$ = 3256, 3228 (m, >N-H), 3023 (w, Ar), 2973, 2920, 2874 (m, CH stretch), 1593 (s, C=O), 1493 (m, Ar), 1434 (m, CH def), 1387 (s, CH₃ sym def), 1233 (m, C-N stretch), 810 (s, 2 adj H) cm⁻¹. ¹H NMR (400.03 MHz, DMSO, 298 K) δ = 2.29 (s, 3H, H11); 2.93 (s, 6H, H1, 5); 4.85 (t, *J* = 8.0 Hz, 1H, H3); 5.63 (d, *J* = 8.0 Hz, 2H, H2, 4); 7.17 (d, *J* = 8.0 Hz, 2H, H9); 7.39 (d, *J* = 8.0 Hz, 2H, H8). ¹³C NMR (100.60 MHz, DMSO, 298 K) δ = 20.73 (C11); 37.71 (C1, 5); 68.51 (C3); 126.97 (C8); 128.80 (C9); 133.77 (C7); 137.11 (C10); 154.53 (C6). Anal. Calcd. for C₁₁H₁₆N₄O: C, 59.98; H, 7.32; N, 25.44. Found: C, 59.72; H, 7.30; N, 25.23. Mass Spectrometry (+ESI-MS) *m/z*: 243.12 [M+Na]⁺.

1.7.3.5. 1,5-dimethyl-3-(4-methoxyphenyl)tetrazinan-6-one⁹⁷ (5)

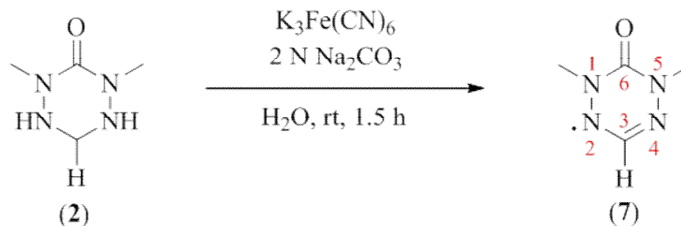


To a solution of **1** (2.36 g, 20.00 mmol) in methanol (25 mL) stirring at ambient temperature was added dropwise a solution of 4-methoxybenzaldehyde (2.72 g, 20.00 mmol) in methanol (5 mL). The resulting solution was left stirring for 1.5 hours. The solvent was removed *in vacuo* to give a white solid with yellow staining which was recrystallised from methanol to give **5** (2.81 g, 59.5%) as white crystalline needles. Melting point: 146–147 °C. IR (neat): $\tilde{\nu}$ = 3246 (s, >N-H), 3038 (w, Ar), 2965, 2920, 2871 (m, CH stretch), 2841 (m, C-OCH₃), 1591 (s, C=O), 1436 (s, CH def), 1404 (s, CH₃ sym def), 1242 (s, C-O stretch), 1170 (m, C-N), 1108 (C-O stretch), 877 (2 adj H) cm⁻¹. ¹H NMR (400.03 MHz, DMSO, 298 K) δ = 2.94 (s, 6H, H1, 5); 3.74 (s, 3H, H11); 4.83 (t, *J* = 8.0 Hz, 1H, H3); 5.61 (d, *J* = 9.0 Hz, 2H, H2,4); 6.92 (d, *J* = 8.0 Hz, 2H, H8); 7.42 (d, *J* = 8.0 Hz, 2H, H9). ¹³C NMR (100.60 MHz, DMSO, 298 K) δ = 37.71 (C1, 5); 55.04 (C11); 68.27 (C3); 113.60 (C8); 128.21 (C9); 128.66 (C7); 154.54 (C10); 158.96 (C6). Anal. Calcd. for C₁₁H₁₆N₄O₂: C, 55.92; H, 6.83; N, 23.71. Found: C, 55.94; H, 6.87; N, 23.65. Mass Spectrometry (+ESI-MS) *m/z*: 259.11 [M+Na]⁺.

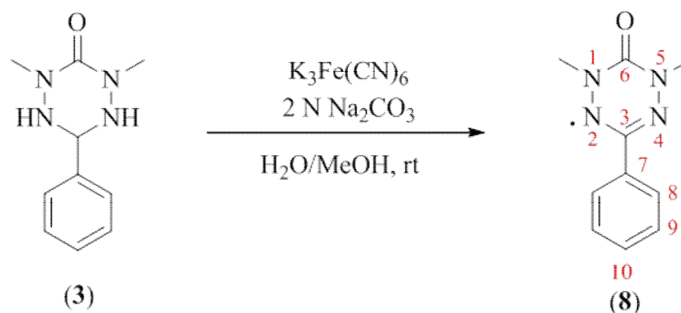
1.7.3.6. 1,5-dimethyl-3-(4-nitrophenyl)tetrazinan-6-one⁹⁷ (6)



To a solution of **1** (1.01 g, 8.55 mmol) in methanol (20 mL) stirring at ambient temperature was added dropwise a solution of 4-nitrobenzaldehyde (0.92 g, 6.09 mmol) in methanol (50 mL). The methanol required gentle heating in order to get the aldehyde to dissolve. The resulting solution was stirred for 1 hour. During this time a yellow precipitate formed and was collected by suction filtration. The resulting yellow powder was recrystallised from methanol to give **6** (0.25 g, 16.6%) as pale yellow needles. Melting point: 172–175 °C. IR (neat): $\tilde{\nu}$ = 3268, 3227 (s, >N-H), 3073 (w, Ar), 2952, 2910, 2865 (br w, CH stretch), 1628, 1607 (NO₂), 1606 (m, Ar), 1517 (s, C=O), 1490 (m, CH₃ sym def), 1432 (m, CH def), 1345 (s, C-NO₂), 1201 (m, C-N), 858 (s, C-OCH₃) cm⁻¹. ¹H NMR (400.03 MHz, DMSO, 298 K) δ = 2.94 (s, 6H, H1, 5); 5.12 (t, *J* = 6.0 Hz, 1H, H3); 5.91 (d, *J* = 6.0 Hz, 2H, H2, 4); 7.82 (d, *J* = 9.0 Hz, 2H, H8); 8.25 (d, *J* = 9.0 Hz, 2H, H9). ¹³C NMR (100.60 MHz, DMSO, 298 K) δ = 37.50 (C1, 5); 67.69 (C3); 123.34 (C8); 128.70 (C9); 144.95 (C10); 147.11 (C7); 154.18 (C6). Anal. Calcd. for C₁₀H₁₃N₅O₃: C, 47.81; H, 5.22; N, 27.87. Found: C, 47.78; H, 5.01; N, 27.96. Mass Spectrometry (+ESI-MS) *m/z*: 247.09 [M+Na]⁺.

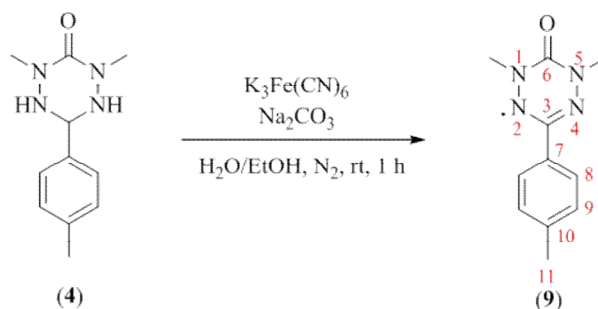
1.7.3.7. 1,5-dimethyl oxoverdazyl⁶³ (7)

To a solution of **2** (3.30 g, 25.6 mmol) in water (26 mL) stirring at ambient temperature was added dropwise a solution potassium ferricyanide (25.30 g, 76.8 mmol) dissolved in water (128 mL) and 2 N sodium carbonate solution (38.5 mL). The resulting solution was stirred for 1.5 hours and then extracted eight times with diethyl ether (60 mL). The combined extracts were dried using magnesium sulphate and the solvent removed *in vacuo* to give a dark red solid. The compound was purified by neutral alumina column chromatography using 1:1 dichloromethane/petroleum ether 40-60 to give **7** (2.67 g, 82.1%) as a dark red crystalline solid, which can be recrystallised from petroleum ether but the crystals are not stable at ambient temperature and require storage in the freezer. Melting point: 36–38 °C. IR (neat): $\tilde{\nu} = 3072$ (br w, Ar), 2942 (br w, CH stretch), 1672 (br s, C=O), 1452 (br m, CH def), 1347 (br m, CH₃ sym def), 1262 (br m, C-O) cm⁻¹. EPR (9.77 GHz, toluene, 298K): $a(\text{N}_{2,4}) = 6.50$ G; $a(\text{N}_{1,5}) = 5.19$ G; $a(\text{H}_{\text{CH}_3}) = 5.45$ G (6H); $a(\text{H}_{\text{CH}}) = 0.78$ G; $g = 2.0045$. UV-vis (1,4-dioxane): λ_{max} (lg ϵ) = 254 nm (3.08), 378 nm (2.84), 416 nm, (2.75), 430 nm (2.79), 446 nm (2.69). Anal. Calcd. for C₂₄H₃₁NO₃: C, 37.79; H, 5.55; N, 44.07. Found: C, 36.37; H, 5.25; N, 41.25. Mass Spectrometry (+ESI-MS) m/z : 127.06 [M]⁺.

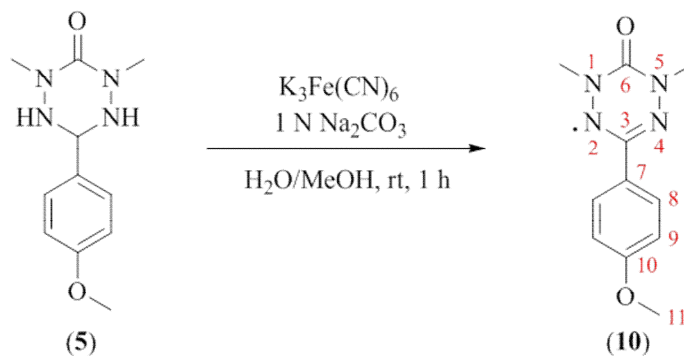
1.7.3.8. 1,5-dimethyl-3-phenyl-6-oxoverdazyl⁶³ (**8**)

To a solution of **3** (1.00 g, 4.85 mmol) dissolved in water (23 mL) and methanol (15 mL) stirring at ambient temperature was added dropwise a solution of potassium ferricyanide (5.24 g, 15.9 mmol) in water (30 mL) and 2 N sodium carbonate solution (7 mL). The addition of an excess of water precipitated **8** (0.88 g, 89.3%) as an orange powder which was collected by suction filtration, washed thoroughly with water and dried in a vacuum oven. Melting point: 63–65 °C. IR (neat): $\tilde{\nu}$ = 3034 (w, Ar), 2945 (w, CH stretch), 1670 (s, C=O), 1456 (m, CH def), 1375 (m, CH₃ sym def), 1248 (s, C-O), 1162 (w, C-O), 776 (s, 5 adj H) cm⁻¹. EPR (9.77 GHz, toluene, 298K): $a(\text{N}_{2,4}) = 6.50 \text{ G}$; $a(\text{N}_{1,5}) = 5.10 \text{ G}$; $a(\text{H}_{\text{CH}_3}) = 5.45 \text{ G (6H)}$; $g = 2.0045$. UV-vis (1,4-dioxane): $\lambda_{\text{max}} (\lg \epsilon) = 248 \text{ nm (4.43)}$, 389 nm (2.91), 400 nm (3.03), 440 nm, (3.17), 492 nm (2.48), 526 nm (2.34), 552 nm (1.29). Anal. Calcd. for C₂₄H₃₁NO₃: C, 59.10; H, 5.46; N, 27.57. Found: C, 57.50; H, 5.25; N, 26.61. Mass Spectrometry (+ESI-MS) m/z : 203.09 [M]⁺.

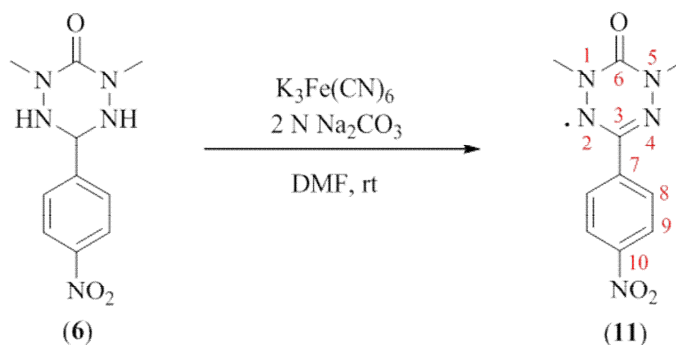
1.7.3.9. 1,5-dimethyl-3-(4-methylphenyl)-6-oxoverdazyl⁹⁹ (9)



To a solution of **4** (0.40 g, 1.80 mmol) in ethanol (30 mL) and water (10 mL) stirring at ambient temperature under nitrogen in a two-necked round bottom flask was added dropwise a solution of potassium ferricyanide (2.00 g, 6.10 mmol) and sodium carbonate (0.50 g, 4.70 mmol) in water (10 mL). The resulting solution was stirred for 1 hour before being poured into ice cold water (100 mL) to precipitate **9** (0.18 g, 46.1%) as an orange powder which was recrystallised from methanol to give dark orange needles. Melting point: 95–96 °C. IR (neat): $\tilde{\nu}$ = 3014 (w, Ar), 2974, 2941, 2923 (w, CH stretch), 1677 (s, C=O), 1516 (m, Ar), 1450 (m, CH def), 1400 (m, CH₃ sym def), 1295 (m, C-N stretch), 823 (s, 2 adj H) cm⁻¹. EPR (9.86 GHz, toluene, 298K): $a(\text{N}_{2,4}) = 6.52$ G; $a(\text{N}_{1,5}) = 5.15$ G; $a(\text{H}_{\text{CH}_3}) = 5.42$ G (6H); $g = 2.0099$. UV-vis (1,4-dioxane): λ_{max} (lg ϵ) = 253 nm (3.34), 391 nm (2.80), 404 nm (2.88), 416 nm (3.00), 451 nm (2.40), 495 nm (2.53), 528 nm (2.42), 557 nm (2.07). Anal. Calcd. for C₁₁H₁₃N₄O: C, 60.81; H, 6.03; N, 25.79. Found: C, 60.39; H, 5.66; N, 25.52. Mass Spectrometry (+ESI-MS) m/z : 240.10 [M]⁺.

1.7.3.10. 1,5-dimethyl-3-(4-methoxyphenyl)-6-oxoverdazyl⁶³ (**10**)

To a solution of **5** (1.50 g, 6.40 mmol) in methanol (77 mL) and water (52 mL) stirring at ambient temperature was added dropwise a solution of potassium ferricyanide (6.32 g, 19.2 mmol) in 1 N sodium carbonate solution (19 mL). The resulting solution was stirred for 1 hour. During which time a mixture of red and cream solids precipitated and was collected by suction filtration and washed thoroughly with water to give **10** (1.20 g, 80.5%) as a red powder which was recrystallised from methanol to give a dark red crystalline solid. Melting point: 86–88 °C. IR (neat): $\tilde{\nu} = 3028$ (w, Ar), 2941, 2912 (m, CH stretch), 2833 (m, C-OCH₃), 1678 (s, C=O), 1606, 1517 (m, Ar), 1469 (m, CH₃ sym def), 1433 (m, CH def), 1298 (s, C-N), 1244, 1110 (m, C-O), 840 (s, 2 adj H) cm⁻¹. EPR (9.81 GHz, toluene, 298K): $a(\text{N}_{2,4}) = 6.53$ G; $a(\text{N}_{1,5}) = 5.37$ G; $a(\text{H}_{\text{CH}_3}) = 5.15$ G (6H); $g = 2.0100$. UV-vis (1,4-dioxane): λ_{max} (lg ϵ) = 263 nm (4.46), 318 nm (2.17), 394 nm (2.82), 407 nm (2.79), 417 nm (2.88), 499 nm (2.57), 523 nm (2.61), 557 nm (2.30). Anal. Calcd. for C₁₁H₁₃N₄O₂: C, 56.64; H, 5.62; N, 24.02. Found: C, 56.41; H, 5.35; N, 23.85. Mass Spectrometry (+ESI-MS) m/z : 240.10 [M]⁺.

1.7.3.11. 1,5-dimethyl-3-(4-nitrophenyl)-6-oxoverdazyl⁶³ (**11**)

To a solution of **6** in dimethylformamide (40 mL) stirring at ambient temperature was added dropwise a solution of potassium ferricyanide (1.74 g, 5.28 mmol) in water (20 mL) and 2 N sodium carbonate solution (2.64 mL). The solution got warm during the addition and a cream precipitate formed. On cooling a brown precipitate formed. The solids were collected by suction filtration and washed thoroughly with water to give **11** (0.26 g, 65.5%) as a *fluffy* brown solid which was recrystallised from methanol to give fine brown needles. Melting point: 144–146 °C. IR (neat): $\tilde{\nu}$ = 3087 (w, Ar), 2947 (w, CH stretch), 1688 (s, NO₂), 1604 (m, NO₂), 1595 (m, Ar), 1520 (s, C=O), 1413 (m, CH def), 1402 (m, CH₃ sym def), 1341 (s, C-NO₂), 1292 (s, C-N stretch), 1248, 1107 (m, C-O), 854 (s, 2 adj H) cm⁻¹. EPR (9.81 GHz, toluene, 298K): $a(\text{N}_{2,4}) = 6.45 \text{ G}$; $a(\text{N}_{1,5}) = 5.35 \text{ G}$; $a(\text{H}_{\text{CH}_3}) = 5.48 \text{ G (6H)}$; $g = 2.0101$. UV-vis (1,4-dioxane): λ_{max} (lg ϵ) = 293 nm (4.27), 408 nm (3.17), 424 nm (3.33), 487 nm (2.43). Anal. Calcd. for C₁₀H₁₀N₅O₃: C, 48.39; H, 4.06; N, 28.21. Found: C, 48.03; H, 3.82; N, 27.95. Mass Spectrometry (+ESI-MS) m/z : 271.07 [M+Na]⁺.

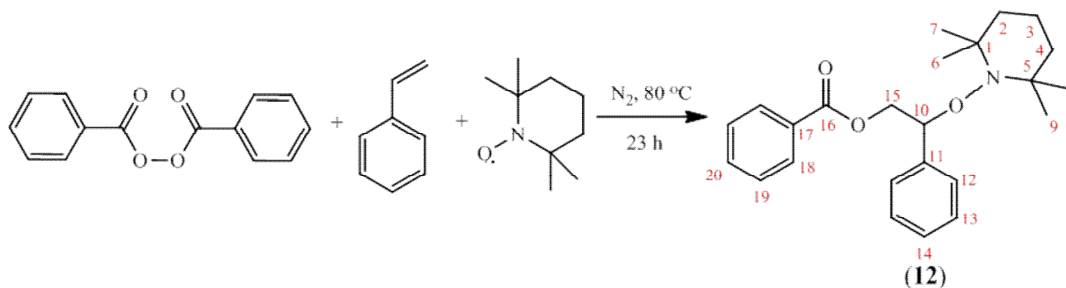
1.7.3.12. Sample preparation of TEMPO and verdazyl radicals
7, 8, 9, 10 and 11 for EPR

To an oven dried Schlenk tube was added the verdazyl radical and toluene to make up the desired concentration. The solution was degassed using three freeze-pump-thaw cycles and kept under nitrogen. Using a gas tight syringe, 0.5 mL of solution was introduced to a degassed EPR tube which was then capped and sealed with parafilm. The EPR parameters used varied for each radical. This enabled the best spectrum to be obtained to determine the hyperfine couplings constants.

Table 1.7-1. Quantities of sample for the EPR of verdazyl radicals

Radical	R	Solution concentration	Radical		Toluene
		mM	mg	mmol	mL
TEMPO		1	0.3	0.0020	2
7	H	1	0.3	0.0024	2
8	Ph	0.2	0.2	0.0010	5
9	PhMe	0.05	0.3	0.0011	27
10	PhOMe	0.05	0.6	0.0008	17
11	PhNO ₂	0.05	0.9	0.0036	72

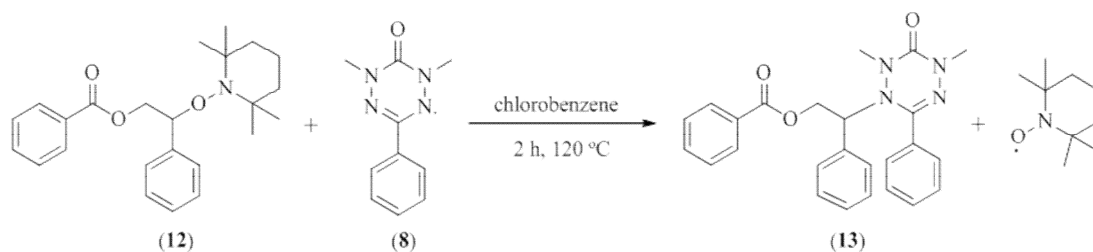
1.7.3.13. 2-phenyl-2-(2,2,6,6-tetramethylpiperidin-1-oxyl)ethyl benzoate²⁴ (12)



To styrene (320 mL, 279 mmol) was added benzoyl peroxide (8.04 g, 33.19 mmol) and 2,2,6,6-tetramethyl-piperidin-1-yloxy (TEMPO) (11.36 g, 72.7 mmol) producing a deep red solution. The solution was degassed by bubbling with nitrogen for 1 hour. The reaction mixture was kept under nitrogen and stirred at 80 °C for 23 hours. The solution was cooled to ambient temperature before removing the styrene on a high vacuum line to give a dark orange oil. The product was purified by repeated silica gel column chromatography with 1:1 dichloromethane/petroleum ether 40-60 changing to 9:1 dichloromethane/petroleum ether 40-60, 30:1 petroleum ether 40-60/diethyl ether changing to 20:1 petroleum ether 40-60/diethyl ether to give **12** (2.47 g, 19.5%) as white crystalline solid. Melting point: 73–74 °C. IR (neat): $\tilde{\nu}$ = 3002 (w, Ar), 2967, 2923 (m, CH stretch), 1602 (w, Ar), 1712 (s, C=O), 1450 (m, CH def), 1364, 1311 (m, N-O asym stretch), 1295 (m, C-N stretch), 1264 (s, C-O stretch), 1132 (m, C-O stretch), 764 (m, 5 adj H) cm^{-1} . ^1H NMR (300.13 MHz, CDCl_3 , 298 K) δ = 0.75, 1.06, 1.20, 1.36 (br s, 12H, H6, 7, 8, 9); 1.50 (br s, 6H, H2, 3, 4); 4.52 (dd, J = 6.0, 11.0 Hz, 1H, H15); 4.82 (dd, J = 5.0, 11.0 Hz, 1H, H15); 5.05 (dd, J = 5.0, 6.0 Hz, 1H, H10); 7.23 – 7.28 (m, 7H, H12-14, 19); 7.38 (tt, J = 7.0, 1.0 Hz, 1H, H20); 7.92 (dd, J = 8.0, 1.0 Hz, 2H, H18). ^{13}C NMR (75.47 MHz, CDCl_3 , 298 K) δ = 17.15 (C3); 20.40 (C7, 8); 34.00 (C6, 9); 40.41 (C2, 4);

60.11 (C1, 5); 66.78 (C15); 83.94 (C10); 127.61 – 129.57 (C12-15, 18, 19); 130.20 (C18); 132.83 (C20); 140.691 (C11); 166.50 (C16). Anal. Calcd. for C₂₄H₃₁NO₃: C, 75.56; H, 8.19; N, 3.67. Found: C, 75.59; H, 8.19; N, 3.64. Mass Spectrometry (+ESI-MS) *m/z*: 382.26 [M+H]⁺, 404.22[M+Na]⁺.

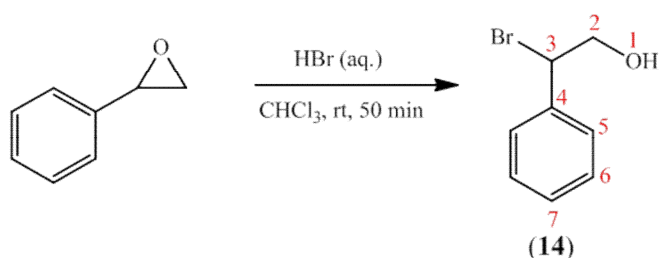
1.7.3.14. Synthesis of 2-phenyl-2-(1,5-dimethyl-3-Phenyl-6-oxoverdazyl)ethyl benzoate (**13**) via an exchange reaction⁵³



To an oven dried Schlenk tube was added **8** (1.2 mg, 0.006 mmol) dissolved in chlorobenzene (3 mL) and **12** (1.1 mg, 0.003 mmol) dissolved in chlorobenzene (3 mL). The resulting solution was degassed using 4 freeze-pump-thaw cycles and stirred at 120 °C for 2 hours during which time the solution changed from pale orange to pale purple in colour. Using a gas tight syringe samples were taken at $t = 0$ and then every 30 minutes and put into degassed EPR tubes which were then capped. The samples were run at ambient temperature in the EPR spectrometer.

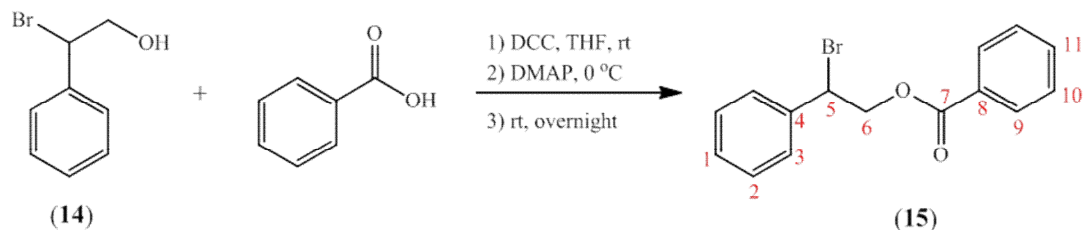
This reaction was repeated using ascorbic acid (0.6 equivalents with respect to **12**) which was mixed with chlorobenzene, degassed and syringed into the reaction mixture after it had been heating for 10 minutes.

1.7.3.15. 2-bromo-2-phenyl ethanol¹¹⁶ (**14**)



To a stirring solution of styrene oxide (3.8 mL, 33.33 mmol) in chloroform (350 mL) at ambient temperature was added dropwise 48% aqueous hydrobromic acid (100 mL, 184 mmol). The resulting orange mixture was stirred for 50 minutes before being washed twice with water (100 mL), and twice with saturated sodium hydrogen carbonate solution (200 mL). The resulting organic solution was dried with magnesium sulphate and the solvent removed *in vacuo* to give **14** (6.1 g, 91%) as a pale orange oil. IR (neat): $\tilde{\nu}$ = 3349 (w, OH), 3030, 1492 (w, Ar), 1453 (m, CH def), 1060, 1021 (s, C-O), 694 (s, C-Br) cm^{-1} . ^1H NMR (300.13 MHz, CDCl_3 , 298 K) δ = 1.98 (br s, 1H, H1); 3.93-4.11 (m, 2H, H2); 5.06 (dd, J = 6.0, 2.0 Hz, 1H, H3); 7.31-7.44 (m, 5H, H5-7). ^{13}C NMR (75.47 MHz, CDCl_3 , 298 K) δ = 56.40 (C3); 66.94 (C2); 127.32-128.40 (C5-7); 137.58 (C4). Anal. Calcd. for $\text{C}_8\text{H}_9\text{BrO}$: C, 47.79; H, 4.51. Found: C, 47.97; H, 4.56. Mass Spectrometry (+ESI-MS) m/z : 224.97 $[\text{M}+\text{Na}]^+$; 183.98 $[\text{M}-\text{OH}]^+$.

1.7.3.16. 2-bromo-2-phenylethyl benzoate (15)



Compound **15** was synthesised using a slightly modified procedure to that described in the literature.¹¹⁷ To a solution of **14** (5.01 g, 24.92 mmol) in tetrahydrofuran (100 mL) stirring at ambient temperature was added benzoic acid (3.35 g, 27.41 mmol). Once dissolved, the solution was cooled to 0 °C, and *N,N'*-dicyclohexylcarbodiimide (5.99 g, 24.93 mmol) added followed by 4-(dimethylamino)pyridine (0.27 g, 2.27 mmol) once dissolved. The solution was left stirring overnight at ambient temperature. The solvent was removed *in vacuo* to give an off white solid. The solid was dissolved in diethyl ether and filtered before washing twice with water. The resulting solution was dried with magnesium sulphate and the solvent removed *in vacuo* to give a yellow oil and white solid. The oil was dissolved in 3:1 petroleum ether 40-60/dichloromethane and the white solid removed by suction filtration before purification of the filtrate by silica gel column chromatography using 3:1 petroleum ether 40-60/dichloromethane. The solvent was removed *in vacuo* to give **15** (3.82 g, 50.4%) as a pale blue oil which solidified overnight during storage in the fridge. Melting point: 36–38 °C. IR (neat): $\tilde{\nu}$ = 3031 (w, Ar), 2955, 2876 (w, CH stretch), 1600 (w, Ar), 1710 (br s, (C=O)), 1109 (s, C-O stretch), 761, 707 (5 adj H), 692 (s, C-Br) cm^{-1} . ¹H NMR (300.13 MHz, CDCl₃, 298 K) δ = 4.74 (dd, *J* = 6.0, 12 Hz, 1H, H₆), 4.84 (dd, *J* = 7.0, 12 Hz, 1H, H₆); 5.27 (dd, *J* = 8.0, 10.0 Hz, 1H, H₅); 7.12 – 7.32 (m, 7H, H₁₋₃, 10), 7.38 (tt, *J* = 1.0, 7.0 Hz, H₁₁), 7.81 (dd, *J* = 1.0, 10.0 Hz, H₉). ¹³C NMR (75.48 MHz, CDCl₃, 298 K) δ = 50.00 (C₅); 67.89 (C₆), 127.80

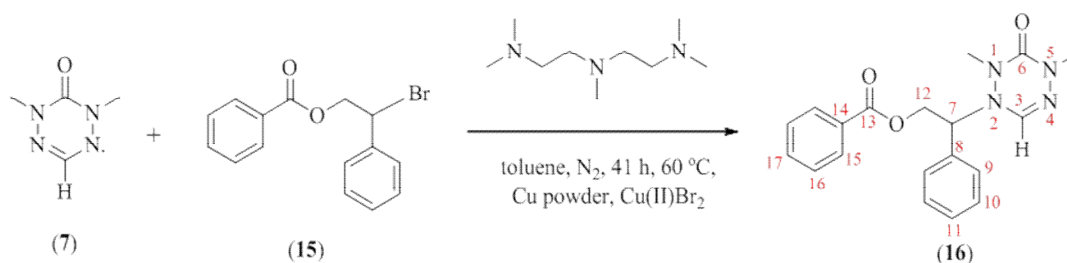
– 129.61 (C1-3, 9, 10), 129.50 (C8), 133.25 (C11), 138.05 (C4), 165.84 (C7). Anal.

Calcd. for C₁₅H₁₃BrO₂: C, 59.04; H, 4.29. Found: C, 59.02; H, 4.33. Mass

Spectrometry (+ESI-MS) *m/z*: 326.99 [M + Na]⁺.

1.7.3.17. 2-phenyl-2-(1,5-dimethyl-6-oxoverdazyl) ethyl benzoate

unimer (16)

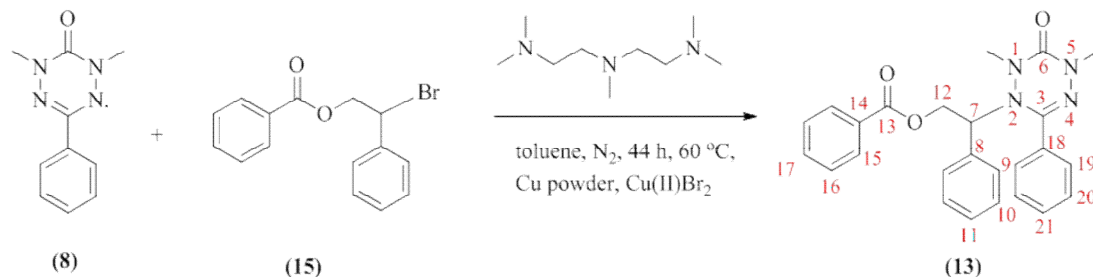


Compound **16** was synthesised using a slightly modified procedure to that described in the literature.⁵³ A solution of **7** (0.52 g, 3.90 mmol), **15** (1.00 g, 3.50 mmol) and *N,N,N',N'',N'''*-pentamethyldiethylenetriamine (PMDETA, 0.15 mL, 0.7 mmol) in toluene (15 mL) was degassed by five freeze-pump-thaw cycles and cannulated into a nitrogen filled round bottom flask containing Cu powder (0.22 g, 3.50 mmol) and Cu(II)Br₂ (16 mg, 0.072 mmol). The reaction mixture was stirred at 60 °C under nitrogen for 41 hours. The reaction mixture was filtered and the solvent removed. The resulting pale yellow oil was dissolved in the minimum amount of dichloromethane and washed with water (3 x 15 mL). The resulting solution was dried using magnesium sulphate and the solvent removed to yield an off white solid. The compound was purified by silica gel column chromatography using 5:4:1 dichloromethane/petroleum ether 40-60/diethyl ether to give **16** (0.39 g, 31.6%) as white powder which was recrystallised from 9:1 petroleum ether 40-60/isopropanol

to give a white crystalline solid. Melting point: 110–111 °C. IR (neat): $\tilde{\nu} = 3034$ (w, Ar), 2925, 2873, 2853 (w, CH stretch), 1717, 1657 (s, C=O), 1619 (m, Ar), 1452 (m, CH def), 1371 (s, CH₃ sym def), 1282 (br s, C-O stretch), 1178 (m, C-N stretch), 1116 (m, C-O stretch), 761, 707 (s, 5 adj H) cm⁻¹. ¹H NMR (400.03 MHz, CDCl₃, 298 K) $\delta = 2.91$ (s, 3H, H5); 3.00 (s, 3H, H1); 4.59 (dd, $J = 5.0, 8.0$ Hz, 1H, H7); 4.72 (dd, $J = 5.0, 12.0$ Hz, 1H, H14); 4.89 (dd, $J = 9.0, 12.0$ Hz, 1H, H14); 6.77 (s, 1H, H3); 7.34 – 7.42 (m, 5H, H9-11); 7.45 (br tt, $J = 8.0$ Hz, 2H, 16), 7.58 (tt, $J = 1.0, 7.0$ Hz, 1H, H17); 8.02 (dd, $J = 1.0, 7.0$ Hz, 2H, H15). ¹³C NMR (100.60 MHz, CDCl₃, 298 K) $\delta = 36.33$ (C5); 38.60 (C1); 62.95 (C12); 64.95 (C7); 128.14 – 128.96 (phenyl C); 129.59 (C8); 129.83 (C15); 133.47 (C17); 134.97 (C14); 137.84 (C3); 157.06 (C6); 166.26 (C13). Anal. Calcd. for C₁₉H₂₀N₄O₃: C, 64.76; H, 5.72; N, 15.90. Found: C, 64.78; H, 5.75; N, 15.47. Mass Spectrometry (+ESI-MS) m/z : 375.14 [M+Na]⁺.

This reaction was repeated on a smaller scale for EPR analysis. Using a gas tight syringe samples were taken at $t = 0, 0.5$ and 40.5 hours and put into degassed EPR tubes, which were then capped. The samples were run at ambient temperature in the EPR spectrometer.

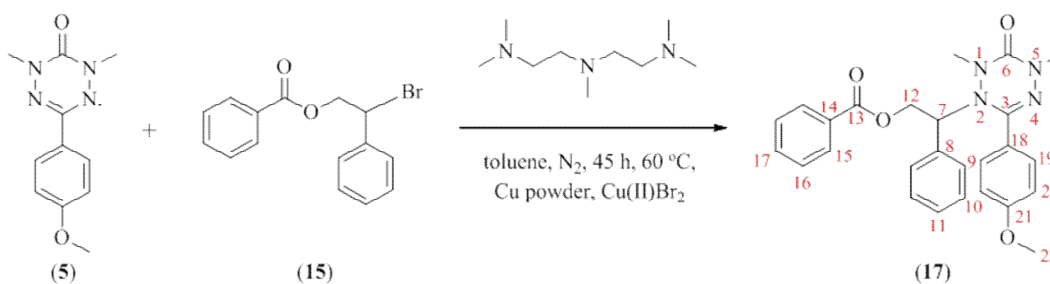
1.7.3.18. Synthesis of 2-phenyl-2-(1,5-dimethyl-3-Phenyl-6-oxoverdazyl)ethyl benzoate (**13**)



Compound **13** was synthesised using the same procedure as described for **16** to give **13** (0.94 g, 62.7%) as a white solid which was recrystallised from isopropanol to give a white crystalline solid. Melting point: 102-104 °C. IR (neat): $\tilde{\nu}$ = 3063 (w, Ar), 2964, 2941, 2895, 2869 (w, CH stretch), 1721, 1617 (s, C=O), 1447 (m, CH def), 1360 (s, CH₃ sym def), 1276 (s, C-O stretch), 1254 (m, C-N stretch), 1118 (s, C-O), 769, 705 (s, 5 adj H) cm⁻¹. ¹H NMR (500.13 MHz, CDCl₃, 253 K) major conformer (78%) δ = 2.63 (s, 3H, H5); 3.33 (s, 3H, H1); 4.48 (dd, J = 4.0 Hz, 1H, H7); 4.60 (dd, J = 4.0, 12.0 Hz, 1H, H12); 5.02 (t, J = 12.0 Hz, 1H, H12); 7.21-7.26 (m, 2H, H9); 7.28 (t, J = 8Hz, 2H, H21); 7.34-7.40 (m, 3 H, H10, 11); 7.43-7.53 (m, 2H, H20); 7.50 (t, J = 8Hz, 2H, H16); 7.67 (br t, J = 7.0 Hz, 1H, H17); 7.88 (br d, J = 7.0 Hz, 2H, H19), 8.12 (br d, J = 7.0 Hz, 2H, H15); minor conformer (22%) δ = 2.68 (s, 3H, H1); 3.02 (s, 3H, H5); 4.49 (m, 1H, H12); 4.75 (br dd, J = 4.0, 10.0 Hz, 1H, H7); 5.08 (br dd, J = 10.0, 12.0 Hz, 1H, H12); 7.20 – 7.53 (m, 10 H, H9-11, 16, 20, 21); 7.63 (br t, J = 7.0 Hz, H17); 7.81 (br d, J = 7.0 Hz, 2H, H19); 8.02 (br d, J = 7.0 Hz, 2H, H15). ¹³C NMR (125.77 MHz, CDCl₃, 253 K) δ = major conformer (78%) δ = 35.74 (C5); 40.59 (C1); 62.32 (C12); 64.43 (C7); 127.00 – 129.84 (C9-11, 16, 19-21); 129.53 (C8); 130.58 (C18); 130.93 (C15); 133.76 (C17); 134.35 (C14); 147.43 (C3); 157.38 (C6); 166.31 (C13); minor conformer (22%) δ = 36.89

(C5); 40.26 (C1); 63.41 (C12); 63.98 (C7); 127.00 – 129.84 (C9-11, 16, 19-21); 129.37 (C8); 130.85 (C18); 131.08 (C15); 133.61 (C17); 135.38 (C14); 149.47 (C3); 159.63 (C6); 166.20 (C13). Anal. Calcd. for C₂₅H₂₄N₄O₃: C, 70.08; H, 5.65; N, 13.08. Found: C, 69.86; H, 5.66; N, 12.99. Mass Spectrometry (+ESI-MS) *m/z*: 451.17 [M+Na]⁺.

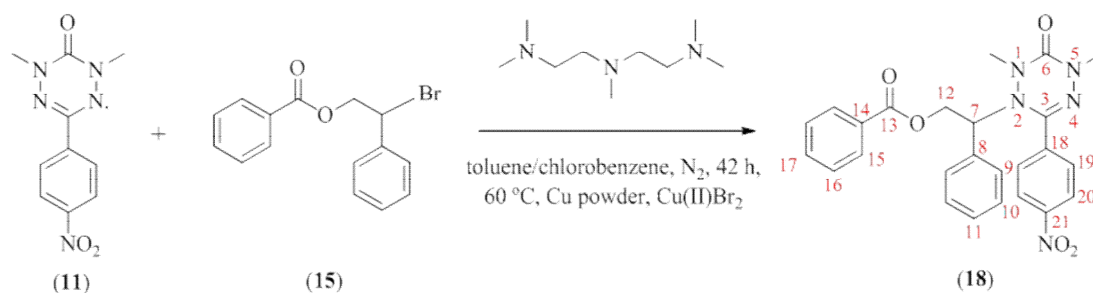
1.7.3.19. Synthesis of 2-phenyl-2-(1,5-dimethyl-3-methoxyphenyl-6-oxoverdazyl)ethyl benzoate (17)



Compound **17** was synthesised using the same procedure as described for **16** to give **17** (0.44 g, 36.1%) as an off white solid which was recrystallised from isopropanol to give a white crystalline solid. Melting point: 101-102 °C. IR (neat): $\tilde{\nu}$ = 3032 (w, Ar), 3005, 2935, 2911 (w, CH stretch), 2838 (w, C-OCH₃), 1719, 1670 (s, C=O), 1605, 1511 (m, Ar), 1452 (m, CH def), 1350 (m, CH₃ sym def), 1267 (s, C-O stretch), 1250 (s, C-N stretch), 1170 (m, C-O stretch), 837 (s, 2 adj H), 752, 709 (s, 5 adj H) cm⁻¹. ¹H NMR (500.13 MHz, CDCl₃, 253 K) major conformer (76%) δ = 2.63 (s, 3H, H5); 3.34 (s, 3H, H1); 3.84 (s, H22); 4.51 (dd, *J* = 4.0, 11.0 Hz, 1H, H7); 4.63 (dd, *J* = 4.0, 12.0 Hz, 1H, H12); 5.03 (t, *J* = 11.0 Hz, 1H, H12); 6.77 (d, *J* = 9.0 Hz, 2H, H20); 7.23 – 7.25 (m, 2 H, H9), 7.36 – 7.50 (m, 3H, H10-11); 7.58 (t, *J* = 8 Hz, 2H, H16); 7.70 (t, *J* = 8 Hz, 1H, H17); 7.81 (d, *J* = 9 Hz, 2H, H19); 8.18 (d, *J* =

7 Hz, 2H, H15); minor conformer (24%) $\delta = 2.69$ (s, 3H, H1); 3.04 (s, 3H, H5); 3.90 (s, 3H, H22); 4.51 (m, 1H, H12); 4.77 (dd, $J = 4.0, 10.0$ Hz, 1H, H7); 5.10 (br dd, $J = 10.0, 12.0$ Hz, 1H, 12); 7.00 (d, $J = 9.0$ Hz, 2H, H20); 7.23 – 7.46 (m, 5 H, H9-11), 7.52 (t, $J = 8$ Hz, 2H, H16); 7.65 (t, $J = 8$ Hz, 1H, H17); 7.76 (d, $J = 9$ Hz, 2H, H19); 8.03 (d, $J = 7$ Hz, 2H, H15). ^{13}C NMR (125.77 MHz, CDCl_3 , 253 K) $\delta =$ major conformer (76%) $\delta = 35.48$ (C5); 40.45 (C1); 55.54 (C22); 62.27 (C12); 64.26 (C7); 114.10 (C20); 122.65 (18); 127.00 – 129.80 (C8-11, 15, 16, 19); 133.61 (C17); 134.20 (C14); 147.58 (C3); 157.41 (C6); 161.41 (C21); 166.17 (C23); minor conformer (24%) $\delta = 36.65$ (C5); 40.13 (C1); 55.52 (C22); 63.31 (C12); 63.84 (C7); 114.25 (C20); 122.83 (C18); 127.00 – 129.80 (C8-11, 15, 16, 19); 133.46 (C17); 135.36 (C14); 149.56 (C3); 159.74 (C6); 161.55 (C21); 166.07 (C13). Anal. Calcd. for $\text{C}_{26}\text{H}_{26}\text{N}_4\text{O}_4$: C, 68.11; H, 5.72; N, 12.22. Found: C, 67.43; H, 5.55; N, 11.90. Mass Spectrometry (+ESI-MS) m/z : 459.20 $[\text{M}+\text{H}]^+$, 451.17 $[\text{M}+\text{Na}]^+$.

1.7.3.20. Synthesis of 2-phenyl-2-(1,5-dimethyl-3-nitrophenyl-6-oxoverdazyl)ethyl benzoate (18)

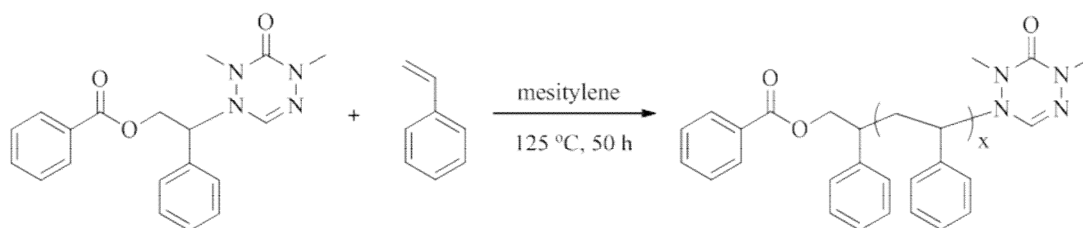


Compound **18** was synthesised using the same procedure as described for **16** except toluene and chlorobenzene (2:1) were used as the reaction solvent to give **18** (0.39 g, 48.5%) as a yellow solid. Melting point: $158\text{--}159^\circ\text{C}$. IR (neat): $\tilde{\nu} = 3064$ (w, Ar),

2939, 2877 (w, CH stretch), 1723, 1714 (s, NO₂), 1684 (s, C=O), 1454 (m, CH def), 1342 (s, CH₃ sym def), 1272 (s, C-N stretch), 1103 (m, C-O stretch), 853 (m, 5 adj H), 749, 703 (s, 2 adj H) cm⁻¹. ¹H NMR (600.13 MHz, CDCl₃, 253 K) major conformer (81%) δ = 2.65 (s, 3H, H5); 3.35 (s, 3H, H1); 4.41 (dd, *J* = 4.0, 7.0 Hz, 1H, H7); 4.61 (dd, *J* = 4.0, 8.0 Hz, 1H, H12); 5.01 (t, *J* = 11.0 Hz, 1H, H12); 7.10 – 7.22 (m, 2H, H9); 7.35 - 7.40 (m, 3H, H10, 11), 7.58 (t, *J* = 8 Hz, 2H, H16); 7.71 (t, *J* = 7 Hz, 1H, H17); 8.01 (d, *J* = 9 Hz, 2H, H19); 8.11 (d, *J* = 9 Hz, 2H, H20); 8.14 (d, *J* = 7 Hz, 2H, H15); minor conformer (19%) δ = 2.76 (s, 3H, H1); 3.08 (s, 3H, H5); 4.52 (dd, *J* = 4.0, 8.0 Hz, 1H, H12); 4.67 (dd, *J* = 4.0, 6.0 Hz, 1H, H7); 4.99 – 5.04 (m, 1H, 12); 7.10 – 7.45 (m, 5H, H9-11); 7.51 (t, *J* = 8 Hz, 2H, H16); 7.64 (t, *J* = 8 Hz, 1H, H17); 7.91 (d, *J* = 8 Hz, 2H, H19); 7.95 (d, *J* = 8 Hz, 2H, H15); 8.27 (d, *J* = 8 Hz, 2H, H20). ¹³C NMR (150.92 MHz, CDCl₃, 253 K) δ = major conformer (81%) δ = 35.93 (C5); 37.05 (C1); 62.17 (C12); 62.27 (C7); 124.27 (C20); 127.70 – 130.00 (C9-11, 15, 16, 19); 133.71 (C18); 134.07 (C17); 137.14 (C14); 148.53 (C3); 156.48 (C6); 166.22 (C13); minor conformer (19%) δ = 37.13 (C5); 39.78 (C1); 63.43 (C12); 64.75 (C7); 127.70 – 130.00 (C9-11, 15, 16, 19, 20); 133.81 (C17); 134.66 (C18); 146.25 (C21); 148.60 (C3); 158.37 (C6); 166.06 (C13). Anal. Calcd. for C₂₅H₂₃N₅O₅: C, 63.42; H, 4.90; N, 14.79. Found: C, 63.05; H, 4.70; N, 14.61. Mass Spectrometry (+ESI-MS) *m/z*: 496.16 [M+Na]⁺.

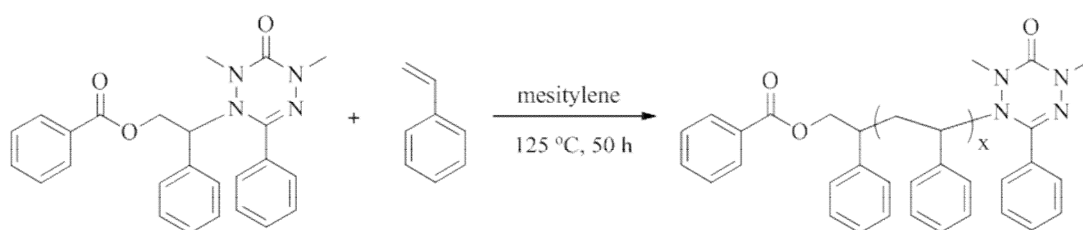
1.7.4. Polymerisation procedures for Chapter 1

1.7.4.1. Polymerisation of verdazyl stabilised and non stabilised styrene using **16** (R = H)



To two separate oven Schlenk tubes was added either styrene or verdazyl stabilised styrene (2 mL, 17.46 mmol), **16** (R = H, 16.2 mg, 0.046 mmol) and mesitylene (1.2 mL). The solution was degassed using three freeze-pump-thaw cycles and stirred at 125 °C under nitrogen for 50 hours. The polymerisation was terminated by bubbling with air for 10 minutes followed by the addition of dichloromethane (2 mL). The crude polymer was precipitated twice into methanol using dichloromethane to dissolve the polymer. $M_n = 11,800$ g/mol; PDI = 1.32 (stabilised styrene). $M_n = 11,900$ g/mol; PDI = 1.29.

1.7.4.2. Polymerisation of styrene with 0, 25 and 50% toluene using **13** (R = Ph)



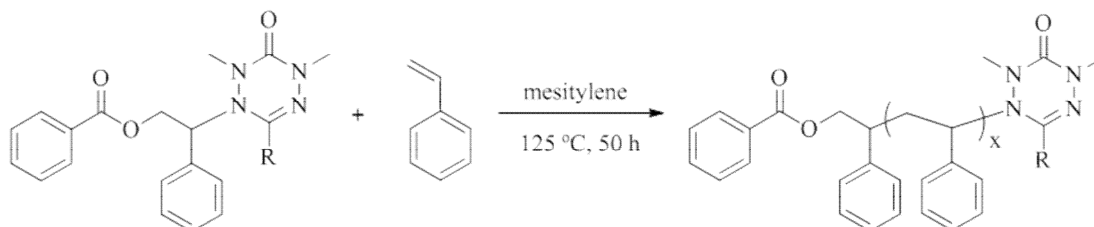
To three separate oven dried Schlenk tubes was added styrene (2 mL, 17.46 mmol), **13** (R = Ph, 15.5 mg, 0.036 mmol) and mesitylene (1.2 mL). To one Schlenk was added 0.5 mL of toluene and to another 1 mL. The solution was degassed using three freeze-pump-thaw cycles and stirred at 125 °C under nitrogen for 50 hours. The polymerisation was terminated by bubbling with air for 10 minutes followed by the addition of dichloromethane (2 mL). The crude polymer was precipitated twice into methanol using dichloromethane to dissolve the polymer.

Table 1.7-2. Final polymerisation data for the polymerisation of styrene with 0, 25 and 50% toluene using **13 (R = Ph)**

Toluene (%)	M_n (g/mol)*	PDI*
0	7,500	1.63
25	7,100	1.78
50	7,500	1.75

*precipitated polymer

1.7.4.3. Polymerisation of styrene using **13** (R = Ph), **16** (R = H), **17** (R = PhOMe) and **18** (PhNO₂)



To an oven dried Schlenk tube was added styrene (2 mL, 17.46 mmol), verdazyl initiator (0.036 mmol) and mesitylene (1.2 mL). The solution was degassed using

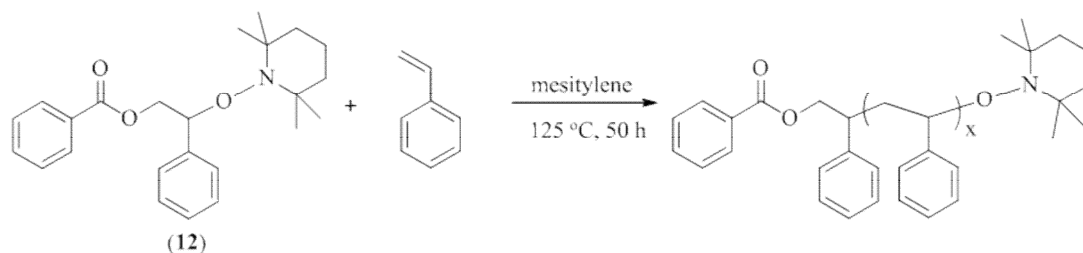
three freeze-pump-thaw cycles and stirred at 125 °C under nitrogen for 50 hours. The polymerisation was terminated by bubbling with air for 10 minutes followed by the addition of dichloromethane (2 mL). The crude polymer was precipitated twice into methanol using dichloromethane to dissolve the polymer.

Table 1.7-3. Final polymerisation data for the verdazyl mediated polymerisation of styrene

Initiator	R	Conversion (%)	M_n (g/mol)*	PDI*
16	H	77.0	20,300	1.29
13	Ph	60.6	7,500	1.63
17	PhOMe	63.6	9,609	1.71
18	PhNO ₂	56.1	5,200	1.50

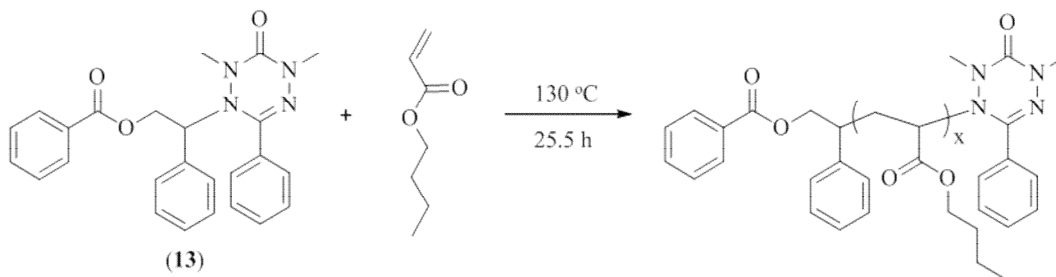
*precipitated polymer

1.7.4.4. Polymerisation of styrene using **12**



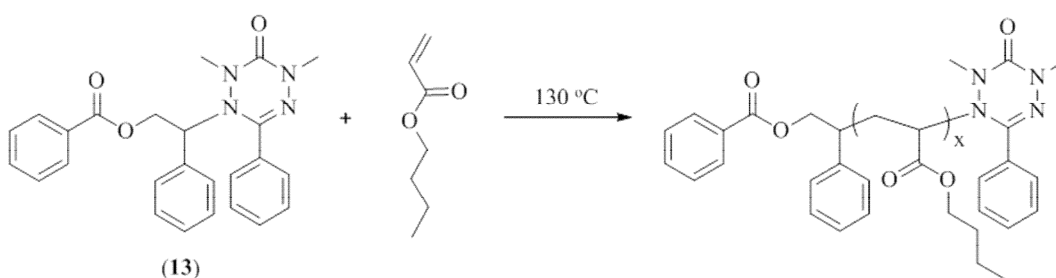
Using the same procedure as described in Section 1.7.4.3, **12** (0.036 mmol) was used to polymerise 125 °C under nitrogen for 50 hours where conversion had reached 76.9%. The polymerisation was terminated by bubbling with air for 10 minutes followed by the addition of dichloromethane (2 mL). The crude polymer was precipitated twice into methanol using dichloromethane to dissolve the polymer. $M_n = 17,100$ g/mol; PDI = 1.28.

1.7.4.5. Polymerisation of *n*-butyl acrylate using **13** (R = Ph)



To an oven dried Schlenk tube was added *n*-butyl acrylate (1 mL, 14 mmol), **13** (11.7 mg, 0.05 mmol). The solution was degassed using three freeze-pump-thaw cycles and stirred at 130 °C under nitrogen for 25.5 hours where conversion had reached 89.3%. The polymerisation was terminated by bubbling with air for 10 minutes followed by the addition of dichloromethane (15 mL). The crude polymer was not precipitated.

1.7.4.6. Polymerisation of verdazyl stabilised *n*-butyl acrylate at different volumes using **13** (R = Ph)



Into two separate oven dried Schlenk tubes were added verdazyl stabilised (1 mg/ 40 mL) *n*-butyl acrylate (15 mL, 0.11 mol), **13** (0.1 g, 0.23 mmol). From one Schlenk tube, aliquots of 3 and 9 mL were taken and put into two separate Schlenk tubes. Each solution was degassed using three freeze-pump-thaw cycles and stirred at 130

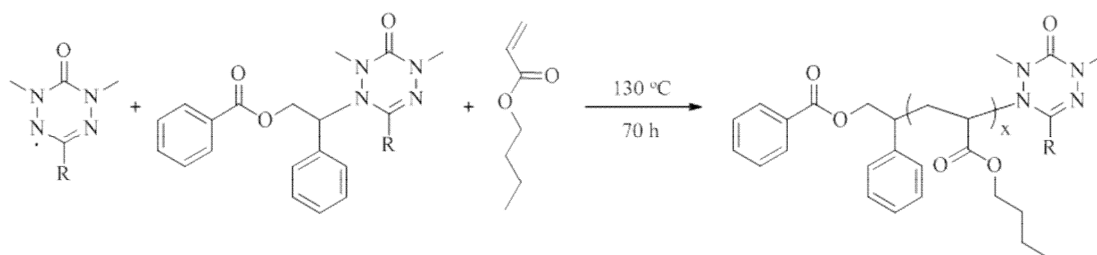
°C under nitrogen. The polymerisation was terminated by bubbling with air for 10 minutes followed by the addition of dichloromethane (15 mL). The crude polymer was precipitated once into 80:20 methanol/ water using dichloromethane to dissolve the polymer.

Table 1.7-4. Final polymerisation data for the verdazyl mediated polymerisation of *n*-butyl acrylate by 13 (R = Ph) at different volumes

Reaction size (mL)	Time (h)	Conversion (%)	M _n (g/mol)*	PDI*
3	47	59.0	28,500	1.50
9	47.25	20.7	10,500	1.12
15	70	42.4	21,200	1.23

*precipitated polymer

1.7.4.7. Polymerisation of verdazyl stabilised *n*-butyl acrylate using verdazyl initiators 16 (R = H), 17 (R = PhOMe) and 18 (R = PhNO₂)



Butyl acrylate polymerisations were performed using a slightly modified procedure described in the literature.⁵³ To an oven dried Schlenk tube was added verdazyl stabilised (1 mg/ 40 mL) *n*-butyl acrylate (15 mL, 0.11 mol) and verdazyl initiator (0.23 mmol). The solution was degassed using three freeze-pump-thaw cycles and

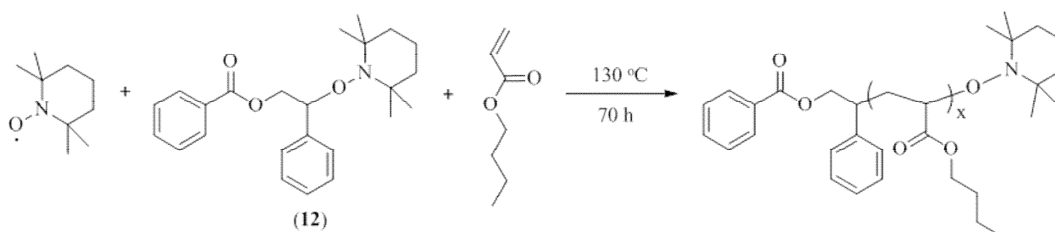
stirred at 130 °C under nitrogen for 70 hours except for with **17** which was stopped after 2 hours. The polymerisation was terminated by bubbling with air for 10 minutes followed by the addition of dichloromethane (15 mL). The crude polymer was precipitated once into 80:20 methanol/ water using dichloromethane to dissolve the polymer.

Table 1.7-5. Final polymerisation data for the verdazyl mediated polymerisation of *n*-butyl acrylate

Initiator	R	Conversion (%)	M_n (g/mol)*	PDI*
16	H	23.3	11,200	1.17
17	PhOMe	50.4	41,400	4.41
18	PhNO ₂	21.4	11,100	1.17

*precipitated polymer

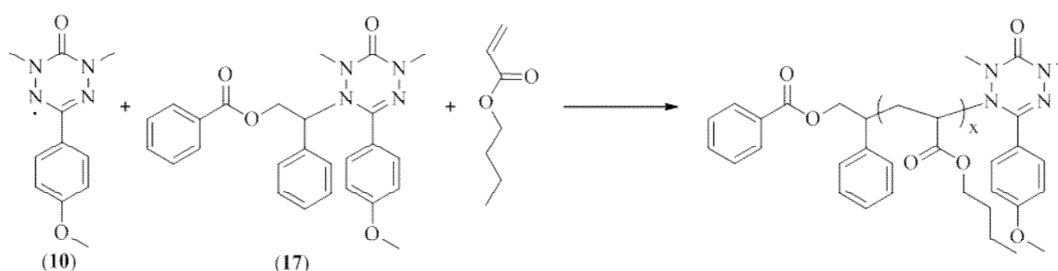
1.7.4.8. Polymerisation of verdazyl stabilised *n*-butyl acrylate using **12**



Using the same procedure as described in Section 1.7.4.7, **12** (0.23 mmol) was used to polymerise *n*-butyl acrylate at 130 °C under nitrogen for 70 hours where conversion had reached 7.4%. The polymerisation was terminated by bubbling with air for 10 minutes followed by the addition of dichloromethane (50 mL). The crude

polymer was precipitated once into 80:20 methanol/ water using dichloromethane to dissolve the polymer. $M_n = 2,900$ g/mol; PDI = 1.40.

1.7.4.9. Polymerisation of *n*-butyl acrylate at different temperatures using **17** (R = PhOMe)



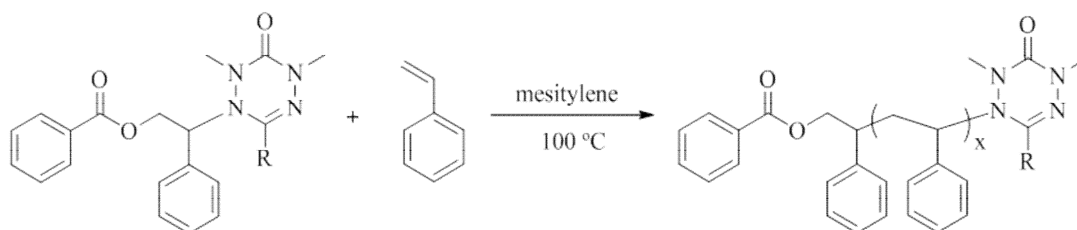
To an oven dried Schlenk tube was added verdazyl stabilised (1 mg/ 40 mL) *n*-butyl acrylate (15 mL, 0.11 mol) and **17** (95.7 mg, 0.21 mmol). Aliquots of 1.5mL were added to eight separate Schlenk tubes. Each solution was degassed using three freeze-pump-thaw cycles and stirred under nitrogen at various temperatures.

Table 1.7-6. Final polymerisation data for the verdazyl mediated polymerisation of *n*-butyl acrylate by **17 (R = PhOMe) at different temperatures**

Temperature (°C)	Time (h)	Conversion (%)	M_n (g/mol)*	PDI*
50	22	1.57	-	-
60	22	0.69	-	-
70	22.5	1.32	-	-
80	22.5	1.89	-	-
90	22	13.8	-	-
100	22	77.4	21,700	1.43
110	22	82.8	340,500	1.74

*precipitated polymer

1.7.4.10. Polymerisation of styrene at a lower temperature



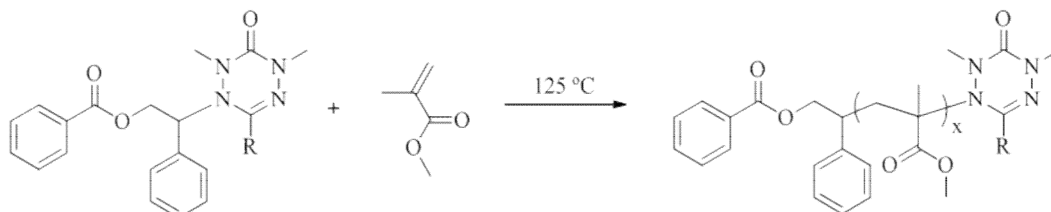
Using the same procedure described in Section 1.7.4.3 verdazyl initiators **13** (R = Ph) and **17** (R = PhOMe, 0.036 mmol) were used to polymerise styrene at 100 °C under nitrogen for 44 hours. The polymerisation was terminated by bubbling with air for 10 minutes followed by the addition of dichloromethane (2 mL). The crude polymer was precipitated once into methanol using dichloromethane to dissolve the polymer.

Table 1.7-7. Final polymerisation data for the verdazyl mediated polymerisation of styrene by **13 (R = Ph) and **17** (R = PhOMe) at 100 °C**

Initiator	R	Time (h)	Conversion (%)	M _n (g/mol)*	PDi*
13	Ph	44	28.3	4,900	1.45
17	PhOMe	47	41.8	13,200	1.30

*precipitated polymer

**1.7.4.11. Polymerisation of MMA using 13 (R = Ph), 16 (R = H),
17 (R = PhOMe) and 18 (R = PhNO₂)**



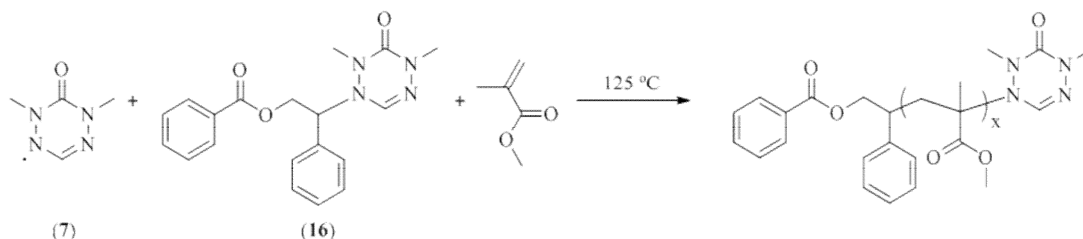
To an oven dried Schlenk tube was added verdazyl initiator (0.036 mmol), mesitylene (0.9 mL) and MMA (1.9 mL, 17.46 mmol). The solution was degassed using three freeze-pump-thaw cycles and heated at 125 °C under nitrogen. The polymerisation was terminated by bubbling with air for 10 minutes. The crude polymer was precipitated once into methanol using dichloromethane to dissolve the polymer.

Table 1.7-8. Final polymerisation data for the verdazyl mediated polymerisation of MMA

Initiator	R	Time (h)	Conversion (%)	M _n (g/mol)*	PDI*
16	H	25.5	61.0	21,900	1.37
13	Ph	7	71.1	23,600	1.56
17	PhOMe	25	55.4	18,600	1.86
18	PhNO ₂	25	76.0	14,800	1.66

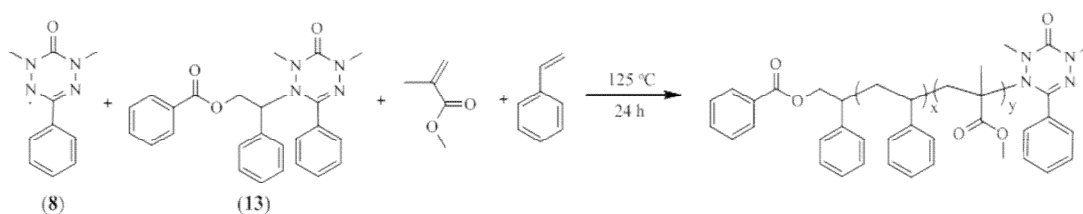
*precipitated polymer

1.7.4.12. Polymerisation of verdazyl stabilised MMA using **16** (R = H)



To an oven dried Schlenk tube was added **16** (0.036 mmol), mesitylene (0.9 mL) and verdazyl stabilised MMA (1.9 mL, 17.46 mmol). The solution was degassed using three freeze-pump-thaw cycles and heated at 125 °C under nitrogen for 22 h. The polymerisation was terminated by bubbling with air for 10 minutes. The crude polymer was precipitated once into methanol using dichloromethane to dissolve the polymer. $M_n = 13,000$ g/mol; PDI = 1.70.

1.7.4.13. Copolymerisation of styrene and MMA using **13** (R = Ph) with the addition of 0.05 equivalents of **8**³¹



To an oven dried Schlenk tube was added styrene, MMA, **13** (42.2 mg, 0.0984 mmol), **8** (0.9 mg, 0.0005 mmol) and mesitylene (0.5 mL). The solution was degassed using three freeze-pump-thaw cycles and stirred at 125 °C under nitrogen for 24 hours. The polymerisation was terminated by bubbling with air for 10

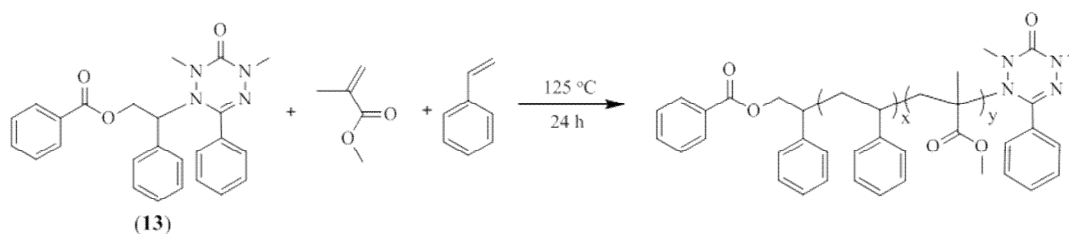
minutes. The crude polymer was precipitated once into methanol using dichloromethane to dissolve the polymer.

Table 1.7-9. Final polymerisation data for the verdazyl mediated copolymerisation of verdazyl stabilised styrene and MMA

Sty:MMA	Styrene		MMA		Conversion (%)	M_n (g/mol)*	PDI*
	mL	mmol	mL	mmol			
1:1	1.13	9.84	1.05	9.84	58.3	3,600	1.28
1:3	0.6	4.92	1.6	14.8	66.2	3,100	1.42
1:9	0.23	1.97	1.89	17.7	50.2	3,100	1.33

*precipitated polymer

1.7.4.14. Copolymerisation of styrene and MMA using **13** (R = Ph)



To an oven dried Schlenk tube was added styrene, MMA, **13** (42.2 mg, 0.0984 mmol) and mesitylene (0.5 mL). The solution was degassed using three freeze-pump-thaw cycles and stirred at 125 °C under nitrogen for 24 hours. The polymerisation was terminated by bubbling with air for 10 minutes. The crude polymer was precipitated once into methanol using dichloromethane to dissolve the polymer.

Table 1.7-10. Final polymerisation data for the verdazyl mediated copolymerisation of styrene and MMA by 13 (R = Ph)

Sty:MMA	Styrene		MMA		Conversion (%)	M_n (g/mol)*	PDI*
	mL	mmol	mL	mmol			
1:1	1.13	9.84	1.05	9.84	63.8	3,800	1.36
1:3	0.6	4.92	1.6	14.8	73.6	4,200	1.56
1:9	0.23	1.97	1.89	17.7	60.2	6,300	1.51

*precipitated polymer

1.7.5. High Temperature EPR procedures for Chapter 1

For all high temperature experiments the following experimental parameters used: centre field = 3443 G; sweep width 100 G; modulation frequency = 100 kHz; modulation amplitude = 0.2 G; conversion time = 40.96 ms, time constant = 40.96 ms and resolution = 2048. The receiver gain was varied depending on sample concentration. One spectrum consists of 10 scans, taking 83.98 seconds per scan.

1.7.5.1. Polymer end-group analysis by EPR

To an oven dried Schlenk tube was added polymer (approximately 0.4 g) and mesitylene (0.3–0.5 mL). The solution was degassed using three freeze-pump-thaw cycles and kept under nitrogen. Using a gas tight syringe, the solution was introduced to a degassed EPR tube which was then capped and sealed with parafilm. The parafilm was removed at prior to running the sample at high temperature. The sample was run at 142 °C for between 15 minutes and 2 hours.

1.7.5.2. High temperature cavity calibration

Solutions of **8** (R = Ph) in mesitylene were degassed using three freeze-pump-thaw cycles and kept under nitrogen. Using a gas tight syringe, 0.4 mL of each solution as introduced into individual degassed EPR tubes which was then capped and sealed with parafilm. The parafilm was removed at prior to running the sample at high temperature. Spectra were recorded at ambient temperature prior to heating at 122 °C to obtain spectra. The samples were then cooled back to ambient temperature to obtain final spectra.

Table 1.7-11. Quantities of **8 (R = H) for calibration of high temperature cavity**

8		Mesitylene	Concentration
mg	mmol	mL	mM
1.6	0.008	1	7.87
1.2	0.006	2.46	2.40
1.2	0.006	4.92	1.20
1.0	0.005	9.84	0.50
1.2	0.006	49.21	0.11
0.4	0.002	24.60	0.08

1.7.5.3. High temperature EPR study of the polymerisation of styrene using **13**

To an oven dried Schlenk tube was added styrene (2 mL, 17.46 mmol), **13** (R = Ph, 15.4 mg, 0.036 mmol) and mesitylene (1.2 mL). The solution was degassed using three freeze-pump-thaw cycles and kept under nitrogen. Using a gas tight syringe, 0.5 mL of solution was introduced to a degassed EPR tube which was then capped and sealed with parafilm. The parafilm was removed at prior to running the sample at high temperature. The sample was run for approximately 68 hours at 122 °C where conversion had reached 64.0%. $M_n = 33,400$ g/mol; PDI = 1.48.

1.7.5.4. High temperature EPR study of radical decomposition using **8**

To an oven dried Schlenk tube was added **8** (R = Ph, 0.04 mmol, 7.4 mg) and mesitylene (3.2 mL). The solution was degassed using three freeze-pump-thaw cycles and kept under nitrogen. Using a gas tight syringe, 0.5 mL of solution was introduced to a degassed EPR tube which was then capped and sealed with parafilm. The parafilm was removed at prior to running the sample at high temperature. The ample was heated at 122 °C for approximately 57 hours.

1.7.5.5. Initiator characterisation

Solutions of verdazyl initiators **13** (R = Ph), **16** (R = H), **17** (R = PhOMe) and **18** (R = PhNO₂) and TEMPO initiator **12** in mesitylene were degassed using three freeze-pump-thaw cycles and kept under nitrogen. Using a gas tight syringe, the solutions were transferred to individual degassed EPR tubes which were capped and sealed with parafilm. The parafilm was removed prior to running the sample at high temperature. Spectra were recorded at ambient temperature prior to running at 122 °C for a set of scans. The sample was cooled back to ambient temperature and further scans were run over time.

Table 1.7-12. Sample preparation of verdazyl initiators for high temperature EPR analysis

R	Initiator		Mesitylene	
	mmol	mg	mL	
H	0.004	1.5	0.34	
Ph	0.004	1.5	0.32	
PhOMe	0.004	1.7	0.34	
PhNO ₂	0.003	1.6	0.31	
TEMPO	0.005	2.0	0.48	

1.7.5.6. High temperature EPR study of initiator decomposition using **13**

To an oven dried Schlenk tube was added **13** (R = Ph, 15.4 mg, 0.036 mmol) and mesitylene (3.2 mL). The solution was degassed using three freeze-pump-thaw cycles and kept under nitrogen. Using a gas tight syringe, 0.5 mL of solution was introduced to a degassed EPR tube which was then capped and sealed with parafilm. The parafilm was removed at prior to running the sample at high temperature. The sample was run for approximately 50 hours at 122 °C.

1.8. Appendix

1.8.1. Crystallographic data

1.8.1.1. 1,5-dimethyl-tetrazinan-6-one

Table 1.8-1. Crystal data for 1,5-dimethyl-tetrazinan-6-one

Compound reference	1,5-dimethyl-tetrazinan-6-one
Chemical formula	C ₄ H ₁₀ N ₄ O
Formula Mass	130.16
Crystal system	Tetragonal
<i>a</i> /Å	7.6562(2)
<i>b</i> /Å	7.6562(2)
<i>c</i> /Å	21.5935(13)
α /°	90.00
β /°	90.00
γ /°	90.00
Unit cell volume/Å ³	1265.75(9)
Temperature/K	100(2)
Space group	<i>P</i> 4(1)2(1)2
No. of formula units per unit cell, <i>Z</i>	8
No. of reflections measured	15503
No. of independent reflections	1052
<i>R</i> _{int}	0.0823
Final <i>R</i> _{<i>I</i>} values (<i>I</i> > 2σ(<i>I</i>))	0.0354
Final <i>wR</i> (<i>F</i> ²) values (<i>I</i> > 2σ(<i>I</i>))	0.0807
Final <i>R</i> _{<i>I</i>} values (all data)	0.0618
Final <i>wR</i> (<i>F</i> ²) values (all data)	0.0847

data_1,5-dimethyl-tetrazinan-6-one

```

_audit_creation_method      SHELXL-97
_chemical_name_systematic;?;
_chemical_name_common      ?
_chemical_melting_point    ?
_chemical_formula_moiety   ?
_chemical_formula_sum      'C4 H10 N4 O'
_chemical_formula_weight   130.16

```

```

loop_
_atom_type_symbol
_atom_type_description
_atom_type_scatter_dispersion_real
_atom_type_scatter_dispersion_imag
_atom_type_scatter_source
'C' 'C' 0.0033 0.0016
'International Tables Vol C Tables 4.2.6.8 and 6.1.1.4'

```

Verdazyl Radicals as Mediators in Living Radical Polymerisation

```

'H'  'H'  0.0000  0.0000
'International Tables Vol C Tables 4.2.6.8 and 6.1.1.4'
'N'  'N'  0.0061  0.0033
'International Tables Vol C Tables 4.2.6.8 and 6.1.1.4'
'O'  'O'  0.0106  0.0060
'International Tables Vol C Tables 4.2.6.8 and 6.1.1.4'

_symmetry_cell_setting      Tetragonal
_symmetry_space_group_name_H-M  P4(1)2(1)2

loop_
  _symmetry_equiv_pos_as_xyz
    'x, y, z'
    '-x, -y, z+1/2'
    '-y+1/2, x+1/2, z+1/4'
    'y+1/2, -x+1/2, z+3/4'
    '-x+1/2, y+1/2, -z+1/4'
    'x+1/2, -y+1/2, -z+3/4'
    'y, x, -z'
    '-y, -x, -z+1/2'

_cell_length_a              7.6562(2)
_cell_length_b              7.6562(2)
_cell_length_c              21.5935(13)
_cell_angle_alpha           90.00
_cell_angle_beta            90.00
_cell_angle_gamma           90.00
_cell_volume                 1265.75(9)
_cell_formula_units_Z       8
_cell_measurement_temperature 100(2)
_cell_measurement_reflms_used 4668
_cell_measurement_theta_min  2.65
_cell_measurement_theta_max  29.00

_exptl_crystal_description  block
_exptl_crystal_colour       colourless
_exptl_crystal_size_max     0.35
_exptl_crystal_size_mid     0.20
_exptl_crystal_size_min     0.08
_exptl_crystal_density_meas ?
_exptl_crystal_density_diffn 1.366
_exptl_crystal_density_method 'not measured'
_exptl_crystal_F_000        560
_exptl_absorpt_coefficient_mu 0.103
_exptl_absorpt_correction_type multi-scan
_exptl_absorpt_correction_T_min 0.87
_exptl_absorpt_correction_T_max 1.00
_exptl_absorpt_process_details 'ABSPACK(Crystalis,Oxford
Diffraction)'
```

```
_exptl_special_details
```

```
;
```

The temperature of the crystal was controlled using the Oxford Cryosystem Cobra Cooler. The data collection nominally covered over a hemisphere of Reciprocal space, by a combination of four sets of exposures with different θ angles for the crystal; each 10 s exposure covered 0.3% in ω .

The crystal-to-detector distance was 5.5 cm.

Crystal decay was found to be negligible by repeating the initial frames at the end of data collection and analyzing the duplicate

reflections.

Hydrogen atoms were added at calculated positions and refined using a riding model with freely rotating methyl groups except the NHs which were located in a difference map.

Anisotropic displacement parameters were used for all non-H atoms; H-atoms were given isotropic displacement parameters equal to 1.2 (or 1.5 for methyl or NH hydrogen atoms) times the equivalent isotropic displacement parameter of the atom to which the H-atom is attached.

There was insufficient anomalous scattering to define the handedness of the crystal chosen (Mo radiation, no atom heavier than oxygen) so the Friedels were merged.

;

```

_diffn_ambient_temperature      100(2)
_diffn_radiation_wavelength     0.71073
_diffn_radiation_type           MoK\alpha
_diffn_radiation_source         'Enhance (Mo) X-ray Source'
_diffn_radiation_monochromator   graphite
_diffn_measurement_device_type   'Oxford Diffraction Gemini R'
_diffn_measurement_method       '\f & \w scans'
_diffn_detector_area_resol_mean 10.2833
_diffn_standards_number         ?
_diffn_standards_interval_count  ?
_diffn_standards_interval_time  ?
_diffn_standards_decay_%        nil
_diffn_reflns_number            15503
_diffn_reflns_av_R_equivalents  0.0823
_diffn_reflns_av_sigmaI/netI    0.0437
_diffn_reflns_limit_h_min       -8
_diffn_reflns_limit_h_max       10
_diffn_reflns_limit_k_min       -10
_diffn_reflns_limit_k_max       10
_diffn_reflns_limit_l_min       -27
_diffn_reflns_limit_l_max       29
_diffn_reflns_theta_min         2.82
_diffn_reflns_theta_max         29.18
_reflns_number_total            1052
_reflns_number_gt               774
_reflns_threshold_expression     >2sigma(I)

_computing_data_collection       'CrysAlis CCD, Oxford Diffraction
Ltd'
_computing_cell_refinement       'CrysAlis RED, Oxford Diffraction
Ltd'
_computing_data_reduction        'CrysAlis RED, Oxford Diffraction
Ltd'
_computing_structure_solution    'SHELXS-97 (Sheldrick, 1990)'
_computing_structure_refinement  'SHELXL-97 (Sheldrick, 1997)'
_computing_molecular_graphics    'SHELXTL (Sheldrick, 1997)'
_computing_publication_material  'SHELXTL (Sheldrick, 1997)'

```

_refine_special_details

;

Refinement of F^2 against ALL reflections. The weighted R-factor wR and goodness of fit S are based on F^2 , conventional R-factors R are based on F , with F set to zero for negative F^2 . The threshold expression of $F^2 > 2\sigma(F^2)$ is used only for

Verdazyl Radicals as Mediators in Living Radical Polymerisation

calculating R-factors(gt) etc. and is not relevant to the choice of reflections for refinement. R-factors based on F^2 are statistically about twice as large as those based on F , and R-factors based on ALL data will be even larger.

```

;

_refine_ls_structure_factor_coef  Fsqd
_refine_ls_matrix_type            full
_refine_ls_weighting_scheme       calc
_refine_ls_weighting_details
'calc          w=1/[\s^2^(Fo^2^)+(0.0483P)^2^+0.0000P]      where
P=(Fo^2^+2Fc^2^)/3'
_atom_sites_solution_primary      direct
_atom_sites_solution_secondary    difmap
_atom_sites_solution_hydrogens    geom
_refine_ls_hydrogen_treatment     mixed
_refine_ls_extinction_method       none
_refine_ls_extinction_coef         ?
_refine_ls_number_reflns           1052
_refine_ls_number_parameters       90
_refine_ls_number_restraints       0
_refine_ls_R_factor_all            0.0618
_refine_ls_R_factor_gt             0.0354
_refine_ls_wR_factor_ref           0.0847
_refine_ls_wR_factor_gt           0.0807
_refine_ls_goodness_of_fit_ref     1.014
_refine_ls_restrained_S_all        1.014
_refine_ls_shift/su_max            0.000
_refine_ls_shift/su_mean           0.000

loop_
  _atom_site_label
  _atom_site_type_symbol
  _atom_site_fract_x
  _atom_site_fract_y
  _atom_site_fract_z
  _atom_site_U_iso_or_equiv
  _atom_site_adp_type
  _atom_site_occupancy
  _atom_site_symmetry_multiplicity
  _atom_site_calc_flag
  _atom_site_refinement_flags
  _atom_site_disorder_assembly
  _atom_site_disorder_group
C1 C 0.6309(2) 0.2131(3) 0.16747(9) 0.0347(5) Uani 1 1 d . . .
H1A H 0.6754 0.1755 0.1271 0.052 Uiso 1 1 calc R . .
H1B H 0.6932 0.1507 0.2004 0.052 Uiso 1 1 calc R . .
H1C H 0.6493 0.3391 0.1723 0.052 Uiso 1 1 calc R . .
N2 N 0.44614(19) 0.1749(2) 0.17148(6) 0.0264(4) Uani 1 1 d . . .
N3 N 0.3767(2) 0.1851(2) 0.23321(6) 0.0263(4) Uani 1 1 d . . .
H3 H 0.386(3) 0.077(3) 0.2487(10) 0.039 Uiso 1 1 d . . .
C4 C 0.1925(2) 0.2259(2) 0.23007(7) 0.0260(4) Uani 1 1 d . . .
H4A H 0.1790 0.3504 0.2187 0.031 Uiso 1 1 calc R . .
H4B H 0.1407 0.2098 0.2717 0.031 Uiso 1 1 calc R . .
N5 N 0.0958(2) 0.1206(2) 0.18617(7) 0.0268(4) Uani 1 1 d . . .
H5 H 0.111(3) 0.008(3) 0.1926(8) 0.040 Uiso 1 1 d . . .
N6 N 0.1715(2) 0.1428(2) 0.12603(6) 0.0258(4) Uani 1 1 d . . .
C7 C 0.0493(3) 0.2091(3) 0.08016(8) 0.0345(5) Uani 1 1 d . . .
H7A H 0.1117 0.2337 0.0415 0.052 Uiso 1 1 calc R . .
H7B H -0.0047 0.3167 0.0956 0.052 Uiso 1 1 calc R . .

```

Verdazyl Radicals as Mediators in Living Radical Polymerisation

```
H7C H -0.0416 0.1215 0.0725 0.052 Uiso 1 1 calc R . .  
C8 C 0.3447(2) 0.1825(2) 0.12020(8) 0.0241(4) Uani 1 1 d . . .  
O9 O 0.40795(17) 0.21935(17) 0.06851(5) 0.0295(3) Uani 1 1 d . . .
```

```
loop_  
  _atom_site_aniso_label  
  _atom_site_aniso_U_11  
  _atom_site_aniso_U_22  
  _atom_site_aniso_U_33  
  _atom_site_aniso_U_23  
  _atom_site_aniso_U_13  
  _atom_site_aniso_U_12  
C1 0.0278(11) 0.0396(12) 0.0367(12) 0.0032(9) 0.0002(8) 0.0005(8)  
N2 0.0263(8) 0.0348(9) 0.0182(8) 0.0043(7) 0.0020(7) 0.0006(7)  
N3 0.0326(9) 0.0300(9) 0.0163(7) 0.0030(6) 0.0000(6) -0.0001(7)  
C4 0.0323(10) 0.0290(10) 0.0167(8) 0.0010(7) 0.0062(7) 0.0014(8)  
N5 0.0283(9) 0.0296(9) 0.0224(8) 0.0029(7) 0.0061(7) -0.0012(7)  
N6 0.0282(8) 0.0331(9) 0.0161(8) 0.0007(6) 0.0013(6) -0.0019(6)  
C7 0.0306(11) 0.0461(13) 0.0268(10) 0.0040(10) -0.0039(8) -0.0047(9)  
C8 0.0278(10) 0.0239(10) 0.0206(9) -0.0008(8) 0.0021(8) 0.0020(7)  
O9 0.0326(7) 0.0378(7) 0.0180(6) 0.0011(5) 0.0071(6) 0.0002(6)
```

```
_geom_special_details
```

```
;  
All esds (except the esd in the dihedral angle between two l.s.  
planes) are estimated using the full covariance matrix. The cell  
esds are taken into account individually in the estimation of esds  
in distances, angles and torsion angles; correlations between esds  
in cell parameters are only used when they are defined by crystal  
symmetry. An approximate (isotropic) treatment of cell esds is used  
for estimating esds involving l.s. planes.;
```

```
loop_  
  _geom_bond_atom_site_label_1  
  _geom_bond_atom_site_label_2  
  _geom_bond_distance  
  _geom_bond_site_symmetry_2  
  _geom_bond_publ_flag  
O9 C8 1.249(2) . ?  
N6 C8 1.366(2) . ?  
N6 N5 1.4323(19) . ?  
N6 C7 1.454(2) . ?  
N5 C4 1.448(2) . ?  
N5 H5 0.88(2) . ?  
N2 C8 1.354(2) . ?  
N2 N3 1.437(2) . ?  
N2 C1 1.448(2) . ?  
N3 C4 1.446(2) . ?  
N3 H3 0.90(2) . ?  
C4 H4A 0.9900 . ?  
C4 H4B 0.9900 . ?  
C1 H1A 0.9800 . ?  
C1 H1B 0.9800 . ?  
C1 H1C 0.9800 . ?  
C7 H7A 0.9800 . ?  
C7 H7B 0.9800 . ?  
C7 H7C 0.9800 . ?
```

```
loop_  


---


```

```
_geom_angle_atom_site_label_1
_geom_angle_atom_site_label_2
_geom_angle_atom_site_label_3
_geom_angle
_geom_angle_site_symmetry_1
_geom_angle_site_symmetry_3
_geom_angle_publ_flag
C8 N6 N5 120.20(13) . . ?
C8 N6 C7 118.96(14) . . ?
N5 N6 C7 113.46(14) . . ?
N6 N5 C4 108.70(14) . . ?
N6 N5 H5 101.8(13) . . ?
C4 N5 H5 111.8(13) . . ?
C8 N2 N3 122.94(14) . . ?
C8 N2 C1 120.22(14) . . ?
N3 N2 C1 113.96(14) . . ?
N2 N3 C4 109.22(13) . . ?
N2 N3 H3 105.5(13) . . ?
C4 N3 H3 107.2(13) . . ?
O9 C8 N2 121.19(16) . . ?
O9 C8 N6 120.60(15) . . ?
N2 C8 N6 118.16(15) . . ?
N3 C4 N5 114.15(14) . . ?
N3 C4 H4A 108.7 . . ?
N5 C4 H4A 108.7 . . ?
N3 C4 H4B 108.7 . . ?
N5 C4 H4B 108.7 . . ?
H4A C4 H4B 107.6 . . ?
N2 C1 H1A 109.5 . . ?
N2 C1 H1B 109.5 . . ?
H1A C1 H1B 109.5 . . ?
N2 C1 H1C 109.5 . . ?
H1A C1 H1C 109.5 . . ?
H1B C1 H1C 109.5 . . ?
N6 C7 H7A 109.5 . . ?
N6 C7 H7B 109.5 . . ?
H7A C7 H7B 109.5 . . ?
N6 C7 H7C 109.5 . . ?
H7A C7 H7C 109.5 . . ?
H7B C7 H7C 109.5 . . ?

loop_
  _geom_hbond_atom_site_label_D
  _geom_hbond_atom_site_label_H
  _geom_hbond_atom_site_label_A
  _geom_hbond_distance_DH
  _geom_hbond_distance_HA
  _geom_hbond_distance_DA
  _geom_hbond_angle_DHA
  _geom_hbond_site_symmetry_A
N5 H5 O9 0.88(2) 2.23(2) 3.074(2) 160.8(17) 5_545
N3 H3 O9 0.90(2) 2.14(2) 2.904(2) 142.2(18) 3_545

_diffn_measured_fraction_theta_max 0.974
_diffn_reflns_theta_full 28.00
_diffn_measured_fraction_theta_full 0.999
_refine_diff_density_max 0.190
_refine_diff_density_min -0.144
_refine_diff_density_rms 0.036
```

1.8.1.2. 1,5-dimethyl-3-phenyl-tetrazinan-6-one

Table 1.8-2. Crystal data for 1,5-dimethyl-3-phenyl-tetrazinan-6-one

Compound reference	1,5-dimethyl-3-phenyl-tetrazinan-6-one
Chemical formula	C ₁₀ H ₁₄ N ₄ O
Formula Mass	206.25
Crystal system	Triclinic
<i>a</i> /Å	5.3871(5)
<i>b</i> /Å	8.398(3)
<i>c</i> /Å	12.752(3)
<i>α</i> /°	71.78(3)
<i>β</i> /°	84.421(14)
<i>γ</i> /°	79.857(16)
Unit cell volume/Å ³	538.9(2)
Temperature/K	296(2)
Space group	<i>P</i> 1
No. of formula units per unit cell, <i>Z</i>	2
No. of reflections measured	5867
No. of independent reflections	2452
<i>R</i> _{int}	0.0358
Final <i>R</i> _{<i>I</i>} values (<i>I</i> > 2σ(<i>I</i>))	0.0540
Final <i>wR</i> (<i>F</i> ²) values (<i>I</i> > 2σ(<i>I</i>))	0.1339
Final <i>R</i> _{<i>I</i>} values (all data)	0.1360
Final <i>wR</i> (<i>F</i> ²) values (all data)	0.1589

data_1,5-dimethyl-3-phenyl-tetrazinan-6-one

```
_audit_creation_method      SHELXL-97
_chemical_name_systematic   ;?;
_chemical_name_common       ?
_chemical_melting_point     ?
_chemical_formula_moiety    ?
_chemical_formula_sum        'C10 H14 N4 O'
_chemical_formula_weight    206.25
```

```
loop_
  _atom_type_symbol
  _atom_type_description
  _atom_type_scatter_dispersion_real
  _atom_type_scatter_dispersion_imag
  _atom_type_scatter_source
  'C'  'C'  0.0033  0.0016
  'International Tables Vol C Tables 4.2.6.8 and 6.1.1.4'
  'H'  'H'  0.0000  0.0000
  'International Tables Vol C Tables 4.2.6.8 and 6.1.1.4'
  'N'  'N'  0.0061  0.0033
  'International Tables Vol C Tables 4.2.6.8 and 6.1.1.4'
  'O'  'O'  0.0106  0.0060
  'International Tables Vol C Tables 4.2.6.8 and 6.1.1.4'
```

```
_symmetry_cell_setting      Triclinic
_symmetry_space_group_name_H-M  P-1
```

loop_

```

_symmetry_equiv_pos_as_xyz
  'x, y, z'
  '-x, -y, -z'

_cell_length_a          5.3871(5)
_cell_length_b          8.398(3)
_cell_length_c          12.752(3)
_cell_angle_alpha       71.78(3)
_cell_angle_beta        84.421(14)
_cell_angle_gamma       79.857(16)
_cell_volume            538.9(2)
_cell_formula_units_Z   2
_cell_measurement_temperature 296(2)
_cell_measurement_reflns_used 1523
_cell_measurement_theta_min 3.36
_cell_measurement_theta_max 29.98

_exptl_crystal_description rod
_exptl_crystal_colour    colourless
_exptl_crystal_size_max  0.80
_exptl_crystal_size_mid  0.10
_exptl_crystal_size_min  0.04
_exptl_crystal_density_meas ?
_exptl_crystal_density_diffn 1.271
_exptl_crystal_density_method 'not measured'
_exptl_crystal_F_000     220
_exptl_absorpt_coefficient_mu 0.087
_exptl_absorpt_correction_type multi-scan
_exptl_absorpt_correction_T_min 0.87
_exptl_absorpt_correction_T_max 1.00
_exptl_absorpt_process_details 'ABSPACK(CrysAlis, Oxford
Diffraction)'
```

_exptl_special_details

```

;
The crystal was glued to a glass fibre with Araldite and the data
recorded at 296 K.
The data collection nominally covered over a hemisphere of
Reciprocal space, by a combination of four sets of exposures with
different \f angles for the crystal; each 10 s exposure covered
0.3\% in \w.
The crystal-to-detector distance was 5.5 cm.
Crystal decay was found to be negligible by by repeating the initial
frames at the end of data collection and analyzing the duplicate
reflections.
```

Hydrogen atoms were added at calculated positions and refined using
a riding model except the NHs which were located in a difference
map.
Anisotropic displacement parameters were used for all
non-H atoms; H-atoms were given isotropic displacement parameter
equal to 1.2 (or 1.5 for methyl and NH H-atoms) times the equivalent
isotropic displacement parameter of the atom to which they are
attached.

```

;

_diffn_ambient_temperature 296(2)
_diffn_radiation_wavelength 0.71073
_diffn_radiation_type      MoK\alpha
_diffn_radiation_source    'Enhance (Mo) X-ray Source'
```

Verdazyl Radicals as Mediators in Living Radical Polymerisation

```

_diffrn_radiation_monochromator  graphite
_diffrn_measurement_device_type  'Oxford Diffraction Gemini R'
_diffrn_measurement_method      '\f & \w scans'
_diffrn_detector_area_resol_mean 10.2833
_diffrn_standards_number         ?
_diffrn_standards_interval_count ?
_diffrn_standards_interval_time  ?
_diffrn_standards_decay_%       nil
_diffrn_reflns_number           5867
_diffrn_reflns_av_R_equivalents 0.0358
_diffrn_reflns_av_sigmaI/netI   0.0592
_diffrn_reflns_limit_h_min      -6
_diffrn_reflns_limit_h_max      6
_diffrn_reflns_limit_k_min      -10
_diffrn_reflns_limit_k_max      10
_diffrn_reflns_limit_l_min      -16
_diffrn_reflns_limit_l_max      16
_diffrn_reflns_theta_min        3.37
_diffrn_reflns_theta_max        27.49
_reflns_number_total            2452
_reflns_number_gt               1159
_reflns_threshold_expression    >2sigma(I)

_computing_data_collection      'CrysAlis CCD, Oxford Diffraction
Ltd'
_computing_cell_refinement     'CrysAlis RED, Oxford Diffraction
Ltd'
_computing_data_reduction      'CrysAlis RED, Oxford Diffraction
Ltd'
_computing_structure_solution  'SHELXS-97 (Sheldrick, 1990)'
_computing_structure_refinement 'SHELXL-97 (Sheldrick, 1997)'
_computing_molecular_graphics  'SHELXTL (Sheldrick, 1997)'
_computing_publication_material 'SHELXTL (Sheldrick, 1997)'

_refine_special_details
;
  Refinement of F2 against ALL reflections. The weighted R-factor
  wR and goodness of fit S are based on F2, conventional R-factors R
  are based on F, with F set to zero for negative F2. The threshold
  expression of F2 > 2sigma(F2) is used only for calculating R-
  factors(gt) etc. and is not relevant to the choice of reflections
  for refinement. R-factors based on F2 are statistically about
  twice as large as those based on F, and R- factors based on ALL data
  will be even larger.
;

_refine_ls_structure_factor_coef Fsqd
_refine_ls_matrix_type          full
_refine_ls_weighting_scheme     calc
_refine_ls_weighting_details
'calc          w=1/[\s2(Fo2)+(0.0794P)2+0.0000P]          where
P=(Fo2+2Fc2)/3'
_atom_sites_solution_primary    direct
_atom_sites_solution_secondary  difmap
_atom_sites_solution_hydrogens  geom
_refine_ls_hydrogen_treatment   mixed
_refine_ls_extinction_method    none
_refine_ls_extinction_coef      ?
_refine_ls_number_reflns        2452
_refine_ls_number_parameters    142

```

Verdazyl Radicals as Mediators in Living Radical Polymerisation

```

_refine_ls_number_restraints      2
_refine_ls_R_factor_all           0.1360
_refine_ls_R_factor_gt            0.0540
_refine_ls_wR_factor_ref          0.1589
_refine_ls_wR_factor_gt           0.1339
_refine_ls_goodness_of_fit_ref     0.947
_refine_ls_restrained_S_all        0.948
_refine_ls_shift/su_max            0.000
_refine_ls_shift/su_mean           0.000

loop_
  _atom_site_label
  _atom_site_type_symbol
  _atom_site_fract_x
  _atom_site_fract_y
  _atom_site_fract_z
  _atom_site_U_iso_or_equiv
  _atom_site_adp_type
  _atom_site_occupancy
  _atom_site_symmetry_multiplicity
  _atom_site_calc_flag
  _atom_site_refinement_flags
  _atom_site_disorder_assembly
  _atom_site_disorder_group
C1 C 0.6496(5) 0.3164(4) 0.1242(2) 0.0954(9) Uani 1 1 d . . .
H1A H 0.5550 0.4181 0.0854 0.115 Uiso 1 1 calc R . .
C2 C 0.8511(6) 0.2429(4) 0.0714(3) 0.1096(11) Uani 1 1 d . . .
H2A H 0.8869 0.2940 -0.0032 0.132 Uiso 1 1 calc R . .
C3 C 0.9983(5) 0.0976(4) 0.1256(3) 0.0907(9) Uani 1 1 d . . .
H3A H 1.1383 0.0517 0.0900 0.109 Uiso 1 1 calc R . .
C4 C 0.9376(5) 0.0211(4) 0.2324(3) 0.0883(8) Uani 1 1 d . . .
H4A H 1.0342 -0.0803 0.2703 0.106 Uiso 1 1 calc R . .
C5 C 0.7318(5) 0.0921(3) 0.2865(2) 0.0770(7) Uani 1 1 d . . .
H5A H 0.6918 0.0372 0.3601 0.092 Uiso 1 1 calc R . .
C6 C 0.5870(4) 0.2423(3) 0.23259(19) 0.0609(6) Uani 1 1 d . . .
C7 C 0.3602(4) 0.3250(3) 0.2877(2) 0.0670(7) Uani 1 1 d . . .
H7A H 0.2117 0.2817 0.2753 0.080 Uiso 1 1 calc R . .
N8 N 0.3173(3) 0.5076(3) 0.23782(17) 0.0667(6) Uani 1 1 d D . .
H8 H 0.179(4) 0.552(3) 0.266(2) 0.100 Uiso 1 1 d D . .
N9 N 0.5143(3) 0.5783(2) 0.26668(16) 0.0602(5) Uani 1 1 d . . .
C9 C 0.6011(5) 0.7164(4) 0.1790(2) 0.0917(9) Uani 1 1 d . . .
H9A H 0.7328 0.7561 0.2049 0.138 Uiso 1 1 calc R . .
H9B H 0.4631 0.8074 0.1570 0.138 Uiso 1 1 calc R . .
H9C H 0.6648 0.6774 0.1170 0.138 Uiso 1 1 calc R . .
O10 O 0.8451(2) 0.5491(2) 0.37021(13) 0.0701(5) Uani 1 1 d . . .
C10 C 0.6554(3) 0.4953(3) 0.35571(18) 0.0533(6) Uani 1 1 d . . .
N11 N 0.5823(3) 0.3545(2) 0.42771(15) 0.0584(5) Uani 1 1 d . . .
C11 C 0.7351(4) 0.2522(3) 0.51832(19) 0.0756(7) Uani 1 1 d . . .
H11A H 0.8643 0.3128 0.5259 0.113 Uiso 1 1 calc R . .
H11B H 0.8119 0.1482 0.5043 0.113 Uiso 1 1 calc R . .
H11C H 0.6312 0.2272 0.5852 0.113 Uiso 1 1 calc R . .
N12 N 0.3863(3) 0.2761(3) 0.40684(17) 0.0705(6) Uani 1 1 d D . .
H12 H 0.247(4) 0.324(3) 0.433(2) 0.106 Uiso 1 1 d D . .

loop_
  _atom_site_aniso_label
  _atom_site_aniso_U_11
  _atom_site_aniso_U_22
  _atom_site_aniso_U_33
  _atom_site_aniso_U_23

```

```
_atom_site_aniso_U_13
_atom_site_aniso_U_12
C1 0.105(2) 0.099(2) 0.0627(18) -0.0155(16) -0.0127(16) 0.0251(17)
C2 0.126(2) 0.116(3) 0.0697(19) -0.0260(18) 0.0066(18) 0.018(2)
C3 0.095(2) 0.094(2) 0.089(2) -0.0484(19) -0.0109(17) 0.0121(17)
C4 0.109(2) 0.0664(18) 0.093(2) -0.0344(17) -0.0303(17) 0.0094(15)
C5 0.0984(19) 0.0634(18) 0.0741(17) -0.0254(14) -0.0080(15) -
0.0142(15)
C6 0.0584(13) 0.0650(16) 0.0649(16) -0.0222(13) -0.0138(11) -
0.0130(12)
C7 0.0468(12) 0.080(2) 0.0836(18) -0.0299(14) -0.0099(11) -
0.0217(11)
N8 0.0391(9) 0.0781(15) 0.0853(15) -0.0283(12) -0.0095(9) -0.0049(9)
N9 0.0444(9) 0.0677(13) 0.0681(13) -0.0176(10) -0.0023(9) -0.0127(9)
C9 0.0758(16) 0.087(2) 0.098(2) -0.0037(17) -0.0050(15) -0.0182(15)
O10 0.0472(8) 0.0907(13) 0.0842(12) -0.0369(10) -0.0013(7) -
0.0232(8)
C10 0.0357(10) 0.0711(16) 0.0587(14) -0.0306(13) 0.0086(10) -
0.0084(10)
N11 0.0457(9) 0.0779(14) 0.0535(11) -0.0201(10) 0.0037(8) -0.0176(9)
C11 0.0714(15) 0.092(2) 0.0604(16) -0.0193(14) 0.0000(12) -
0.0134(14)
N12 0.0495(10) 0.0924(16) 0.0735(14) -0.0241(12) 0.0070(9) -
0.0276(10)

_geom_special_details
;
All esds (except the esd in the dihedral angle between two l.s.
planes) are estimated using the full covariance matrix. The cell
esds are taken into account individually in the estimation of esds
in distances, angles and torsion angles; correlations between esds
in cell parameters are only used when they are defined by crystal
symmetry. An approximate (isotropic) treatment of cell esds is used
for estimating esds involving l.s. planes.
;

loop_
_geom_bond_atom_site_label_1
_geom_bond_atom_site_label_2
_geom_bond_distance
_geom_bond_site_symmetry_2
_geom_bond_publ_flag
C1 C6 1.363(3) . ?
C1 C2 1.376(4) . ?
C1 H1A 0.9300 . ?
C2 C3 1.354(4) . ?
C2 H2A 0.9300 . ?
C3 C4 1.347(4) . ?
C3 H3A 0.9300 . ?
C4 C5 1.392(3) . ?
C4 H4A 0.9300 . ?
C5 C6 1.374(3) . ?
C5 H5A 0.9300 . ?
C6 C7 1.520(3) . ?
C7 N8 1.450(3) . ?
C7 N12 1.459(3) . ?
C7 H7A 0.9800 . ?
N8 N9 1.431(2) . ?
N8 H8 0.868(16) . ?
N9 C10 1.356(3) . ?
```

N9 C9 1.446(3) . ?
 C9 H9A 0.9600 . ?
 C9 H9B 0.9600 . ?
 C9 H9C 0.9600 . ?
 O10 C10 1.239(2) . ?
 C10 N11 1.346(3) . ?
 N11 N12 1.424(2) . ?
 N11 C11 1.437(3) . ?
 C11 H11A 0.9600 . ?
 C11 H11B 0.9600 . ?
 C11 H11C 0.9600 . ?
 N12 H12 0.878(16) . ?

 loop_
 _geom_angle_atom_site_label_1
 _geom_angle_atom_site_label_2
 _geom_angle_atom_site_label_3
 _geom_angle
 _geom_angle_site_symmetry_1
 _geom_angle_site_symmetry_3
 _geom_angle_publ_flag
 C6 C1 C2 120.9(3) . . ?
 C6 C1 H1A 119.6 . . ?
 C2 C1 H1A 119.6 . . ?
 C3 C2 C1 121.5(3) . . ?
 C3 C2 H2A 119.3 . . ?
 C1 C2 H2A 119.3 . . ?
 C4 C3 C2 118.6(3) . . ?
 C4 C3 H3A 120.7 . . ?
 C2 C3 H3A 120.7 . . ?
 C3 C4 C5 120.7(3) . . ?
 C3 C4 H4A 119.7 . . ?
 C5 C4 H4A 119.7 . . ?
 C6 C5 C4 120.8(3) . . ?
 C6 C5 H5A 119.6 . . ?
 C4 C5 H5A 119.6 . . ?
 C1 C6 C5 117.5(2) . . ?
 C1 C6 C7 119.5(2) . . ?
 C5 C6 C7 122.9(2) . . ?
 N8 C7 N12 112.4(2) . . ?
 N8 C7 C6 111.32(19) . . ?
 N12 C7 C6 110.8(2) . . ?
 N8 C7 H7A 107.4 . . ?
 N12 C7 H7A 107.4 . . ?
 C6 C7 H7A 107.4 . . ?
 N9 N8 C7 109.03(17) . . ?
 N9 N8 H8 105.1(18) . . ?
 C7 N8 H8 110.4(18) . . ?
 C10 N9 N8 122.23(19) . . ?
 C10 N9 C9 120.66(19) . . ?
 N8 N9 C9 114.7(2) . . ?
 N9 C9 H9A 109.5 . . ?
 N9 C9 H9B 109.5 . . ?
 H9A C9 H9B 109.5 . . ?
 N9 C9 H9C 109.5 . . ?
 H9A C9 H9C 109.5 . . ?
 H9B C9 H9C 109.5 . . ?
 O10 C10 N11 121.3(2) . . ?
 O10 C10 N9 120.5(2) . . ?
 N11 C10 N9 118.18(18) . . ?

Verdazyl Radicals as Mediators in Living Radical Polymerisation

```
C10 N11 N12 122.89(19) . . ?
C10 N11 C11 120.99(18) . . ?
N12 N11 C11 114.63(19) . . ?
N11 C11 H11A 109.5 . . ?
N11 C11 H11B 109.5 . . ?
H11A C11 H11B 109.5 . . ?
N11 C11 H11C 109.5 . . ?
H11A C11 H11C 109.5 . . ?
H11B C11 H11C 109.5 . . ?
N11 N12 C7 108.52(16) . . ?
N11 N12 H12 105.5(19) . . ?
C7 N12 H12 105.9(19) . . ?

loop_
  _geom_hbond_atom_site_label_D
  _geom_hbond_atom_site_label_H
  _geom_hbond_atom_site_label_A
  _geom_hbond_distance_DH
  _geom_hbond_distance_HA
  _geom_hbond_distance_DA
  _geom_hbond_angle_DHA
  _geom_hbond_site_symmetry_A
N8 H8 O10 0.868(16) 2.132(19) 2.943(2) 155(2) 1_455
N12 H12 O10 0.878(16) 2.62(2) 3.349(3) 141(2) 1_455

_diffrn_measured_fraction_theta_max 0.998
_diffrn_reflns_theta_full 27.49
_diffrn_measured_fraction_theta_full 0.998
_refine_diff_density_max 0.160
_refine_diff_density_min -0.126
_refine_diff_density_rms 0.030
```

1.8.1.3. 2-phenyl-2-(1,5-dimethyl-3-phenyl-6-oxoverdazyl)ethyl benzoate

Table 1.8-3. Crystal data for 2-phenyl-2-(1,5-dimethyl-3-phenyl-6-oxoverdazyl)ethyl benzoate

Compound reference	2-phenyl-2-(1,5-dimethyl-3-phenyl-6-oxoverdazyl)ethyl benzoate
Chemical formula	C ₂₅ H ₂₄ N ₄ O ₃
Formula Mass	428.48
Crystal system	Monoclinic
<i>a</i> /Å	8.56617(18)
<i>b</i> /Å	34.5561(6)
<i>c</i> /Å	7.35229(14)
<i>α</i> /°	90.00
<i>β</i> /°	95.2700(18)
<i>γ</i> /°	90.00
Unit cell volume/Å ³	2167.18(7)
Temperature/K	100(2)
Space group	<i>P</i> 2(1)/ <i>c</i>
No. of formula units per unit cell, <i>Z</i>	4
No. of reflections measured	10435
No. of independent reflections	4052
<i>R</i> _{int}	0.0183
Final <i>R</i> _{<i>I</i>} values (<i>I</i> > 2σ(<i>I</i>))	0.0380
Final <i>wR</i> (<i>F</i> ²) values (<i>I</i> > 2σ(<i>I</i>))	0.0982
Final <i>R</i> _{<i>I</i>} values (all data)	0.0401
Final <i>wR</i> (<i>F</i> ²) values (all data)	0.0998

data_2-phenyl-2-(1,5-dimethyl-3-phenyl-6-oxoverdazyl)ethyl benzoate

```

_audit_creation_method          SHELXL-97
_chemical_name_systematic      ;?;
_chemical_name_common          ?
_chemical_melting_point        ?
_chemical_formula_moiety       'C25 H24 N4 O3'
_chemical_formula_sum          'C25 H24 N4 O3'
_chemical_formula_weight       428.48

loop_
  _atom_type_symbol
  _atom_type_description
  _atom_type_scatter_dispersion_real
  _atom_type_scatter_dispersion_imag
  _atom_type_scatter_source
  'C'  'C'  0.0181  0.0091
  'International Tables Vol C Tables 4.2.6.8 and 6.1.1.4'
  'H'  'H'  0.0000  0.0000
  'International Tables Vol C Tables 4.2.6.8 and 6.1.1.4'
  'N'  'N'  0.0311  0.0180
  'International Tables Vol C Tables 4.2.6.8 and 6.1.1.4'
  'O'  'O'  0.0492  0.0322
  'International Tables Vol C Tables 4.2.6.8 and 6.1.1.4'

_symmetry_cell_setting         monoclinic
_symmetry_space_group_name_H-M P2(1)/c

```

Verdazyl Radicals as Mediators in Living Radical Polymerisation

```

_symmetry_space_group_name_Hall      '-P 2ybc'

loop_
  _symmetry_equiv_pos_as_xyz
    'x, y, z'
    '-x, y+1/2, -z+1/2'
    '-x, -y, -z'
    'x, -y-1/2, z-1/2'

_cell_length_a                        8.56617(18)
_cell_length_b                        34.5561(6)
_cell_length_c                        7.35229(14)
_cell_angle_alpha                     90.00
_cell_angle_beta                      95.2700(18)
_cell_angle_gamma                     90.00
_cell_volume                          2167.18(7)
_cell_formula_units_Z                 4
_cell_measurement_temperature         100(2)
_cell_measurement_reflns_used         3745
_cell_measurement_theta_min           3.83
_cell_measurement_theta_max           70.01

_exptl_crystal_description            block
_exptl_crystal_colour                 colourless
_exptl_crystal_size_max               0.38
_exptl_crystal_size_mid               0.30
_exptl_crystal_size_min               0.12
_exptl_crystal_density_meas           ?
_exptl_crystal_density_diffn          1.313
_exptl_crystal_density_method         'not measured'
_exptl_crystal_F_000                  904
_exptl_absorpt_coefficient_mu         0.714
_exptl_absorpt_correction_type        multi-scan
_exptl_absorpt_correction_T_min       0.58
_exptl_absorpt_correction_T_max       1.00
_exptl_absorpt_process_details        'ABSPACK(CrysAlis, Oxford
Diffraction)')

_exptl_special_details
;
  The temperature of the crystal was controlled using the Oxford
  Cryosystem Cryostream Cobra.
  The data collection nominally covered over a hemisphere of
  Reciprocal space, by a combination of seventeen sets of exposures
  with different \f angles for the crystal; low angles were recorded
  at 4 s and high angles at 16 s exposure covering 1.0 \% in \w.
  The crystal-to-detector distance was 5.5 cm.
  Crystal decay was found to be negligible by by repeating the initial
  frames at the end of data collection and analyzing the duplicate
  reflections.

  Hydrogen atoms were added at calculated positions and refined using
  a riding model. Anisotropic displacement parameters were used for
  all non-H atoms; H-atoms were given isotropic displacement parameter
  equal to 1.2 (or 1.5 for methyl H-atoms) times the equivalent
  isotropic displacement parameter of the atom to which they are
  attached.
;

_diffn_ambient_temperature            100(2)

```

Verdazyl Radicals as Mediators in Living Radical Polymerisation

```

_diffrn_radiation_wavelength      1.54184
_diffrn_radiation_type            CuK\alpha
_diffrn_radiation_source          'Enhance (Mo) X-ray Source'
_diffrn_radiation_monochromator    graphite
_diffrn_measurement_device_type    'Oxford Diffraction Gemini R'
_diffrn_measurement_method        '\f & \w scans'
_diffrn_detector_area_resol_mean  10.2833
_diffrn_standards_number          ?
_diffrn_standards_interval_count   ?
_diffrn_standards_interval_time   ?
_diffrn_standards_decay_%         nil
_diffrn_reflns_number             10435
_diffrn_reflns_av_R_equivalents    0.0183
_diffrn_reflns_av_sigmaI/netI     0.0178
_diffrn_reflns_limit_h_min        -10
_diffrn_reflns_limit_h_max        10
_diffrn_reflns_limit_k_min        -29
_diffrn_reflns_limit_k_max        42
_diffrn_reflns_limit_l_min        -8
_diffrn_reflns_limit_l_max        8
_diffrn_reflns_theta_min          5.19
_diffrn_reflns_theta_max          70.81
_reflns_number_total              4052
_reflns_number_gt                 3859
_reflns_threshold_expression       >2sigma(I)

_computing_data_collection         'CrysAlis CCD, Oxford Diffraction
Ltd'
_computing_cell_refinement         'CrysAlis RED, Oxford Diffraction
Ltd'
_computing_data_reduction         'CrysAlis RED, Oxford Diffraction
Ltd'
_computing_structure_solution     'SHELXS-97 (Sheldrick, 1990)'
_computing_structure_refinement   'SHELXL-97 (Sheldrick, 1997)'
_computing_molecular_graphics     'SHELXTL (Sheldrick, 1997)'
_computing_publication_material   'SHELXTL (Sheldrick, 1997)'

_refine_special_details
;
  Refinement of F2 against ALL reflections. The weighted R-factor
  wR and goodness of fit S are based on F2, conventional R-factors
  R are based on F, with F set to zero for negative F2. The
  threshold expression of F2 > 2sigma(F2) is used only for
  calculating R-factors(gt) etc. and is not relevant to the choice of
  reflections for refinement. R-factors based on F2 are
  statistically about twice as large as those based on F, and R-
  factors based on ALL data will be even larger.
;

_refine_ls_structure_factor_coef   Fsqd
_refine_ls_matrix_type            full
_refine_ls_weighting_scheme        calc
_refine_ls_weighting_details
  'calc          w=1/[\s2(Fo2)+(0.0588P)2+0.5743P]          where
P=(Fo2+2Fc2)/3'
_atom_sites_solution_primary       direct
_atom_sites_solution_secondary     difmap
_atom_sites_solution_hydrogens     geom
_refine_ls_hydrogen_treatment      constr
_refine_ls_extinction_method       none

```

Verdazyl Radicals as Mediators in Living Radical Polymerisation

_refine_ls_extinction_coef	?
_refine_ls_number_reflns	4052
_refine_ls_number_parameters	291
_refine_ls_number_restraints	0
_refine_ls_R_factor_all	0.0401
_refine_ls_R_factor_gt	0.0380
_refine_ls_wR_factor_ref	0.0998
_refine_ls_wR_factor_gt	0.0982
_refine_ls_goodness_of_fit_ref	1.042
_refine_ls_restrained_S_all	1.042
_refine_ls_shift/su_max	0.000
_refine_ls_shift/su_mean	0.000
loop_	
_atom_site_label	
_atom_site_type_symbol	
_atom_site_fract_x	
_atom_site_fract_y	
_atom_site_fract_z	
_atom_site_U_iso_or_equiv	
_atom_site_adp_type	
_atom_site_occupancy	
_atom_site_symmetry_multiplicity	
_atom_site_calc_flag	
_atom_site_refinement_flags	
_atom_site_disorder_assembly	
_atom_site_disorder_group	
C1 C 0.20819(14) 0.91257(3) 0.40204(16) 0.0236(2) Uani 1 1 d . . .	
H1A H 0.1977 0.8858 0.4283 0.028 Uiso 1 1 calc R . .	
C2 C 0.13569(15) 0.92764(4) 0.24093(17) 0.0299(3) Uani 1 1 d . . .	
H2A H 0.0752 0.9113 0.1581 0.036 Uiso 1 1 calc R . .	
C3 C 0.15133(17) 0.96644(4) 0.20073(18) 0.0349(3) Uani 1 1 d . . .	
H3A H 0.1028 0.9767 0.0897 0.042 Uiso 1 1 calc R . .	
C4 C 0.23830(18) 0.99036(4) 0.32325(19) 0.0354(3) Uani 1 1 d . . .	
H4A H 0.2487 1.0171 0.2961 0.042 Uiso 1 1 calc R . .	
C5 C 0.30995(15) 0.97557(4) 0.48463(17) 0.0279(3) Uani 1 1 d . . .	
H5A H 0.3688 0.9922 0.5680 0.033 Uiso 1 1 calc R . .	
C6 C 0.29618(13) 0.93628(3) 0.52572(15) 0.0206(2) Uani 1 1 d . . .	
C7 C 0.37809(13) 0.91998(3) 0.69416(15) 0.0194(2) Uani 1 1 d . . .	
N8 N 0.44388(12) 0.94288(3) 0.81581(13) 0.0225(2) Uani 1 1 d . . .	
N9 N 0.53343(12) 0.92532(3) 0.96047(13) 0.0233(2) Uani 1 1 d . . .	
C9 C 0.60946(17) 0.95223(4) 1.09265(18) 0.0332(3) Uani 1 1 d . . .	
H9A H 0.7041 0.9402 1.1530 0.050 Uiso 1 1 calc R . .	
H9B H 0.5374 0.9587 1.1842 0.050 Uiso 1 1 calc R . .	
H9C H 0.6381 0.9758 1.0298 0.050 Uiso 1 1 calc R . .	
O10 O 0.53190(10) 0.87789(2) 1.17694(11) 0.0261(2) Uani 1 1 d . . .	
C10 C 0.49426(13) 0.88917(3) 1.02173(15) 0.0208(2) Uani 1 1 d . . .	
N11 N 0.40429(11) 0.86786(3) 0.89679(13) 0.0208(2) Uani 1 1 d . . .	
C11 C 0.31526(14) 0.83509(3) 0.95587(17) 0.0256(3) Uani 1 1 d . . .	
H11A H 0.2663 0.8421 1.0666 0.038 Uiso 1 1 calc R . .	
H11B H 0.3857 0.8130 0.9817 0.038 Uiso 1 1 calc R . .	
H11C H 0.2338 0.8281 0.8591 0.038 Uiso 1 1 calc R . .	
N12 N 0.38238(11) 0.87902(3) 0.71069(12) 0.0184(2) Uani 1 1 d . . .	
C13 C 0.49313(13) 0.86028(3) 0.59076(15) 0.0190(2) Uani 1 1 d . . .	
H13A H 0.4740 0.8728 0.4682 0.023 Uiso 1 1 calc R . .	
C14 C 0.45487(13) 0.81764(3) 0.56277(16) 0.0225(2) Uani 1 1 d . . .	
H14A H 0.5236 0.8060 0.4764 0.027 Uiso 1 1 calc R . .	
H14B H 0.4707 0.8036 0.6803 0.027 Uiso 1 1 calc R . .	
O15 O 0.29245(9) 0.81533(2) 0.48969(11) 0.02303(19) Uani 1 1 d . . .	
C16 C 0.25007(14) 0.78391(3) 0.38855(15) 0.0217(2) Uani 1 1 d . . .	

Verdazyl Radicals as Mediators in Living Radical Polymerisation

```
C25 0.0248(6) 0.0273(6) 0.0280(6) -0.0016(5) 0.0066(5) -0.0025(5)
C26 0.0189(6) 0.0394(7) 0.0267(6) -0.0044(5) 0.0017(5) -0.0011(5)
C27 0.0222(6) 0.0397(7) 0.0227(6) 0.0034(5) 0.0007(5) 0.0040(5)
C28 0.0229(6) 0.0279(6) 0.0204(6) 0.0018(4) 0.0041(4) 0.0013(4)
```

```
_geom_special_details
```

```
;
```

All esds (except the esd in the dihedral angle between two l.s. planes) are estimated using the full covariance matrix. The cell esds are taken into account individually in the estimation of esds in distances, angles and torsion angles; correlations between esds in cell parameters are only used when they are defined by crystal symmetry. An approximate (isotropic) treatment of cell esds is used for estimating esds involving l.s. planes.

```
;
```

```
loop_
```

```
_geom_bond_atom_site_label_1
_geom_bond_atom_site_label_2
_geom_bond_distance
_geom_bond_site_symmetry_2
_geom_bond_publ_flag
```

```
C1 C2 1.3874(18) . ?
C1 C6 1.3929(16) . ?
C1 H1A 0.9500 . ?
C2 C3 1.3821(19) . ?
C2 H2A 0.9500 . ?
C3 C4 1.388(2) . ?
C3 H3A 0.9500 . ?
C4 C5 1.3827(19) . ?
C4 H4A 0.9500 . ?
C5 C6 1.3983(17) . ?
C5 H5A 0.9500 . ?
C6 C7 1.4777(16) . ?
C7 N8 1.2849(15) . ?
C7 N12 1.4208(14) . ?
N8 N9 1.3921(14) . ?
N9 C10 1.3797(15) . ?
N9 C9 1.4551(15) . ?
C9 H9A 0.9800 . ?
C9 H9B 0.9800 . ?
C9 H9C 0.9800 . ?
O10 C10 1.2208(14) . ?
C10 N11 1.3601(15) . ?
N11 N12 1.4173(13) . ?
N11 C11 1.4538(15) . ?
C11 H11A 0.9800 . ?
C11 H11B 0.9800 . ?
C11 H11C 0.9800 . ?
N12 C13 1.5002(14) . ?
C13 C23 1.5111(16) . ?
C13 C14 1.5193(15) . ?
C13 H13A 1.0000 . ?
C14 O15 1.4469(14) . ?
C14 H14A 0.9900 . ?
C14 H14B 0.9900 . ?
O15 C16 1.3470(13) . ?
C16 O16 1.2033(15) . ?
C16 C17 1.4919(16) . ?
C17 C22 1.3927(16) . ?
```

C17 C18 1.3985(16) . ?
 C18 C19 1.3841(17) . ?
 C18 H18A 0.9500 . ?
 C19 C20 1.3921(17) . ?
 C19 H19A 0.9500 . ?
 C20 C21 1.3869(18) . ?
 C20 H20A 0.9500 . ?
 C21 C22 1.3844(18) . ?
 C21 H21A 0.9500 . ?
 C22 H22A 0.9500 . ?
 C23 C28 1.3929(16) . ?
 C23 C24 1.3960(16) . ?
 C24 C25 1.3852(17) . ?
 C24 H24A 0.9500 . ?
 C25 C26 1.3869(19) . ?
 C25 H25A 0.9500 . ?
 C26 C27 1.3863(19) . ?
 C26 H26A 0.9500 . ?
 C27 C28 1.3867(18) . ?
 C27 H27A 0.9500 . ?
 C28 H28A 0.9500 . ?

loop_
 _geom_angle_atom_site_label_1
 _geom_angle_atom_site_label_2
 _geom_angle_atom_site_label_3
 _geom_angle
 _geom_angle_site_symmetry_1
 _geom_angle_site_symmetry_3
 _geom_angle_publ_flag

C2 C1 C6 120.63(11) . . ?
 C2 C1 H1A 119.7 . . ?
 C6 C1 H1A 119.7 . . ?
 C3 C2 C1 120.14(12) . . ?
 C3 C2 H2A 119.9 . . ?
 C1 C2 H2A 119.9 . . ?
 C2 C3 C4 119.72(12) . . ?
 C2 C3 H3A 120.1 . . ?
 C4 C3 H3A 120.1 . . ?
 C5 C4 C3 120.42(12) . . ?
 C5 C4 H4A 119.8 . . ?
 C3 C4 H4A 119.8 . . ?
 C4 C5 C6 120.31(12) . . ?
 C4 C5 H5A 119.8 . . ?
 C6 C5 H5A 119.8 . . ?
 C1 C6 C5 118.77(11) . . ?
 C1 C6 C7 120.65(10) . . ?
 C5 C6 C7 120.54(10) . . ?
 N8 C7 N12 123.21(10) . . ?
 N8 C7 C6 119.52(10) . . ?
 N12 C7 C6 117.25(9) . . ?
 C7 N8 N9 116.04(9) . . ?
 C10 N9 N8 120.71(9) . . ?
 C10 N9 C9 117.90(10) . . ?
 N8 N9 C9 114.40(9) . . ?
 N9 C9 H9A 109.5 . . ?
 N9 C9 H9B 109.5 . . ?
 H9A C9 H9B 109.5 . . ?
 N9 C9 H9C 109.5 . . ?
 H9A C9 H9C 109.5 . . ?

H9B C9 H9C 109.5 . . ?
 O10 C10 N11 122.90(11) . . ?
 O10 C10 N9 122.88(11) . . ?
 N11 C10 N9 114.16(10) . . ?
 C10 N11 N12 121.42(9) . . ?
 C10 N11 C11 120.01(9) . . ?
 N12 N11 C11 118.28(9) . . ?
 N11 C11 H11A 109.5 . . ?
 N11 C11 H11B 109.5 . . ?
 H11A C11 H11B 109.5 . . ?
 N11 C11 H11C 109.5 . . ?
 H11A C11 H11C 109.5 . . ?
 H11B C11 H11C 109.5 . . ?
 N11 N12 C7 110.71(9) . . ?
 N11 N12 C13 114.53(8) . . ?
 C7 N12 C13 113.11(8) . . ?
 N12 C13 C23 112.47(9) . . ?
 N12 C13 C14 110.98(9) . . ?
 C23 C13 C14 113.57(9) . . ?
 N12 C13 H13A 106.4 . . ?
 C23 C13 H13A 106.4 . . ?
 C14 C13 H13A 106.4 . . ?
 O15 C14 C13 106.98(9) . . ?
 O15 C14 H14A 110.3 . . ?
 C13 C14 H14A 110.3 . . ?
 O15 C14 H14B 110.3 . . ?
 C13 C14 H14B 110.3 . . ?
 H14A C14 H14B 108.6 . . ?
 C16 O15 C14 116.79(9) . . ?
 O16 C16 O15 123.55(11) . . ?
 O16 C16 C17 124.71(10) . . ?
 O15 C16 C17 111.74(9) . . ?
 C22 C17 C18 119.27(11) . . ?
 C22 C17 C16 117.92(10) . . ?
 C18 C17 C16 122.81(10) . . ?
 C19 C18 C17 120.32(11) . . ?
 C19 C18 H18A 119.8 . . ?
 C17 C18 H18A 119.8 . . ?
 C18 C19 C20 119.93(11) . . ?
 C18 C19 H19A 120.0 . . ?
 C20 C19 H19A 120.0 . . ?
 C21 C20 C19 119.97(11) . . ?
 C21 C20 H20A 120.0 . . ?
 C19 C20 H20A 120.0 . . ?
 C22 C21 C20 120.17(11) . . ?
 C22 C21 H21A 119.9 . . ?
 C20 C21 H21A 119.9 . . ?
 C21 C22 C17 120.33(11) . . ?
 C21 C22 H22A 119.8 . . ?
 C17 C22 H22A 119.8 . . ?
 C28 C23 C24 118.96(11) . . ?
 C28 C23 C13 122.70(10) . . ?
 C24 C23 C13 118.26(10) . . ?
 C25 C24 C23 120.60(11) . . ?
 C25 C24 H24A 119.7 . . ?
 C23 C24 H24A 119.7 . . ?
 C24 C25 C26 119.98(11) . . ?
 C24 C25 H25A 120.0 . . ?
 C26 C25 H25A 120.0 . . ?
 C27 C26 C25 119.86(11) . . ?

Verdazyl Radicals as Mediators in Living Radical Polymerisation

C27 C26 H26A 120.1 . . ?
C25 C26 H26A 120.1 . . ?
C26 C27 C28 120.26(12) . . ?
C26 C27 H27A 119.9 . . ?
C28 C27 H27A 119.9 . . ?
C27 C28 C23 120.34(11) . . ?
C27 C28 H28A 119.8 . . ?
C23 C28 H28A 119.8 . . ?

_diffirn_measured_fraction_theta_max 0.972
_diffirn_reflns_theta_full 68.50
_diffirn_measured_fraction_theta_full 0.983
_refine_diff_density_max 0.224
_refine_diff_density_min -0.213
_refine_diff_density_rms 0.044

1.9. References

1. K. Matyjaszewski and T. P. Davis, *Handbook of Radical Polymerisation*, 1st edn., Wiley-Interscience, Hoboken, New Jersey, 2002.
2. M. Szwarc, M. Levy and R. Milkovich, *J. Am. Chem. Soc.*, 1956, **78**, 2656-2657.
3. M. Szwarc, *Nature*, 1956, **178**, 1168-1169.
4. M. Szwarc, *J. Pol. Sci. Part A - Polym. Chem.*, 1998, **36**, v-xiii.
5. R. P. Quirk and B. Lee, *Polym. Int.*, 1992, **27**, 359-367.
6. M. Kato, M. Kamigaito, M. Sawamoto and T. Higashimura, *Macromolecules*, 1995, **28**, 1721-1723.
7. J.-S. Wang and K. Matyjaszewski, *Macromolecules*, 1995, **28**, 7901-7910.
8. M. S. Kharasch, E. V. Jensen and W. H. Urry, *Science*, 1945, **102**, 128.
9. F. Minisci, *Acc. Chem. Res.*, 1975, **8**, 165-171.
10. G. Moad and D. H. Solomon, *The Chemistry of Radical Polymerisation*, 2nd edn., Elsevier, 2006.
11. K. Matyjaszewski and J. Xia, *Chem. Rev.*, 2001, **101**, 2921-2990.
12. G. F. Meijs and E. Rizzardo, *Makromol. Chem. Rapid. Commun.*, 1988, **9**, 547-551.
13. G. F. Meijs, E. Rizzardo and S. H. Thang, *Macromolecules*, 1988, **21**, 3122-3124.
14. J. Chiefari, Y. K. Chong, F. Ercole, J. Krstina, J. Jeffery, T. P. T. Le, R. T. A. Mayadunne, G. F. Meijs, C. L. Moad, G. Moad, E. Rizzardo and S. H. Thang, *Macromolecules*, 1998, **31**, 5559-5562.
15. G. Moad, E. Rizzardo and S. H. Thang, *Polymer*, 2008, **49**, 1079-1131.

16. T. Otsu, M. Yoshida and T. Tazaki, *Makromol. Chem. Rapid. Commun.*, 1982, **3**, 133-140.
17. H. Fischer, *J. Pol. Sci. Part A - Polym. Chem.*, 1999, **37**, 1885-1901.
18. H. Fischer, *Chem. Rev.*, 2001, **101**, 3581-3610.
19. M. Souaille and H. Fischer, *Macromolecules*, 2000, **33**, 7378-7394.
20. M. Souaille and H. Fischer, *Macromolecules*, 2001, **35**, 248-261.
21. E. Rizzardo and D. Solomon, *Polym. Bull.*, 1979, **1**, 529-534.
22. G. Moad, E. Rizzardo and D. H. Solomon, *Macromolecules*, 1982, **15**, 909-914.
23. M. K. Georges, R. P. N. Veregin, P. M. Kazmaier and G. K. Hamer, *Macromolecules*, 1993, **26**, 2987-2988.
24. C. J. Hawker, *J. Am. Chem. Soc.*, 1994, **116**, 11185-11186.
25. C. J. Hawker, G. G. Barclay, A. Orellana, J. Dao and W. Devonport, *Macromolecules*, 1996, **29**, 5245-5254.
26. C. J. Hawker, A. W. Bosman and E. Harth, *Chem. Rev.*, 2001, **101**, 3661-3688.
27. M. K. Georges, J. L. Lukkarila and A. R. Szkurhan, *Macromolecules*, 2004, **37**, 1297-1303.
28. C. J. Hawker, E. Elce, J. Dao, W. Volksen, T. P. Russell and G. G. Barclay, *Macromolecules*, 1996, **29**, 2686-2688.
29. F. R. Mayo, *J. Am. Chem. Soc.*, 1968, **90**, 1289-1295.
30. C. M. Paleos and P. Dais, *J. Chem. Soc., Chem. Commun.*, 1977, 345-346.
31. D. Benoit, V. Chaplinski, R. Braslau and C. J. Hawker, *J. Am. Chem. Soc.*, 1999, **121**, 3904-3920.

-
32. D. Benoit, S. Grimaldi, S. Robin, J.-P. Finet, P. Tordo and Y. Gnanou, *J. Am. Chem. Soc.*, 2000, **122**, 5929-5939.
33. A. Nilsen and R. Braslau, *J. Pol. Sci. Part A - Polym. Chem.*, 2006, **44**, 697-717.
34. G. Moad, G. Anderson Albert, F. Ercole, H. J. Johnson Charles, J. Krstina, L. Moad Catherine, E. Rizzardo, H. Spurling Thomas and H. Thang San, in *Controlled Radical Polymerization*, American Chemical Society, 1998, vol. 685, pp. 332-360.
35. G. S. Ananchenko, M. Souaille, H. Fischer, C. Le Mercier and P. Tordo, *J. Pol. Sci. Part A - Polym. Chem.*, 2002, **40**, 3264-3283.
36. B. Charleux, J. Nicolas and O. Guerret, *Macromolecules*, 2005, **38**, 5485-5492.
37. J. Nicolas, S. Brusseau and B. Charleux, *J. Pol. Sci. Part A - Polym. Chem.*, 2010, **48**, 34-47.
38. Y. Guillaneuf, D. Gigmes, S. R. A. Marque, P. Astolfi, L. Greci, P. Tordo and D. Bertin, *Macromolecules*, 2007, **40**, 3108-3114.
39. M. Edeleva, S. R. A. Marque, D. Bertin, D. Gigmes, Y. Guillaneuf, S. V. Morozov and E. G. Bagryanskaya, *J. Pol. Sci. Part A - Polym. Chem.*, 2008, **46**, 6828-6842.
40. A. C. Greene and R. B. Grubbs, *Macromolecules*, **43**, 10320-10325.
41. O. E. Ansong, S. Jansen, Y. Wei, G. Pomrink, H. Lu, A. Patel and S. Li, *Polym. Int.*, 2009, **58**, 54-65.
42. B. Grignard, T. Phan, D. Bertin, D. Gigmes, C. Jerome and C. Detrembleur, *Polym. Chem.*, 2010, **1**, 837-840.
43. D. Colombani, M. Steenbock, M. Klapper and K. Müllen, *Macromol. Rapid Commun.*, 1997, **18**, 243-251.

-
44. M. Steenbock, M. Klapper and K. Müllen, *Macromol. Chem. Phys.*, 1998, **199**, 763-769.
 45. A. Dasgupta, T. Brand, M. Klapper and K. Müllen, *Polym. Bull.*, 2001, **46**, 131-138.
 46. N. S. Khelfallah, M. Peretolchin, M. Klapper and K. Müllen, *Polym. Bull.*, 2005, **53**, 295-304.
 47. T. C. Chung and H. Hong, in *Advances in Controlled/Living Radical Polymerization*, American Chemical Society, 2003, vol. 854, pp. 481-495.
 48. J. D. Druliner, *Macromolecules*, 1991, **24**, 6079-6082.
 49. *US Pat.*, J. D. Druliner, *Polymerisation of Vinyl Monomers with a New Catalytic System*, WO9202561, 1992.
 50. B. Yamada, H. Tanaka, K. Konishi and T. Otsu, *Macromol. Sci. Pure Appl. Chem.*, 1994, **31**, 351 - 366.
 51. B. Yamada, Y. Nobukane and Y. Miura, *Pol. Bull.*, 1998, **41**, 539-544.
 52. S. J. Teertstra, E. Chen, D. Chan-Seng, P. O. Otieno, R. G. Hicks and M. K. Georges, *Macromol. Symp.*, 2007, **248**, 117-125.
 53. E. K. Y. Chen, S. J. Teertstra, D. Chan-Seng, P. O. Otieno, R. G. Hicks and M. K. Georges, *Macromolecules*, 2007, **40**, 8609-8616.
 54. R. G. Hicks, *Stable Radicals: Fundamentals and Applied Aspects of Odd-Electron Compounds*, 1st edn., Wiley, 2010.
 55. G. R. Eaton, S. S. Eaton, D. P. Barr and R. T. Weber, *Quantitative EPR*, 1st edn., SpringerWeinNewYork, New York, 2010.
 56. J. A. Weil and J. R. Bolton, *Electron Paramagnetic Resonance Elemental Theory and Practical Applications*, 2nd edn., J. Wiley & Sons, Inc., 2007.
 57. R. S. Alger, *Electron Paramagnetic Resonance Techniques and Applications*, 1st edn., Interscience Publishers, 1968.

58. J. Krzystek, A. Sienkiewicz, L. Pardi and L. C. Brunel, *J. Magn. Reson.*, 1997, **125**, 207-211.
59. A. R. Forrester, J. M. Hay and R. H. Thompson, *Organic Chemistry of Stable Radicals*, 1st edn., Academic Press, 1968.
60. R. Kuhn and H. Trischmann, *Angew. Chem. Int. Ed. Engl.*, 1963, **2**, 155.
61. D. Griller and K. U. Ingold, *Acc. Chem. Res.*, 1976, **9**, 13-19.
62. F. A. Neugebauer and H. Fischer, *Angew. Chem.*, 1980, **92**, 766.
63. F. A. Neugebauer, H. Fischer and R. Siegel, *Chem. Ber.*, 1988, **121**, 815-822.
64. R. Milcent, G. Barbier, S. Capelle and J.-P. Catteau, *J. Heterocycl. Chem.*, 1994, **31**, 319-324.
65. C. L. Barr, P. A. Chase, R. G. Hicks, M. T. Lemaire and C. L. Stevens, *J. Org. Chem.*, 1999, **64**, 8893-8897.
66. E. C. Pare, D. J. R. Brook, A. Brieger, M. Badik and M. Schinke, *Org. Biomol. Chem.*, 2005, **3**, 4258-4261.
67. *French Pat.*, R. Milcent, G. Barbier, F. Mazouz and A. K. Ben, *Preparation of 1,4,5,6-tetrahydro-1,2,4,5-tetrazin-3-ones and their conversion to stable radicals for use as nuclear magnetic resonance tomography contrast agents*, WO8904309A2, 1989.
68. R. G. Hicks, *Org. Biomol. Chem.*, 2007, **5**, 1321-1338.
69. Franz A. Neugebauer, *Angew. Chem. Int. Ed. Engl.*, 1973, **12**, 455-464.
70. A. Yang, T. Kasahara, E. K. Y. Chen, G. K. Hamer and M. K. Georges, *Eur. J. Org. Chem.*, 2008, 4571-4574.
71. F. A. Neugebauer, *Tetrahedron*, 1970, **26**, 4853-4857.
72. V. Chemistruck, D. Chambers and D. J. R. Brook, *J. Org. Chem.*, 2009, **74**.
73. D. B. E. Kennedy, University of British Columbia, 1974.

-
74. F. A. Neugebauer, H. Fischer and C. Krieger, *J. Chem. Soc., Perkin Trans. 2*, 1993, 535-544.
75. R. Kuhn and H. Trischmann, *Monatsh. Chem.*, 1964, **95**, 457-479.
76. P. H. Fischer, *Tetrahedron*, 1967, **23**, 1939-1952.
77. L. N. Markovskiy, O. M. Polumbrik and A. M. Nesterenko, *Int. J. Quantum Chem.*, 1979, **16**, 891-895.
78. F. A. Neugebauer, H. Brunner and K. H. Hausser, *Tetrahedron*, 1971, **27**, 3623-3628.
79. L. Degtyarev and Y. Gorlov, *J. Struct. Chem.*, 1976, **16**, 715-718.
80. L. S. Degtyarev, A. A. Stetsenko and Y. I. Gorlov, *Chem. Phys. Lett.*, 1980, **69**, 323-326.
81. O. Polumbrik, A. Nesterenko and L. Markovskii, *J. Struct. Chem.*, 1980, **20**, 487-490.
82. J. Jornet, M. Deumal, J. Ribas-Ariño, M. J. Bearpark, M. A. Robb, R. G. Hicks and J. J. Novoa, *Chem. Eur. J.*, 2006, **12**, 3995-4005.
83. J. B. Gilroy, S. D. J. McKinnon, P. Kennepohl, M. S. Zsombor, M. J. Ferguson, L. K. Thompson and R. G. Hicks, *J. Org. Chem.*, 2007, **72**, 8062-8069.
84. A. R. Katritzky, S. A. Belyakov, S. Strah, B. Cage and N. S. Dalal, *Tetrahedron Lett.*, 1999, **40**, 407-410.
85. J. B. Gilroy, B. D. Koivisto, R. McDonald, M. J. Ferguson and R. G. Hicks, *J. Mater. Chem.*, 2006, **16**, 2618-2624.
86. D. J. R. Brook, S. Fornell, J. E. Stevens, B. Noll, T. H. Koch and W. Einfeld, *Inorg. Chem.*, 2000, **39**, 562-567.
87. R. G. Hicks, B. D. Koivisto and M. T. Lemaire, *Org. Lett.*, 2004, **6**, 1887-1890.
88. B. D. Koivisto and R. G. Hicks, *Coord. Chem. Rev.*, 2005, **249**, 2612-2630.
-

-
89. M. H. Chahma, X. Wang, A. van der Est and M. Pilkington, *J. Org. Chem.*, 2006, **71**, 2750-2755.
90. C. Train, L. Norel and M. Baumgarten, *Coord. Chem. Rev.*, 2009, **253**, 2342-2351.
91. I. Ratera and J. Veciana, *Chem. Soc. Rev.*, 2011 Advanced article.
92. M. Bancercz and M. K. Georges, *J. Org. Chem.*, 2011, **76**, 6377-6382.
93. M. Kinoshita and Y. Miura, *Makromol. Chem.*, 1969, **124**, 211-221.
94. *United States Pat.*, R. G. Hicks and M. Georges, *Verdazyl Agents for the Production of Free Standing Polymers*, US 0244274, 2007.
95. E. K.-Y. Chen, University of Toronto, 2010.
96. M. K. Georges, R. A. Kee, R. P. N. Veregin, G. K. Hamer and P. M. Kazmaier, *J. Phys. Org. Chem.*, 1995, **8**, 301-305.
97. F. A. Neugebauer, H. Fischer, R. Siegel and C. Krieger, *Chem. Ber.*, 1983, **116**, 3461-3481.
98. M. J. Plater, J. P. Sinclair, S. Kemp, T. Gelbrich, M. B. Hursthouse and C. J. Gomez-Garcia, *J. Chem. Res.*, 2006, 515-520.
99. K. Mukai, N. Wada, J. B. Jamali, N. Achiwa, Y. Narumi, K. Kindo, T. Kobayashi and K. Amaya, *Chem. Phys. Lett.*, 1996, **257**, 538-544.
100. M. J. Frisch, G. W. Trucks and G. E. S. H. B. Schlegel, M. A. Robb, J. R. Cheeseman, J. A. Montgomery, Jr., T. Vreven, K. N. Kudin, J. C. Burant, J. M. Millam, S. S. Iyengar, J. Tomasi, V. Barone, B. Mennucci, M. Cossi, G. Scalmani, N. Rega, G. A. Petersson, H. Nakatsuji, M. Hada, M. Ehara, K. Toyota, R. Fukuda, J. Hasegawa, M. Ishida, T. Nakajima, Y. Honda, O. Kitao, H. Nakai, M. Klene, X. Li, J. E. Knox, H. P. Hratchian, J. B. Cross, V. Bakken, C. Adamo, J. Jaramillo, R. Gomperts, R. E. Stratmann, O. Yazyev, A. J. Austin, R. Cammi, C. Pomelli, J. W. Ochterski, P. Y. Ayala, K. Morokuma, G. A. Voth, P. Salvador, J. J. Dannenberg, V. G. Zakrzewski, S. Dapprich, A. D. Daniels, M. C. Strain, O. Farkas, D. K. Malick, A. D. Rabuck, K. Raghavachari, J. B. Foresman, J. V. Ortiz, Q. Cui, A. G. Baboul,
-

S. Clifford, J. Cioslowski, B. B. Stefanov, G. Liu, A. Liashenko, P. Piskorz, I. Komaromi, R. L. Martin, D. J. Fox, T. Keith, M. A. Al-Laham, C. Y. Peng, A. Nanayakkara, M. Challacombe, P. M. W. Gill, B. Johnson, W. Chen, M. W. Wong, C. Gonzalez, and J. A. Pople, *Gaussian 03, Revision C.02*; Gaussian 03, Revision C.02, Wallingford CT, **2004**.

101. M. J. Plater, S. Kemp, E. Coronado, C. J. Gómez-García, R. W. Harrington and W. Clegg, *Polyhedron*, 2006, **25**, 2433-2438.

102. H. Kurreck, B. Kirste and W. Lubitz, *Angew. Chem. Int. Ed. Eng.*, 1984, **23**, 173-194.

103. K. Matyjaszewski, B. E. Woodworth, X. Zhang, S. G. Gaynor and Z. Metzner, *Macromolecules*, 1998, **31**, 5955-5957.

104. J. M. Evans, *Polymer Engineering & Science*, 1973, **13**, 401-408.

105. M. K. Georges, email correspondance, December 2009.

106. A. Kajiwarra and K. Matyjaszewski, in *Advanced ESR methods in polymer research*, ed. S. Schlich, John Wiley & Sons, Inc., Hoboken, New Jersey, **2006**, pp. 101-131.

107. G. Odian, *Principles of Polymerisation*, 4th edn., John Wiley & Sons, Hoboken, New Jersey, 2004.

108. B. Ranby and J. F. Rabek, *ESR Spectroscopy in Polymer Research*, 1st edn., Springer, New York, 1977.

109. B. Yamada, D. G. Westmoreland, S. Kobatake and O. Konosu, *Prog. Polym. Sci.*, 1999, **24**, 565-630.

110. H.-R. Chang, W. Lau, H.-Y. Parker and D. G. Westmoreland, *Macromol. Symp.*, 1996, **111**, 253-263.

111. Y. Mao, R. Song, Y. Zheng and J. Shen, *Macromolecules*, 1994, **27**, 6746-6749.

112. M. Kamachi and A. Kajiwarra, *Macromol. Symp.*, 2002, **179**, 53-74.

113. A. Matsumoto, in *Handbook of Radical Polymerization*, John Wiley & Sons, Inc., 2003, pp. 691-773.
114. A. Lund, M. Shiotani and S. Shimada, *Principles and Applications of ESR Spectroscopy*, 1st edn., Springer, New York, 2011.
115. M. Newton, conversation, April 2011.
116. M. Chini, P. Crotti, C. Gardelli and F. Macchia, *Tetrahedron*, 1992, **48**, 3805-3812.
117. D. L. J. Clive, J. Zhang, R. Subedi, V. Bouetard, S. Hiebert and R. Ewanuk, *J. Org. Chem.*, 2001, **66**, 1233-1241.

2. Dopamine End-Functionalised Polymers for Application as Friction Modifiers

2.1. Introduction

2.1.1. Dopamine and polymer adhesion

2.1.1.1. Taking inspiration from nature

Common marine mussels display a unique ability of being able to anchor themselves permanently to uneven, dirty, slippery and wet surfaces with bonds strong enough to survive often turbulent conditions (Figure 2.1-1). This method of adhesion has been of particular interest in the scientific community.



Figure 2.1-1. Mussels in their natural environment¹

The mussels attach themselves to a surface by a byssus or ‘beard’ which consists of 50–100 threads with adhesive plaques on the end (Figure 2.1-2).² The mussel has an organ called a foot which serves to produce the threads for the byssus. The foot is best modelled as a rubber plunger equipped with injectors (Figure 2.1-3).³ In the first step the foot extends and explores the surface before making contact. The foot mediates scrubbing of the surface and by depression of the ‘plunger’ extrudes water. Muscles in the foot then contract reforming the dome of the plunger and creating a cavity under vacuum, known as the distal depression. The adhesive protein precursor is injected into the cavity forming a foam. Once the foam has hardened, the foot retreats leaving the thread attached to the surface.

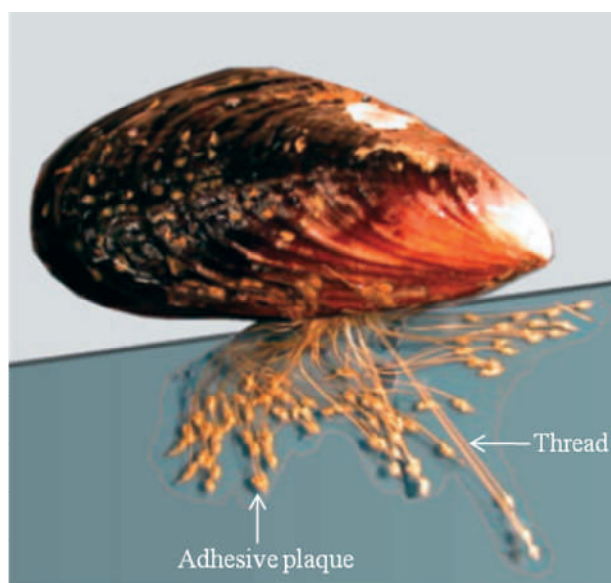


Figure 2.1-2. Mussel with the byssus used to adhere to a rock⁴

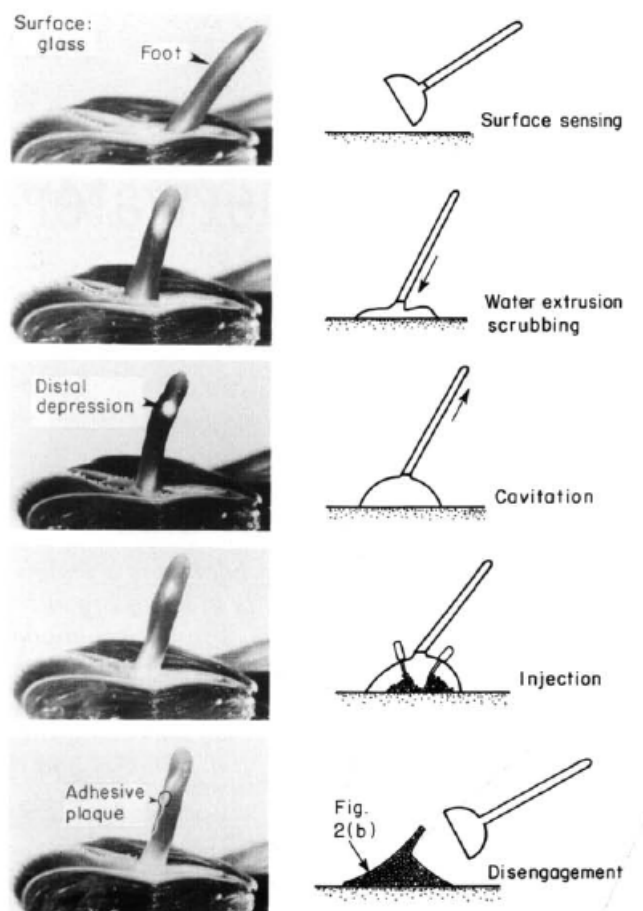


Figure 2.1-3. Time lapse photography showing the mussel foot (left) and the rubber plunger model (right) for the five steps of thread formation³

The byssus contains approximately 25–30 different proteins, five of which are found only in the adhesive plaque.⁴ The core of the thread is mainly composed of silk and collagen-like proteins.^{5, 6} The adhesive proteins located in the adhesive plaque, best characterised for the common blue mussel, *Mytilus edulis*, are the so called mussel foot proteins (mfp) -2, -3, -4, -5 and -6. Mfp-1 is found in the cuticle of the byssal thread.⁷ Each of these proteins contain 3,4-dihydroxyphenyl-L-alanine (DOPA), a catechol containing compound with a primary amine functional group, formed from

the post translational modification of tyrosine, in varying amounts as shown in Figure 2.1-4.⁴

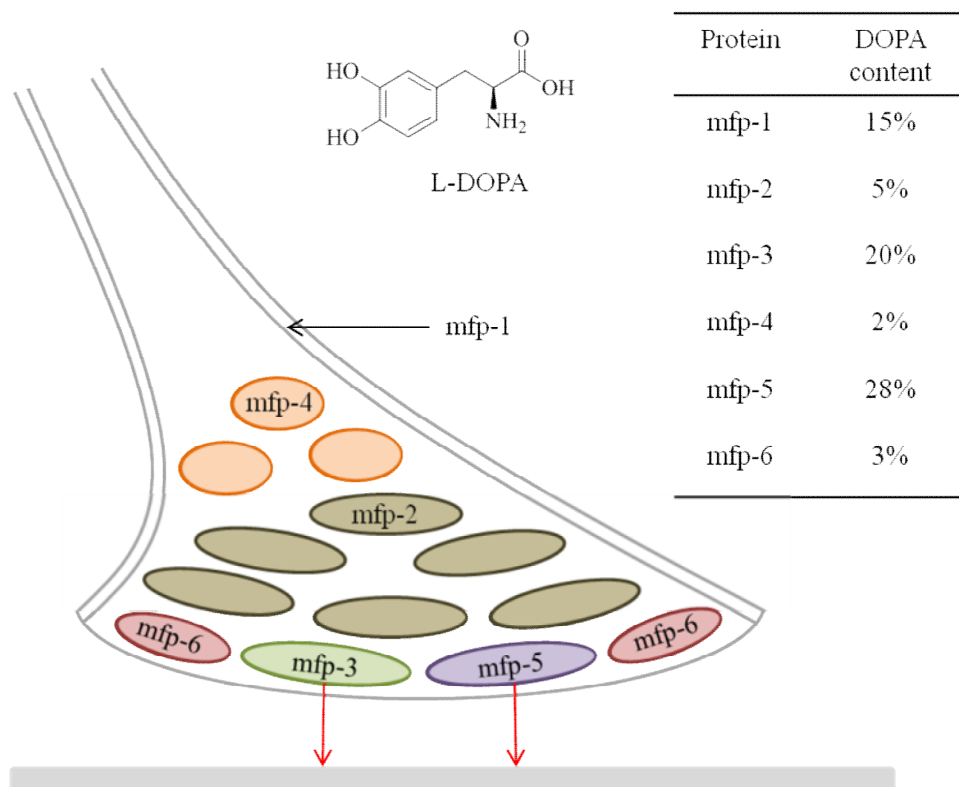
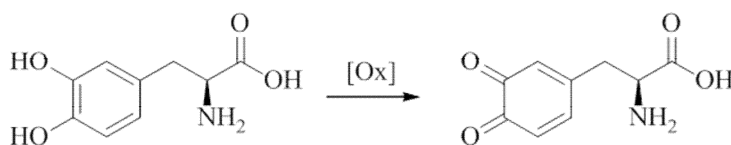


Figure 2.1-4. Schematic of the mussel adhesive plaque and the approximate location of the mussel foot proteins and their DOPA content

2.1.1.2. The role of DOPA in adhesion

Mfp-3 and mfp-5 contain the highest DOPA content and are accepted as being the proteins responsible for surface adhesion.^{4, 7} The mechanism of adhesion by DOPA is not fully understood and is the subject of ongoing investigations.

It is generally accepted that DOPA is mainly responsible for adhesion, whereas dopaquinone, the oxidised form of DOPA, is mainly responsible for cross-linking reactions, particularly in thread formation.⁸⁻¹¹ This was illustrated by Yu *et al.*^{8, 12} who investigated the adhesion of both DOPA and its oxidised form dopaquinone (Scheme 2.1-1). DOPA copolymers with L-lysine or L-glutamic acid either in the presence or absence of oxidising agent on aluminium exhibited a strong moisture resistant bond. Oxidation of DOPA to dopaquinone resulted in a weaker bond to the surface and the formation of a cross-linked network on the aluminium substrate.



Scheme 2.1-1. Oxidation of DOPA to dopaquinone

The strength of adhesion of DOPA to organic substrates has been investigated using single molecule atomic force microscopy (AFM) by Lee *et al.*¹³ A DOPA functionalised AFM tip was produced by tethering a DOPA molecule with a PEG chain and the force required to break the DOPA-substrate bond was measured. The amine group was protected to ensure no interaction was observed with the substrate. Strong, reversible coordination bonds were observed for DOPA with titanium oxide (Figure 2.1-5). It was suggested by the authors that although a reversible interaction was seen in the single molecule experiments, the same may not be seen in mfps as multiple DOPA interactions with a metal oxide surface should produce a much stronger overall bond. Oxidation of DOPA to dopaquinone substantially reduced

adhesion to the titanium oxide surface; however, with organic surfaces the dopaquinone formed strong covalent bonds possibly by a route similar to a Michael addition reaction (Figure 2.1-5).¹³

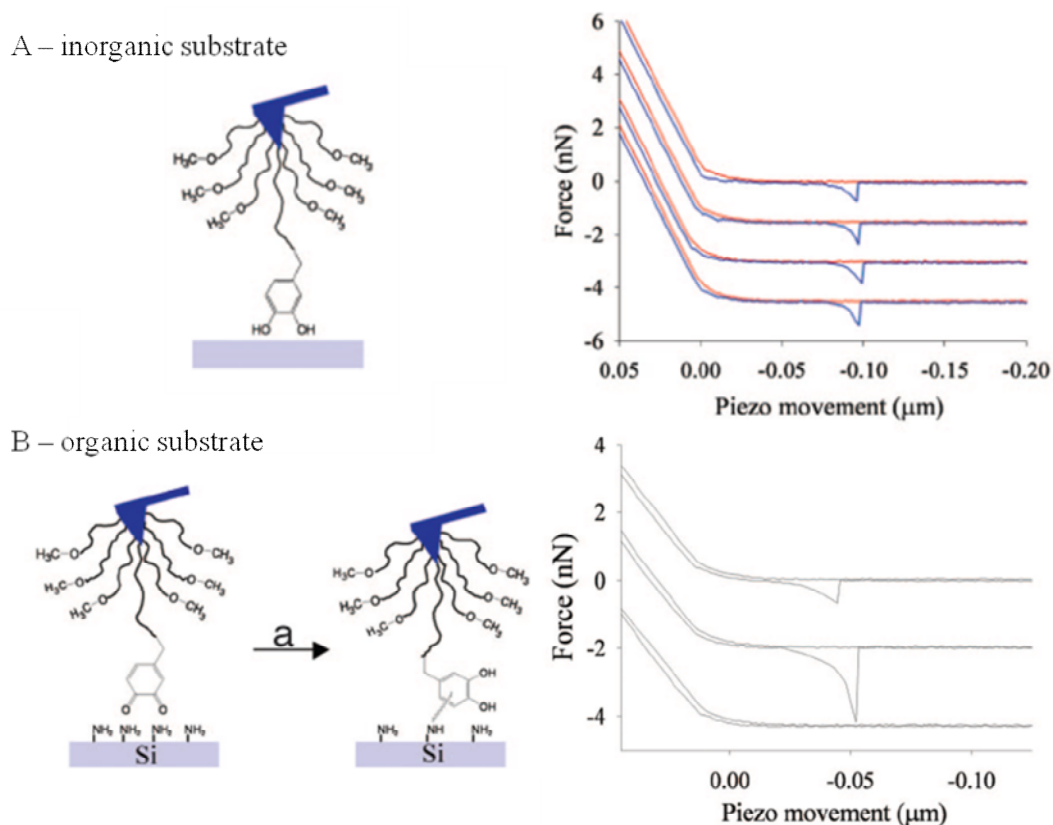
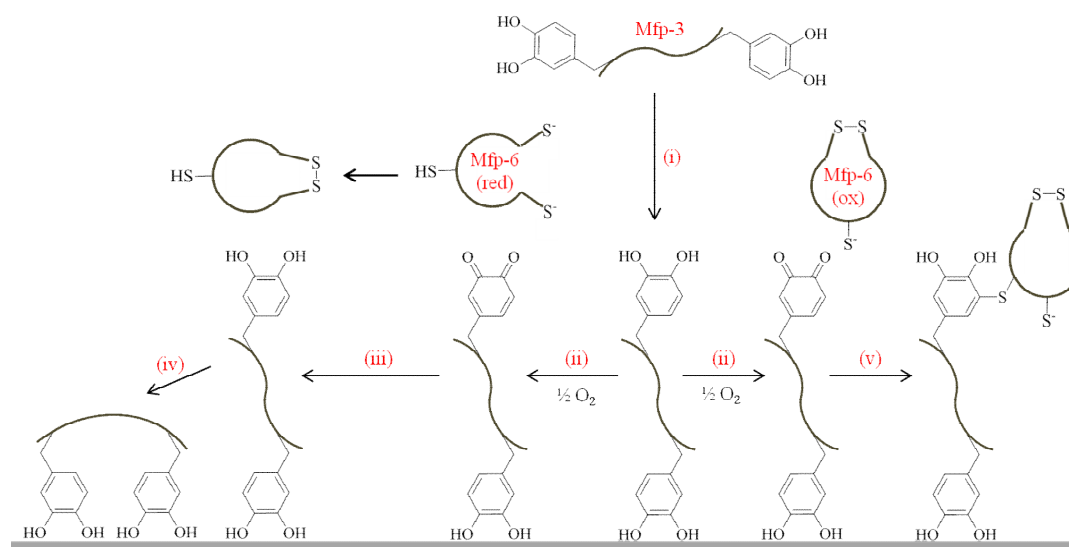


Figure 2.1-5. A) Schematic of the DOPA functionalised AFM tip and the force-distance curves for the single molecule interaction of DOPA with a titanium surface; B) Schematic of the oxidised DOPA functionalised AFM tip and force-distance curves for the single molecule interaction of dopaquinone with an organic surface¹³

At marine pH (~ 8.2) DOPA is easily oxidised to dopaquinone, raising many questions as to why a mussel relies on DOPA for adhesion. Yu and co-workers addressed this in a recent report which demonstrated that oxidation of DOPA to

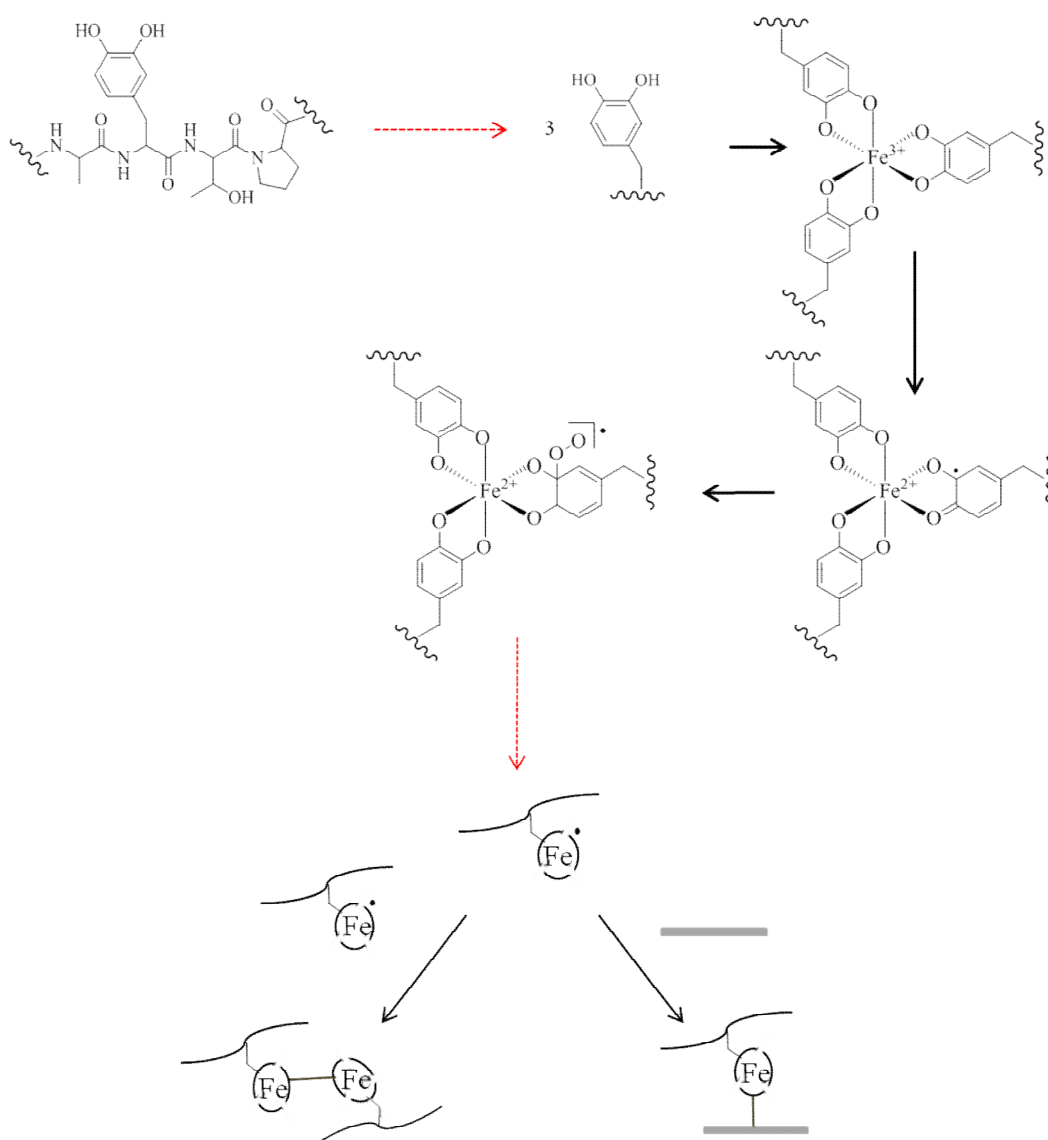
dopaquinone is reversed *in situ* by the oxidation of thiols (Scheme 2.1-2).¹⁴ Mfp-3 and mfp-5 are housed by the adhesive plaque in a reducing environment (around pH 5-6) maintained by mfp-6, a thiol rich protein, found near the interface between the adhesive plaque and the substrate.



Scheme 2.1-2. Oxidation and reduction of DOPA in mfp-3 by thiols present in mfp-6¹⁴

In Scheme 2.1-2, mfp-3 is bound to a mica surface through a series of DOPA mediated hydrogen bonds (i). Any DOPA residues not initially bound to the substrate are liable to undergo oxidation to form dopaquinone (ii). Mfp-6 serves to reduce the dopaquinone back to DOPA making the full adsorption possible (iii, iv). The supply of thiols available for reduction in mfp-6 is limited and eventually S-cysteinyl-dopa adducts form from the cross-linking of dopaquinone and the oxidised thiol (v).¹⁴

The presence of inorganic ions, in particular Fe^{3+} , has been established in the cuticle of the thread and it has been proposed that an iron-DOPA coordination complex cross-links mfp-1 causing hardening of the cuticle, making it resistant to wear.^{15, 16} Recently it has been proposed that the same iron-DOPA coordination complex may also be involved in the adhesion mechanism (Scheme 2.1-3).¹⁷



Scheme 2.1-3. Proposed mechanism of mussel adhesion and crosslinking based on by the formation of an $\text{Fe}(\text{DOPA})_3$ complex¹⁷

In the mechanism, DOPA containing protein chains form a $\text{Fe}(\text{DOPA})_3$ complex. Reduction of Fe^{3+} to Fe^{2+} and oxidation of DOPA forms a semiquinone radical. The semiquinone radical reacts with oxygen to form a different radical species. This radical can undergo a crosslinking reaction or react with a surface creating a covalent bond and adhesion to a surface.¹⁷

Studies thus far have shown that DOPA or dopaquinone adhere to a multitude of substrates, both organic and inorganic, including Teflon (PTFE), glass, steel, aluminium, quartz, mica and copper.¹⁸

2.1.1.3. Mussel inspired adhesive polymers

The catechol end-group of DOPA is finding increased applications, particularly in the development and synthesis of functional polymers for multifunctional coatings such as anti-biofouling surfaces.^{6, 19-21} The catechol is generally incorporated through the use of dopamine, the precursor of which is DOPA. Other applications include, but are not limited to, using dopamine to attach functionality to nanoparticles²²⁻²⁴ and as medical adhesives^{25, 26}.

Synthetic approaches to DOPA functional polymers generally proceed via the polymerisation of a dopamine monomer^{21, 27-30} or by the incorporation of dopamine as the end-group on the polymer chain^{19, 22, 31, 32}. Other approaches have included the

incorporation of dopamine into polymer chains via conjugation³³ or through the use of a dopamine functionalised RAFT agent³⁴.

Polymer films can be attached to a substrate by growth of a film *in situ* by autopolymerisation of dopamine onto a substrate immersed in an aqueous solution of the catechol.¹⁸ Alternately functionalisation of a substrate prior to surface initiated polymerisation can be performed^{19, 35} or preformed polymers can also be adsorbed onto the surface^{20, 21, 36} in either ‘graft from’ or ‘graft to’ approaches (Figure 2.1-6).⁶

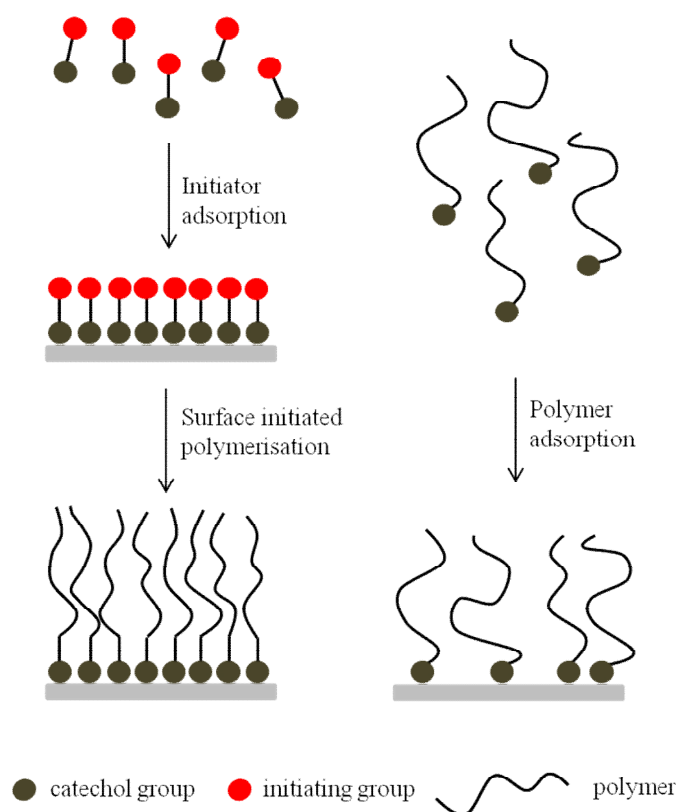


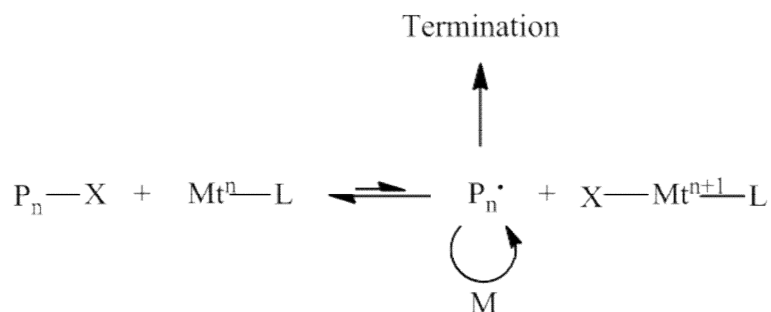
Figure 2.1-6. Modification of surfaces by DOPA by ‘grafting from’ or ‘grafting to’ approaches

2.1.2. Living radical polymerisation

The history behind the development of living radical polymerisation was discussed in Section 1.1.1. In this chapter, work was focussed on the use of transition metal mediated living radical polymerisation and will be discussed in the following sections.

2.1.2.1. Atom transfer radical polymerisation

Atom transfer radical polymerisation (ATRP) was previously introduced in Section 1.1.2.1 and a proposed mechanism is reproduced in Scheme 2.1-4.



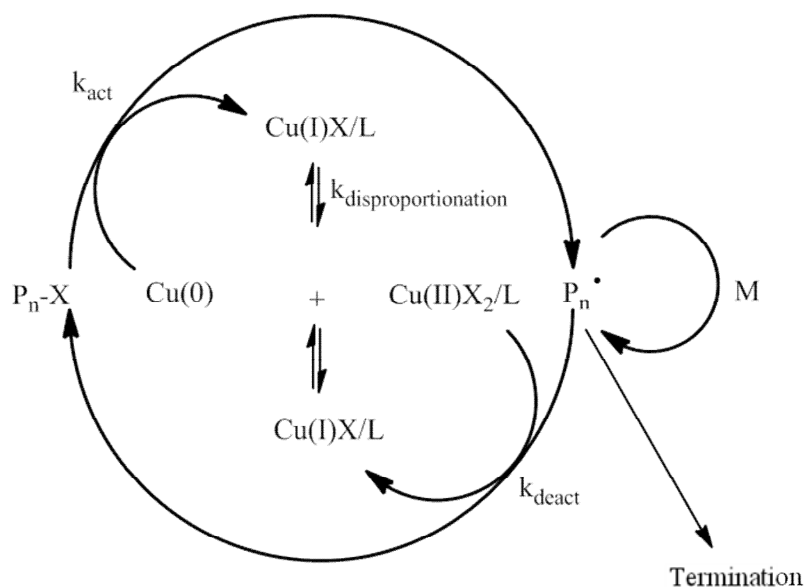
Scheme 2.1-4. A proposed mechanism for ATRP

The transition metal/ligand complex acts as the mediating agent through the reversible transfer of a halogen atom to and from the propagating polymer chain, thus deactivating or activating the chain. Copper is the most widely used metal in ATRP and exists as Cu(I)X when the polymer chain is dormant and Cu(II)X₂ when

propagation is occurring. ATRP reactions typically use nitrogen based ligands with an alkyl halide initiator.³⁷ ATRP is believed to proceed via an inner sphere electron transfer mechanism in which the propagating radical and Cu(II)X_2 are formed through homolytic bond cleavage between $\text{P}_n\text{-X}$ and transfer of the halogen to Cu(I)X .³⁸

2.1.2.2. Single electron transfer living radical polymerisation

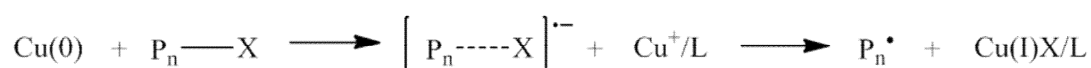
In 2006 Percec *et al.* reported the living radical polymerisation of vinyl chloride and acrylates using nitrogen based ligands and an alkyl halide initiator at 25 °C in polar solvents mediated by Cu(0) .³⁹ The authors called the system single electron transfer living radical polymerisation (SET-LRP) and the proposed mechanism is shown in Scheme 2.1-5.



Scheme 2.1-5. Proposed mechanism for SET-LRP

Like ATRP, SET-LRP proceeds via an equilibrium between the dormant polymer chain and the propagating polymer chain and copper is used as the mediating metal. Rather than using Cu(I)X, Cu(0) is used and is referred to as the active catalyst. The deactivating group is still Cu(II)X₂. In this mechanism, the Cu(I)X species disproportionates to form Cu(0) and Cu(II)X₂ allowing the polymerisation to continue.³⁹

It is suggested by the authors that SET-LRP proceeds via an outer sphere electron transfer mechanism in which Cu(I)X forms from heterolytic bond cleavage by the abstraction of a halogen atom from P_n-X by Cu(0) to give a radical anion intermediate shown in Scheme 2.1-6.³⁹



Scheme 2.1-6. Proposed route to the propagating radical by the outer sphere electron transfer

Computational studies of both ATRP and SET-LRP systems have shown the R-X (or P_n-X) bond dissociation energy is much lower in the outer sphere mechanism proposed for SET-LRP than for the inner sphere mechanism proposed for ATRP.⁴⁰ As a result, fast polymerisations can be run at ambient temperature in SET-LRP as there is only a small dependence on the nature of the halide group in P_n-X.⁴¹

The presence of Cu(II)Br_2 in the polymerisation was confirmed by UV-vis (Figure 2.1-7).³⁹ The absorbance of deoxygenated solutions of Cu(I)Br and Cu(II)Br_2 in DMSO with N,N,N',N',N'',N'' -hexamethyl-tris[2-(dimethylamino)ethyl]amine (Me_6Tren) were studied. Interestingly, an absorbance for Cu(II)Br_2 was seen in the Cu(I)Br solution. Different solvents and ligands were studied. Disproportionation occurs in water, protic solvents such as methanol, ethanol and triethylene glycol and dipolar aprotic solvents including DMSO and DMF. The nitrogen containing ligand should destabilise the Cu(I)Br complex to encourage disproportionation. Ligands suitable include 2,2'-bipyridine, PMDETA and Me_6Tren . It was discovered that Cu(I)Br did not dissociate in the presence of N -R-2-pyridyl-methanimine.³⁹

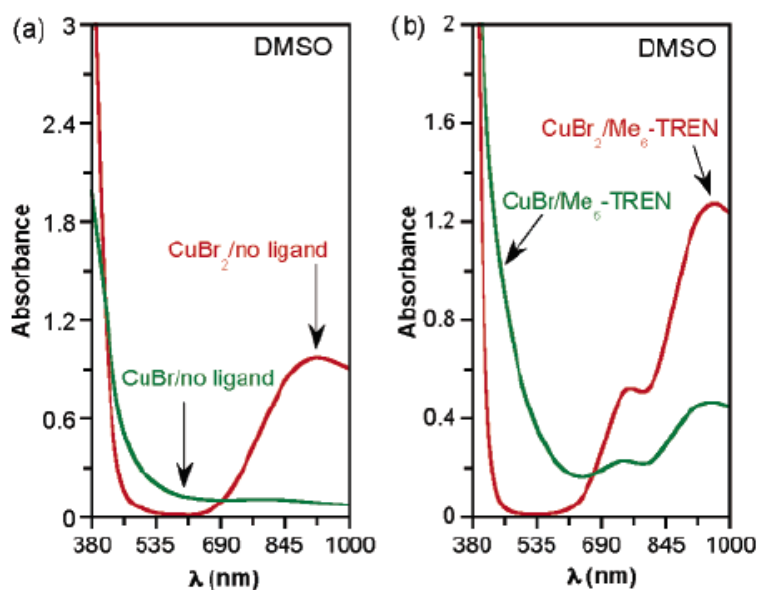


Figure 2.1-7. UV-vis spectra of Cu(II)Br_2 (red) and Cu(I)Br (green) in (a) DMSO and (b) DMSO and Me_6Tren ³⁹

This result has led to controversy as it suggests that any mechanism mediated by copper in the presence of polar solvents with ligands other than a pyridyl-methanimine should proceed via the disproportionation pathway and the SET-LRP mechanism. Publications have been published both trying to prove and disprove the mechanism.^{42, 43} Investigations are still ongoing, however, further review is beyond the scope of this thesis.

2.1.3. Reduction of friction and wear by lubrication

2.1.3.1. Friction and wear

Friction and wear occur as the result of contact between two surfaces in motion. Friction is defined as resistance to motion and occurs due to asperities which are peaks raised from the surfaces.⁴⁴ These asperities are even present in carefully prepared materials. Wear is defined as the physical loss of material, which often results from high friction.⁴⁴

2.1.3.2. The role of lubricants

The primary role of a lubricant is to reduce friction and wear in a system. Lubricants are typically fluids that form films at the surfaces in contact with one another effectively forming a physical barrier.⁴⁵ As such, one of the most important properties of a lubricant is its viscosity. A liquid with a high viscosity will flow

slowly and create a thicker film whereas thin films are formed with low viscosity liquids.⁴⁶ However, viscosity is often temperature and pressure dependant. This is seen with motor oils, which are used to lubricate automotive systems, and has led to the development of additives to improve viscosity at elevated temperature and pressure.^{44, 45}

2.1.3.3. The Stribeck curve

The Stribeck curve illustrates how friction is influenced by a fluids viscosity, the speed of the two surfaces and the load on the interface (Figure 2.1-8).⁴⁷ Changes in the curve are caused by four main lubrication regimes; i) hydrodynamic lubrication; ii) elastohydrodynamic lubrication; iii) mixed lubrication and iv) boundary lubrication. The lubrication regime is determined by the thickness of the film formed between two surfaces, illustrated in Figure 2.1-9.⁴⁴

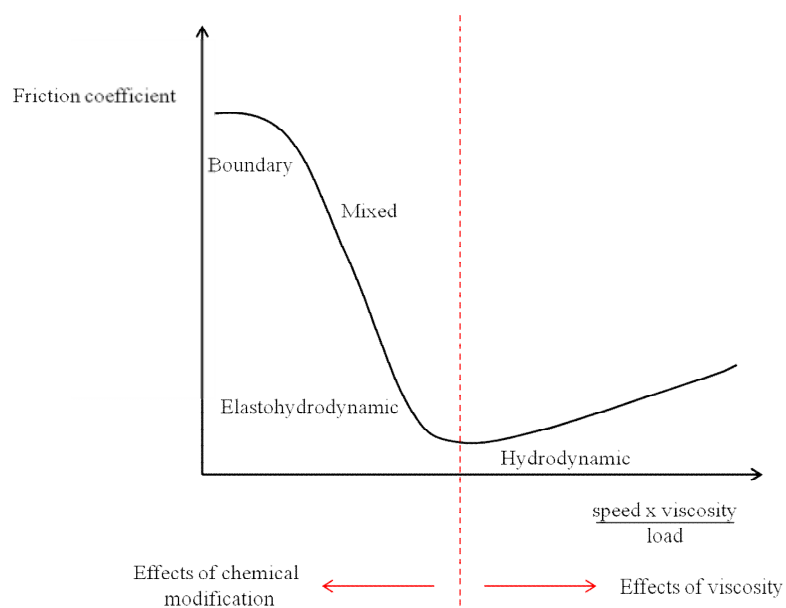


Figure 2.1-8. The Stribeck curve

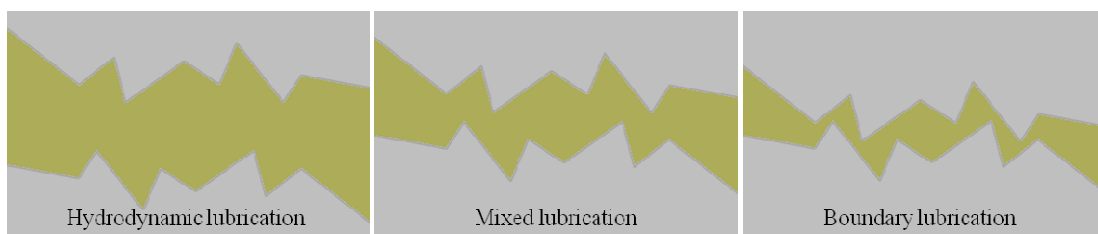


Figure 2.1-9. Schematic of hydrodynamic, mixed and boundary lubrication regimes

In hydrodynamic lubrication, the film is produced by an increase in fluid pressure created by the motion between two surfaces.⁴⁶ No surface contact is observed resulting in low friction and no wear. This is illustrated in the Stribeck curve by a minimum in the friction coefficient. An increase in friction in the hydrodynamic region is sometimes observed and is due to fluid drag caused by a thick film at high

viscosity. In the hydrodynamic region lubrication is the result of purely viscosity effects. In the elastohydrodynamic lubrication region pressure is affecting viscosity. An increase in pressure increases the viscosity of the film so that it becomes solid like. This process forms a very thin, highly viscous film.⁴⁶ The mixed lubrication regime is the result of a combination of boundary and hydrodynamic lubrication. The film thickness is an intermediate between that observed between boundary and hydrodynamic and there is increased contact between asperities. This is illustrated in the Stribeck curve by a sharp drop in the friction coefficient.⁴⁶ The higher the measured friction coefficient more effects from boundary lubrication is observed and vice versa. Boundary lubrication displays the highest friction coefficients. Thin films are formed between the two surfaces and result in increased contact between asperities.⁴⁶ In this lubrication regime wear is observed increasingly. The design of lubricants to decrease friction and wear in boundary lubrication regimes generally utilises modification of the two surfaces to form a protective layer.⁴⁴

Different mechanisms of film formation are possible.⁴⁴ Of particular interest is the chemical modification of surfaces, such as the adsorption of polar molecules with long non-polar tails onto the surfaces by van der Waals forces (Figure 2.1-10). These layers display shear strength and movement between the two surfaces is possible without high friction and wear.⁴⁴

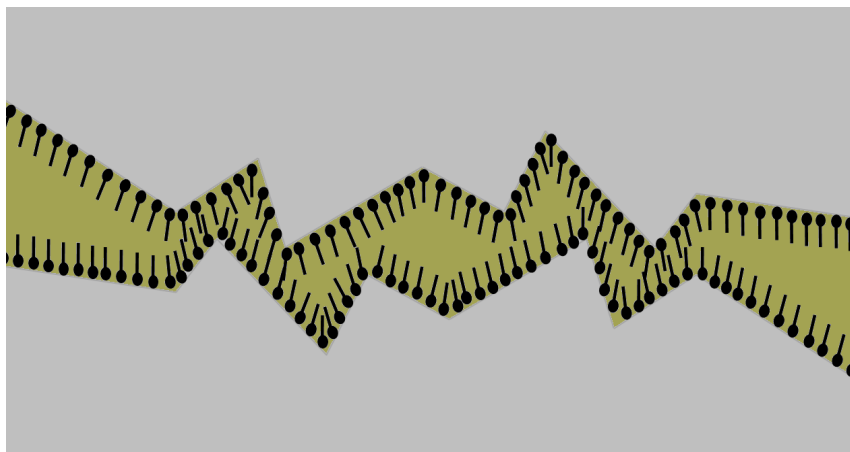


Figure 2.1-10. Schematic of the use of chemical modification to reduce friction by the adsorption of molecules onto a surface

2.1.4. Mechanical measurement of friction

The friction coefficient for an automotive system at predetermined loads and speed is measured by tribological testing which utilises mechanical tests to measure the interaction between surfaces in motion. In this work mechanical tests have been run using a high frequency reciprocating rig (HFRR) and a mini traction machine (MTM) as shown in Figures 2.1-11 and 2.1-12.^{48, 49} Both techniques allow for variable temperature measurements so changes in viscosity as a result of temperature can be related to friction.

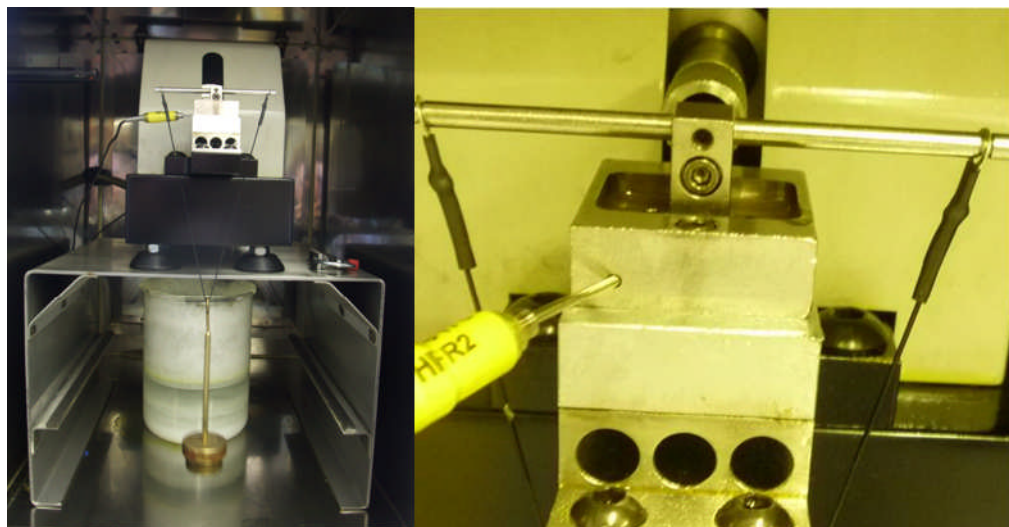


Figure 2.1-11. High frequency reciprocating rig



Figure 2.1-12. Mini traction machine

The HFRR is used to study the behaviour of lubricants and coatings purely in the boundary lubrication regime.⁵⁰ It studies the effects of the lubricant on friction and

wear. This process uses a purely sliding contact system where the steel ball is slid back and forth on a static steel surface to maximise friction (Figure 2.1-13).

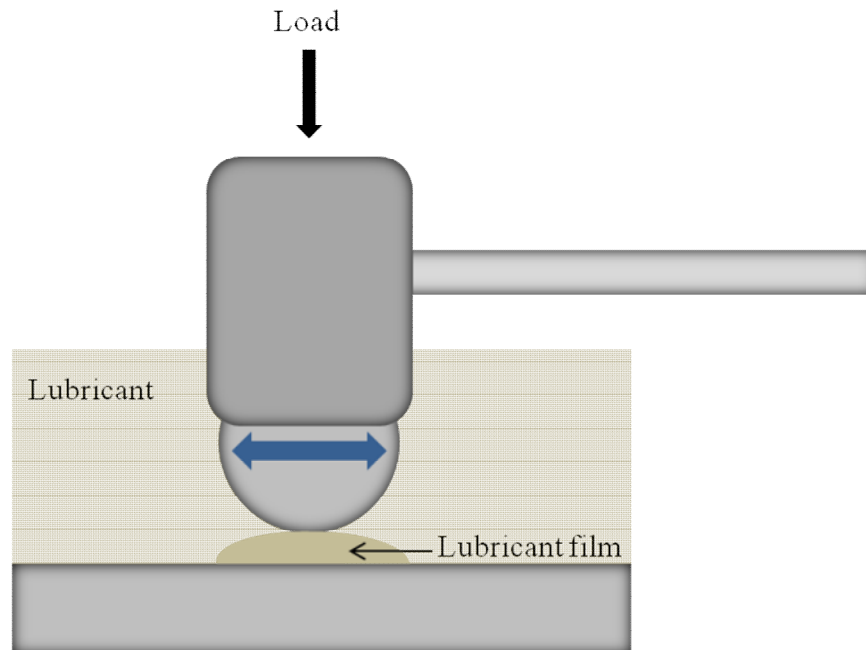


Figure 2.1-13. Schematic of the HFRR system

The MTM also measures how a lubricant affects friction and wear. It studies the behaviour of coatings and thin films in the elastohydrodynamic, mixed and boundary lubrication regimes.⁵⁰ In the process a steel ball and disk are spun independently to create a mixed sliding rolling contact as illustrated in (Figure 2.1-14).

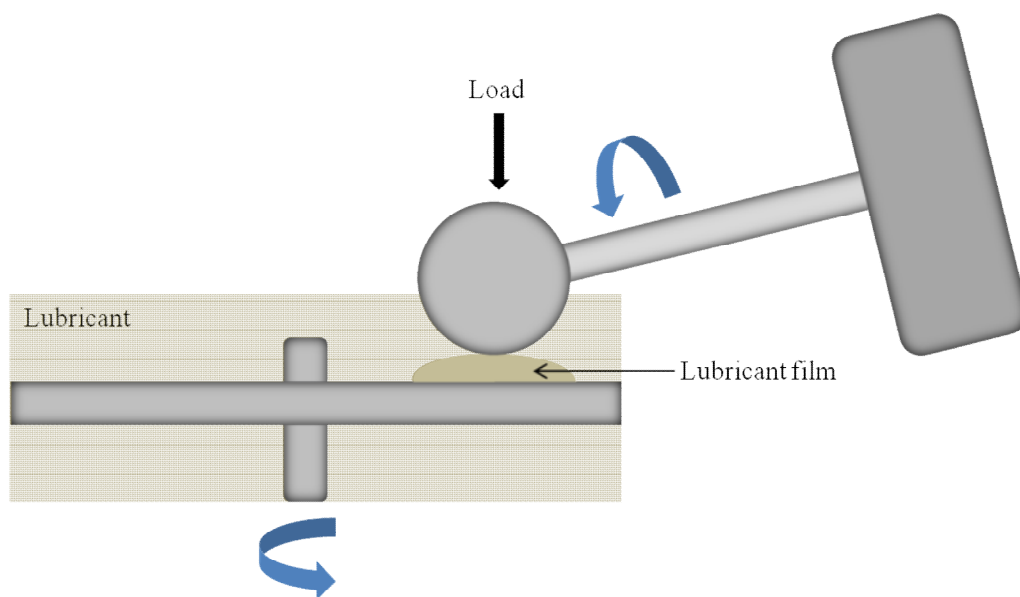


Figure 2.1-14. Schematic of the MTM system

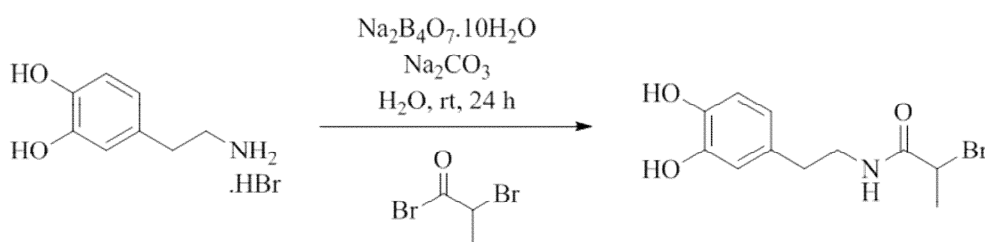
2.1.5. The aim of this work

The ability of the catecholic end-group of DOPA to adhere to a variety of surfaces is finding applications in the formation of films to obtain functionalised surfaces. The same functional chemistry may be applicable to automotive systems that experience friction and wear through the use of chemically modified surfaces. This work aims to synthesise oil soluble dopamine end-functionalised polymers for preliminary mechanical testing. This should establish the viability of the system to reduce friction, therefore preventing wear, through film formation by interaction of the catechol with the metal surface.

2.2. Initiator synthesis and characterisation

2.2.1. Initiator synthesis

The procedure for the synthesis of 2-bromo-*N*-[2-(3,4-dihydroxyphenyl)ethyl] propionamide, referred to throughout this body of work as the unprotected dopamine initiator, followed a slightly modified procedure to that described by Messersmith *et al.*¹⁹ and is shown in Scheme 2.2-1.

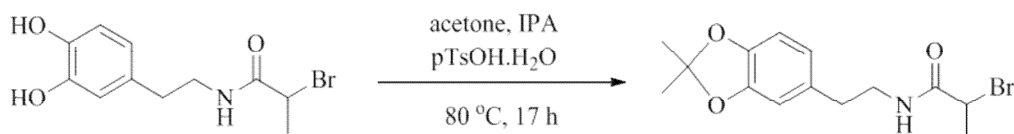


Scheme 2.2-1. Synthesis of 2-bromo-*N*-[2-(3,4-dihydroxyphenyl)ethyl] propionamide

Borax was dissolved in ultrapure 18 Mega Ohm water and bubbled with nitrogen for approximately 3 hours. Dopamine hydrobromide was added and once dissolved the pH of the solution was adjusted to 10 using sodium carbonate. At pH 10 the borax forms a complex with the catechol protecting it from oxidation during the reaction.⁵¹ Then 2-bromopropionyl bromide was added dropwise to the solution after it has been cooled to below 0 °C. The reaction was left stirring at ambient temperature for approximately 24 hours before acidifying to pH 2 with 6 M HCl, followed by extraction into ethyl acetate. The volatiles were removed *in vacuo* before purification by silica gel column chromatography using 25:23:2 petroleum ether

46:60/ethyl acetate/methanol. The compound was crystallised from methanol/water. This reaction was repeated on numerous occasions due to low yields (~ 40%) being continuously encountered, a problem also seen in the literature where the reported yield is 33 %.¹⁹

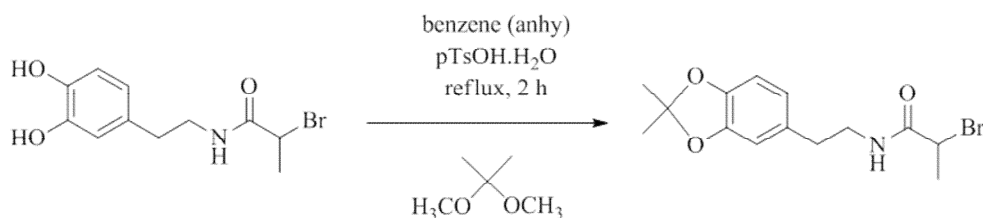
The catechol end-group on dopamine is highly reactive and prone to oxidation. It was therefore anticipated that reactions may need to be performed using a protected dopamine initiator. Initially the reaction was attempted using a similar procedure to that described by Soloshonok and Ueki (Scheme 2.2-2).⁵²



Scheme 2.2-2. Soloshonok and Ueki method for the acetonide protection of 2-bromo-N-[2-(3,4-dihydroxyphenyl)ethyl] propionamide

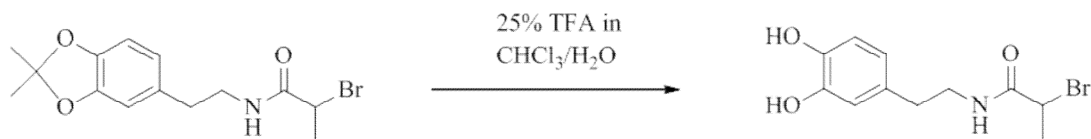
A mixture of unprotected dopamine initiator, *p*-toluenesulfonic acid monohydrate, acetone and isopropyl alcohol was heated at 80 °C. A Dean Stark trap was attached to the reaction to collect water removed azeotropically by the isopropyl alcohol. After the suggested 17 hour reaction time thin layer chromatography (TLC) analysis showed that starting material was still present and after a further 48 hours no desired product was observed.

The acetonide protection of the dopamine initiator was successfully performed by refluxing the initiator with 2,2-dimethoxypropane and *p*-toluenesulfonic acid monohydrate in benzene, as described by Messersmith *et al.* (Scheme 2.2-3).⁵³ The progress of the reaction was determined using a ferric chloride test for phenols that produces a black spot when they are present. When no spot was seen, after approximately 2 hours, the reaction was stopped and the protected dopamine initiator was purified.



Scheme 2.2-3. Messersmith method for the acetonide protection of 2-bromo-N-[2-(3,4-dihydroxyphenyl)ethyl] propionamide

The deprotection reaction, also described by Messersmith *et al.*⁵³, was attempted to confirm that it worked (Scheme 2.2-4). The protected initiator was stirred with 25% trifluoroacetic acid (TFA) in chloroform/water at ambient temperature for 3 hours and the volatiles removed *in vacuo*. The ferric chloride test confirmed the presence of the phenol groups on the deprotected dopamine initiator by a black spot.



Scheme 2.2-4. Deprotection of 2-bromo-N-[2-(3,4-dihydroxyphenyl)ethyl] propionamide acetone

2.2.2. Initiator characterisation

NMR was also used to confirm that protection and deprotection had taken place, Figure 2.2-1. In the aromatic region of the ¹H NMR, between 6 and 7 ppm, both the unprotected and deprotected initiator display two distinct peaks that generally appear as a broad triplet and a broad doublet for the three hydrogen atoms on the aromatic ring. The doublet in particular sometimes appears as a doublet of doublets in the spectra but in general is too broad to determine the *J* couplings. In comparison the protected dopamine initiator displays a single peak. It should be noted that the peaks seen in the aromatic region vary depending on the choice of solvent used to run the NMR. In chloroform, both the unprotected (and deprotected) and the protected dopamine initiator generally display a doublet, singlet, doublet pattern in the aromatic region although sometimes this signal is broadened and appears as a triplet and a doublet. An additional peak is visible in the spectrum of the protected dopamine initiator at 1.61 ppm from the hydrogen atoms on the acetonide protecting group, in chloroform this signal appears at 1.66 ppm.

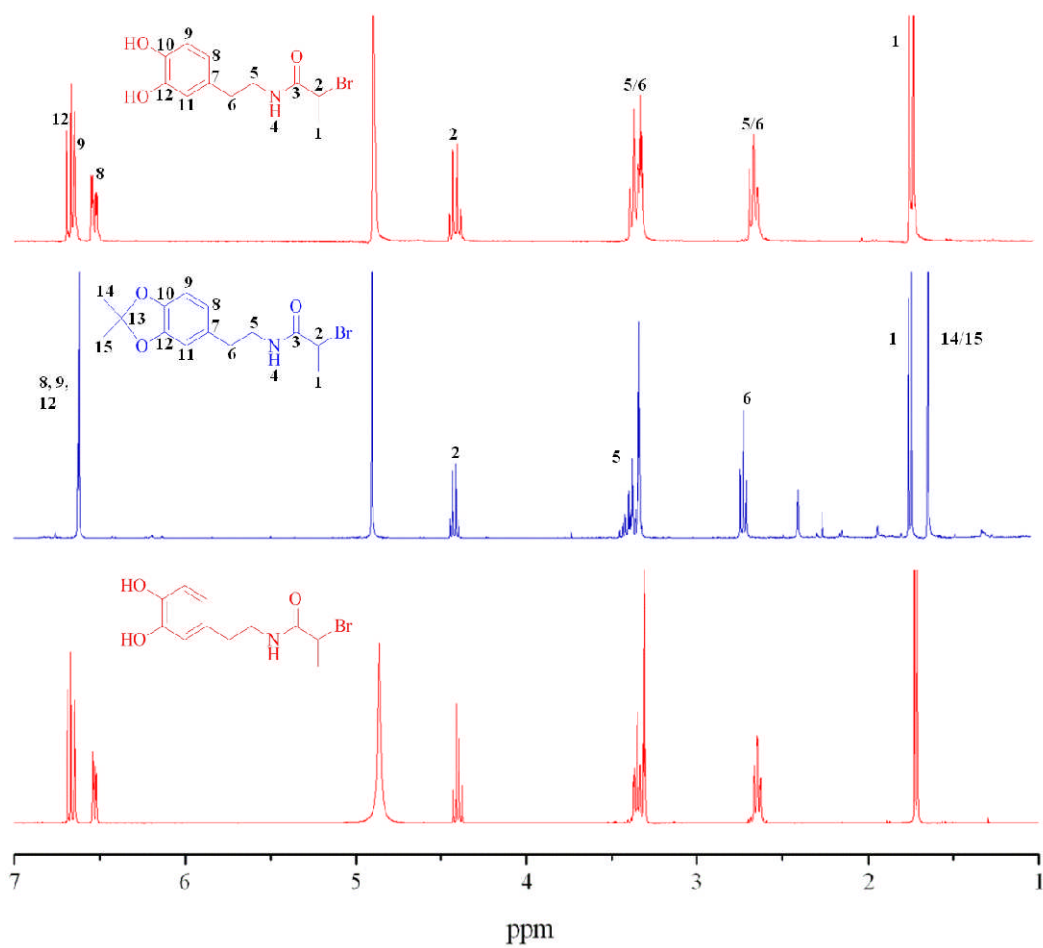


Figure 2.2-1. ^1H NMR spectra of unprotected dopamine initiator (top), protected dopamine initiator (middle) and deprotected dopamine initiator (bottom) in deuterated methanol

2.3. Initial polymerisation studies

2.3.1. Cu(I) mediated polymerisation of MMA

Both the unprotected and protected dopamine initiators were used in the Cu(I) mediated polymerisation of MMA. Following a standard procedure outlined by Haddleton *et al.*⁵⁴, Cu(I)Br, *N*-propyl-2-pyridylmethanimine and the dopamine initiators (1:2:1 equivalents respectively) were used at 90 °C. The solvent system was altered from 100% toluene to 50:50 toluene/isopropyl alcohol in order to solubilise the unprotected dopamine initiator.

Polymerisation from the unprotected dopamine initiator gave a linear kinetic plot indicating that the concentration of active species remained constant over the duration of the polymerisation (Figure 2.3-1). A slower rate was observed for the protected dopamine initiator and the plot plateaued after approximately 5 hours suggesting the polymerisation had stopped. An increase in molecular weight with conversion was not seen for the unprotected initiator (Figure 2.3-2). After the first hour the molecular weight had jumped to 30,000 g/mol and the molecular weight remained relatively constant over the duration of the reaction. An increase in molecular weight with conversion was seen up until 25% conversion had been reached and the polymerisation stalled with no further increase in conversion or molecular weight.

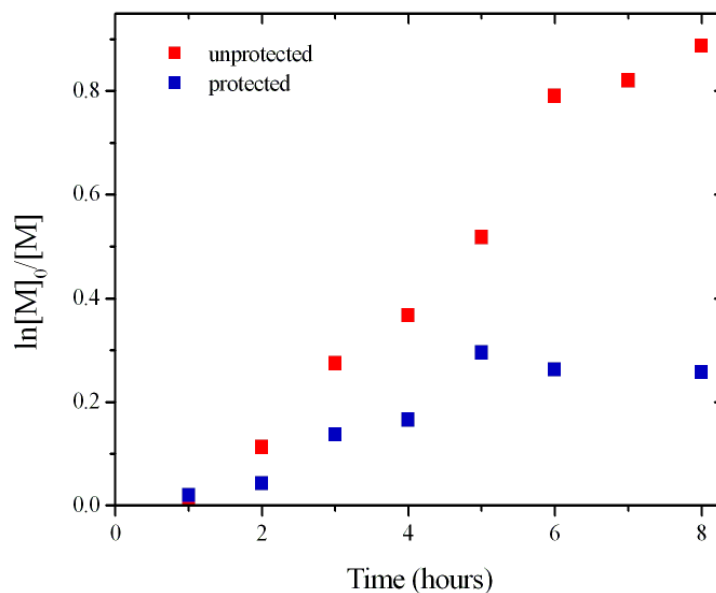


Figure 2.3-1. First order kinetic plot for the Cu(I) mediated polymerisation of MMA using the unprotected dopamine initiator (■) and protected dopamine initiator (■)

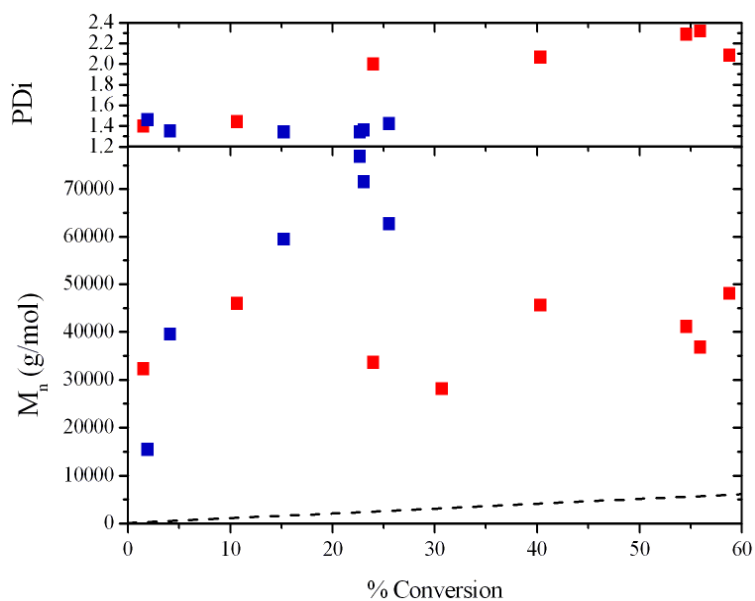


Figure 2.3-2. Evolution of molecular weight (M_n) and PDI versus conversion for the Cu(I) mediated polymerisation of MMA using the unprotected dopamine initiator (■) and protected dopamine initiator (■), DP = 100, target M_n = 10,000 g/mol (---)

In both cases the observed molecular weights were higher than the calculated theoretical molecular weight. Lower polydispersities were seen for the protected initiator than for the unprotected dopamine initiator, although they were generally > 1.3. It was deemed that under these conditions, both dopamine initiators failed to polymerise MMA in a living fashion. The copper containing residues were removed from the polymerisation mixture by diluting the mixture in toluene before passing through a short basic alumina column. The solvent was then removed *in vacuo* before the polymer was redissolved in dichloromethane and precipitated into methanol.

2.3.1.1. Polymer end-group analysis

The presence of dopamine end-groups on both polymers synthesised using the unprotected and protected dopamine initiators was investigated using ^1H NMR (Figure 2.3-3). The characteristic peaks in the aromatic region were not visible in the polymer prepared with the unprotected dopamine initiator but were visible for the protected dopamine initiator. The peak corresponding to the hydrogen atoms on the acetonide protecting group was also visible at 1.66 ppm.

To further confirm the presence of the dopamine end group on the polymer synthesised using the protected dopamine initiator both the initiator and polymer were investigated using UV-vis GPC (Figure 2.3-4). Both showed an absorbance at 292 nm with a reduced retention time for the polymer in comparison to the initiator

(18.36 mins for the initiator and 12.89 mins for the polymer). This result confirms the dopamine moiety as the end group of the polymer.

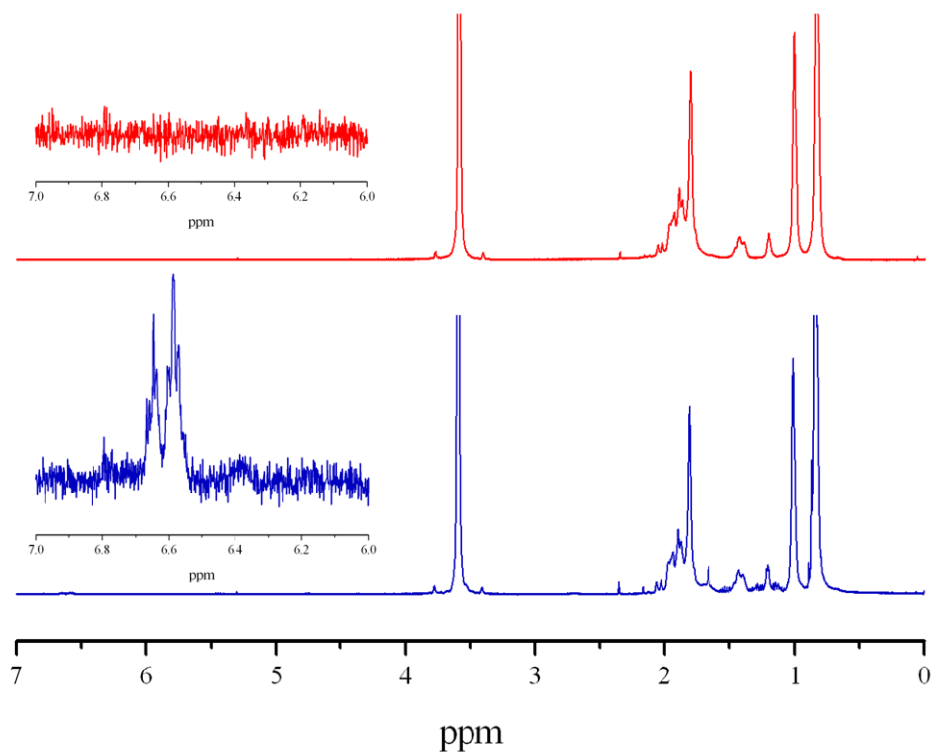


Figure 2.3-3. ^1H NMR of precipitated polymers from the Cu(I) mediated polymerisation of MMA by the unprotected dopamine initiator (top) and protected dopamine initiator (bottom) in deuterated chloroform

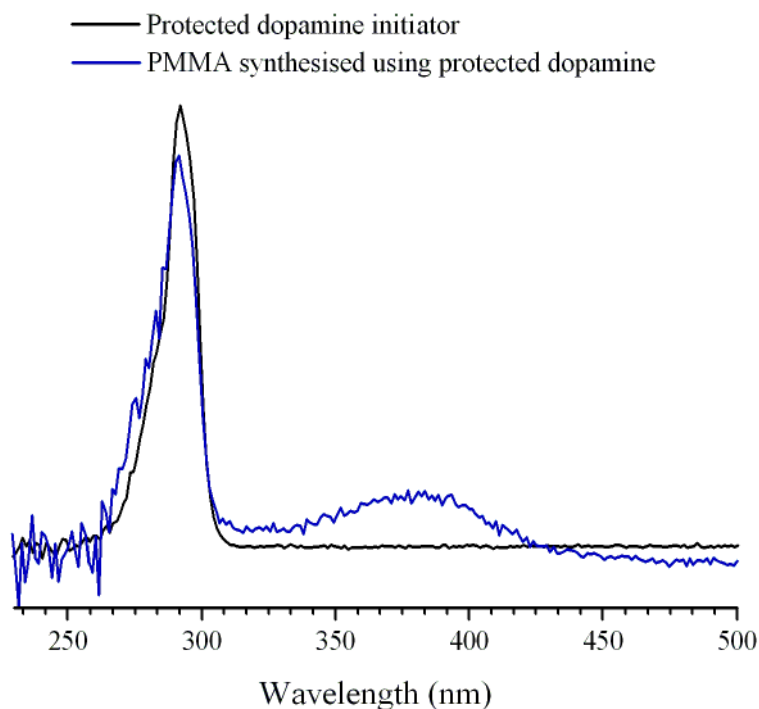


Figure 2.3-4. UV-vis GPC traces for the protected dopamine initiator at a retention time of 18.36 mins (—) and for PMMA synthesised using the protected dopamine initiator at 12.89 mins (—).

2.3.2. Cu(0) mediated polymerisation of *t*-butyl acrylate

The poor initiator efficiencies seen for the both the dopamine initiators in polymerisations mediated by Cu(I) can be related back to the amide group as similar effects have been observed before for other amide initiators.⁵⁵⁻⁵⁷ In the Cu(0) mediated LRP, the R-X bond dissociation energy is lower than in ATRP and as a result a wider range of initiators are possible, including amide based initiators.

The Cu(0) mediated polymerisation of *t*-butyl acrylate was attempted for both the unprotected and protected dopamine initiator using a method developed within the Haddleton group. The polymerisation set up consisted of Cu(0), Cu(II)Br₂, Me₆Tren and the unprotected/protected dopamine initiator (2:0.3:2.3:1 equivalents respectively) in toluene/methanol (14:1) and was attempted at 25 °C.

Firstly a polymerisation aiming for a molecular weight of approximately 25,000 g/mol was undertaken for both initiators. The degree of polymerisation (DP) was slightly different for both initiators as the same equivalents rather than moles of initiator were kept constant. Figure 2.3-5 displays the kinetic data for the two polymerisations. The unprotected dopamine initiator displayed a 5 hour inhibition period and by 22 hours the reaction had stopped. Reasonably linear kinetic data was observed for the polymerisation using the protected initiator. The observed molecular weight was much higher than the theoretical for the unprotected dopamine polymerisation and the polydispersity was high (Figure 2.3-6). For the protected initiator a linear increase in molecular weight with conversion was observed, although the molecular weight was still higher than the theoretical, polydispersities were generally < 1.3. Using the Cu(0) system, the polymerisation using the protected initiator proceeded in a reasonably living fashion, a marked improvement on the Cu(I) mediated technique.

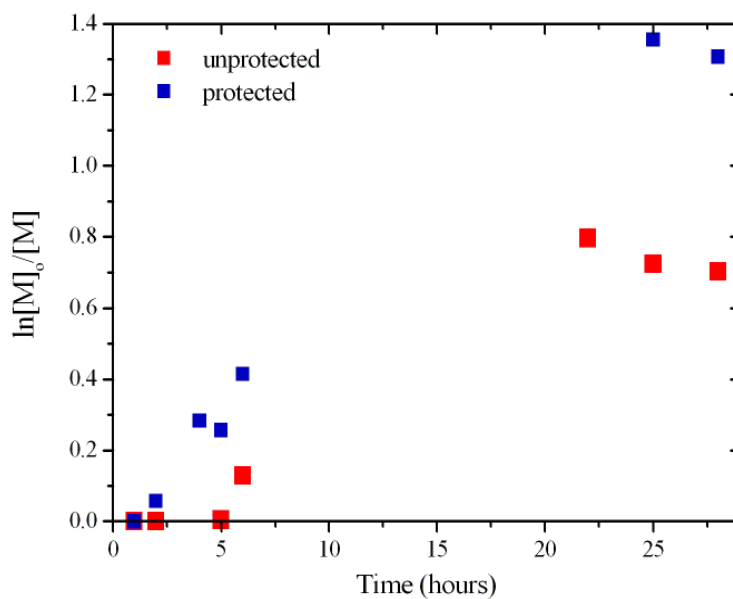


Figure 2.3-5. First order kinetic plot for the Cu(0) mediated polymerisation of *t*-butyl acrylate using the unprotected dopamine initiator (■, DP = 200) and protected dopamine initiator (■, DP = 160)

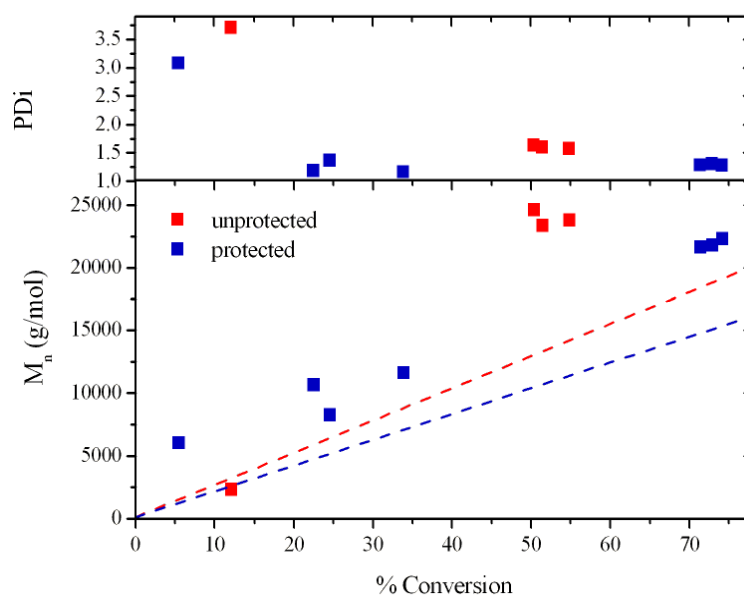


Figure 2.3-6. Evolution of molecular weight (M_n) and PDI versus conversion for the Cu(0) mediated polymerisation of *t*-butyl acrylate using the unprotected dopamine initiator (■) and protected dopamine initiator (■), DP = 200, target M_n = 25,600 g/mol (---), DP = 160, target M_n = 20,500 g/mol (- - -)

The difference between the unprotected and protected dopamine Cu(0) mediated polymerisations is further illustrated by their colour (Figure 2.3-7). The unprotected dopamine initiator polymerisation is dark brown and the protected dopamine initiator polymerisation is green. This suggests that something occurs in the unprotected dopamine polymerisation that causes a colour change and may impede the polymerisation.

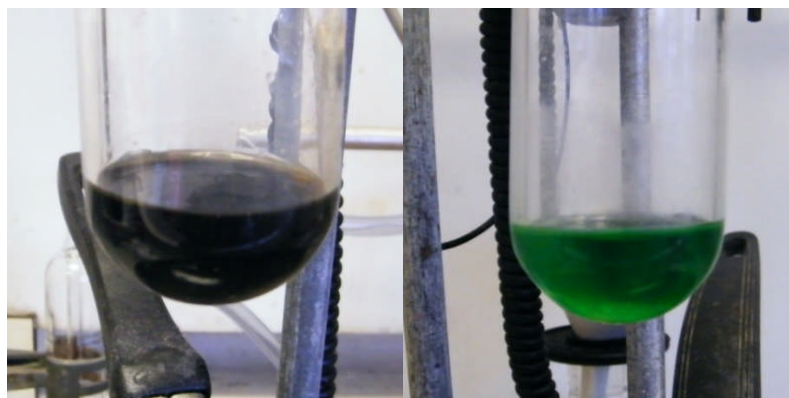
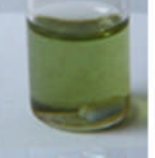
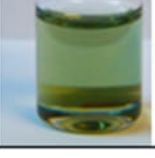


Figure 2.3-7. Cu(0) mediated polymerisation of *t*-butyl acrylate by the unprotected dopamine initiator (left) and protected dopamine initiator (right)

A short investigation was completed to investigate the origin of the colour, Table 2.3-1. Cu(0), Cu(I)Br, Cu(II)Br₂ and Me₆Tren were added to toluene/methanol solution (14:1, 1.2 mL) using the ratios of 2:1:0.3:2.3 respectively with regards to initiator. Solutions were degassed before adding the unprotected dopamine initiator, protected dopamine initiator, Me₆Tren or a combination of initiator and ligand and were stirred for 24 hours. The colour associated with the protected dopamine polymerisation was observed in the vial with Cu(I) with added Me₆Tren and initiator. For the unprotected dopamine initiator the colour associated with the

polymerisation was seen when either Cu(0) or Cu(II) were mixed with the initiator and Me₆Tren. These results indicate different copper complexes are potentially formed in solution depending on which initiating system is used. Further investigations are required to determine the nature of the species.

Table 2.3-1. Effect of initiator on the species formed in solution with Cu(0), Cu(I)Br and Cu(II)Br₂

	Solvent	Solvent + Cu(0)	Solvent + Cu(I)	Solvent + Cu(II)	Solvent + Me ₆ Tren
Unprotected I					
Protected I					
Me ₆ Tren					
Unprotected I + Me ₆ Tren					
Protected I + Me ₆ Tren					

Using the same technique, polymerisations aiming for a molecular weight of 5,000 g/mol were also investigated for both initiators (Figures 2.3-8 and 2.3-9). The unprotected initiator displayed a slow rate at the start and towards the end of the polymerisation. An almost linear increase in molecular weight was observed although molecular weight was again higher than the theoretical value and the polydispersity increased continuously over the duration of the reaction. In comparison, the protected initiator displayed linear first order kinetics with respect to monomer, a linear increase in molecular weight with conversion closely matching the theoretical and with polydispersity values < 1.2 , characteristic of a living polymerisation. The residues were removed from all four polymerisations before precipitation as previously described in Section 2.3.1.

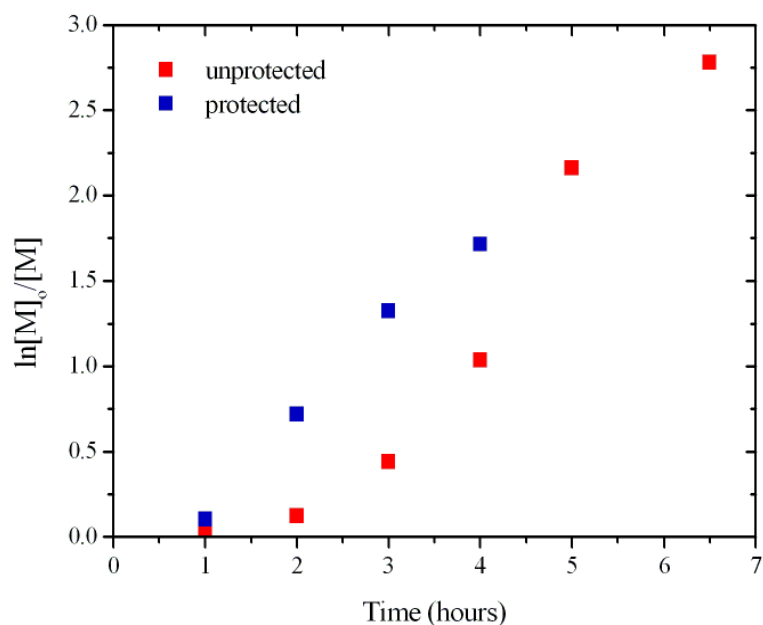


Figure 2.3-8. First order kinetic plot for the Cu(0) mediated polymerisation of *t*-butyl acrylate using the unprotected dopamine initiator (■) and protected dopamine initiator (■)

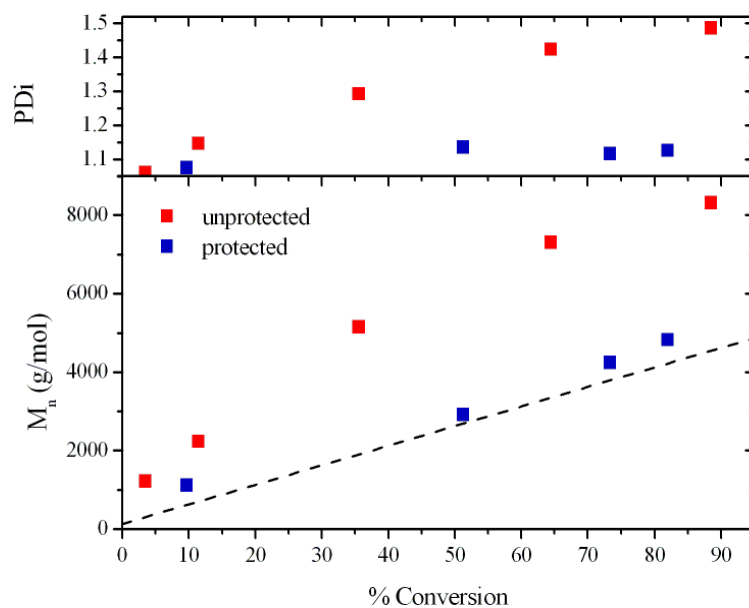


Figure 2.3-9. Evolution of molecular weight (M_n) and PDI versus conversion for the Cu(0) mediated polymerisation of *t*-butyl acrylate using the unprotected dopamine initiator (■) and protected dopamine initiator (■), DP = 39, target M_n = 5,000 g/mol (---)

2.3.2.1. Low molecular weight polymer end-group analysis

The end-groups of the two low molecular weight polymers were investigated (Figure 2.3-10). As seen in the Cu(I) mediated polymerisations, the characteristic doublet singlet doublet pattern in the aromatic region of the ^1H NMR was missing for the unprotected dopamine polymerisation. The peaks for the protected initiator were clearly visible in the aromatic region and at 1.66 ppm. The same result was also seen for the higher molecular weight polymer. From these initial polymerisations it was deemed necessary to use the protected initiator for further polymerisations.

The presence of the dopamine end group on the polymer synthesised using the protected dopamine initiator was again confirmed by UV-vis GPC (Figure 2.3-11). Both showed an absorbance at 292 nm with a reduced retention time for the polymer in comparison to the initiator (18.36 mins for the initiator and 14.77 mins for the polymer).

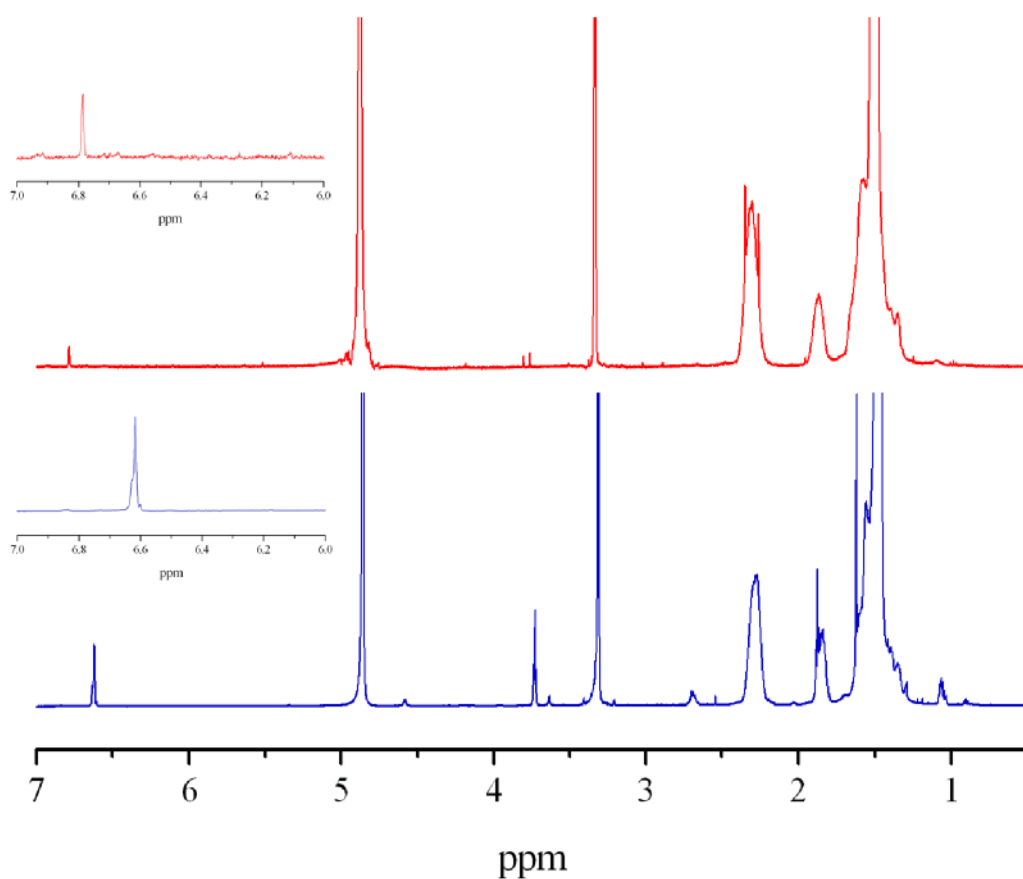


Figure 2.3-10. ^1H NMR of precipitated polymers from the Cu(0) mediated polymerisation of *t*-butyl acrylate using the unprotected dopamine initiator (top) and protected dopamine initiator (bottom) in deuterated methanol

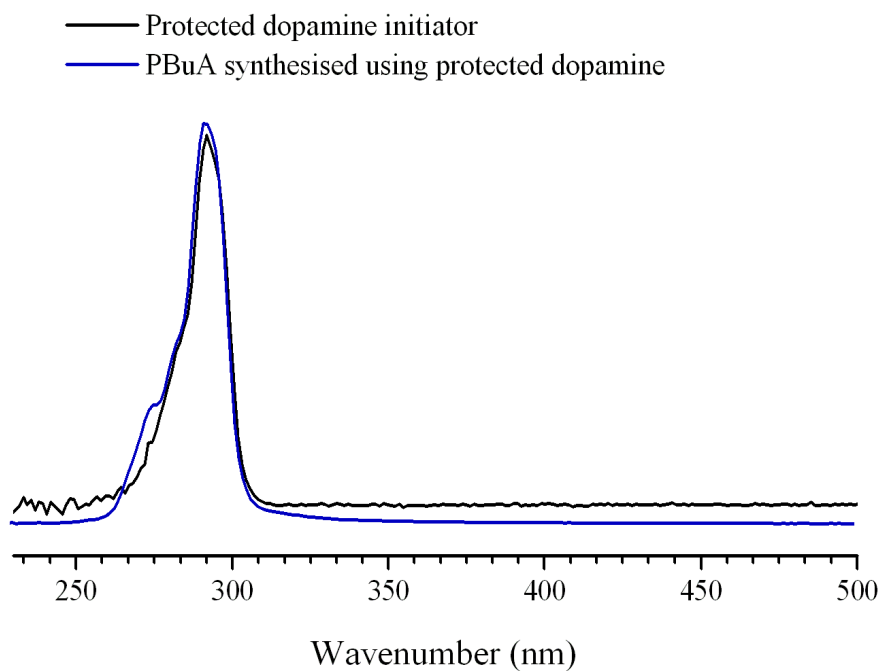


Figure 2.3-11. UV-vis GPC traces for the protected dopamine initiator at a retention time of 18.36 mins (—) and for PBUA synthesised using the protected dopamine initiator at 14.77 mins (—).

2.3.2.2. Deprotection of low molecular weight polymer

The method used to deprotect the dopamine initiator was applied to the low molecular weight *t*-butyl acrylate polymer. The polymer was stirred with 25% TFA in chloroform/water at ambient temperature for 2 hours after which precipitation of the polymer was observed. The ^1H NMR in deuterated methanol for both the protected dopamine and deprotected dopamine polymers are shown in Figure 2.3-12.

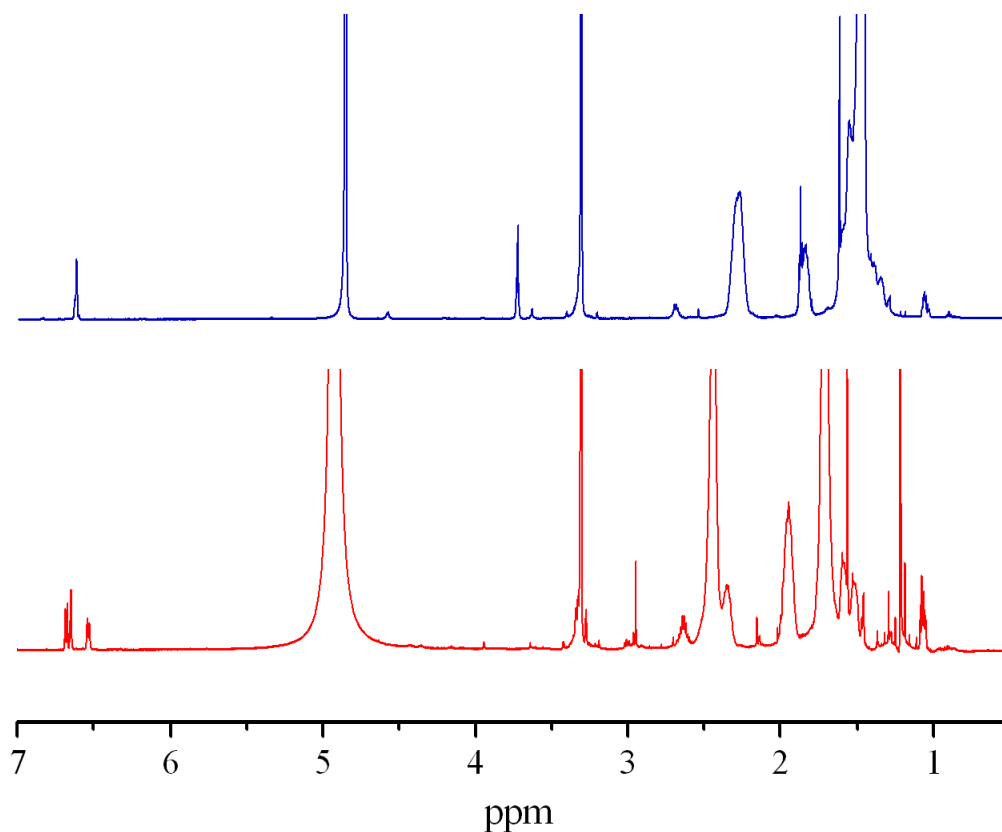


Figure 2.3-12. ^1H NMR of the precipitated polymer from the Cu(0) mediated polymerisation of *t*-butyl acrylate using the protected dopamine initiator (top) and after deprotection (bottom) in deuterated methanol

The characteristic peaks in the aromatic region changed from a singlet for the protected dopamine to a triplet and doublet for the deprotected dopamine consistent with the ^1H NMRs observed for the initiator as described in Section 2.2.2. The peak corresponding to the protecting group at 1.61 ppm was absent from the deprotected polymer. The changes observed in the polymer peaks are due to the elimination of the *t*-butyl groups by hydrolysis using TFA to give poly acrylic acid. As a result a water soluble dopamine functionalised poly acrylic acid was obtained.

2.4. Polymerisation of lauryl methacrylate

The required composition of the polymers for mechanical testing was required to be 80% lauryl methacrylate and 20% MMA. Lauryl methacrylate is a non-polar long chain molecule and is utilised as the resulting polymers are oil soluble. Ten grams of 20,000 g/mol molecular weight polymer was required.

2.4.1. Initial investigations

Small scale polymerisations (approximately 2 mL) were initially attempted to find an appropriate polymerisation technique to produce the desired polymer. Initially, the Cu(I) and Cu(0) mediated polymerisations described earlier were attempted, however, these were unsuccessful. When Cu(I) was used no polymerisation was observed after 24 hours and with Cu(0) the polymerisation reached 85% conversion with a molecular weight of 40,000 g/mol and a polydispersity of 1.70 with a 6 hour induction period. Further investigations in the Cu(I) mediated polymerisation included using 100% toluene as the solvent and changing the ligand to *N*-2-octylpyridylmethanimine. In particular, changing to a longer alkyl chain ligand was expected to help solubilise the catalyst in the increased non-polar medium; however, this reaction was unsuccessful. The Cu(0) mediated polymerisation was reinvestigated using PMDETA as the ligand instead of Me₆Tren as PMDETA is generally used for methacrylate polymerisation when using SET-LRP.⁵⁸ The use of 20 equivalents of phenol in toluene, similar to a system used previously to polymerise lauryl acrylate was also investigated.⁵⁹

2.4.2. Polymerisation of lauryl methacrylate using a Cu(I)Cl system

As the previous polymerisation systems were unsuccessful, an alternative procedure designed specifically for the polymerisation of lauryl methacrylate was found in the literature. Xu *et al.* reported the living polymerisation of lauryl methacrylate using Cu(I)Cl with ethyl 2-bromoisobutyrate (EBiB) in a variety of solvents at 110 °C.⁶⁰ Initially a polymerisation as described in the literature was attempted using anisole as the solvent and EBiB as the initiator. The polymerisation was carried out for 240 minutes before being terminated due to the increased viscosity of the polymerisation reaction. First order kinetics with respect to monomer was linear for the polymerisation (Figure 2.4-1). A reasonably linear increase in molecular weight observed although conversion had only reached 16% and the molecular weight was higher than the theoretical value towards the end of the polymerisation (Figure 2.4-2). The observed polydispersity values started low but began to increase as the polymerisation viscosity increased. The copper was removed from the polymerisation mixtures as previously described in Section 2.3.1. The polymer was precipitated into methanol cooled by dry ice/acetone bath. Under these conditions the polymer precipitates as a fine powder. If the temperature is raised slightly the polymer begins to coagulate, forming lumps that can be easily collected with a spatula and placed in a vial. The polymer was then dried in a vacuum oven to give the pure, highly viscous polymer. All lauryl methacrylate-containing polymers were precipitated in this way.

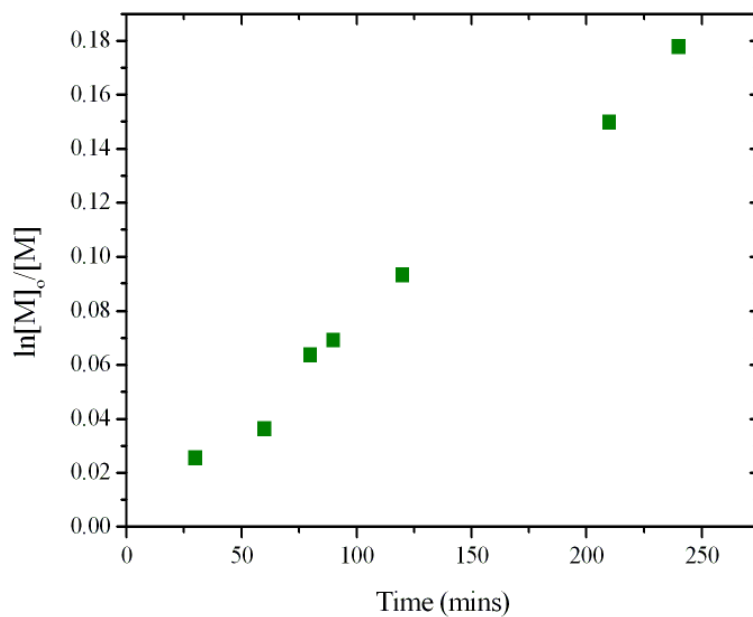


Figure 2.4-1. First order kinetic plot for the polymerisation of lauryl methacrylate by EBiB using Cu(I)Cl

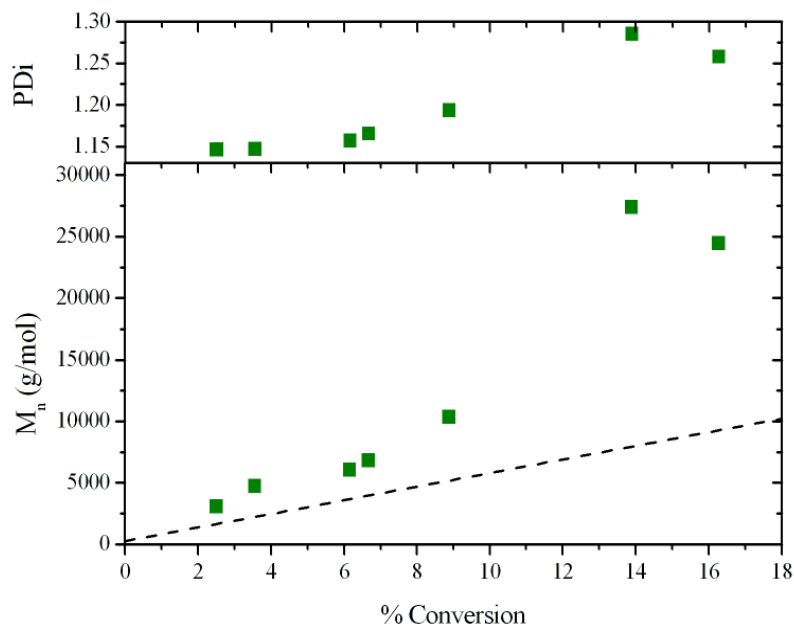


Figure 2.4-2. Evolution of molecular weight (M_n) and PDI versus conversion for the polymerisation of lauryl methacrylate by EBiB using Cu(I)Cl, DP = 200, target $M_n = 55,300$ g/mol (- - -)

2.4.2.1. Copolymerisation of lauryl methacrylate and MMA

The copolymerisation of lauryl methacrylate and MMA (80:20) was then investigated, however, this time aiming for a molecular weight of 20,000 g/mol (Figures 2.4-3 and 2.4-4). The polymerisation proceeded quickly reaching nearly 90% conversion in 90 minutes. The observed molecular weight increased linearly although was higher than the calculated theoretical and the polydispersity remained < 1.2 .

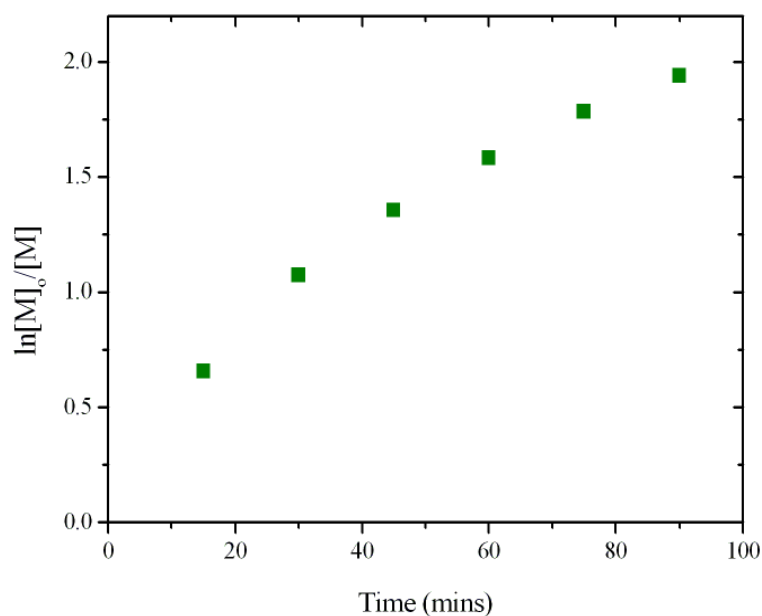


Figure 2.4-3. First order kinetic plot for the copolymerisation of lauryl methacrylate and MMA by EBiB using Cu(I)Cl

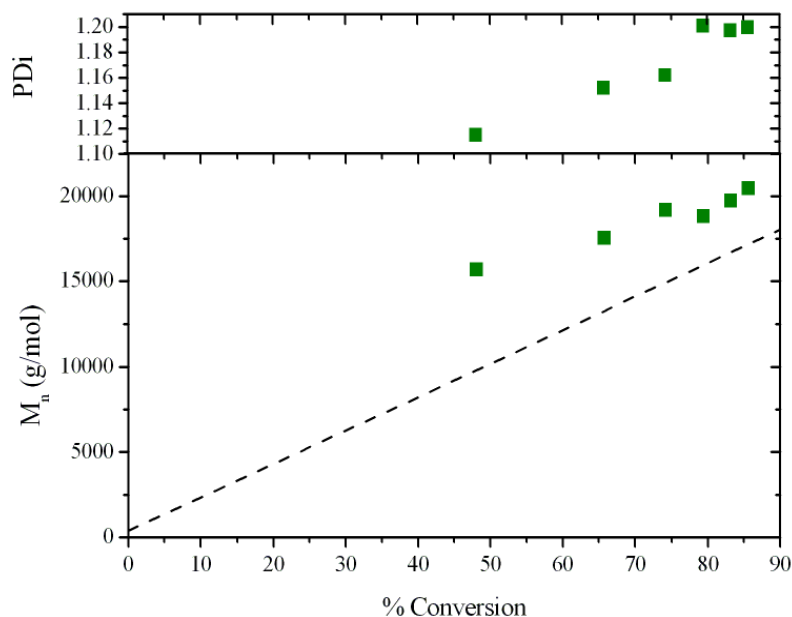


Figure 2.4-4. Evolution of molecular weight (M_n) and PDI versus conversion for the copolymerisation of lauryl methacrylate and MMA by EBiB using Cu(I)Cl, target $M_n = 20,000$ g/mol (---)

The copolymerisation of lauryl methacrylate and MMA was then attempted under the same conditions using the protected dopamine initiator (Figures 2.4-5 and 2.4-6, ■). The polymerisation proceeded quickly, reaching 85% conversion in 90 minutes. The rate of polymerisation slowed towards the end of the reaction and the observed molecular weight was found to be double the theoretical. The polydispersity values were reasonable but still a little higher than would be expected for a living system. The polymerisation was repeated, this time aiming for a molecular weight of 10,000 g/mol (●). The reaction was fast reaching nearly full conversion at 90 minutes. The molecular weight was again observed to be double the theoretical, so a polymer with the desired molecular weight of 20,000 g/mol had been obtained. A polymerisation

aiming for 15,000 g/mol was also completed to ensure that the reaction would follow the same observed trends to obtain double the targeted molecular weight, and this was observed (▲) although the reaction only took 40 minutes to reach 85% conversion. These results illustrate that under the described polymerisation conditions the initiator has an efficiency of 0.5. As a result only half the initiators initiate chains leading to double the expected molecular weight. Therefore, to obtain the desired molecular weight of 20,000 g/mol, a polymerisation aiming for 10,000 g/mol would need to be undertaken. In general the polydispersity values were quite high ranging from 1.3 – 1.5.

Finally a polymerisation aiming for 10,000 g/mol was carried out at 50% solids instead of 75% (★). The increased volume of solvent was speculated to slow down the polymerisation and improve control with the effect of reducing the polydispersity by reducing the viscosity thus reducing termination reactions. The reaction proceeded slower than the analogous 10,000 g/mol polymerisation (●), however, the reaction was still fast reaching 90% conversion in 90 minutes. As expected a polymer with a molecular weight of approximately 20,000 g/mol was obtained but on this occasion lower polydispersities were observed with values generally less than 1.3. If the polymerisation was terminated at around 70% conversion, where the rate starts to noticeably slow, the polydispersity would be around 1.2 and a molecular weight close to the desired 20,000 g/mol would be obtained (Figure 2.4-6, ★). It was therefore vital in the large scale polymerisations to carefully monitor the conversion of the polymerisation to enable well defined polymers to be obtained.

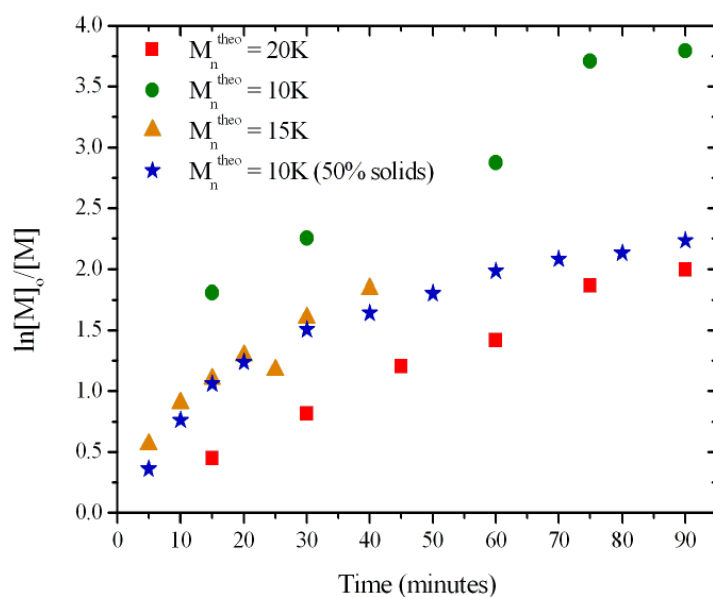


Figure 2.4-5. First order kinetic plot for the copolymerisation lauryl methacrylate and MMA using the protected dopamine initiator using Cu(I)Cl aiming for 20,000 g/mol (■), 10,000 g/mol (●), 15,000 g/mol (▲) and 10,000 g/mol at 50% solids (★)

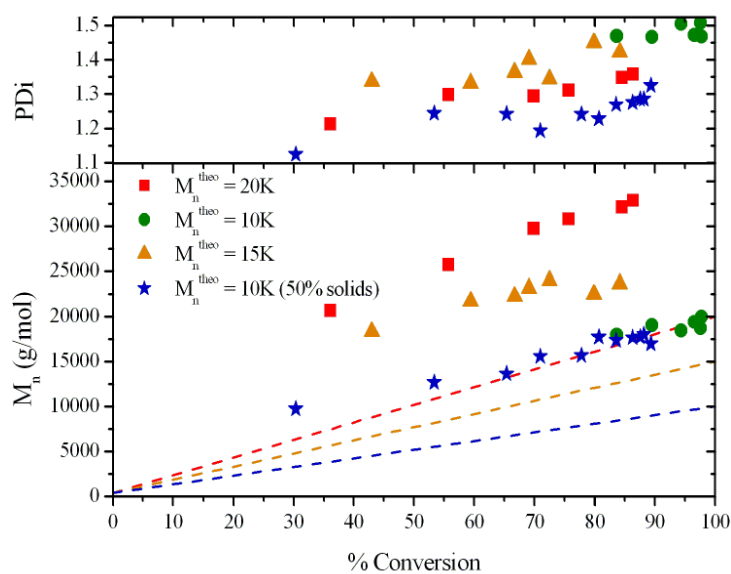


Figure 2.4-6. Evolution of molecular weight (M_n) and PDI versus conversion for the copolymerisation of lauryl methacrylate and MMA using the protected dopamine initiator with Cu(I)Cl aiming for 20,000 g/mol (■), 10,000 g/mol (●), 15,000 g/mol (▲) and 10,000 g/mol at 50% solids (★), target M_n = 20,000 g/mol (---), target M_n = 10,000 g/mol (---), target M_n = 15,000 g/mol (---)

Before performing the scale up reactions, the deprotection of the polymerisation run at 50% solids was attempted. As expected, the peak at 1.66 ppm associated with the acetonide group disappeared after deprotection.

2.4.2.2. Initiator scale up

In order to complete the large scale polymerisations a large scale initiator synthesis had to be undertaken. Two 5 g scale reactions were completed to give approximately 4 g of the unprotected initiator which was subsequently protected, yielding 3.2 g of protected dopamine initiator after recrystallisation and drying.

2.4.2.3. Scale up polymerisations

The large scale polymerisations, all at 50% solids, were then attempted. The baseline polymer, initiated using EBiB, was run for 90 minutes reaching approximately 90% conversion and reaching the desired molecular weight of 20,000 g/mol with a polydispersity less than 1.2. Two protected dopamine initiated polymerisations were also completed, both aiming for 10,000 g/mol. Both polymerisations reached approximately 90% conversion in 60 minutes with molecular weights close to 20,000 g/mol and polydispersities < 1.25. One of the polymers was deprotected as previously described and the deprotection confirmed by ¹H NMR, Table 2.4-1.

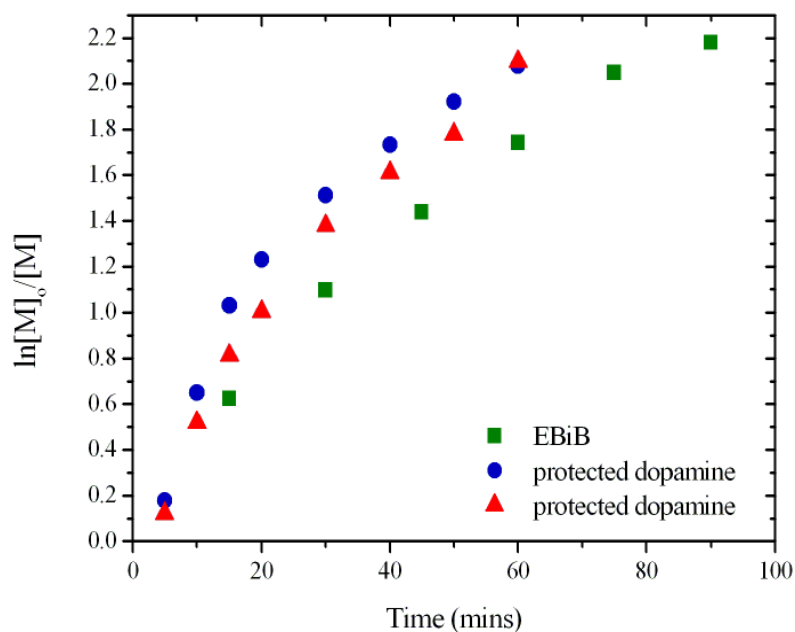


Figure 2.4-7. First order kinetic plot for the copolymerisation lauryl methacrylate and MMA using EBiB aiming for 20,000 g/mol (■) and the protected dopamine initiator aiming for 10,000 g/mol (●, ▲) with Cu(I)Cl

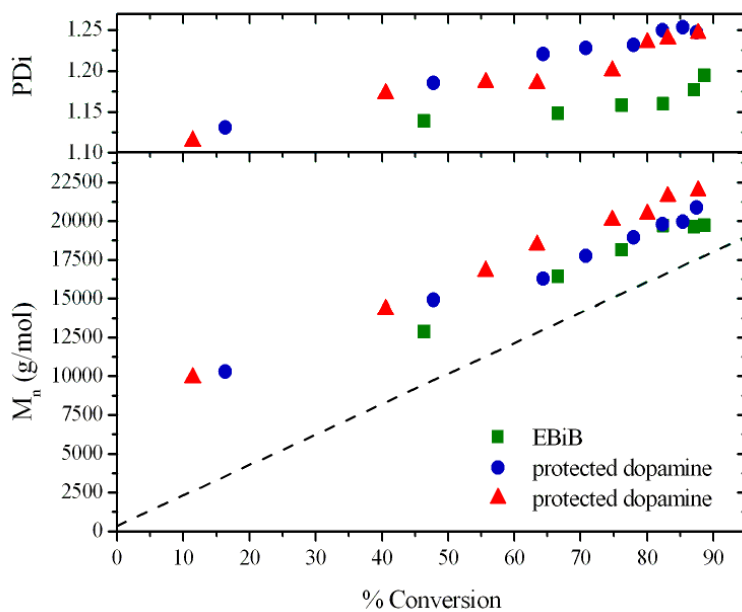


Figure 2.4-8. Evolution of molecular weight (M_n) and PDI versus conversion for the copolymerisation of lauryl methacrylate and MMA using EBiB aiming for 20,000 g/mol (■), and the protected dopamine initiator aiming for 10,000 g/mol (●, ▲) with Cu(I)Cl

Table 2.4-1. Final polymerisation data for the scale up polymerisations for mechanical testing

Polymer	M_n (g/mol)*	PDI*
Baseline	20,800	1.21
Protected dopamine	19,900	1.31
Protected dopamine ^a	18,700	1.31
Deprotected	18,000	1.34

*precipitated polymer; ^adeprotected polymer

2.5. Tribological testing

The three scaled-up polymers were tested by MTM and HFRR to ascertain whether they had any tribological benefits. The aim was to determine whether the deprotected dopamine polymer showed any reduction in wear. The testing was carried out by John Durham and Zahra Hussain at the Lubrizol site in Derby, UK.

Each polymer was dissolved in Yubase 4 oil, a high grade colourless oil, to obtain kinematic viscosity (KV) of 6 centistokes (cSt) at 100 °C. Kinematic viscosity is a measure of viscosity without any applied force. Table 2.5-1 displays the experimental data for the three prepared blends. The baseline polymer is the polymer prepared using EBiB. The amount of each polymer dissolved in the oil had to be varied for each polymer to obtain approximately the same KV.

The HFRR tests were conducted on the three polymer blends at a load of 200 g. The samples were heated at 40 °C for 15 minutes before ramping the temperature to 160 °C at a rate of 2 °C/min. The MTM tests were conducted on the three polymer blends at a load of 37 N. The speed was varied from 3,000 to 10 mm/s using a slide to roll ratio of 50% with measurements recorded at 40, 60, 80, 100, 120 and 140 °C.

Table 2.5-1. Polymer blend formulation

Sample	Baseline polymer	Protected dopamine polymer	Deprotected dopamine polymer
Warwick M_w *	21,400 g/mol	25,900 g/mol	24,200 g/mol
Lubrizol M_w *	25,800 g/mol	31,700 g/mol	33,000 g/mol
% Additives	100	100	100
Treat/% wt	6	6	6
KV100/cSt	5.97	6.18	5.73
Treat/% wt	6.08	5.57	6.82
KV100/cSt	5.96	5.98	6.14

*Molecular weights were recorded in CHCl_3 at Warwick and in THF at Lubrizol. KV100 is the kinematic viscosity measured according to the D445_100 method.

The data from the HFRR testing is plotted in Figures 2.5-1, 2.5-2 and 2.5-3 for the baseline, protected dopamine and deprotected dopamine polymers respectively. In each plot the red trace is a measure of the lubrication film (as a percentage), the green trace is the temperature and the blue trace is the measured friction coefficient. From the plots it can be seen that as the temperature increases the lubrication film started to collapse for both the baseline and protected dopamine polymers. The lubrication film collapsed at a noticeably lower temperature for the deprotected dopamine initiator. The measured friction coefficient was lower for the deprotected dopamine polymer between 40 and 100 °C compared to the baseline and protected polymer. The average friction coefficient by temperature range for the three polymer blends is shown in Table 2.5-2. The wear scars for each sample are shown in Figure 2.5-4.

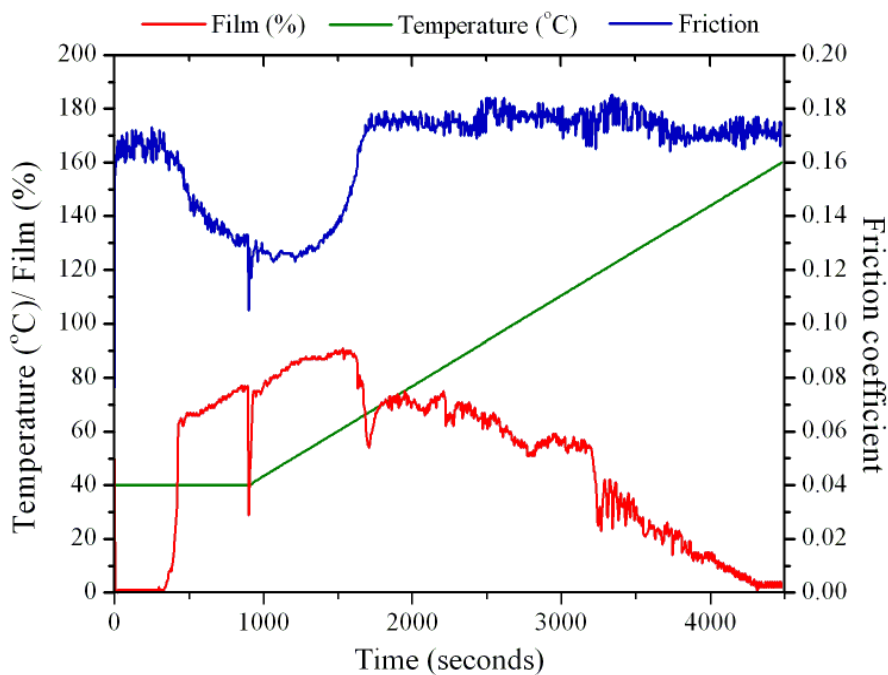


Figure 2.5-1. Plot of test run on HFRR for the baseline polymer

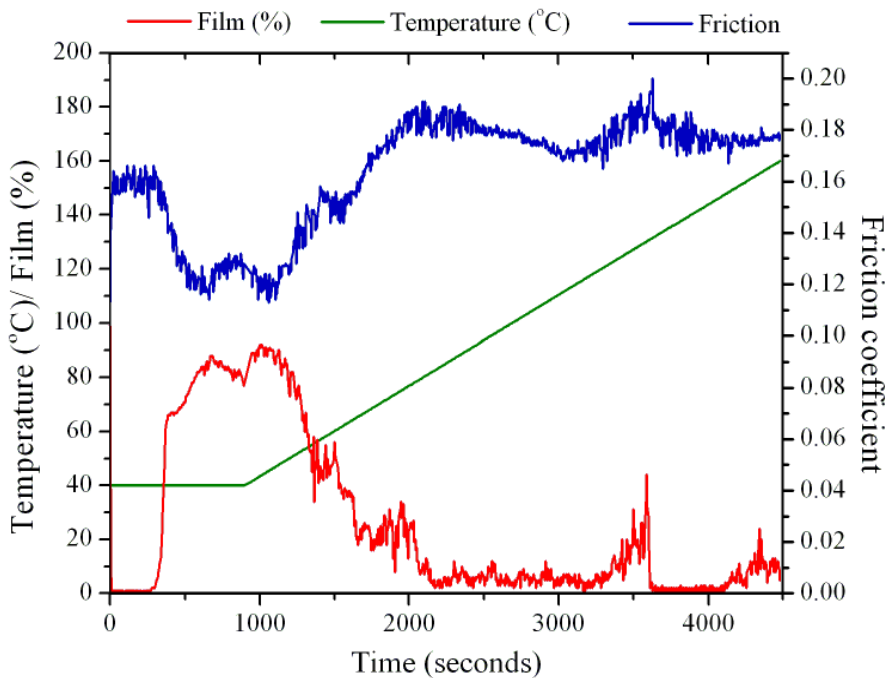


Figure 2.5-2. Plot of test run on HFRR for the protected dopamine polymer

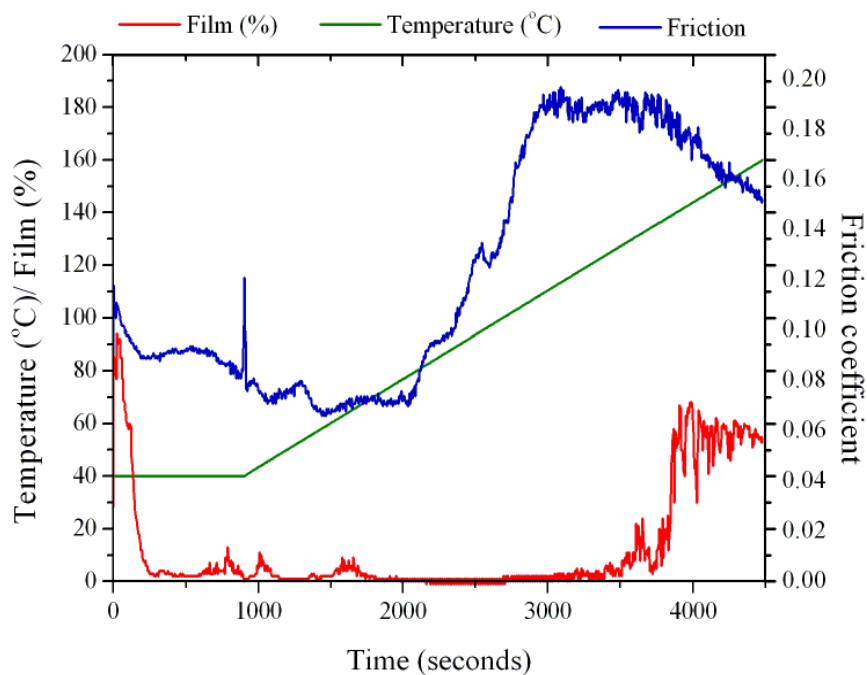


Figure 2.5-3. Plot of test run on HFRR for the deprotected dopamine polymer

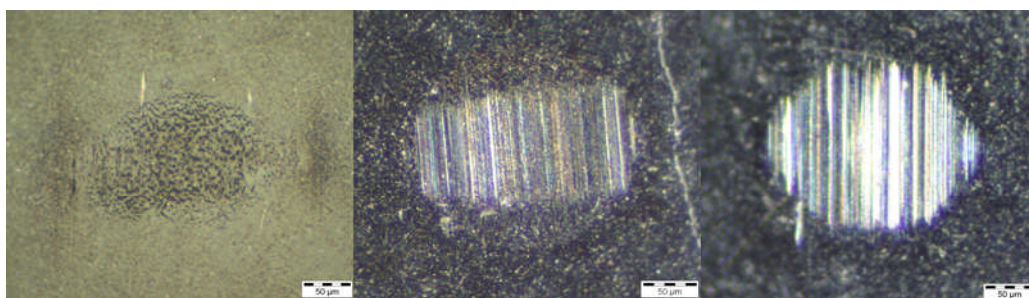


Figure 2.5-4. Wear scars for the base line (left), protected dopamine (middle) and deprotected dopamine (right) polymers from HFRR

Table 2.5-2. Average friction coefficients for the baseline, protected dopamine and deprotected dopamine polymers recorded using HFRR

Sample	Average friction coefficient by temperature range													
	40	40-50	50-60	60-70	70-80	80-90	90-	100-	110-	120-	130-	140-	150-	160
Baseline polymer	0.151	0.126	0.129	0.160	0.175	0.174	0.178	0.177	0.175	0.178	0.172	0.171	0.172	0.172
Protected dopamine polymer	0.140	0.123	0.147	0.162	0.182	0.183	0.179	0.174	0.172	0.184	0.180	0.176	0.176	0.176
Deprotected dopamine polymer	0.092	0.077	0.073	0.071	0.073	0.095	0.126	0.170	0.189	0.190	0.186	0.172	0.159	0.159

Visual inspection of the test pieces has determined that both the protected and deprotected dopamine polymers showed a small reduction in the wear of the surface compared to the baseline polymer. Corrosion of the test pieces was observed for the deprotected dopamine polymer. This is best illustrated in Figures 2.5-5 and 2.5-6 which shows the test pieces from the HFRR and MTM. The test pieces for the deprotected dopamine polymer shown on the right have become dull in comparison to the baseline (left) and the protected dopamine polymer (middle) which both retain their shiny surface.



Figure 2.5-5. Test pieces from the HFRR tests for the baseline (left), protected dopamine (middle) and deprotected dopamine (right) polymers



Figure 2.5-6. Test pieces from the MTM tests for the baseline (left), protected dopamine (middle) and deprotected dopamine (right) polymers

The overlaid Stribeck curves obtained from the recorded MTM data for each polymer blend at different temperatures are shown in Figures 2.5-7, 2.5-8 and 2.5-9.

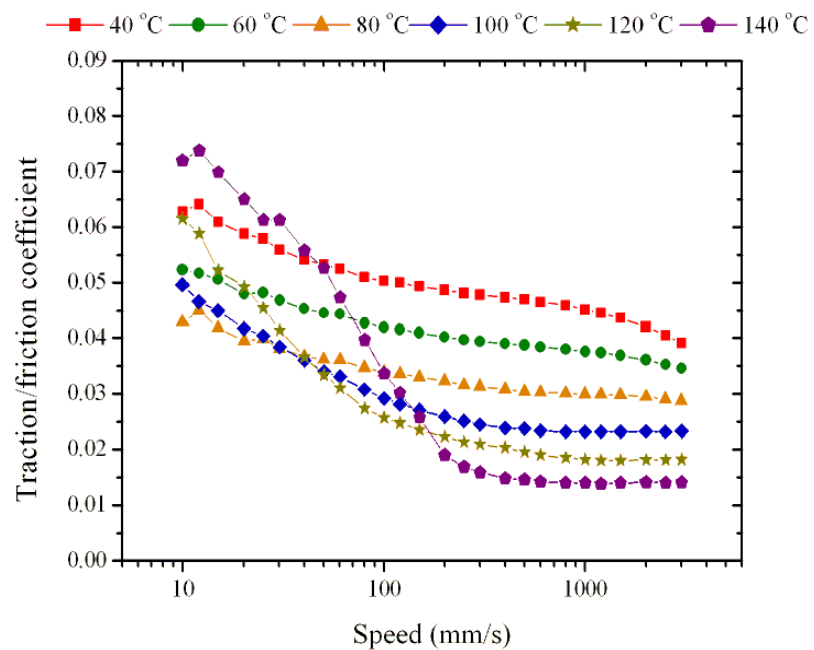


Figure 2.5-7. Overlaid Stribeck curves from the MTM tests for the baseline polymer

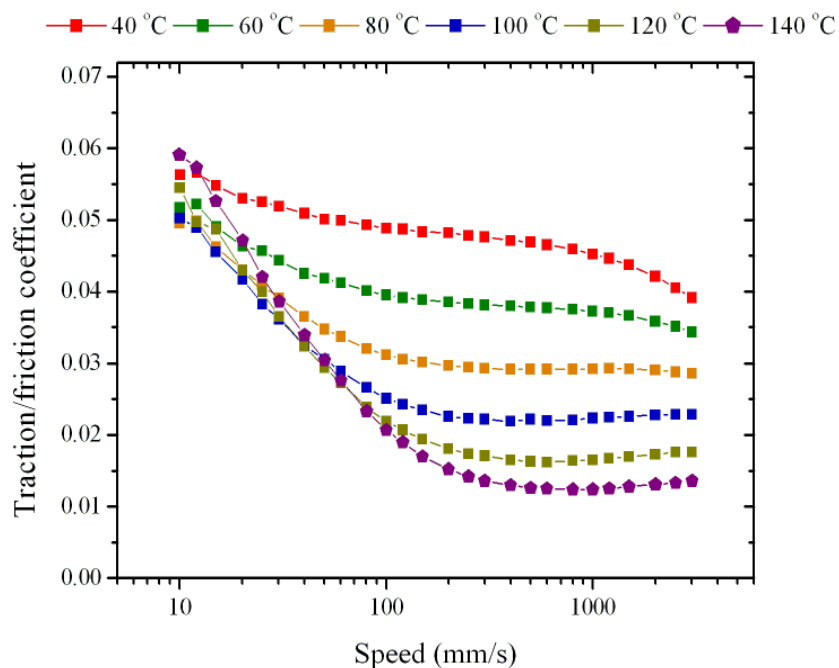


Figure 2.5-8. Overlaid Stribeck curves from the MTM tests for the protected dopamine polymer

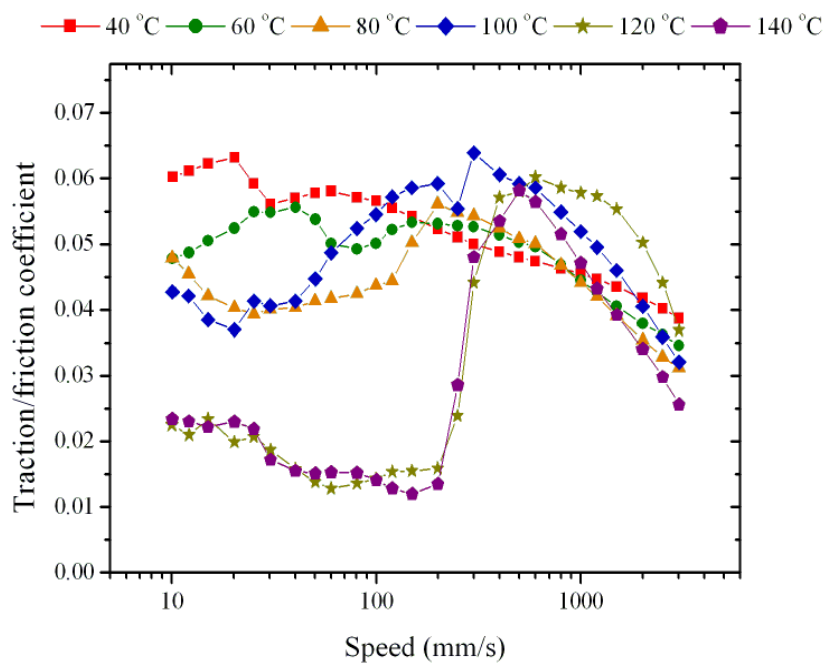


Figure 2.5-9. Overlaid Stribeck curves from the MTM tests for the deprotected dopamine polymer

From the graphs it can be seen that the baseline and protected dopamine polymer show very similar curves up until the higher temperatures. The deprotected polymer showed some unusual curves. These curves are potentially very interesting as a reduction in friction was observed for the deprotected polymer. However, because corrosion of the test piece was observed these unusual curves may be due to the change in surface structure.

It was concluded that these initial tests were successful. The observed reduction in friction for the deprotected dopamine polymer suggests that the polymer may be interacting with the surface and as a result reduce friction. The observed reduction in wear for both dopamine polymers was also considered a positive result. However, due to the observed corrosion the results for the deprotected dopamine polymer may not be accurate. It was speculated that the corrosion may have been caused by increased acidity of the deprotected polymer due to its method of preparation.

2.6. Conclusions and future work

In conclusion, a dopamine based initiator was synthesised and used in the Cu(I) mediated polymerisation of MMA and the Cu(0) mediated polymerisation of *t*-butyl acrylate with little success. The synthesis of an acetonide protected version of the dopamine initiator was used in the same polymerisations and proceeded under living conditions in the Cu(0) mediated polymerisation. The protected dopamine catecholic end-group was identified as the polymer end-group and was completely deprotected post polymerisation. The polymerisation of lauryl methacrylate was achieved using a technique designed for the long chain, non-polar molecule which utilised Cu(I)Cl and anisole. A baseline, protected dopamine polymer and deprotected dopamine polymer were synthesised on a 10 g scale and submitted for MTM and HFRR testing. A reduction in friction and wear was observed for the deprotected polymer, however, corrosion of the test pieces was also observed.

Following on from the results discussed in this thesis, more work can be done to investigate the dopamine end-functionalised polymers as friction modifiers once the corrosion problem, assumed to be due to the acidity of the polymer after deprotection, has been addressed. Tests should be done to investigate how long the polymer should be left in contact with the test piece to allow the dopamine to fully adsorb onto the surface and to investigate whether the oil soluble polymer can be lost in the oil environment overtime. The percentage of dopamine in the polymer may also need to be increased to match the percentages observed in the mfps involved in adhesion either by using a lower molecular weight polymer or by

incorporating dopamine in the back bone of the polymer. The viscosity of the polymer blend at various temperatures also needs to be measured to see how the polymers viscosity changes with temperature as it have been assumed in this work that it remains relatively constant.

2.7. Experimental

2.7.1. Materials

All chemicals were purchased from Sigma Aldrich and used as received unless otherwise stated. Lauryl methacrylate was supplied by The Lubrizol Corporation. High quality (nanoporous) copper used for Cu(0) polymerisations was supplied by Exeter Analytical. Inhibitors were removed from all monomers by passing through a short basic alumina column.

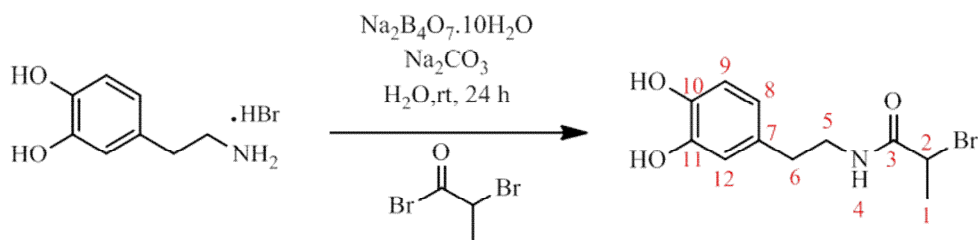
2.7.2. Characterisation techniques

Melting points were recorded using a Stuart Scientific SMP3 melting point apparatus at a rate of 3 °C/minute. Infra-red spectra were recorded using a Bruker Vector 22 FTIR spectrometer fitted with a Golden Gate attenuated total reflection cell. IR transmissions are reported as wavenumbers (cm^{-1}). The following abbreviations have been used; br = broad, w = weak, m = medium, s = strong, Ar = aromatic, adj = adjacent, def = deformation, sym = symmetrical and asym = asymmetrical. NMR spectra were recorded using Bruker DPX-300, DPX-400, DRX-500 and AV III-600 instruments as solutions in deuterated NMR solvents. Chemical shifts are reported in parts per million (ppm) relative to tetramethylsilane (TMS). The following abbreviations are used to abbreviate multiplicities; s = singlet, d = doublet, t = triplet, q = quartet and m = multiplet. Conversion was determined by measuring the disappearance of the monomer vinyl peaks with the appearance of

polymer in NMR spectra. Microanalyses were performed in duplicate where possible by Warwick Analytical Service. High resolution mass spectrometry were performed by the Mass Spectroscopy Facility at Warwick. Gel permeation chromatography samples were run on an Agilent 390-LC system equipped with a PL-AS RT autosampler, a 100 μ L injection loop, a 5 μ m PLgel guard column (50 mm x 7.5 mm), 2 5 μ m PLgel Mixed D columns (50 mm x 300) and a differential refractive index (DRI) detector. The system was eluted with chloroform at a rate of 1 mL/minute and the detector was calibrated with PL narrow polystyrene (162–371,100 g/mol) and poly methyl methacrylate (200–467,400 g/mol) standard easy vials. UV-vis gel permeation chromatography samples were run an Agilent 390MDS system equipped with a PL-AS RT autosampler, a 100 μ L injection loop, a 5 μ m PLgel guard column (50 mm x 7.5 mm), 2 5 μ m PLgel Mixed D columns (50 mm x 300) a differential refractive index (DRI) detector and a Shimadzu SPD-M20A photodiode array UV-vis detector. The system was eluted with TFA with 100 ppm Topanol and 2% v/v TEA at a rate of 1 mL/minute and the RI detector was calibrated with PL narrow polystyrene (162–371,100 g/mol) and poly methyl methacrylate (200–467,400 g/mol) standard easy vials.

2.7.3. Synthesis of compounds for Chapter 2

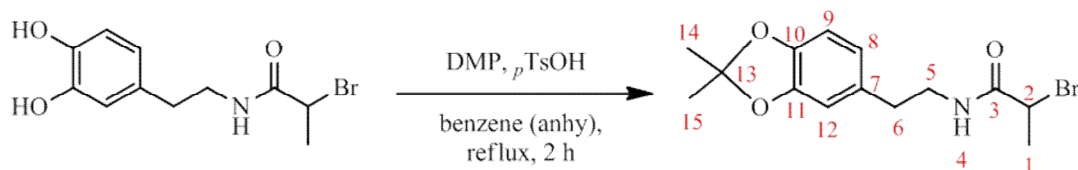
2.7.3.1. Synthesis of 2-bromo-*N*-[2-(3,4-dihydroxyphenyl)ethyl]propionamide (unprotected dopamine initiator)



The unprotected dopamine initiator was synthesised using a slightly modified procedure to that described in the literature.¹⁹ To a three-necked 250 mL round bottomed flask which contained stirring ultrapure water (100 mL) was slowly added borax (3.83 g, 10 mmol). The resulting solution was stirred and bubbled with nitrogen for approximately 2 hours before adding dopamine hydrobromide (2.34 g, 10 mmol). The solution was stirred for 15 minutes before adding sodium carbonate (3.39 g, 32 mmol) and cooled in an ice bath before adding 2-bromopropionyl bromide (1.05 mL, 10 mmol) dropwise. The reaction mixture was stirred at ambient temperature for 20 hours under nitrogen. The pH was monitored during the reaction adding more sodium carbonate as necessary to keep the pH = 10. The reaction mixture was acidified to pH = 2 using 6 M aqueous HCl solution and extracted three times with ethyl acetate (100 mL). The organic fractions were combined and dried with magnesium sulphate before removing the solvent *in vacuo* to give an off white oil. The compound was purified by silica gel column chromatography using 25:23:2 petroleum ether 46:60/ethyl acetate/methanol to give the unprotected dopamine initiator (0.77 g, 26.8%) as a colourless oil. The compound was crystallised from

methanol/water and recrystallised using chloroform to give colourless crystals. Melting point: 71-73 °C. IR (neat): $\tilde{\nu}$ = 3269 (s, OH), 2970, 2921, 2973 (w, CH stretch), 1650 (s, C=O), 1563, 1469 (m, Ar), 1441 (m, CH def), 1349 (s, CH₃ sym def), 1261 (s, OH), 1150 (s, C-OH), 863 (m, C-O-CH₃), 698 (s, C-Br) cm⁻¹. ¹H NMR (400.03 MHz, MeOD, 298 K) δ = 1.72 (d, *J* = 7.0 Hz, 3H, H1); 2.65, 3.35 (AA'XX', *J*_{AA'} = 10.55, *J*_{AX} = 12.42, *J*_{AX'} = -10.66, *J*_{XX} = 4.64, 4H, H5,6); 4.40 (q, *J* = 7.0, 14.0 Hz, 1H, H2); 6.55 (br dd, *J* = 2.0, 8.0 Hz, 1H, H8); 6.64 (s, 1H, H9); 6.67 (t, *J* = 8.0 Hz, H12). ¹³C NMR (100.60 MHz, MeOD, 298 K) δ = 22.47 (C1); 35.58 (C5); 42.64 (C6); 44.05 (C2); 116.37 (C8); 116.93 (C9); 121.13 (C12); 131.79 (C7); 144.84, 146.28 (C10,11); 172.36 (C3). Anal. Calcd. for C₁₁H₁₄NO₃Br: C, 45.85; H, 4.90; N, 4.86. Found: C, 42.53; H, 4.67; N, 4.58. Mass Spectrometry (+ESI-MS) *m/z*: 310.00 [M+Na]⁺.

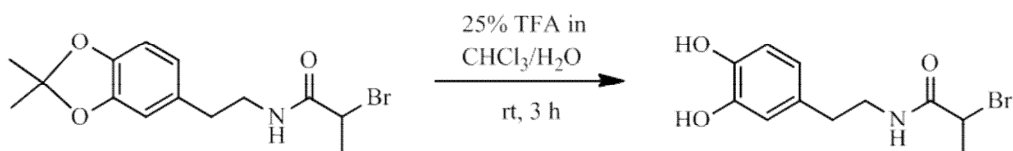
2.7.3.2. Synthesis of 2-bromo-*N*-[2-(3,4-dihydroxyphenyl)ethyl]propionamide acetone (protected dopamine initiator)



The procedure used for the synthesis of the protected dopamine initiator was taken from the literature.⁵³ To a two-necked 100 mL round bottomed flask was added unprotected dopamine initiator (0.53 g, 1.84 mmol), 2,2-dimethoxypropane (0.85 mL, 6.94 mmol) and anhydrous benzene (40 mL). One neck of the flask was fitted with a Soxhlet extractor and the thimble was filled with anhydrous granular calcium

chloride (4 g). The other neck was sealed with a septum. The flask was flushed with nitrogen and then heated to reflux for 5 minutes before adding *p*-toluenesulfonic acid monohydrate (13.5 mg, 0.071 mmol) dissolved in a minimal amount of anhydrous benzene. The reaction was monitored using the ferric chloride test. Once a negative test had been observed, approximately after 2 hours, the reflux was stopped. Once cooled the solution was passed through a short silica gel column and washed through using dichloromethane. The solvent was removed *in vacuo* to give a yellow solid which was recrystallised from dichloromethane/petroleum ether 40:60 to give the protected dopamine initiator (0.41 g, 68.1%) as a white crystalline solid. Melting point: 106-107 °C. IR (neat): $\tilde{\nu}$ = 3243 (m, -CONH-), 2971, 2926, 2859 (w, CH stretch), 1652 (s, C=O), 1575 (m), 1496 (s, Ar), 1445 (m, CH def), 1380 (m, CH₃ sym def), 863 (s, C-O-CH₃), 723 (m, C-Br) cm⁻¹. ¹H NMR (400.03 MHz, CDCl₃, 298 K) δ = 1.67 (s, 6H, H14,15); 1.85 (d, *J* = 7.0 Hz, 3H, H1); 2.74 (t, *J* = 7.0 Hz, 2H, H6); 3.49 (m, 2H, H5); 4.37 (q, *J* = 7.0, 14.0 Hz, 1H, H2); 6.39 (br s, 1H, H4); 6.59 (br dd, *J* = 2.0, 6.0 Hz, 2H, H8,12); 6.66 (q, *J* = 3.0, 6.0 Hz, 1H, H9). ¹³C NMR (100.60 MHz, CDCl₃, 298 K) δ = 23.39 (C1); 25.96 (C14,15); 35.27 (C6); 41.60 (C5); 45.59 (C2); 108.31, 109.00 (C8,9); 117.97 (C13), 121.23 (C12), 131.57 (C7), 146.32, 147.86 (C10,11), 169.23 (C3). Anal. Calcd. for C₁₄H₁₈NO₃Br: C, 51.23; H, 5.53; N, 4.27. Found: C, 50.68; H, 5.35; N, 4.25. Mass Spectrometry (+ESI-MS) *m/z*: 350.04 [M+Na]⁺.

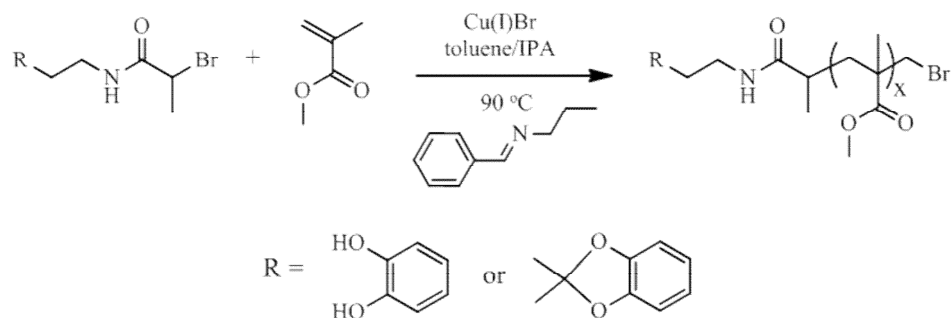
2.7.3.3. Deprotection 2-bromo-*N*-[2-(3,4-dihydroxyphenyl)ethyl]propionamide acetone (deprotected dopamine initiator)



The deprotection was completed using a slightly modified procedure to that described in the literature.⁵³ To a 25 mL round bottomed flask was added the protected dopamine initiator (0.13 g, 0.4 mmol). The flask was sealed with a septum and flushed in nitrogen. To an oven dried Schlenk tube was added trifluoroacetic acid (1.25 mL, 16.3 mmol), chloroform (3.7 mL) and water (0.05 mL). The solution was degassed using three freeze-pump-thaw cycles before being cannulated into the round bottom flask. The reaction mixture was stirred at ambient temperature for 3 hours. The volatiles were removed *in vacuo* to give the deprotected dopamine initiator (0.1 g, 87.5%) as a colourless oil which was crystallised from methanol/water.

2.7.4. Polymerisation procedures for Chapter 2

2.7.4.1. Cu(I) mediated polymerisation of MMA using the unprotected/protected dopamine initiators



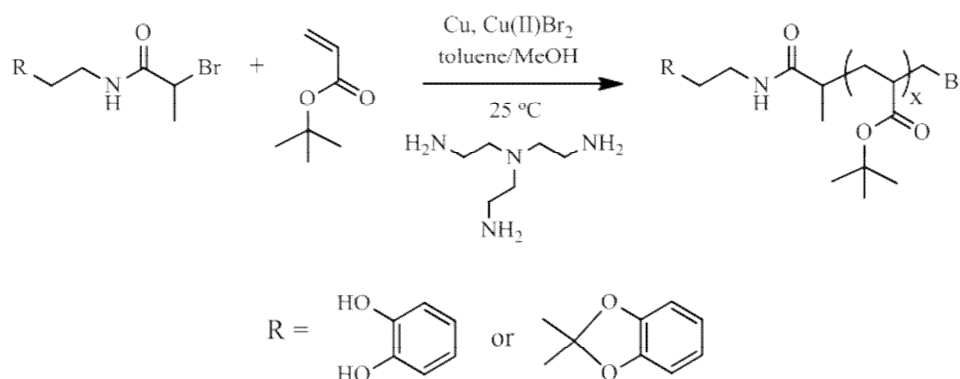
The polymerisation of MMA was carried out using a slightly modified procedure to that described in the literature.⁵⁴ To an oven dried Schlenk tube was added either the unprotected or protected dopamine initiator (0.21 mmol) and 50:50 toluene/isopropyl alcohol (1 mL). To another Schlenk tube was added Cu(I)Br (28 mg, 0.21 mmol), *N*-ethyl-2-pyridylmethanimine (28 μL , 0.10 mmol), 50:50 toluene/isopropyl alcohol (1.2 mL) and MMA (1.12 mL, 10.4 mmol) in that order. Both solutions were degassed using three freeze-pump-thaw cycles. The reaction mixture was heated at 90 $^\circ\text{C}$ under nitrogen for 5 minutes prior to adding the initiator solution via a degassed syringe. The polymerisation was terminated by bubbling with air for 10 minutes followed by the addition of dichloromethane (5 mL). The crude polymer was precipitated once into methanol using dichloromethane to dissolve the polymer.

Table 2.7-1. Final polymerisation data for the Cu(I) mediated polymerisation of MMA using the unprotected/protected dopamine initiators

Initiator	Time (h)	Conversion (%)	M_n (g/mol)*	PDI*
Unprotected	116	64.9	54,700	1.46
Protected	23	87.1	18,073	1.39

*precipitated polymer

2.7.4.2. Cu(0) mediated polymerisation of *t*-butyl acrylate using the unprotected/protected dopamine initiators



To an oven dried Schlenk tube was added either the unprotected or protected dopamine initiator (0.4 g) and 14:1 toluene/methanol (0.8 mL). To another Schlenk tube was added was added Cu, Cu(II)Br₂, Me₆Tren, the remaining 14:1 toluene/methanol, and *t*-butyl acrylate in that order. Both solutions were degassed using three freeze-pump-thaw cycles. The reaction mixture was heated at 25 °C under nitrogen for 5 minutes prior to adding the initiator solution via a degassed syringe. The polymerisation was terminated by bubbling with air for 10 minutes followed by the addition of dichloromethane (approximately 5 mL). The crude

polymer was precipitated once into methanol using dichloromethane to dissolve the polymer.

Table 2.7-2. Reagent quantities for the Cu(0) mediated polymerisation of *t*-butyl acrylate using the unprotected/protected dopamine initiators

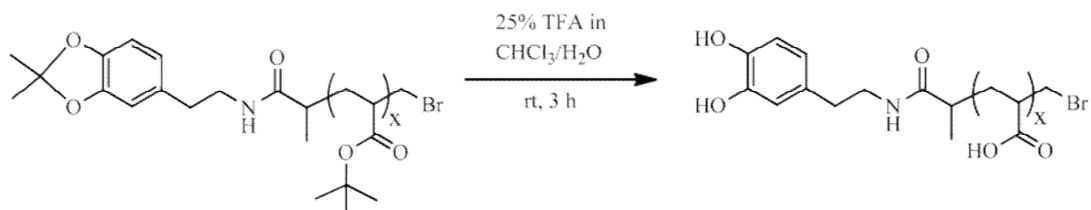
Initiator	Cu		Cu(II)Br ₂		Me ₆ Tren		<i>t</i> -butyl acrylate		Toluene/MeOH (14:1)	
	mmol	mg	mmol	mg	mmol	μL	mmol	mL	mmol	mL
Unprotected	0.14	17.8	0.28	9.5	0.04	85	0.32	4	27.3	6.1 mL
Unprotected	0.14	17.3	0.27	10.0	0.04	85	0.32	0.8	5.46	1.5 mL
Protected	0.12	15.9	0.24	8.5	0.04	75	0.28	3.7	25.3	5.4 mL
Protected	0.12	18.3	0.28	9.5	0.04	85	0.32	0.7	4.78	1.3 mL

Table 2.7-3. Final polymerisation data for the Cu(0) mediated polymerisation of *t*-butyl acrylate using the unprotected/protected dopamine initiators

Initiator	Time (h)	Conversion (%)	M _n (g/mol)*	PDI*
Unprotected	28	50.4	33,600	1.70
Unprotected	6.5	93.8	7,300	2.55
Protected	28	72.9	23,200	1.27
Protected	4	82.0	4,700	1.14

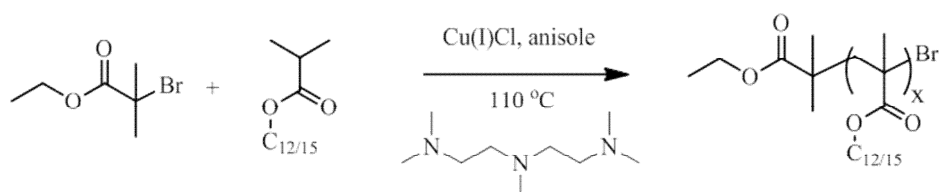
*precipitated polymer

2.7.4.3. Deprotection of poly *t*-butyl acrylate made using the protected dopamine initiator



The procedure described for the deprotection of the protected dopamine initiator was used to deprotect the two butyl acrylate polymers synthesised using the protected dopamine initiator (0.2 g).

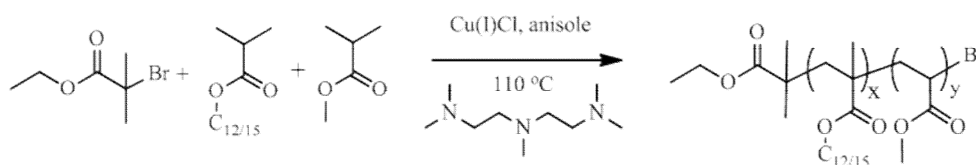
2.7.4.4. Polymerisation of lauryl methacrylate using Cu(I)Cl



The procedure described by Xu *et al.*⁶⁰ was followed. To an oven dried Schlenk tube was added Cu(I)Cl (8.5 mg, 0.086 mmol), *N,N,N',N'',N'''*-pentamethyldiethylenetriamine (PMDETA, 53 μ L, 0.23 mmol), anisole (1.5 mL), ethyl 2-bromoisobutyrate (12.5 μ L, 0.086 mmol) and lauryl methacrylate (5 mL, 17.1 mmol) in that order. The reaction mixture was degassed using three freeze-pump-thaw cycles and heated at 110 °C under nitrogen for 4 hours where conversion had reached 16.3%. The polymerisation was terminated by bubbling with air for 10 minutes followed by the addition of dichloromethane (10 mL). A small amount

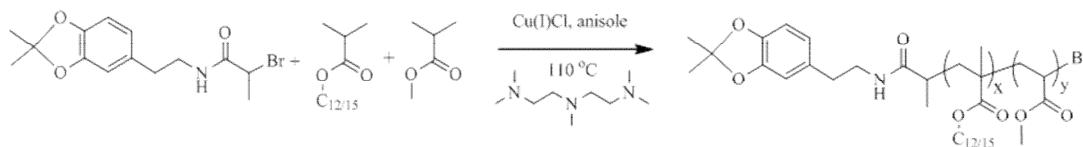
crude polymer was passed through a short basic alumina column before being precipitated once into methanol. The polymer was dried in a vacuum oven for 3 hours and used for analysis. $M_n = 31,300$ g/mol; $PDi = 1.27$.

2.7.4.5. Copolymerisation of lauryl methacrylate and MMA using Cu(I)Cl



The method for the copolymerisation of lauryl methacrylate and MMA was adapted from that described by Xu *et al.*⁶⁰ for this polymerisation. To an oven dried Schlenk tube was added Cu(I)Cl (8.5 mg, 0.086 mmol), PMDETA (53 μ L, 0.26 mmol), anisole (0.6 mL), ethyl 2-bromoisobutyrate (12.5 μ L, 0.085 mmol), lauryl methacrylate (1.35 g, 4.89 mmol) and MMA (0.34 g, 3.43 mmol). The reaction mixture was degassed using four freeze-pump-thaw cycles and heated at 110 °C under nitrogen for 120 minutes where conversion had reached 96.8%. The polymerisation was terminated by bubbling with air for 10 minutes followed by the addition of dichloromethane (10 mL). A small amount crude polymer was passed through a short basic alumina column before being precipitated once into methanol. The polymer was dried in a vacuum oven for 3 hours and used for analysis. $M_n = 19,600$ g/mol; $PDi = 1.29$.

2.7.4.6. Copolymerisation of lauryl methacrylate and MMA using Cu(I)Cl and the protected dopamine initiator



The method for the copolymerisation of lauryl methacrylate and MMA was adapted from that described in Section 2.7.4.5 for this polymerisation. To an oven dried Schlenk tube was added Cu(I)Cl, PMDETA, anisole, the protected dopamine initiator, lauryl methacrylate (1.35 g, 4.89 mmol) and MMA (0.34 g, 3.43 mmol). The reaction mixture was degassed using four freeze-pump-thaw cycles and heated at 110 °C under nitrogen for 90 minutes. The polymerisation was terminated by bubbling with air for 10 minutes followed by the addition of dichloromethane (10 mL). The crude polymer was passed through a basic alumina column before being precipitated once into methanol using a dry ice/acetone bath using dichloromethane to dissolve the polymer. The polymer was dried in a vacuum oven at 40 °C overnight.

Table 2.7-4. Reagent quantities for the Cu(I)Cl mediated copolymerisation of lauryl methacrylate and MMA using the unprotected dopamine initiator

Cu(I)Cl		PMDETA		Unprotected I		Anisole
mg	mmol	μL	mmol	mg	mmol	(mL)
8.5	0.09	53	0.26	27.9	0.09	0.6
12.7	0.13	80	0.38	42.1	0.13	0.6
16.9	0.17	107	0.51	55.8	0.17	0.6
16.9	0.17	107	0.51	55.8	0.17	1.86

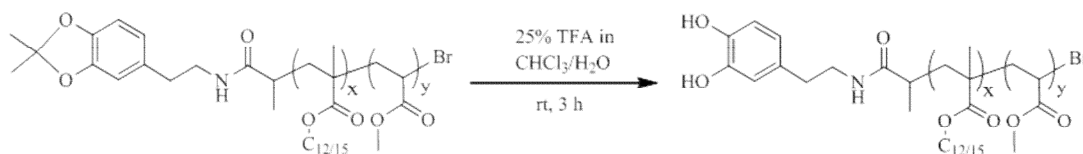
Table 2.7-5. Final polymerisation data for the Cu(I)Cl mediated copolymerisation of lauryl methacrylate and MMA using the unprotected dopamine initiator

Time (mins)	Conversion (%)	M_n (g/mol)*	PDI*
90	86.4	39,800	1.29
40	84.1	38,600	1.71
90	97.7	20,700	1.46
90	89.3	18,900	1.29

*precipitated polymer

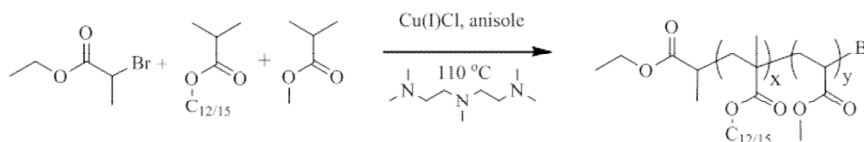
2.7.4.7. Deprotection of lauryl methacrylate/MMA copolymer

($M_n = 18,900$ g/mol; PDI = 1.29)



The method described for the deprotection of the protected dopamine initiator was used to deprotect a lauryl methacrylate/MMA copolymer synthesised in Section 2.7.4.6 ($M_n = 18,900$ g/mol; PDI = 1.29) with the amounts of reagents adjusted to the weight of the polymer (0.44 g).

2.7.4.8. Copolymerisation of lauryl methacrylate and MMA using Cu(I)Cl and ethyl 2-bromopropionate



The method for the copolymerisation of lauryl methacrylate and MMA was adapted from that described in Section 2.7.4.6. To an oven dried Schlenk tube was added Cu(I)Cl (8.6 mg, 0.09 mmol), PMDETA (53 μ L, , 0.26 mmol), anisole (1.8 mL), ethyl 2-bromopropionate (11 μ L, 0.09 mmol), lauryl methacrylate (1.35 g, 4.89 mmol) and MMA (0.34 g, 3.43 mmol). The reaction mixture was degassed using four freeze-pump-thaw cycles and heated at 110 °C under nitrogen for 90 minutes where conversion had reached 85.6%. The polymerisation was terminated by bubbling with air for 10 minutes followed by the addition of dichloromethane (10 mL). A small amount crude polymer was passed through a short basic alumina column before being precipitated once into methanol. The polymer was dried in a vacuum oven for 3 hours and used for analysis. $M_n = 13,358$ g/mol; PDI = 1.25.

2.7.5. Scale up polymerisations for industrial testing

2.7.5.1. Copolymerisation of lauryl methacrylate and MMA using Cu(I)Cl and ethyl 2-bromopropionate

The method described in Section 2.7.4.8 was repeated with the reagents scaled up as follows: Cu(I)Cl (182 mg, 1.84 mmol), PMDETA (1.15 mL, 5.51 mmol), anisole (38 mL), ethyl 2-bromopropionate (0.24 mL, 1.84 mmol), lauryl methacrylate (29.03 g, 0.11 mol) and MMA (7.31 g, 73.0 mmol). The polymerisation was stopped after 90 minutes where conversion had reached 88.7%. The polymerisation was terminated by bubbling with air for 10 minutes followed by the addition of dichloromethane (50 mL). The crude polymer was passed through a basic alumina column before being precipitated once into methanol using a dry ice/acetone bath using dichloromethane to dissolve the polymer. The polymer was dried in a vacuum oven at 40 °C for 3 days. $M_n = 20,800$ g/mol; PDI = 1.21.

2.7.5.2. Copolymerisation of lauryl methacrylate and MMA using Cu(I)Cl and the protected dopamine initiator

The method described in Section 2.7.4.6 was repeated with the reagents scaled up as follows: Cu(I)Cl (363 mg, 3.67 mmol), PMDETA (2.3 mL, 11.0 mmol), anisole (40 mL), protected dopamine initiator (1.2 g, mmol), lauryl methacrylate (29.03 g, 0.11 mol) and MMA (7.31 g, 73.0 mmol). The polymerisation was stopped after 60 minutes where conversion had reached 87.7%. The polymerisation was terminated

by bubbling with air for 10 minutes followed by the addition of dichloromethane (50 mL). The crude polymer was passed through a basic alumina column before being precipitated once into methanol using a dry ice/acetone bath using dichloromethane to dissolve the polymer. The polymer was dried in a vacuum oven at 40 °C for 3 days. $M_n = 19,900$ g/mol; PDI = 1.31.

This reaction was repeated to obtain a second polymer. $M_n = 18,700$ g/mol; PDI = 1.31.

2.7.5.3. Deprotection of lauryl methacrylate/MMA copolymer

The method described for the deprotection of the protected dopamine initiator was used to deprotect one polymer from Section 2.7.5.2 ($M_n = 18,700$ g/mol; PDI = 1.31) with the amounts of reagents adjusted to the weight of the protected dopamine initiator used in the polymerisation (1.2 g). The polymer was dried in a vacuum oven at ambient temperature for 4 days.

2.8. References

1. J. H. Waite, *Nat. Mater.*, 2008, **7**, 8-9.
2. J. H. Waite, N. H. Andersen, S. Jewhurst and C. Sun, *J. Adhes.*, 2005, **81**, 297-317.
3. J. H. Waite, *Int. J. Adhes. Adhes.*, 1987, **7**, 9-14.
4. B. P. Lee, P. B. Messersmith, J. N. Israelachvili and J. H. Waite, *Annu. Rev. Mater. Res.*, 2011, **41**, 99-132.
5. X.-X. Qin, K. J. Coyne and J. H. Waite, *J. Biol. Chem.*, 1997, **272**, 32623-32627.
6. J. L. Dalsin and P. B. Messersmith, *Materials Today*, 2005, **8**, 38-46.
7. Q. Lin, D. Gourdon, C. Sun, N. Holten-Andersen, T. H. Anderson, J. H. Waite and J. N. Israelachvili, *Proc. Natl. Acad. Sci.*, 2007, **104**, 3782-3786.
8. M. Yu, J. Hwang and T. J. Deming, *J. Am. Chem. Soc.*, 1999, **121**, 5825-5826.
9. L. A. Burzio and J. H. Waite, *Biochemistry*, 2000, **39**, 11147-11153.
10. S. Haemers, G. J. M. Koper and G. Frens, *Biomacromolecules*, 2003, **4**, 632-640.
11. J. Monahan and J. J. Wilker, *Langmuir*, 2004, **20**, 3724-3729.
12. M. Yu and T. J. Deming, *Macromolecules*, 1998, **31**, 4739-4745.
13. H. Lee, N. F. Scherer and P. B. Messersmith, *Proc. Natl. Acad. Sci.*, 2006, **103**, 12999-13003.
14. J. Yu, W. Wei, E. Danner, R. K. Ashley, J. N. Israelachvili and J. H. Waite, *Nat. Chem. Biol.*, 2011, **7**, 588-590.

15. M. J. Harrington, A. Masic, N. Holten-Andersen, J. H. Waite and P. Fratzl, *Science*, 2010, **328**, 216-220.
16. J. J. Wilker, *Angew. Chem. Int. Ed.*, 2010, **49**, 8076-8078.
17. J. J. Wilker, *Curr. Opin. Chem. Biol.*, 2010, **14**, 276-283.
18. H. Lee, S. M. Dellatore, W. M. Miller and P. B. Messersmith, *Science*, 2007, **318**, 426-430.
19. X. Fan, L. Lin, J. L. Dalsin and P. B. Messersmith, *J. Am. Chem. Soc.*, 2005, **127**, 15843-15847.
20. J. L. Dalsin, L. Lin, S. Tosatti, J. Voros, M. Textor and P. B. Messersmith, *Langmuir*, 2004, **21**, 640-646.
21. A. Charlot, V. Sciannamea, S. Lenoir, E. Faure, R. Jerome, C. Jerome, C. Van De Weerd, J. Martial, C. Archambeau, N. Willet, A.-S. Duwez, C.-A. Fustin and C. Detrembleur, *J. Mater. Chem.*, 2009, **19**, 4117-4125.
22. A. S. Goldmann, C. Schödel, A. Walther, J. Yuan, K. Loos and A. H. E. Müller, *Macromol. Rapid Commun.*, 2010, **31**, 1608-1615.
23. C. Xu, K. Xu, H. Gu, R. Zheng, H. Liu, X. Zhang, Z. Guo and B. Xu, *J. Am. Chem. Soc.*, 2004, **126**, 9938-9939.
24. K. C. L. Black, Z. Liu and P. B. Messersmith, *Chem. Mater.*, 2011, **23**, 1130-1135.
25. G. Bilic, C. Brubaker, P. B. Messersmith, A. S. Mallik, T. M. Quinn, C. Haller, E. Done, L. Gucciardo, S. M. Zeisberger, R. Zimmermann, J. Deprest and A. H. Zisch, *Am. J. Obstet. Gynecol.*, 2010, **202**, 85.e81-85.e89.
26. C. E. Brubaker, H. Kissler, L.-J. Wang, D. B. Kaufman and P. B. Messersmith, *Biomaterials*, 2010, **31**, 420-427.
27. P. Glass, H. Chung, N. R. Washburn and M. Sitti, *Langmuir*, 2009, **25**, 6607-6612.

28. G. Westwood, T. N. Horton and J. J. Wilker, *Macromolecules*, 2007, **40**, 3960-3964.
29. H. Shao, K. N. Bachus and R. J. Stewart, *Macromol. Biosci.*, 2009, **9**, 464-471.
30. H. Lee, B. P. Lee and P. B. Messersmith, *Nature*, 2007, **448**, 338-341.
31. K. G. Neoh and E. T. Kang, *ACS Applied Materials & Interfaces*, 2011, **3**, 2808-2819.
32. X.-D. Pan, Z. Qin, Y.-Y. Yan and P. Sadhukhan, *Polymer*, 2010, **51**, 3453-3461.
33. H. Lee, K. D. Lee, K. B. Pyo, S. Y. Park and H. Lee, *Langmuir*, 2010, **26**, 3790-3793.
34. C. D. Zobrist, J. Sobocinski, J. L. Lyskawa, D. Fournier, V. R. Miri, M. Traisnel, M. Jimenez and P. Woisel, *Macromolecules*, 2011, **44**, 5883-5892.
35. L. M. Hamming, X. W. Fan, P. B. Messersmith and L. C. Brinson, *Compos. Sci. Technol.*, 2008, **68**, 2042-2048.
36. J. L. Dalsin, B.-H. Hu, B. P. Lee and P. B. Messersmith, *J. Am. Chem. Soc.*, 2003, **125**, 4253-4258.
37. K. Matyjaszewski, *Current Opinion in Solid State and Materials Science*, 1996, **1**, 769-776.
38. K. Matyjaszewski, *Macromol. Symp.*, 1998, **134**, 105-118.
39. V. Percec, T. Guliashvili, J. S. Ladislaw, A. Wistrand, A. Stjerndahl, M. J. Sienkowska, M. J. Monteiro and S. Sahoo, *J. Am. Chem. Soc.*, 2006, **128**, 14156-14165.
40. T. Guliashvili and V. Percec, *J. Pol. Sci. Part A - Polym. Chem.*, 2007, **45**, 1607-1618.
41. M. J. Monteiro, T. Guliashvili and V. Percec, *J. Pol. Sci. Part A - Polym. Chem.*, 2007, **45**, 1835-1847.

-
42. K. Matyjaszewski, N. V. Tsarevsky, W. A. Braunecker, H. Dong, J. Huang, W. Jakubowski, Y. Kwak, R. Nicolay, W. Tang and J. A. Yoon, *Macromolecules*, 2007, **40**, 7795-7806.
43. B. M. Rosen and V. Percec, *Chem. Rev.*, 2009, **109**, 5069-5119.
44. C. V. Bovington, in *Chemistry and Technology of Lubricants*, eds. R. M. Mortier, M. F. Fox and S. T. Orszulik, Springer, **2010**.
45. B. Edward, M. Michael, T. Simon and S. Shirley, in *Handbook of Lubrication and Tribology*, CRC Press, **2006**, pp. 1-26.
46. STLE, *Fundamentals of Lubrication and Tribology III - Lubrication*, <http://www.stle.org/resources/lubelearn/lubrication/>, Accessed 15th October 2011.
47. J. Bo, *Tribology International*, 2003, **36**, 781-789.
48. P. Instruments, *HFRR High Frequency Reciprocating Rig Brochure*, http://www.pcs-instruments.com/pdf/hfr/HFRR_Brochure_ENGLISH.pdf, Accessed 15th October, 2011.
49. P. Instruments, *MTM2 Mini Traction Machine Brochure*, <http://www.pcs-instruments.com/pdf/mtm/MTM2.pdf>, Accessed 15th October, 2011.
50. J. Durham, Discussions on tribological testing at Lubrizol site, 29th September 2010.
51. R. Pizer and L. Babcock, *Inorg. Chem.*, 1977, **16**, 1677-1681.
52. V. A. Soloshonok and H. Ueki, *Synthesis*, 2008, **5**, 693-695.
53. Z. Liu, B.-H. Hu and P. B. Messersmith, *Tetrahedron Lett.*, 2010, **51**, 2403-2405.
54. D. M. Haddleton, M. C. Crossman, B. H. Dana, D. J. Duncalf, A. M. Heming, D. Kukulj and A. J. Shooter, *Macromolecules*, 1999, **32**, 2110-2119.
55. A. Limer and D. M. Haddleton, *Macromolecules*, 2006, **39**, 1353-1358.

56. Y. Xia, N. A. D. Burke and H. D. H. Stover, *Macromolecules*, 2006, **39**, 2275-2283.
57. R. M. Broyer, G. M. Quaker and H. D. Maynard, *J. Am. Chem. Soc.*, 2007, **130**, 1041-1047.
58. C. Fidge, University of Warwick, 2009.
59. P. Wright, University of Warwick, 2008.
60. W. Xu, X. Zhu, Z. Cheng and J. Chen, *J. Appl. Polym. Sci.*, 2003, **90**, 1117-1125.